Dyslipidemia at the crossroad of the skin barrier and the arterial wall

Martins Cardoso, R.

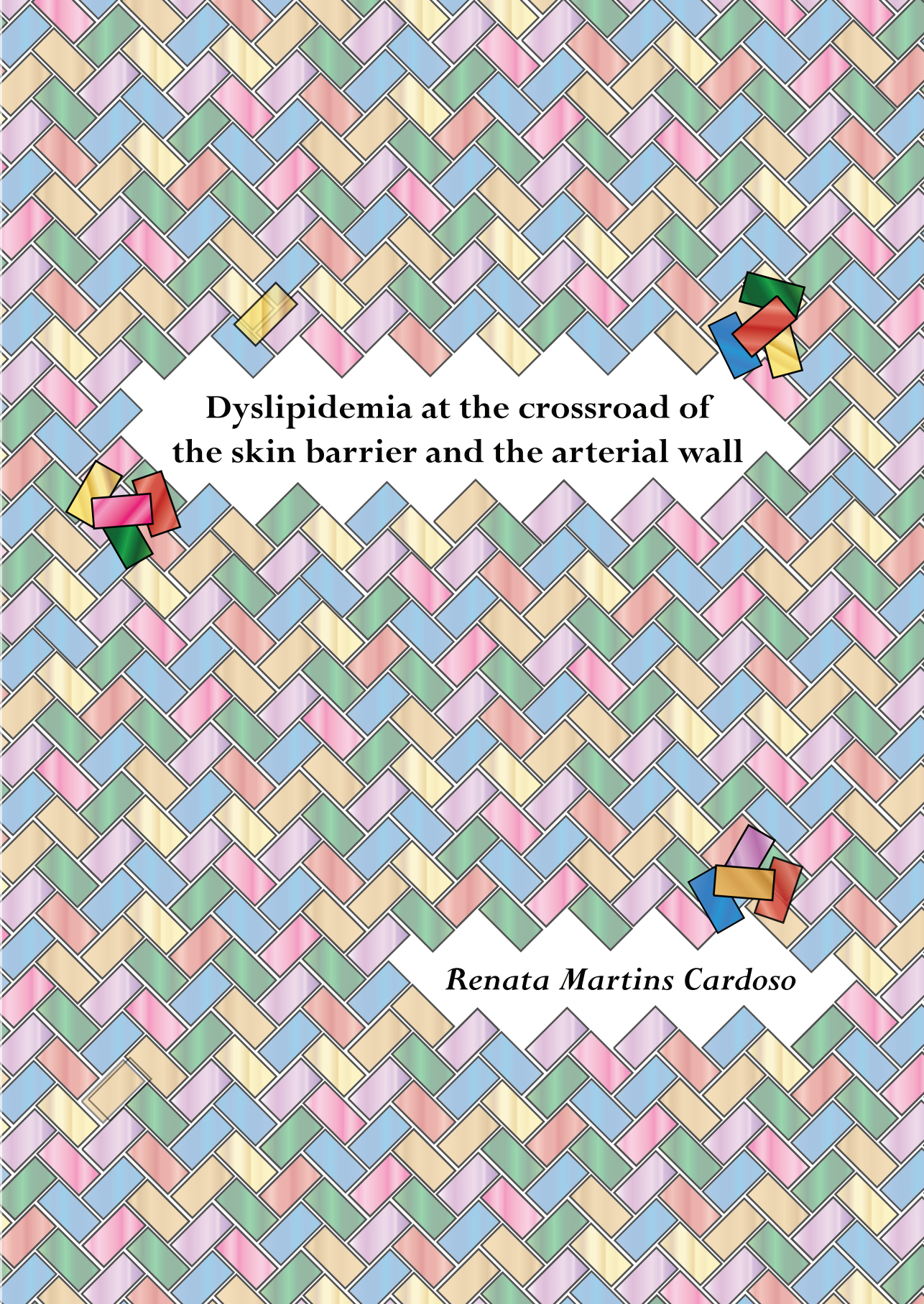

Dyslipidemia at the crossroad of the skin barrier and the arterial wall

Renata Martins Cardoso

Dyslipidemia at the crossroad of the skin barrier and the arterial wall

Renata Martins Cardoso

Dyslipidemia at the crossroad of the skin barrier and the arterial wall
Renata Martins Cardoso
05 October 2021

Institute: Leiden Academic Centre for Drug Research

Cover design: The cover illustrates the classic brick and mortar structure of the stratum corneum layer with a glance of the vascular bed that lies under the skin. Cover design by Renata Martins Cardoso and Richard W. J. Helder with technical support from Science Ink.

Thesis layout: Renata Martins Cardoso

Printer: Ipskamp Printing

ISBN: 978-94-6421-466-6

Dyslipidemia at the crossroad of the skin barrier and the arterial wall

Proefschrift

ter verkrijging van
de graad van doctor aan de Universiteit Leiden,
op gezag van rector magnificus prof.dr.ir. H. Bijl,
volgens besluit van het college voor promoties
te verdedigen op 5 oktober 2021
klokke 13:45 uur

door
Renata Martins Cardoso

geboren te Vitória, Brazilië
in 1986

Promotor: Prof. Dr. J. A. Bouwstra

Promotor: Prof. Dr. M. van Eck

Promotiecommissie:

Prof. Dr. H. Irth	- LACDR (voorzitter)
Prof. Dr. J. Kuiper	- LACDR (secretaris)

Overige leden

Dr. J. van Smeden	- Leiden University
Prof. Dr. P. C. N. Rensen	- LUMC
Prof. Dr. T. Vermonden	- Utrecht University
Dr. M. T. Mulder	- Erasmus Medical Centre

The research described in this thesis was performed at the division of BioTherapeutics at the Leiden Academy Centre for Drug Research (Leiden University, Leiden, The Netherlands). This research was supported by Leiden Academic Centre for Drug Research. The realization of this thesis was also supported by Leiden University.

To my belated grandmother Maria

Table of contents

Chapter 1

General Introduction

SKIN FUNCTION AND STRUCTURE

The skin is the largest organ in mammals and it acts as an interface between the body and the external environment[1]. It naturally functions as a barrier protecting the body from excessive loss of water and electrolytes (inside-outside barrier), and against the permeation of harmful agents and pathogens (outside-inside barrier)[1]. In addition to being a physicochemical barrier, the skin is densely populated with antigen presenting cells; thus, a highly immunogenic organ[2–4].

The skin is morphologically divided into three main layers from the inside to the outside: hypodermis, dermis and epidermis[5,6]. The hypodermis comprises the subcutaneous fat tissue involved in *e.g.* the storage of energy (fat), mechanical protection, and thermoregulation[6]. The dermis is mainly composed of fibroblasts surrounded by an extracellular matrix enriched with collagen and elastin[7,8]. The dermis accommodates all skin appendages (hair follicles, sebaceous glands and sweat glands) as well as nerve endings, blood- and lymphatic vessels. The presence and density distribution of the dermal components varies depending on the mammalian species and on body site[9–12].

The epidermis is the outer layer of the skin composed of melanocytes, Langerhans cells, Merkel cells, and keratinocytes, the latter comprising the predominant epidermal cell type[1,13]. From inside-out the epidermis can be divided into four sub-layers (strata): stratum basale (SB), stratum spinosum (SS), stratum granulosum (SG), and stratum corneum (SC) (Figure 1). In contrast to the human epidermis with multiple keratinocyte layers, murine epidermis is one quarter thinner and contains merely 2-3 layers of keratinocytes[14,15]. Epidermal keratinocytes proliferate in the SB and migrate upwards to the skin surface in a differentiation process to become flat enucleated dead cells called corneocytes[16,17]. As part of the differentiation process in the SS (early differentiation) and SG (late differentiation), the metabolism of the keratinocyte shifts to produce lamellar bodies, that are intracellular vesicles enriched with lipid processing enzymes and lipids[18]. At the terminal differentiation stage, the load of the lamellar bodies is extruded to form a well-structured lamellar lipid matrix surrounding the corneocytes leading to the formation of the SC layer[19].

STRATUM CORNEUM (SC)

The SC is the outermost layer of the epidermis and is primarily responsible for the barrier function of the skin. The SC is mainly composed of corneocytes embedded in an lipid matrix similarly to a “brick and mortar” structure. Corneocytes are dead cells that

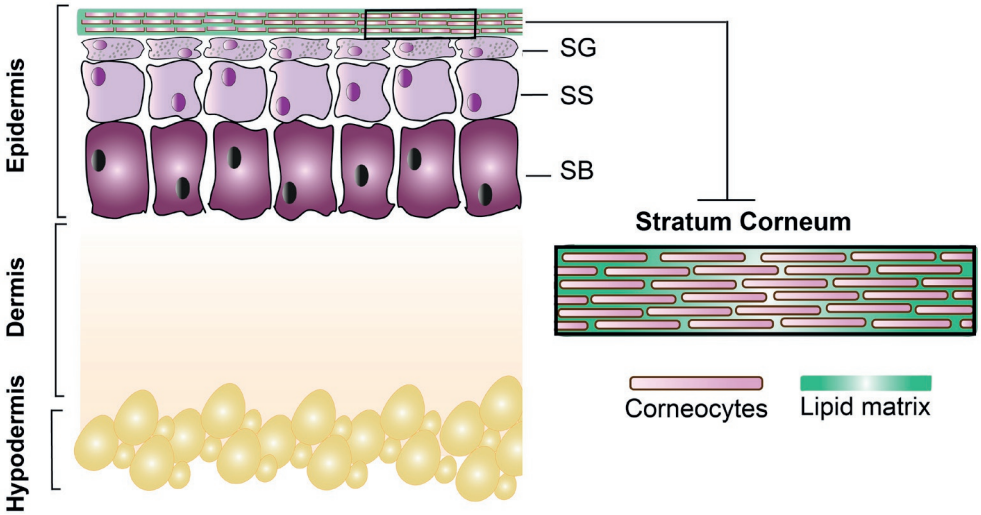

Figure 1. Structure of murine skin. The skin is divided into three main layers: hypodermis, dermis, and epidermis. The hypodermis is the deepest skin layer comprising the subcutaneous fat tissue. The dermis is the intermediate skin layer mostly composed of fibroblasts and collagen and where skin appendages, blood vessels, and nerve endings are found. The epidermis is the most superficial layer of the skin and is subdivided into four strata from inside to outside: stratum basale (SB), stratum spinosum (SS), stratum granulosum (SG), and stratum corneum (SC). In the SC, fully differentiated dead keratinocytes, now called corneocytes, are surrounded by a lipid matrix and undergo desquamation over time.

lost their organelles and replaced their cellular membranes by a highly impermeable crosslinked protein structure chemically attached to a lipid layer, namely the cornified envelope[17,20,21]. This monolayer of lipids serves as a template for the orientation of the SC lipid matrix (the mortar), a well-structured stack of lipid layers filling the intercorneocyte space; hence, the only continuous pathway in the SC. In time, corneocytes at the surface shed off, a process defined as desquamation, leading to SC renewal over time[17]. A complete turnover of keratinocytes in murine skin takes about 3 weeks while in human skin this process takes up to 5 weeks[22]. The thickness of the SC also differs between mouse (approximately 5 μm) and human (10–20 μm) skin[15,23].

The lipids in the SC adopt both a lamellar and a lateral organization (Figure 2). The stacked lipid lamellae are oriented approximately parallel to the skin surface. Two distinct lamellar phases can be identified using small-angle X-ray diffraction (SAXD); a short periodicity phase (SPP) and a long periodicity phase (LPP) with repeated distances of approximately 6 nm and 13 nm in human SC, respectively[24,25]. The presence of a LPP highly correlates with a functional skin barrier[26]. Perpendicular to the skin surface, the lipids can adopt three types of lateral organization based on the distances between the lipid lattice planes: a dense orthorhombic phase (0.375 and 0.416 nm), a

less dense hexagonal phase (0.412 nm), and a liquid disordered phase (approximately 0.46 nm)[27]. In healthy human and murine SC, both orthorhombic and hexagonal phases co-exist. However, most lipids form a dense orthorhombic lipid packing, most favorable for the barrier function of the skin[28–32].

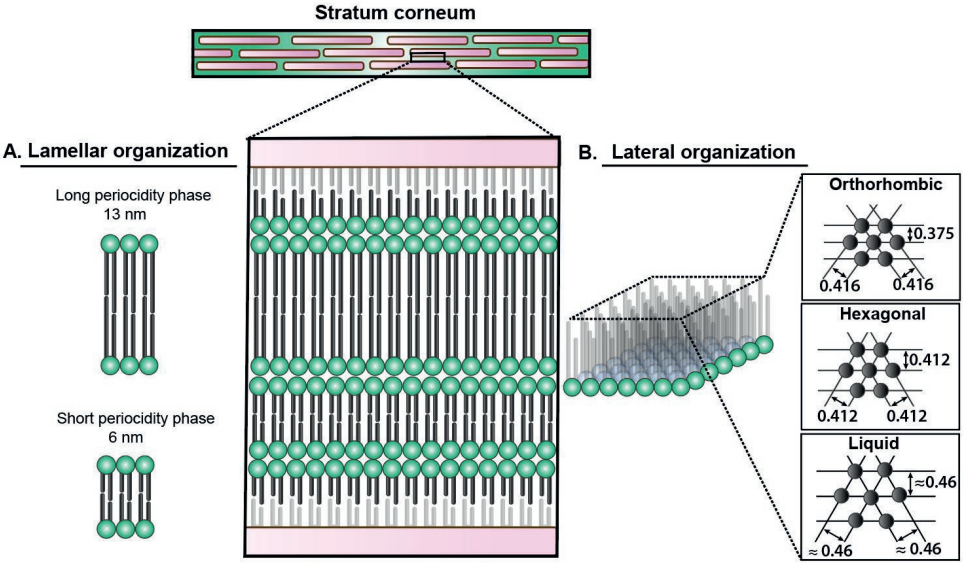

Figure 2. Organization of the lipids composing the stratum corneum (SC) lipid matrix. In the SC, corneocytes and lipid matrix are ordered similarly to a "brick and mortar" structure. In the lipid matrix, the lipids form a lamellar organization and a lateral organization. For the **(A)** lamellar organization two distinct phases are identified: the long periodicity phase and the short periodicity phase with 13 nm and 6 nm repeated distances, respectively. For the **(B)** lateral organization, the lipids can adopt a dense orthorhombic phase, a less dense hexagonal phase, and a liquid disordered phase based on the distance between lipid lattice planes (nm).

The composition of the SC lipids has major impact on the organization of the lipid matrix[33–35]. The main lipid classes composing the SC lipid matrix are cholesterol, ceramides (CERs), and free fatty acids (FFAs), which are present in the matrix in an approximately equimolar ratio (Figure 3)[36]. Other lipids have also been described as part of the skin surface lipids (*e.g.* wax-esters, triglycerides - TG) but at minor fractions and strongly associated with sebum lipids[37–39]. Cholesterol is the most abundant sterol in the SC, constituting 20-25% of the SC lipid mass[40,41]. At much lower levels (2-5% SC lipid mass), cholesterol sulfate is another sterol present in the SC[42,43]. Cholesterol sulfate is particularly expressed in the superficial layer in SC, where it participates as a signaling molecule in the desquamation of corneocytes[42,44].

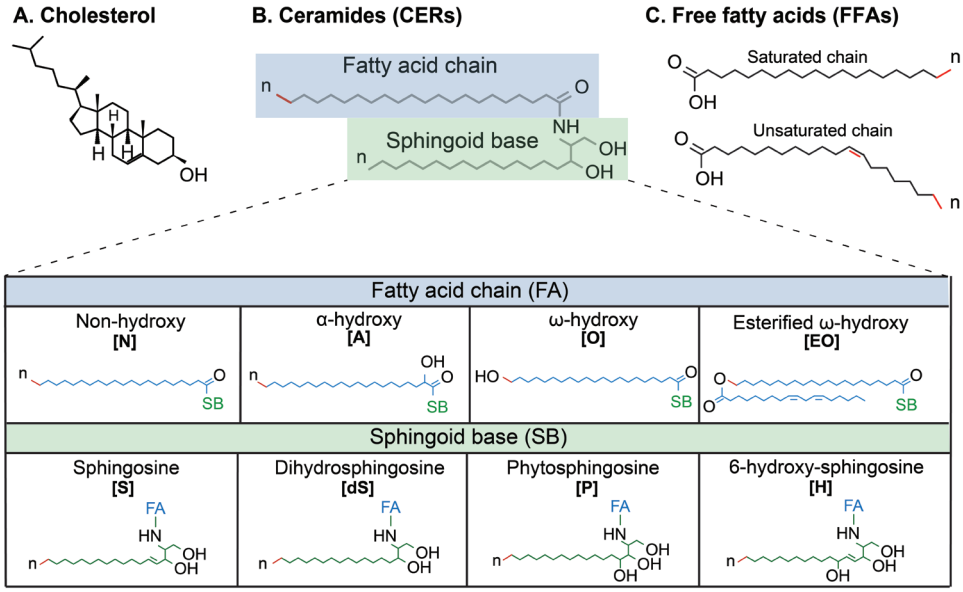

Figure 3. Schematic structure of the three main lipid classes present in the SC lipids matrix. (A) Cholesterol, (B) ceramides (CERs) and (C) free fatty acids (FFAs). CERs are named according to Motta *et. al.* (1993) based on their sphingoid bases (green marked area) and acyl chains (blue marked area)[45]. FFA chains can be (un)saturated and vary in number of carbon atoms (n).

CERs are sphingolipids composed of a sphingoid base linked to an acyl chain and they contribute to nearly 50-60% of lipid mass in the SC[40,41]. In this thesis, CER nomenclature is based on the type of acyl chain and the architecture of the headgroup in the sphingoid base present in their structures (Figure 3)[45]. The acyl chains present in CERs can be non-hydroxylated (N); α-hydroxylated (A); ω-hydroxylated (O) or esterified ω-hydroxylated (EO). The sphingoid bases can be classified as sphingosine (S), dihydrosphingosine (dS), phytosphingosine (P) or 6-hydroxy-sphingosine (H). Other CER groups are present in the SC in lower amounts, including the newly identified sphingoid base dihydroxy sphinganine (CER[T]) and the recently described acyl chain 1-O-acylceramindes (CER [1-O-E])[46,47]. In addition to their structural classification, a wide range of carbon chain length has been described for both the sphingoid base and the acyl chain, yielding CERs with a total chain length between 32-78 carbon atoms[48]. Although less abundant, unsaturated CERs can also be present in the SC[34,47,49].

FFAs are fatty acids in non-esterified form. In contrast to CERs, FFAs have a simpler structure and represent only 15-20% of the SC lipid weight[40,41]. FFA species in the SC vary in carbon chain length (12-36 carbon atoms), unsaturation (saturated or mono/polyunsaturated), and hydroxylation (non- or hydroxylated) (Figure 3)[31,50,51]. However,

in both murine and human skin, saturated long chain FFAs with 24 and 26 carbon atoms are most abundant[50,52]. Both unsaturated and hydroxylated FFAs are present at very low levels in healthy human SC[51]. In contrast, unsaturated FFA species can account for nearly 15% of the FFA content in murine skin[52].

SYNTHESIS OF SC BARRIER LIPIDS

The lipids present in the SC lipid matrix are primarily synthesized by keratinocytes during their differentiation process in the viable epidermis[19,41,53].

Cholesterol

Cholesterol is synthesized in the endoplasmic reticulum and peroxisomes of keratinocytes starting with condensation of three molecules of acetyl-co-enzyme-A (CoA) to form 3-hydroxy-3-methylglutaryl-CoA (HMG-CoA)[54]. The reduction of HMG-CoA to mevalonate by the enzyme HMG-CoA reductase (HMGCR) is the rate-limiting step in cholesterol synthesis[54,55]. Next, in a series of enzyme mediated steps, mevalonate is converted to lanosterol, which can be finally converted into cholesterol.

Ceramides (CERs)

The synthesis of CERs also occurs in the endoplasmic reticulum starting with the condensation of serine with palmitoyl-CoA by the enzyme serine-palmitoyl transferase to produce 3-keto-dihydrosphingosine[41,56,57]. Multiple steps involving the ceramide synthase family result in the acetylation of a FA to form a ceramide with a dihydrosphingosine base (CER[dS]). Next, the CER[dS] can be converted into other CER subclasses [S] and [P] by activity of dihydroceramide desaturase 1 (DESG1) and 2 (DESG2), respectively[41]. The mechanisms underlying the hydroxylation step involved in the conversion of CER [dS] into CER[H] remain unknown. The enzymes patatin like phospholipase domain containing 1 and CYP4F22 have been implicated in the esterification of linoleic acid (FA C18:2) to form the CER[EO] subclass; yet, the contribution of other mediators cannot be excluded[41,58]. At the final step, the CERs are transported to the Golgi complex for the addition of a glucose (glucosyl-CERs) or phosphocholine (sphingomyelin) followed by their storage in the LB as CER precursor lipids. Once extruded at the interface SG-SC, glucosyl-CERs and sphingomyelin are converted by β-glucocerebrosidase (GBA) and acid sphingomyelinase, respectively, into CERs for the lipid matrix[59,60].

Free fatty acids (FFAs)

The synthesis of fatty acids starts in the cytosol with the condensation of one acetyl-CoA and seven malonyl-CoA molecules to form palmitic acid, a saturated fatty acid

with 16 carbon atoms in its chain (FFA C16:0). Palmitic acid is then elongated in the endoplasmic reticulum through a four steps membrane-associated elongation cycle: condensation, reduction, dehydration, and reduction, respectively. The first step, condensation, is mediated by a family of seven elongases (ELOVL1-7) and is the rate limiting step in the fatty acid synthesis[61,62]. In addition to elongation, fatty acids can be desaturated by stearoyl-CoA desaturase (SCD) and fatty acid desaturases (FADS)[62–64]. At the end, fatty acids can be used in the CER synthesis or converted into phospholipids for storage in the LB as FFA precursors for the SC lipids. In fact FFAs and CERs share a common biosynthetic pathway in the epidermis and alterations in the chain length or unsaturation of FFA translate into similar trends in the CER profile[35,41,65]. Finally, as described for the CERs, following extrusion at the interface SG-SC, these precursors can be converted by various phospholipases into FFAs to compose the lipid matrix.

Extracutaneous lipids

In addition to local lipid synthesis by keratinocytes, lipids of extracutaneous origin (*e.g.* FAs, precursors CERs, and cholesterol) enter the skin and can be detected in the epidermis[66–71]. Nearly 20% of circulating low-density lipoprotein (LDL) particles reach the skin, specifically, the cells in the SB[72]. In line, labelled cholesterol can be found in the epidermis following systemic administration[67]. The uptake of CER precursors from the plasma can also contribute to the epidermal lipid pool[66,73,74]. In mice, sphingomyelin and ceramide products can be found in SC after oral administration of radiolabeled sphingomyelin[66]. Furthermore, oral administration of sphingomyelin also improved the hydration of the SC and increased the CER content in the epidermis of mice[66]. Similar effects have been reported after supplementation of rice-derived glucosylceramides to mice and to human skin equivalent[74]. Essential FAs are not produced in the body and enter the circulation via the intake of food[68,70]. These diet-derived FAs are also essential components of the SC lipid matrix[71].

The uptake of cholesterol and FAs from the plasma and from circulating lipoproteins are likely mediated by receptors expressed in the keratinocytes (*e.g.* low-density lipoprotein receptor - LDLR, scavenger receptor class B member I -SR-BI, fatty acid binding protein-FABP, fatty acid transport protein - FATP, and cluster of differentiation 36 - CD36)[68,75–78]. These receptors are especially expressed in the basal layer of the epidermis with reduced expression towards the skin surface[75,78]. Inhibition of local cholesterol synthesis by topical application of pitavastatin leads to upregulation of LDLR in both cultured human keratinocytes and *in vivo* murine skin[75]. The levels of SR-BI and CD36 in the epidermis increase in response to acute barrier disruption, which can be normalized by occlusion of the disrupted barrier area[68,78]. CERs are also transported in the plasma in lipoproteins[79] and are likely delivered to the skin as part of these particles. However, in contrast, the pathways involved in the uptake of extracutaneous CERs remain unclear.

In summary, the importance of plasma lipids for the skin has been demonstrated both *in vitro* and *in vivo* and the contribution of these lipids to skin function becomes further relevant once the SC barrier has been compromised.

TRANSPORT AND METABOLISM OF PLASMA LIPIDS

Lipids are transported through the plasma compartment mainly in the core of 4 groups of lipoproteins: chylomicrons, very-low-density lipoproteins (VLDL), LDL, and high-density lipoproteins (HDL) (Figure 4). Each of these groups of lipoproteins have distinct physicochemical properties, lipid content, and protein composition (Table 1).

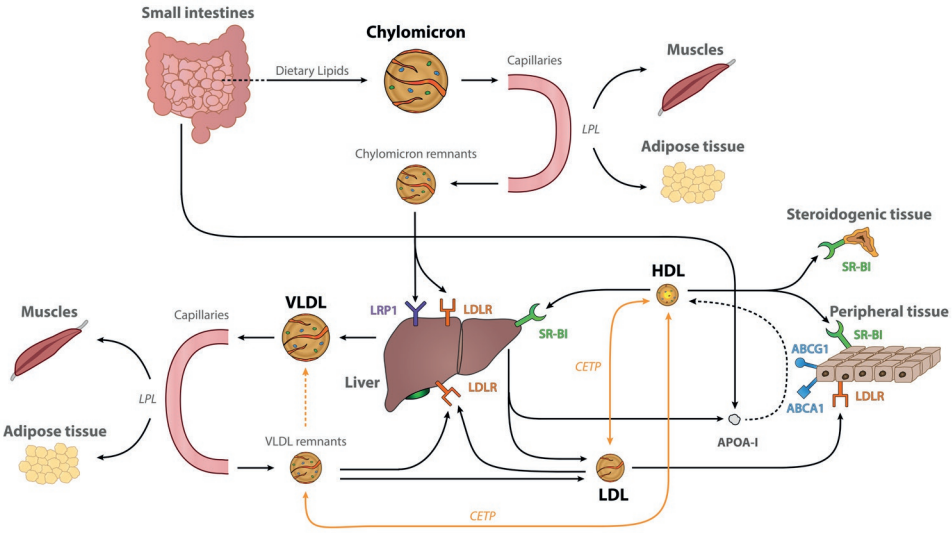

Figure 4. Metabolism of lipoproteins. The four major groups of lipoproteins are depicted: chylomicrons, very low-density lipoprotein (VLDL); low-density lipoprotein (LDL), and high-density lipoprotein (HDL). LPL is an extracellular enzyme present on the surface of the vascular endothelial involved in the metabolism of TG from VLDL and chylomicrons to generate free fatty acids that can be taken up by the muscles and adipose tissue. CETP is a lipid transfer factor present in humans but not in mice and it mediates the exchange of cholesteryl esters from HDL for triglycerides from VLDL/LDL (yellow arrows in the image). ABCA1 – ATP binding cassette A1; ABCG1; ATP binding cassette G1; APOAI-I – apolipoprotein A-I; CETP – cholesteryl ester transfer protein; LPL – lipoprotein lipase; LDLR – low-density lipoprotein receptor; LRP1 – low-density lipoprotein receptor related protein.

Chylomicrons are large particles produced by enterocytes and involved in the transport of lipids originated from the diet (exogenous source)[80,81]. The core of chylomicrons is primarily composed of TG but it also carries also cholesteryl esters (CE) and phospholipids. The main structural apolipoprotein (Apo) in chylomicrons is ApoB-48,

a truncated form of ApoB-100[82,83]. Once excreted by enterocytes into the lymphatic system and subsequently reaching the systemic circulation, the TG transported by chylomicrons are susceptible to the metabolic activity of lipoprotein lipase (LPL), leading to the removal of the FAs moieties. This process results in the formation of smaller cholesterol-rich chylomicron remnant particles that are rapidly taken up by the liver by interaction of ApoE with the LDLR-related protein 1 (LRP1) and LDLR.

VLDL are also TG-rich particles that carry a low amount cholesterol synthesized in the liver from acetyl-CoA molecules (endogenous source)[84]. The Apo profile in VLDL particles comprises ApoC-II and ApoE, and the main structural protein ApoB-100[85]. In rodents, ApoB-48 is also present in VLDL. VLDL is produced in the liver and released into the circulation where the TGs in the core of the particle undergo cleavage by LPL as described for chylomicrons[85]. TG-depleted VLDL remnants will lose ApoE and can be converted into LDL, CE-rich particles[85]. LDL delivers cholesterol to the tissues and is cleared from the circulation by the liver upon interaction with LDLR.

HDL represents another important group of lipoproteins involved in the transport of cholesterol throughout the body. In contrast to chylomicrons, VLDL and LDL that mainly participate in the delivery of lipids to the tissues, HDL especially mediates the transport of cholesterol from peripheral tissues to steroidogenic tissues and to the liver, the latter is part of a process defined as reverse cholesterol transport[86,87]. HDL particles contain ApoA-II, ApoC-II, ApoE, and ApoA-I, the latter comprising nearly 70% of the HDL protein content[88]. ApoA-I is synthesized by enterocytes and hepatocytes and secreted into the plasma in a lipid-poor form. ApoA-I develops into mature HDL particles by acquisition of lipids, in particular free cholesterol and phospholipids from other lipoproteins and via its interaction with the cellular cholesterol efflux pumps ATP-binding cassette (ABC)A1 and ABCG1[89]. Cholesterol is then stored in the core of the lipoprotein after esterification by the enzyme lecithin: cholesterol acyl transferase (LCAT)[90]. Interaction of HDL particles with SR-BI leads to the selective delivery of HDL-CE to steroidogenic tissues for hormone production or to the liver to be redistributed to the body or excreted via the bile, the last step in the reverse cholesterol transport process[91,92].

The distribution of TG and cholesterol within the lipoprotein groups varies according to the species[86,94]. In normolipidemic human subjects TG and CE are mainly transported in the core of VLDL and LDL, respectively. In normolipidemic rodents, VLDL is the main carrier of TG in the fasted state while almost all cholesterol circulates in HDL particles. These distinctions are crucial when translating the research performed in murine models to the human situation.

Table 1. Characteristics of the four main lipoprotein classes involved in the transport of lipids throughout the body: their density, size, lipid, and apolipoprotein composition[95,96] For each lipoprotein class the most representative lipids and apolipoproteins are described.

Lipoprotein	Density (g/ml)	Size (nm)	Lipid composition	Apolipoprotein composition
Chylomicrons	<0.930	75-1200	Triglycerides	ApoB-48, ApoC-II, ApoC-III, ApoE, ApoA-I, ApoA-II
VLDL	0.930-1.006	30-80	Triglycerides	ApoB-100, ApoE, ApoC-II, ApoB-48 (in rodents)
LDL	1.019-1.063	18-25	Cholesterol	ApoB-100, ApoB-48 (in rodents)
HDL	1.063-1.210	5-12	Cholesterol Phospho;lipids	ApoA-I, ApoA-II, ApoC-I, ApoC-II, ApoE

DYSLIPIDEMIA

Abnormalities in the metabolism of lipoproteins lead to the development of dyslipidemia, often marked by a persistent raise in the plasma lipid concentration, especially cholesterol and TG. Dyslipidemic profiles are a common cause of morbidity worldwide and hypercholesterolemia accounts for the majority of the cases. To date, several mutations have been identified in Apo's, enzymes, and receptors involved in the metabolism of lipoproteins.

Mutations in, but not limited to, LDLR and ApoE lead to the development of familial hypercholesterolemia (FH) and familial combined hyperlipidemia, respectively[97–99]. The loss of a functional LDLR hinders the clearance of ApoB- and ApoE-containing lipoproteins from the plasma[100]. These lipoproteins are then only catabolized via LRP1. In contrast, the lack of functional ApoE impacts the clearance chylomicrons remnants and VLDL via both the LDLR and LRP1, as this Apo is their main ligand[100]. Nonetheless, FH is marked by an increased retention time of LDL in the circulation, and thus, a higher concentration of cholesterol in the plasma. FH patients display an increased risk of pre-mature development of cardiovascular diseases (*e.g.* as a result of enhanced atherosclerosis)[98]. In addition, FH patients often present cholesterol deposits (xanthomas) in tendons, cornea, and in various skin sites. Interestingly, the composition of the xanthomas is similar to that described for atherosclerotic plaques in these patients[101].

Accumulation of HDL particles, namely hyperalphalipoproteinemia, can also cause hypercholesterolemia. Among others, mutations in cholesteryl ester transfer protein (CETP) and SR-BI have been identified as underlying causes of hyperalphalipoproteinemia[102–105]. Absence of CETP limits the transfer of CE from

HDL to ApoB-containing lipoproteins, hence, increasing the plasma fraction of HDL-cholesterol[106,107]. Loss of functionality or absence of SR-BI impairs the clearance of plasma HDL leading to a rise in the HDL-cholesterol fraction mainly carried by larger and abnormal HDL particles[104,108,109]. Although HDL is involved in reversed cholesterol transport, higher levels of HDL are not always associated with a reduced risk of cardiovascular diseases[86,110,111]. In addition, accumulation of HDL particles has been described to impact platelet function and steroidogenesis, among others[112,113].

As illustrated in the previous paragraphs, cardiovascular diseases are highly associated with hypercholesterolemia. The epidemiology of this disease can be related to genetic predisposition (as reported for FH patients) but other factors such as age, gender, hypertension, diabetes, obesity, and lifestyle may be contributors to the onset and development of this disease. Interestingly, the skin and nails of individuals with cardiovascular problems can be the first sites to show warning signs for heart conditions[101,114,115]. These individuals may, amongst others, develop yellow deposits under the skin, skin coloring (blue/purple net pattern), and non-itchy rashes.

ATHEROSCLEROSIS

Atherosclerosis is marked by the accumulation of cholesterol in the wall of medium-sized and large arteries leading to a chronic narrowing and hardening disease in these vessels (Figure 5a)[116,117]. This process initiates at early age and can remain asymptomatic through a lifetime or culminate in complications such as myocardial infarction.

According to the response-to-injury hypothesis, the development of atherosclerosis starts with endothelial dysfunction and activation, characterized by enhanced expression of adhesion molecules. LDL can pass the endothelial layer of the arterial wall by passive diffusion or through active transcytosis. Once in the sub-endothelial space, the LDL particles are trapped and undergo extensive modifications (lipolysis, oxidation)[116]. The buildup of oxidized LDL (oxLDL) in the intima of the arterial wall activates the endothelial cells to enhance the production of adhesion molecules and to secrete cytokines and growth factors. Interaction with adhesion molecules leads to an increase in monocyte infiltration from the blood stream into the arterial wall[117]. In the arterial wall, monocytes differentiate into macrophages and phagocyte oxLDL becoming lipid-rich foam cells with reduced mobility and insufficient cholesterol efflux capacity (Figure 5b)[117].

The development of the atherosclerotic plaque progresses as a local chronic inflammatory reaction with further recruitment of monocytes, mast cells, and T-cells[117–119]. Eventually, the overgrown lipid-laden foam cells die releasing their debris and lipid content into the plaque, which in turn aggravate the local inflammatory

response. At this late stage, the core of the atherosclerotic plaque consists of cellular debris, infiltrated immune cells and cholesterol, and is covered by a collagen-rich fibrous cap produced by smooth muscle cells[120]. The thickness of this cap correlates with the stability of the plaque and can ultimately hinder plaque rupture; hence, reducing the likelihood of a thrombotic event[120].

Reducing risk factors is pivotal in lowering atherosclerosis-related risks[117,121]. Thus, patients are advised to switch to a healthy diet, do physical exercise, stop tobacco abuse, and control hypertension and diabetes mellitus[117]. The main benefits of these treatments are to stabilize and to slow down the development of atherosclerotic plaques. Most treatments for atherosclerosis focus on lowering LDL cholesterol (gold standard prevention method)[121–123]. HMG-CoA reductase inhibitors (statins) are the main molecules employed to reduce plasma LDL levels. Interestingly, statins also impact the cholesterol synthesis in the skin and have been associated with increased risk of skin infection[124]. Other approaches to lower cholesterol levels include the use of cholesterol absorption inhibitors, PCSK9 inhibitors, and bile acid sequestrants[117,121]. Lowering TG levels is also important in atherosclerotic patients. For that purpose, statins, fibrates and n-3 fatty acids are the most common therapies[125–127]. As HDL is a key lipoprotein in the reverse cholesterol transport, increasing HDL has also been investigated as a possible therapeutic approach, mostly with unsatisfactory results[128]. CETP inhibitors and ApoA-I mimetics have also been explored as intervention therapies, although late development of these compounds have been complicated when translating to the clinic, with some CETP inhibitors failing at phase III trials[129,130]. As the efficacy of these interventions can vary between individuals and residual risk of coronary event remains over 50%, new therapeutic approaches are required[131–134]. In view of the pivotal role of macrophages in of atherosclerosis, therapies that can reduce local lipid content and inhibit inflammation remain interesting in the treatment of this pathophysiology[135].

LIVER X RECEPTOR (LXR)

The liver X receptor (LXR) is a nuclear transcription factor that functions as an intracellular cholesterol sensor and a suppressor of inflammatory genes[136–138]. Increased intracellular (oxidized) cholesterol levels result in activation of LXR followed by induction of cholesterol efflux pathways by upregulation of ABCA1 and ABCG1[139,140]. In addition, LXR activation impacts cellular fatty acid metabolism by, among others, regulating the expression of genes involved in fatty acid synthesis[136,141]. LXR also has a role in regulation of inflammation by, for instance, repressing the expression of tumor necrosis factor alpha, cyclooxygenase 2, nitric oxide synthase, and matrix metalloprotease[137]. Two isoforms of LXR have been identified; LXRα and LXRβ. LXRα is mostly expressed in the liver, intestines, spleen, and adipose tissue, while LXRβ is ubiquitously expressed[142]. A group of small molecules defined

as synthetic LXR agonists (*e.g.* TO901317 and GW3965) has been described to activate LXR and its downstream targets involved in the regulation of lipid and inflammation pathways[143–145].

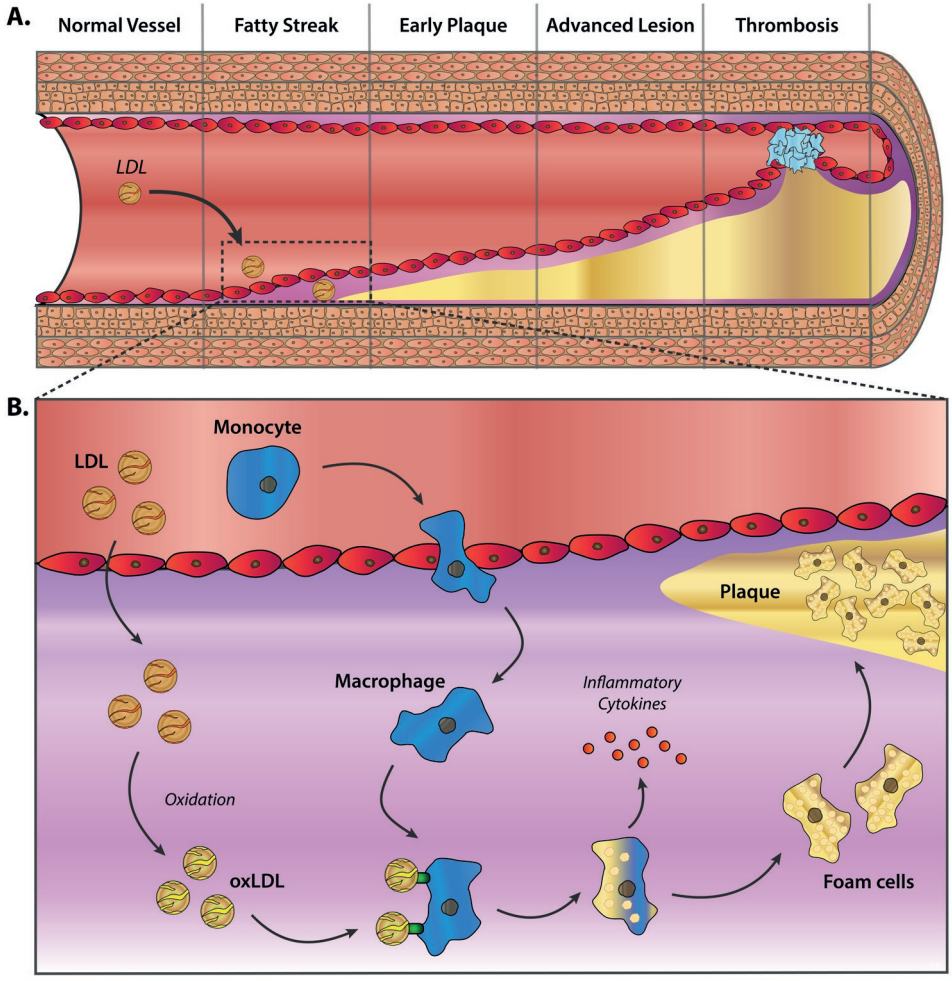

Figure 5. The pathogenesis of atherosclerosis. (A) The stages of atherosclerotic plaque development; from a healthy artery to an atherosclerotic artery with an advanced lesion and, in extreme cases, a thrombotic event. (B) The pivotal role of macrophages in pathogenesis of atherosclerosis. LDL particles can penetrate the intima of the arterial wall where it can undergo modifications (*e.g.* oxidation). Monocytes that penetrate the intima differentiate into macrophages. The oxidized LDL particles can be cleared by the macrophages via interaction with scavenger receptors expressed on the surface of these cells. Macrophages release inflammatory cytokines to recruit more monocytes and other immune cells to the site. The intracellular accumulation of lipids in the macrophages leads to the formation of lipid-rich cells (foam cells), a hallmark in the pathogenesis of atherosclerosis. LDL - low-density lipoprotein; oxLDL - oxidized low-density lipoprotein.

LXR has been extensively investigated as a potential therapeutic target in atherosclerosis as the deletion of LXR in mice is followed by a remarkable increase in susceptibility to atherosclerotic lesion development[143,146–148]. Activation of LXR by a synthetic agonist stimulates cholesterol efflux from foam cells in the arterial wall by upregulation of ABCA1 and ABCG1 expression[146,149,150]. However, severe undesired effects have been reported related to the administration of synthetic LXR agonists as free drug with remarkable impact on hepatic lipid metabolism[147,151]. Hence, various studies focus on the encapsulation of LXR agonist into (targeting) particles to increase the delivery to the atherosclerotic lesion while reducing unwanted effects[152,153].

THESIS AIM AND OUTLINE

The research reported in this thesis focuses on the impact of an imbalanced plasma cholesterol metabolism on skin lipid homeostasis (Figure 6). As patients with cardiovascular diseases are known to develop dermatological problems/signs, we hypothesized that the skin may have its own lipid profile impacted by one of the most important risk factors for atherosclerosis, namely increased cholesterol levels.

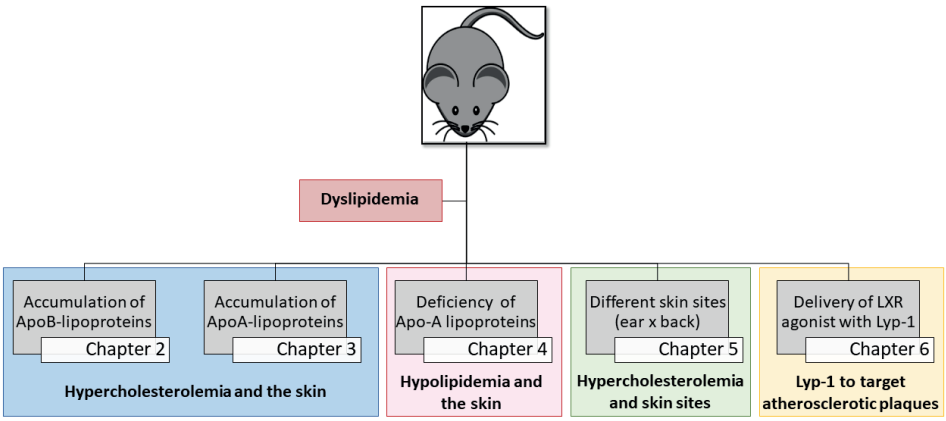

Figure 6. Research chapters presented in this thesis. Chapters 2-5 of this thesis focus on the impact of various dyslipidemic profiles on the skin lipid composition, organization and barrier function. Chapters 6 reports the use of a cyclic peptide (Lyp-1) to deliver LXR-loaded liposomes to atherosclerotic lesion macrophages to reduce hypercholesterolemia associated cardiovascular risk.

In our studies, young adult dyslipidemic mouse models not challenged with lipid rich-diets were used to investigate our hypothesis. In **Chapter 2** we show the impact of mild- and severe hypercholesterolemia associated with increased plasma levels of ApoB-containing lipoproteins (VLDL; LDL) on the skin lipid composition and barrier function of *LDLR*$^{-/-}$ and *APOE*$^{-/-}$ mice. In **Chapter 3** we report the effects of hypercholesterolemia

driven by the accumulation of ApoA-containing lipoproteins (HDL) on the skin lipid profile and lipid barier function in *SR-BI*$^{-/-}$ mice. In a new approach, in **Chapter 4**, we evaluate the changes in the skin lipid homeostasis as a result of the disrupted metabolism of ApoA-containing lipoproteins (HDL) in the hypolipidemic profile of *APOAI*$^{-/-}$ mice. In **Chapter 5**, we use both wild-type and *APOE*$^{-/-}$ mice to investigate the epidermal lipid profile of two commonly skin sites used in research as well as their responses to altered plasma lipid levels.

Hypercholesterolemia is highly associated with the risk of developing cardiovascular diseases. Although effective, nearly 65-70% of the cardiovascular events cannot be prevented with the current therapeutic strategies. Therefore, new strategies are necessary. Specific activation of LXR in atherosclerotic plaques offers the opportunity to lower the residual cardiovascular risk by modulating lesion lipid content and inflammation. Thus, in **Chapter 6** we explore a new peptide-targeting approach to deliver liposomes carrying an LXR agonist to foam cells as a treatment for atherosclerosis in *LDLR*$^{-/-}$ mice. Finally, in **Chapter 7** we present a summary of the findings described in this thesis and discuss the conclusions and implications of this research to the field and for patients.

REFERENCES

1. Elias, P. M. Stratum corneum defensive functions: An integrated view. J. Invest. Dermatol. 125, 183–200 (2005).

2. Kabashima, K., Honda, T., Ginhoux, F. & Egawa, G. The immunological anatomy of the skin. Nat. Rev. Immunol. 19, 19–30 (2019).

3. Ho, A. W. & Kupper, T. S. T cells and the skin: from protective immunity to inflammatory skin disorders. Nat. Rev. Immunol. 19, 490–502 (2019).

4. Pasparakis, M., Haase, I. & Nestle, F. O. Mechanisms regulating skin immunity and inflammation. Nat. Rev. Immunol. 14, 289–301 (2014).

5. Wong, R., Geyer, S., Weninger, W., Guimberteau, J.-C. & Wong, J. K. The dynamic anatomy and patterning of skin. Exp. Dermatol. 25, 92–98 (2016).

6. Driskell, R. R., Jahoda, C. A. B., Chuong, C.-M., Watt, F. M. & Horsley, V. Defining dermal adipose tissue. Exp. Dermatol. 23, 629–631 (2014).

7. Korosec, A. et al. Lineage Identity and Location within the Dermis Determine the Function of Papillary and Reticular Fibroblasts in Human Skin. J. Invest. Dermatol. 139, 342–351 (2019).

8. Kielty, C. M. & Shuttleworth, C. A. Microfibrillar elements of the dermal matrix. Microsc. Res. Tech. 38, 413–427 (1997).

9. Ludovici, M. et al. Influence of the sebaceous gland density on the stratum corneum lipidome. Sci. Rep. 8, 11500 (2018).

10. Huggenberger, R. et al. An important role of lymphatic vessel activation in limiting acute inflammation. Blood 117, 4667–4678 (2011).

11. Liu, F., Smith, J., Zhang, Z., Cole, R. & Herron, B. J. Genetic heterogeneity of skin microvasculature. Dev. Biol. 340, 480–489 (2010).

12. Mangelsdorf, S., Vergou, T., Sterry, W., Lademann, J. & Patzelt, A. Comparative study of hair follicle morphology in eight mammalian species and humans. Ski. Res. Technol. 20, 147–154 (2014).

13. Lippens, S., Denecker, G., Ovaere, P., Vandenabeele, P. & Declercq, W. Death penalty for keratinocytes: apoptosis versus cornification. Cell Death Differ. 12, 1497–1508 (2005).

14. Gudjonsson, J. E., Johnston, A., Dyson, M., Valdimarsson, H. & Elder, J. T. Mouse Models of Psoriasis. J. Invest. Dermatol. 127, 1292–1308 (2007).

15. Todo, H. Transdermal permeation of drugs in various animal species. Pharmaceutics 9, 1–11 (2017).

16. Houben, E., De Paepe, K. & Rogiers, V. A Keratinocyte's Course of Life. Skin Pharmacol. Physiol. 20, 122–132 (2007).

17. Eckhart, L., Lippens, S., Tschachler, E. & Declercq, W. Cell death by cornification. Biochim. Biophys. Acta - Mol. Cell Res. 1833, 3471–3480 (2013).

18. Rassner, U., Feingold, K. R., Crumrine, D. A. & Elias, P. M. Coordinate assembly of lipids and enzyme proteins into epidermal lamellar bodies. Tissue Cell 31, 489–498 (1999).

19. Feingold, K. R. & Elias, P. M. Role of lipids in the formation and maintenance of the cutaneous permeability barrier. Biochim. Biophys. Acta - Mol. Cell Biol. Lipids 1841, 280–294 (2014).

20. Proksch, E., Brandner, J. M. & Jensen, J.-M. The skin: an indispensable barrier. Exp. Dermatol. 17, 1063–1072 (2008).

21. Feingold, K. R. The outer frontier: the importance of lipid metabolism in the skin: Fig. 1. J. Lipid Res. 50, S417–S422 (2009).

22. Lindwall, G. et al. Heavy Water Labeling of Keratin as a Non-Invasive Biomarker of Skin Turnover In Vivo in Rodents and Humans. J. Invest. Dermatol. 126, 841–848 (2006).

23. Wei, J. C. J. et al. Allometric scaling of skin thickness, elasticity, viscoelasticity to mass for micro-medical device translation: from mice, rats, rabbits, pigs to humans. Sci. Rep. 7, 15885 (2017).

24. Bouwstra, J. A., Gooris, G. S., van der Spek, J. A. & Bras, W. Structural Investigations of Human Stratum Corneum by Small-Angle X-Ray Scattering. J. Invest. Dermatol. 97, 1005–1012 (1991).

25. Schreiner, V. et al. Barrier Characteristics of Different Human Skin Types Investigated with X-Ray Diffraction, Lipid Analysis, and Electron Microscopy Imaging. J. Invest. Dermatol. 114, 654–660 (2000).

26. Groen, D., Poole, D. S., Gooris, G. S. & Bouwstra, J. A. Is an orthorhombic lateral packing and a proper lamellar organization important for the skin barrier function? Biochim. Biophys. Acta - Biomembr. 1808, 1529–1537 (2011).

27. Smeden, J. Van et al. Intercellular Skin Barrier Lipid Composition and Organization in Netherton Syndrome Patients. J. Invest. Dermatol. 134, 1238–1245 (2014).

28. Boncheva, M., Damien, F. & Normand, V. Molecular organization of the lipid matrix in intact Stratum corneum using ATR-FTIR spectroscopy. Biochim. Biophys. Acta - Biomembr. 1778, 1344–1355 (2008).

29. Bouwstra, J., Gooris, G. & Ponec, M. The lipid organisation of the skin barrier: liquid and crystalline domains coexist in lamellar phases. J. Biol. Phys. 28, 211–23 (2002).

30. White, S. H., Mirejovsky, D. & King, G. I. Structure of lamellar lipid domains and corneocyte envelopes of murine stratum corneum. An x-ray diffraction study. Biochemistry 27, 3725–3732 (1988).

31. Martins Cardoso, R. et al. Hypercholesterolemia in young adult APOE −/− mice alters epidermal lipid composition and impairs barrier function. Biochim. Biophys. Acta - Mol. Cell Biol. Lipids 1864, 976–984 (2019).

32. Martins Cardoso, R. et al. Hyperalphalipoproteinemic scavenger receptor BI knockout mice exhibit a disrupted epidermal lipid barrier. Biochim. Biophys. Acta - Mol. Cell Biol. Lipids 1865, 158592 (2020).

33. Janssens, M. et al. Increase in short-chain ceramides correlates with an altered lipid organization and decreased barrier function in atopic eczema patients. J. Lipid Res. 53, 2755–2766 (2012).

34. Thakoersing, V. S. et al. Modulation of stratum corneum lipid composition and organization of human skin equivalents by specific medium supplements. Exp. Dermatol. 24, 669–674 (2015).

35. van Smeden, J. et al. The importance of free fatty acid chain length for the skin barrier function in atopic eczema patients. Exp. Dermatol. 23, 45–52 (2014).

36. Ponec, M., Weerheim, A., Lankhorst, P. & Wertz, P. New acylceramide in native and reconstructed epidermis. J. Invest. Dermatol. 120, 581–588 (2003).

37. Pappas, A., Johnsen, S., Liu, J.-C. & Eisinger, M. Sebum analysis of individuals with and without acne. Dermatoendocrinol. 1, 157–161 (2009).

38. Maier, H. et al. Normal Fur Development and Sebum Production Depends on Fatty Acid 2-Hydroxylase Expression in Sebaceous Glands. J. Biol. Chem. 286, 25922–25934 (2011).

39. Feldman, A. et al. Blimp1+ cells generate functional mouse sebaceous gland organoids in vitro. Nat. Commun. 10, 2348 (2019).

40. Weerheim, A. & Ponec, M. Determination of stratum corneum lipid profile by tape stripping in combination with high-performance thin-layer chromatography. Arch. Dermatol. Res. 293, 191–199 (2001).

41. Kihara, A. Synthesis and degradation pathways, functions, and pathology of ceramides and epidermal acylceramides. Prog. Lipid Res. 63, 50–69 (2016).

42. Sjövall, P. et al. Imaging the distribution of skin lipids and topically applied compounds in human skin using mass spectrometry. Sci. Rep. 8, 1–14 (2018).

43. Feingold, K. R. & Jiang, Y. J. The mechanisms by which lipids coordinately regulate the formation of the protein and lipid domains of the stratum corneum: Role of fatty acids, oxysterols, cholesterol sulfate and ceramides as signaling molecules. Dermatoendocrinol. 3, 113–118 (2011).

44. Elias, P. M., Williams, M. L., Choi, E. H. & Feingold, K. R. Role of cholesterol sulfate in epidermal structure and function: Lessons from X-linked ichthyosis. Biochim. Biophys. Acta - Mol. Cell Biol. Lipids 1841, 353–361 (2014).

45. Motta, S. et al. Ceramide composition of the psoriatic scale. BBA - Mol. Basis Dis. 1182, 147–151 (1993).

46. Rabionet, M. et al. 1-O-acylceramides are natural components of human and mouse epidermis. J. Lipid Res. 54, 3312–3321 (2013).

47. t'Kindt, R. et al. Profiling and Characterizing Skin Ceramides Using Reversed-Phase Liquid Chromatography–Quadrupole Time-of-Flight Mass Spectrometry. Anal. Chem. 84, 403–411 (2012).

48. Masukawa, Y. et al. Characterization of overall ceramide species in human stratum corneum. J. Lipid Res. 49, 1466–1476 (2008).

49. Helder, R. W. J. et al. The effects of LXR agonist T0901317 and LXR antagonist GSK2033 on morphogenesis and lipid properties in full thickness skin models. Biochim. Biophys. Acta - Mol. Cell Biol. Lipids 1865, 158546 (2020).

50. Norlén, L., Nicander, I., Lundsjö, A., Cronholm, T. & Forslind, B. A new HPLC-based method for the quantitative analysis of inner stratum corneum lipids with special reference to the free fatty acid fraction. Arch. Dermatol. Res. 290, 508–516 (1998).

51. van Smeden, J. et al. Combined LC/MS-platform for analysis of all major stratum corneum lipids, and the profiling of skin substitutes. Biochim. Biophys. Acta - Mol. Cell Biol. Lipids 1841, 70–79 (2014).

52. Martins Cardoso, R., Absalah, S., Van Eck, M. & Bouwstra, J. A. Barrier lipid composition and response to plasma lipids: A direct comparison of mouse dorsal back and ear skin. Exp. Dermatol. 29, 548–555 (2020).

53. Breiden, B. & Sandhoff, K. The role of sphingolipid metabolism in cutaneous permeabilitybarrier formation. Biochim. Biophys. Acta - Mol. Cell Biol. Lipids 1841, 441–452 (2014).

54. Siefken, W., Höppner, H. & Harris, I. R. Regulation of cholesterol synthesis by oleic and palmitic acid in keratinocytes. Exp. Dermatol. 9, 138–145 (2000).

55. Feingold, K. R. et al. Cholesterol synthesis is required for cutaneous barrier function in mice. J. Clin. Invest. 86, 1738–1745 (1990).

56. Kondo, N. et al. Identification of the phytosphingosine metabolic pathway leading to odd-numbered fatty acids. Nat. Commun. 5, 5338 (2014).

57. Mizutani, Y. et al. Cooperative Synthesis of Ultra Long-Chain Fatty Acid and Ceramide during

Keratinocyte Differentiation. PLoS One 8, 2–9 (2013).

58. Hirabayashi, T., Murakami, M. & Kihara, A. The role of PNPLA1 in ω-O-acylceramide synthesis and skin barrier function. Biochim. Biophys. Acta - Mol. Cell Biol. Lipids 1864, 869–879 (2019).

59. van Smeden, J. et al. In situ visualization of glucocerebrosidase in human skin tissue: zymography versus activity-based probe labeling. J. Lipid Res. 58, 2299–2309 (2017).

60. Schmuth, M. et al. Permeability Barrier Disorder in Niemann–Pick Disease: Sphingomyelin–Ceramide Processing Required for Normal Barrier Homeostasis. J. Invest. Dermatol. 115, 459–466 (2000).

61. Jakobsson, A., Westerberg, R. & Jacobsson, A. Fatty acid elongases in mammals: Their regulation and roles in metabolism. Prog. Lipid Res. 45, 237–249 (2006).

62. Guillou, H., Zadravec, D., Martin, P. G. P. & Jacobsson, A. The key roles of elongases and desaturases in mammalian fatty acid metabolism: Insights from transgenic mice. Prog. Lipid Res. 49, 186–199 (2010).

63. Paton, C. M. & Ntambi, J. M. Biochemical and physiological function of stearoyl-CoA desaturase. Am. J. Physiol. - Endocrinol. Metab. 297, 28–37 (2009).

64. Sampath, H. & Ntambi, J. M. Role of stearoyl-CoA desaturase-1 in skin integrity and whole body energy balance. J. Biol. Chem. 289, 2482–2488 (2014).

65. Sassa, T. et al. Impaired Epidermal Permeability Barrier in Mice Lacking Elovl1, the Gene Responsible for Very-Long-Chain Fatty Acid Production. Mol. Cell. Biol. 33, 2787–2796 (2013).

66. Haruta-Ono, Y. et al. Orally administered sphingomyelin in bovine milk is incorporated into skin sphingolipids and is involved in the water-holding capacity of hairless mice. J. Dermatol. Sci. 68, 56–62 (2012).

67. Bhattacharyya, A. K., Connor, W. E. & Spector, A. A. Excretion of sterols from the skin of normal and hypercholesterolemic humans. Implications for sterol balance studies. J. Clin. Invest. 51, 2060–70 (1972).

68. Khnykin, D., Miner, J. H. & Jahnsen, F. Role of fatty acid transporters in epidermis: Implications for health and disease. Dermatoendocrinol. 3, 53–61 (2011).

69. Hansen, H. S. & Jensen, B. Essential function of linoleic acid esterified in acylglucosylceramide and acylceramide in maintaining the epidermal water permeability barrier. Evidence from feeding studies with oleate, linoleate, arachidonate, columbinate and α-linolenate. Biochim. Biophys. Acta - Lipids Lipid Metab. 834, 357–363 (1985).

70. Feingold, K. R. Thematic review series: Skin Lipids . The role of epidermal lipids in cutaneous permeability barrier homeostasis: Fig. 1. J. Lipid Res. 48, 2531–2546 (2007).

71. Bibel, D. J. et al. Antimicrobial Activity of Stratum Corneum Lipids from Normal and Essential Fatty Acid-Deficient Mice. J. Invest. Dermatol. 92, 632–638 (1989).

72. Ponec, M. et al. LDL Receptors in Keratinocytes. J. Invest. Dermatol. 98, S50–S56 (1992).

73. Tomonaga, N., Manabe, Y., Aida, K. & Sugawara, T. Dietary ceramide 2-aminoethylphosphonate, a marine sphingophosphonolipid, improves skin barrier function in hairless mice. Sci. Rep. 10, 13891 (2020).

74. Shimoda, H. et al. Changes in Ceramides and Glucosylceramides in Mouse Skin and Human Epidermal Equivalents by Rice-Derived Glucosylceramide. J. Med. Food 15, 1064–1072 (2012).

75. Abd El-Latif, M. I. A., Murota, H., Terao, M. & Katayama, I. Effects of a 3-hydroxy-3-methylglutaryl coenzyme A reductase inhibitor and low-density lipoprotein on proliferation and migration of keratinocytes. Br. J. Dermatol. 128–137 (2010). doi:10.1111/j.1365-2133.2010.09694.x

76. Lin, M.-H. & Khnykin, D. Fatty acid transporters in skin development, function and disease. Biochim.

Biophys. Acta 1841, 362–8 (2014).

77. Mommaas, M., Tada, J. & Ponec, M. Distribution of low-density lipoprotein receptors and apolipoprotein B on normal and on reconstructed human epidermis. J. Dermatol. Sci. 2, 97–105 (1991).

78. Tsuruoka, H. et al. Scavenger receptor class B type I is expressed in cultured keratinocytes and epidermis. Regulation in response to changes in cholesterol homeostasis and barrier requirements. J. Biol. Chem. 277, 2916–2922 (2002).

79. Meeusen, J. W. et al. Plasma Ceramides. Arterioscler. Thromb. Vasc. Biol. 38, 1933–1939 (2018).

80. M.J. van Greevenbroek, M. & W.A. de Bruin, T. Chylomicron synthesis by intestinal cells in vitro and in vivo. Atherosclerosis 141, S9–S16 (1998).

81. Mansbach, C. M. & Siddiqi, S. A. The Biogenesis of Chylomicrons. Annu. Rev. Physiol. 72, 315–333 (2010).

82. Tennyson, G. E., Sabatos, C. A., Higuchi, K., Meglin, N. & Brewer, H. B. Expression of apolipoprotein B mRNAs encoding higher- and lower-molecular weight isoproteins in rat liver and intestine. Proc. Natl. Acad. Sci. 86, 500–504 (1989).

83. Nakamuta, M. et al. Complete Phenotypic Characterization of apobec-1 Knockout Mice with a Wild-type Genetic Background and a Human Apolipoprotein B Transgenic Background, and Restoration of Apolipoprotein B mRNA Editing by Somatic Gene Transfer of Apobec-1. J. Biol. Chem. 271, 25981–25988 (1996).

84. Tiwari, S. & Siddiqi, S. A. Intracellular Trafficking and Secretion of VLDL. Arterioscler. Thromb. Vasc. Biol. 32, 1079–1086 (2012).

85. Wolska, A. et al. Apolipoprotein C-II: New findings related to genetics, biochemistry, and role in triglyceride metabolism. Atherosclerosis 267, 49–60 (2017).

86. Rosenson, R. S. et al. Dysfunctional HDL and atherosclerotic cardiovascular disease. Nat. Rev. Cardiol. 13, 48–60 (2016).

87. Tall, A. R. & Yvan-Charvet, L. Cholesterol, inflammation and innate immunity. Nat. Rev. Immunol. 15, 104–116 (2015).

88. Huang, Y. et al. An abundant dysfunctional apolipoprotein A1 in human atheroma. Nat. Med. 20, 193–203 (2014).

89. Vaughan, A. M. & Oram, J. F. ABCA1 and ABCG1 or ABCG4 act sequentially to remove cellular cholesterol and generate cholesterol-rich HDL. J. Lipid Res. 47, 2433–2443 (2006).

90. Nakamura, Y. et al. Molecular Mechanism of Reverse Cholesterol Transport: Reaction of Pre-β-Migrating High-Density Lipoprotein with Plasma Lecithin/Cholesterol Acyltransferase †. Biochemistry 43, 14811–14820 (2004).

91. Acton, S. et al. Identification of Scavenger Receptor SR-BI as a High Density Lipoprotein Receptor. Science (80-.). 271, 518–520 (1996).

92. Out, R. et al. Scavenger receptor class B type I is solely responsible for the selective uptake of cholesteryl esters from HDL by the liver and the adrenals in mice. J. Lipid Res. 45, 2088–2095 (2004).

93. Gordon, S. M. et al. A comparison of the mouse and human lipoproteome: suitability of the mouse model for studies of human lipoproteins. J. Proteome Res. 14, 2686–95 (2015).

94. Kaabia, Z. et al. Plasma lipidomic analysis reveals strong similarities between lipid fingerprints in human, hamster and mouse compared to other animal species. Sci. Rep. 8, 15893 (2018).

95. Feingold, K. R. & Grunfeld, C. Introduction to Lipids and Lipoproteins. Endotext (2000).

96. Hegele, R. A. Plasma lipoproteins: genetic influences and clinical implications. Nat. Rev. Genet. 10, 109–121 (2009).

97. Rashidi, O. M., H.Nazar, F. A., Alama, M. N. & Awan, Z. A. Interpreting the Mechanism of APOE (p.Leu167del) Mutation in the Incidence of Familial Hypercholesterolemia; An In-silico Approach. Open Cardiovasc. Med. J. 11, 84–93 (2017).

98. Defesche, J. C. et al. Familial hypercholesterolaemia. Nat. Rev. Dis. Prim. 3, 17093 (2017).

99. Ellis, K. L., Hooper, A. J., Burnett, J. R. & Watts, G. F. Progress in the care of common inherited atherogenic disorders of apolipoprotein B metabolism. Nat. Rev. Endocrinol. 12, 467–484 (2016).

100. Getz, G. S. & Reardon, C. A. Do the Apoe −/− and Ldlr −/− Mice Yield the Same Insight on Atherogenesis? Arterioscler. Thromb. Vasc. Biol. 36, 1734–1741 (2016).

101. Sugiyama, N. et al. Immunohistochemical distribution of lipoprotein epitopes in xanthomata from patients with familial hypercholesterolemia. Am. J. Pathol. 141, 99–106 (1992).

102. Hirano, K. et al. Disease-associated marked hyperalphalipoproteinemia. Mol. Genet. Metab. Reports 1, 264–268 (2014).

103. Helgadottir, A. et al. Rare SCARB1 mutations associate with high-density lipoprotein cholesterol but not with coronary artery disease. Eur. Heart J. 39, 2172–2178 (2018).

104. Brunham, L. R. et al. Novel mutations in scavenger receptor BI associated with high HDL cholesterol in humans. Clin. Genet. 79, 575–581 (2011).

105. Ljunggren, S. A. et al. Lipoprotein profiles in human heterozygote carriers of a functional mutation P297S in scavenger receptor class B1. Biochim. Biophys. Acta - Mol. Cell Biol. Lipids 1851, 1587–1595 (2015).

106. Calabresi, L. et al. A novel homozygous mutation in CETP gene as a cause of CETP deficiency in a caucasian kindred. Atherosclerosis 205, 506–511 (2009).

107. de Grooth, G. J. et al. A review of CETP and its relation to atherosclerosis. J. Lipid Res. 45, 1967–1974 (2004).

108. Van Eck, M. et al. Differential effects of scavenger receptor BI deficiency on lipid metabolism in cells of the arterial wall and in the liver. J. Biol. Chem. 278, 23699–23705 (2003).

109. Vergeer, M. et al. Genetic Variant of the Scavenger Receptor BI in Humans. N. Engl. J. Med. 364, 136–145 (2011).

110. Vergeer, M., Holleboom, A. G., Kastelein, J. J. P. & Kuivenhoven, J. A. The HDL hypothesis: does high-density lipoprotein protect from atherosclerosis?: Fig. 1. J. Lipid Res. 51, 2058–2073 (2010).

111. Barter, P. & Genest, J. HDL cholesterol and ASCVD risk stratification: A debate. Atherosclerosis 283, 7–12 (2019).

112. van der Stoep, M., Korporaal, S. J. A. & Van Eck, M. High-density lipoprotein as a modulator of platelet and coagulation responses. Cardiovasc. Res. 103, 362–371 (2014).

113. Bochem, A. E. et al. High density lipoprotein as a source of cholesterol for adrenal steroidogenesis: a study in individuals with low plasma HDL-C. J. Lipid Res. 54, 1698–1704 (2013).

114. Dwivedi, S. Cutaneous markers of coronary artery disease. World J. Cardiol. 2, 262 (2010).

115. Shenoy, C., Shenoy, M. & Rao, G. Dyslipidemia in dermatological disorders. N. Am. J. Med. Sci. 7, 421

(2015).

116. Pirillo, A., Norata, G. D. & Catapano, A. L. LOX-1, OxLDL, and Atherosclerosis. Mediators Inflamm. 2013, 1–12 (2013).

117. Libby, P. et al. Atherosclerosis. Nat. Rev. Dis. Prim. 5, 56 (2019).

118. Wolf, D. & Ley, K. Immunity and Inflammation in Atherosclerosis. Circ. Res. 124, 315–327 (2019).

119. Hansson, G. K. & Hermansson, A. The immune system in atherosclerosis. Nat. Immunol. 12, 204–212 (2011).

120. Chen, Y.-C., Huang, A. L., Kyaw, T. S., Bobik, A. & Peter, K. Atherosclerotic Plaque Rupture. Arterioscler. Thromb. Vasc. Biol. 36, (2016).

121. Glass, C. K. & Witztum, J. L. Atherosclerosis. Cell 104, 503–516 (2001).

122. Whayne, T. Atherosclerosis: Current Status of Prevention and Treatment. Int. J. Angiol. 20, 213–222 (2011).

123. Bergheanu, S. C., Bodde, M. C. & Jukema, J. W. Pathophysiology and treatment of atherosclerosis. Netherlands Hear. J. 25, 231–242 (2017).

124. Ko, H. H. T., Lareu, R. R., Dix, B. R., Hughes, J. D. & Parsons, R. W. A sequence symmetry analysis of the interrelationships between statins, diabetes and skin infections. Br. J. Clin. Pharmacol. 85, 2559–2567 (2019).

125. Kim, N. H. & Kim, S. G. Fibrates Revisited: Potential Role in Cardiovascular Risk Reduction. Diabetes Metab. J. 44, 213 (2020).

126. Sahebkar, A., Simental-Mendía, L. E., Watts, G. F., Serban, M.-C. & Banach, M. Comparison of the effects of fibrates versus statins on plasma lipoprotein(a) concentrations: a systematic review and meta-analysis of head-to-head randomized controlled trials. BMC Med. 15, 22 (2017).

127. Skulas-Ray, A. C. et al. Omega-3 Fatty Acids for the Management of Hypertriglyceridemia: A Science Advisory From the American Heart Association. Circulation 140, (2019).

128. Sirtori, C. R. et al. HDL therapy today: from atherosclerosis, to stent compatibility to heart failure. Ann. Med. 51, 345–359 (2019).

129. Tall, A. R. & Rader, D. J. Trials and Tribulations of CETP Inhibitors. Circ. Res. 122, 106–112 (2018).

130. Smith, J. D. Apolipoprotein A-I and its mimetics for the treatment of atherosclerosis. Curr. Opin. Investig. Drugs 11, 989–96 (2010).

131. Armitage, J. et al. Efficacy and safety of statin therapy in older people: a meta-analysis of individual participant data from 28 randomised controlled trials. Lancet 393, 407–415 (2019).

132. Libby, P. & Everett, B. M. Novel Antiatherosclerotic Therapies. Arterioscler. Thromb. Vasc. Biol. 39, 538–545 (2019).

133. Bäck, M. & Hansson, G. K. Anti-inflammatory therapies for atherosclerosis. Nat. Rev. Cardiol. 12, 199–211 (2015).

134. Adhyaru, B. B. & Jacobson, T. A. Safety and efficacy of statin therapy. Nat. Rev. Cardiol. 15, 757–769 (2018).

135. Magida, J. A. & Evans, R. M. Rational application of macrophage-specific LXR agonists avoids the pitfalls of SREBP-induced lipogenesis. Proc. Natl. Acad. Sci. 115, 5051–5053 (2018).

136. Wang, B. & Tontonoz, P. Liver X receptors in lipid signalling and membrane homeostasis. Nat. Rev. Endocrinol. 14, 452–463 (2018).

137. Im, S.-S. & Osborne, T. F. Liver X Receptors in Atherosclerosis and Inflammation. Circ. Res. 108, 996–1001 (2011).

138. Schulman, I. G. Liver X receptors link lipid metabolism and inflammation. FEBS Lett. 591, 2978–2991 (2017).

139. Beyea, M. M. et al. Selective Up-regulation of LXR-regulated Genes ABCA1 , ABCG1 , and APOE in Macrophages through Increased Endogenous Synthesis of 24(S),25-Epoxycholesterol. J. Biol. Chem. 282, 5207–5216 (2007).

140. Kennedy, M. A. et al. ABCG1 has a critical role in mediating cholesterol efflux to HDL and preventing cellular lipid accumulation. Cell Metab. 1, 121–131 (2005).

141. Ulven, S. M., Dalen, K. T., Gustafsson, J.-Å. & Nebb, H. I. LXR is crucial in lipid metabolism. Prostaglandins, Leukot. Essent. Fat. Acids 73, 59–63 (2005).

142. Wójcicka, G., Jamroz-Wiśniewska, A., Horoszewicz, K. & Bełtowski, J. Liver X receptors (LXRs). Part I: structure, function, regulation of activity, and role in lipid metabolism. Postepy Hig. Med. Dosw. (Online) 61, 736–59 (2007).

143. Lund, E. G., Menke, J. G. & Sparrow, C. P. Liver X Receptor Agonists as Potential Therapeutic Agents for Dyslipidemia and Atherosclerosis. Arterioscler. Thromb. Vasc. Biol. 23, 1169–1177 (2003).

144. Peng, D. et al. A novel potent synthetic steroidal liver X receptor agonist lowers plasma cholesterol and triglycerides and reduces atherosclerosis in LDLR −/− mice. (2011). doi:10.1111/j.1476-5381.2011.01202.x

145. Aravindhan, K. et al. Assessing the effects of LXR agonists on cellular cholesterol handling: a stable isotope tracer study. J. Lipid Res. 47, 1250–1260 (2006).

146. Verschuren, L., de Vries-van der Weij, J., Zadelaar, S., Kleemann, R. & Kooistra, T. LXR agonist suppresses atherosclerotic lesion growth and promotes lesion regression in apoE*3Leiden mice: time course and mechanisms. J. Lipid Res. 50, 301–311 (2009).

147. Zhang, Y. et al. Liver LXRα expression is crucial for whole body cholesterol homeostasis and reverse cholesterol transport in mice. J. Clin. Invest. 122, 1688–1699 (2012).

148. Bischoff, E. D. et al. Non-redundant roles for LXR and LXR in atherosclerosis susceptibility in low density lipoprotein receptor knockout mice. J. Lipid Res. 51, 900–906 (2010).

149. Joseph, S. B. et al. Synthetic LXR ligand inhibits the development of atherosclerosis in mice. Proc. Natl. Acad. Sci. 99, 7604–7609 (2002).

150. Kirchgessner, T. G. et al. Beneficial and Adverse Effects of an LXR Agonist on Human Lipid and Lipoprotein Metabolism and Circulating Neutrophils. Cell Metab. 24, 223–233 (2016).

151. Heckmann, B. L. et al. Liver X receptor α mediates hepatic triglyceride accumulation through upregulation of G0/G1 Switch Gene 2 expression. JCI Insight 2, (2017).

152. Yu, M. et al. Targeted Nanotherapeutics Encapsulating Liver X Receptor Agonist GW3965 Enhance Antiatherogenic Effects without Adverse Effects on Hepatic Lipid Metabolism in Ldlr −/− Mice. Adv. Healthc. Mater. 6, 1700313 (2017).

153. Zhang, X.-Q. et al. Nanoparticles Containing a Liver X Receptor Agonist Inhibit Inflammation and Atherosclerosis. Adv. Healthc. Mater. 4, 228–236 (2015).

Chapter 2

Hypercholesterolemia in young adult *APOE*$^{-/-}$ mice alters epidermal lipid composition and impairs barrier function

Biochimica et Biophysica Acta Molecular and Cell Biology of Lipids 1864(7): 976-984 (2019).

Renata Martins Cardoso[1], Eline Creemers[1], Samira Absalah[1], Gert S. Gooris[1], Menno Hoekstra[1], Miranda Van Eck[1*], Joke A. Bouwstra[1*]

[1]Division of BioTherapeutics, Leiden Academic Centre for Drug Research, Leiden University, Leiden, The Netherlands

*Both authors contributed equally

ABSTRACT

Long-term exposure to hypercholesterolemia induces the development of skin xanthoma's characterized by the accumulation of lipid-laden foam cells in humans and in mice. Early skin changes in response to hypercholesterolemia are however unknown. In this study, we investigated the skin lipid composition and associated barrier function in young adult low-density lipoprotein receptor knockout (*LDLR*$^{-/-}$) and apolipoprotein E knockout (*APOE*$^{-/-}$) mice, two commonly used hypercholesterolemic mouse models characterized by the accumulation of apolipoprotein B containing lipoproteins. No effects were observed on cholesterol content in the epidermis in *LDLR*$^{-/-}$ mice or in the more extremely hypercholesterolemic *APOE*$^{-/-}$ mice. Interestingly, the free fatty acids in the *APOE*$^{-/-}$ epidermis shifted towards shorter and unsaturated chains. Genes involved in the synthesis of cholesterol and fatty acids were downregulated in *APOE*$^{-/-}$ skin suggesting a compensation for the higher influx of plasma lipids, most probably as cholesteryl esters. Importantly, *in vivo* transepidermal water loss and permeability studies with murine lipid model membranes revealed that the lipid composition of the *APOE*$^{-/-}$ skin resulted in a reduced skin barrier function. In conclusion, severe hypercholesterolemia associated with increased apolipoprotein B containing lipoproteins affects the epidermal lipid composition and its protective barrier.

Keywords: *skin barrier lipids; apolipoprotein E knockout; low-density lipoprotein receptor knockout; free fatty acids; cholesteryl esters; LC/MS.*

1. INTRODUCTION

Patients suffering from familial hypercholesterolemia often present mutations in the low-density lipoprotein receptor (LDLR) or other proteins (*e.g.* apolipoprotein E - apoE) that result in increased circulating levels of low-density lipoprotein and a higher risk of developing cardiovascular diseases[1–3]. Interestingly, these patients are also reported to develop skin xanthoma's filled with cholesterol-laden macrophages[4,5]. Lipid-lowering therapy with statins is the main choice of treatment for hypercholesterolemic patients[1,4]. However, in some cases statin treatment is not sufficient to reverse the skin phenotypes[3,5].

Hypercholesterolemia has been extensively studied using LDLR knockout (*LDLR*$^{-/-}$) and APOE knockout (*APOE*$^{-/-}$) mice. Both LDLR and apoE play an essential role in the clearance of apolipoprotein B and apoE containing lipoproteins from the circulation by the liver[6,7]. In the absence of a functional LDLR, the clearance of apolipoprotein B and apoE containing lipoproteins is impaired leading to accumulation of these particles in the plasma. However, as apoE containing lipoproteins are also cleared by LDLR-related protein 1 (LRP1), *LDLR*$^{-/-}$ mice develop a mild hypercholesterolemia on a regular chow diet or severe hypercholesterolemia when fed a high fat/high cholesterol diet[6,7]. *APOE*$^{-/-}$ mice, on the other hand, develop a more severe hypercholesterolemic phenotype on chow diet as the lipoprotein clearance by both the LDLR and LRP1 are impaired[6,7].

Similar to hypercholesterolemic patients, xanthoma's have also been described in the skin of *LDLR*$^{-/-}$ mice and *APOE*$^{-/-}$ mice. On a low-fat diet the morphology of the skin of young adult *LDLR*$^{-/-}$ and *APOE*$^{-/-}$ mice is comparable to the wild-type (WT) control of similar age with no signs of inflammation or lipid deposits[8–11]. However, on a high fat/high cholesterol diet both *LDLR*$^{-/-}$ mice and *APOE*$^{-/-}$mice showed accumulation of fat droplets and inflammatory infiltrates in their skin[10–12]. Furthermore, aging of *APOE*$^{-/-}$ mice fed low-fat diet exhibited skin phenotypes characterized by skin thinning, hair follicle loss and premature greying of the hair accompanied by impaired hair regeneration, which appeared earlier than reported for WT controls[13,14]. Also, these age-related skin changes can be accelerated when *APOE*$^{-/-}$ mice received high fat/high cholesterol diet[13].

The skin naturally functions as a barrier protecting the body from excessive water and electrolyte loss and permeation of harmful agents and pathogens. This protective function is mostly performed by corneocytes and an extracellular lipid domain present in the outermost layer of the epidermis, the stratum corneum (SC)[15]. The SC lipid domain mainly comprises cholesterol, ceramides (CERs) and free fatty acids (FFAs), which

are primarily synthesized by keratinocytes during their differentiation process[16]. In addition to local lipid synthesis, keratinocytes express receptors involved in the uptake of lipids from plasma, (*e.g.* LDLR, scavenger receptor class B member I and cluster of differentiation 36) via which plasma lipids likely enter the skin and can be detected in the epidermis[17–19].

Despite the crucial role of lipids in the skin barrier, the early consequences of an impaired metabolism of apolipoprotein B and apoE containing lipoproteins to the skin lipid composition and barrier function are unknown. In this study we compared young adult *LDLR*$^{-/-}$ mice and *APOE*$^{-/-}$ mice with WT controls of the same age and genetic background to specifically analyze the effects of hypercholesterolemia on skin morphology, lipid composition and organization, and barrier functionality prior to the development of inflammatory phenotypes as described for high fat/high cholesterol diets and aging.

2. MATERIALS AND METHODS

2.1 Chemicals

Manufacture's details regarding the chemicals used in these studies are available in the online supplementary information.

2.2 Animals

16-18 weeks old female WT, homozygous *LDLR*$^{-/-}$ mice and homozygous *APOE*$^{-/-}$ mice (obtained from The Jackson laboratory and bred at the Gorlaeus laboratories) all on a C57BL/6 background were kept under standard laboratory conditions (20^{o}C and light cycle of 12h light/12h dark) with water and standard low fat chow diet ad libitum (Rat and Mouse No.3 breeding diet, Special Diets Services, United Kingdom) and not fasted prior sacrifice. All experiments were performed in accordance with National guidelines and approved by the Ethics Committee for Animals Experiments of Leiden University. The mice were anesthetized for retro-orbital bleeding (70 mg/kg body weight xylazine, 1.8 mg/kg body weight atropine, 350 mg/kg body weight ketamine) and shaving of the back skin followed by perfusion with phosphate buffered saline (PBS, pH 7.4 - 8.13 g/L NaCl, 2.87 g/L Na_2HPO_4, 0.2 g/L KH_2PO_4, 0.19 g/L KCl in milliQ water) at room temperature.

2.3 Plasma lipid analysis

Enzymatic colorimetric assays were used to measure non-fasted plasma levels of

cholesterol and triglycerides (Roche Diagnostics, Almere, Netherlands)[20]. All assays were performed according to manufacturer's instructions.

2.4 Skin morphology staining

Paraffin embedded skin sections (4-5 µm) were deparaffinized, rehydrated and stained with hematoxylin and eosin according to manufacturer's instructions or with toluidine blue. In short, toluidine blue stock solution (1% w/v in 70 % ethanol) was diluted 10 times in NaCl solution (1% w/v in demi-water). Skin sections were deparaffinized, rehydrated, stained for 2 min with toluidine blue working solution, and rinsed with demi-water. For both stainings slides were mounted in Entellan® and the sections were imaged with a Zeiss Axioplan 2 light microscope (Zeiss, Best, The Netherlands) and BH-2 polarized microscope (Olympus, Leiderdorp, The Netherlands).

2.5 Liquid chromatography-mass spectrometry (LC/MS)

After removing the hypodermis, skin samples were placed overnight (4°C) on a paper filter soaked with 0.3 % w/v trypsin solution in PBS (pH 7.4). Next day, the samples were incubated at for 1 hour at 37°C to isolate the epidermis. Next, the epidermis was rinsed once in 0.1% w/v trypsin inhibitor in PBS and twice in demi-water. The samples dried at room temperature and were stored under argon atmosphere for lipids extraction and FTIR measurements. Epidermal lipids were extracted as described by Boiten *et al.* (2016)[21] and the extracts were stored in chloroform:methanol (2:1; v/v) at 4°C under argon atmosphere for cholesterol, CER and FFA analyses.

Cholesterol and CER analysis

Lipid extracts were dried and reconstituted in heptane:chloroform:methanol (95:2.5:2.5; v/v/v) to a lipid concentration of 0.3 mg/mL. 5 µl of reconstituted lipid extracts were injected in an Acquity UPLC H-class system (Waters, Milford, MA, USA) connected to a triple-quadrupole XEVO TQ-S mass spectrometer (Waters, Milford, MA, USA). Separation occurred in a normal phase column (PVA-Sil column: 5 µm particle size, 100x2.1 mm i.d., YMC, Kyoto, Japan) at flow rate of 0.8 ml/min with a gradient solvent shift from 98% heptane and 2% heptane:isopropanol:ethanol (50:25:25; v/v/v) to 50% heptane and 50% heptane:isopropanol:ethanol (50:25:25; v/v/v) in 11 minutes (Supplementary Table S1). The mass spectrometer was coupled to atmospheric pressure chemical ionization chamber set to positive ion mode and the detector measured in full scans from 350-1200 amu. Deuterated CER[NS] (C24deuterated; C18protonated) was added to all samples as internal standard prior to injection into UPLC/MS. Software

Waters MassLynx 4.1 was used to determine the area under the curve (AUC) followed by internal standard correction for both cholesterol and CER analysis. Cholesterol AUC was further corrected for the response based on a calibration curve of cholesterol and the data was plotted as absolute amount of cholesterol (µg) per epidermis weight (mg). CER composition was provided as AUC corrected for the internal standard and was plotted as relative percentage of ceramide subclasses. CER subclasses were named as described previously[22] based on different acyl chains (non-hydroxy fatty acid [N]; α-hydroxy fatty acid [A]; esterified ω-hydroxy fatty acid [EO]) and on the sphingoid base (dihydrosphingosine, [dS]; sphingosine [S]; phytosphingosine [P]) (Supplementary Fig. S1).

FFA analysis

Lipid extracts were dried and reconstituted in isopropanol to a lipid concentration of 0.75 mg/mL. 2 µl of reconstituted lipid extracts were injected in the same UPLC-mass spectrometry system described in subsection "Cholesterol and CERs analysis". Deuterated FFA C18 and FFA C24 were added to all samples as internal standard. FFA separation in the UPLC H-class system was done with Purospher Star LiChroCART reverse phase column (3 µm particle size, 55x2 mm i.d., 55x2 mm, Merck, Darmstadt, Germany) with a solvent shift from 100% acetonitrile/milliQ/chloroform/acetic acid (90:10:2:0.005; v/v/v/v) to 100% methanol/heptane/chloroform/acetic acid (90:10:2:0.005; v/v/v/v) in 2.5 minutes at a flow rate of 0.5 mL/min (Supplementary Table S2). The XEVO TQ-S mass spectrometer was connected to an atmospheric pressure chemical ionization chamber (probe temperature: 425°C, discharge current 3 µA.) set to negative mode and detector measured in full scan from 200-550 amu. Data analysis was performed by Waters MassLynx 4.1 and the area under the curve (AUC) was corrected by the internal standard FFA C24 and corrected for the response based on calibration curves of FFA C16-C30. Data was plotted as absolute amounts and relative percentage to the total amount of FFA detected. FFA C16:0 and C18:0 were not included due to manufacturer's contamination of the chloroform extracting solvent with these FAs. Unsaturated FFA C16-C18 were plotted separately as they also are important components of sebum lipids.

2.6 Quantitative real-time PCR (q-PCR)

Total RNA from skin samples without hypodermis were isolated by guanidinium thiocyanate method[23]. cDNA was synthesized from 1 µg RNA with M-MuLV reverse transcriptase. Quantitative gene analysis was done with 7500 Fast real-time PCR system (Applied Biosystems, Foster City, CA, USA) using SYBR Green Technology as detection

method. Ribosomal protein, large, P0 (*RPL0*), cytochrome c-1 (*CYC1*) and ribosomal protein S20 (*RPS20*) were used as housekeeping genes. Relative gene expression was calculated by deducting the average threshold cycle (Ct) of the housekeeping genes from the Ct of the target gene. The difference was then raised to 2 to the power and the data was plotted as relative fold change compared to the WT control group. Primer sequences of the analyzed genes are available in Supplementary Table S3.

2.7 Fourier transform infrared spectroscopy (FTIR)

FTIR measurements were performed with Varian 670-IR spectrometer (Agilent Technologies, Inc., Santa Clara, CA) equipped with a broad-band mercury cadmium telluride detector. Hydrated epidermis (24 hours in 27% NaBr in deuterated water, D_2O) was mounted between 2 silver bromide windows for collection of FTIR spectra (600-4000 cm^{-1}) with resolution of 1 cm^{-1} in a temperature range from 0-90°C (0.5°C/min). Spectra were analyzed and deconvoluted (half width of 4cm-1; enhancement factor of 1.7) with Resolutions Pro 4.1 (Varian Inc.) software. CH_2 rocking vibrations were used to determine the orthorhombicity of the samples and the transition temperature from orthorhombic to hexagonal phases. The area ratio (peak area at 730 cm^{-1}/ peak area at 719 cm^{-1}) was calculated by curve fitting the FTIR spectra at 32°C in the range of CH_2 rocking vibrations (710-740 cm^{-1}). In this range, two peaks were fitted using a Lorentzian peak function. The transition temperature between the orthorhombic and hexagonal phases was determined by the disappearance of the peak at the 730 cm^{-1}. CH_2 asymmetrical stretching vibrations (2840-2860 cm^{-1}) were monitored to assess the conformational ordering of the lipid chains.

2.8 Transepidermal water loss (TEWL)

The barrier function of the skin of WT and *APOE*$^{-/-}$ mice was examined by measuring the transepidermal water loss (TEWL). The measurements were performed under controlled ambient temperature (22°C) and humidity (49.5%). The mice were anesthetized as described in section 2.2, their back skin was shaved and the closed-chamber of the evaporimeter (Aqua Flux AF200, Biox Systems Ltd, London, UK) was placed on their back skin in upright position perpendicular to the skin surface. Transepidermal water loss was measured for 90 seconds.

2.9 Preparation of murine lipid model membranes (mLMM)

Synthetic mLMMs were prepared in a composition representing the epidermal lipid composition of the WT and the *APOE*$^{-/-}$ mice. The membranes contained an equimolar

ratio of synthetic CER, FFA and cholesterol. All mLMM CER mixture were prepared with CER NdS C24, CER NS C24, CER NP C24, CER AS C24, CER EOS C30 lineolate (40.5: 36:5:14.5:4, respective molar ratios). FFA mixtures were composed of FFA C16:0, C18:0, C20:0, C20:1, C22:0, C22:1, C24:0, C26:0 in a molar ratio of 3.5:1.5:2.0: 10.0:4.5:3.5:30.0:45.0, representative of WT epidermis or 4.5:0.5:12.5:31.5:7.5:6.0:22 .0:15.50, mimicking lipid composition of *APOE*$^{-/-}$ epidermis. mLMM were prepared as described previously[24]. In short, lipid mixtures (5 mg/mL in a 100 µL Hamilton syringe, Bonaduz, Switzerland) in hexane:ethanol (2:1, v/v) were sprayed onto a polycarbonate membrane (0.05 µm pore size, 25 mm i.d., Whatmann, Kent, UK) using a Camag Linomat IV with an extended y-axis arm (Muttenz, Switzerland). Mixtures were sprayed at a 5 µL/min flow under a gentle nitrogen flow to form a homogenous square (8x8 mm). Afterwards, the membranes were equilibrated at 85°C for 10 minutes, cooled down to room temperature and stored in the dark under argon atmosphere for characterization by X-ray diffraction studies and permeability studies.

2.10 X-ray diffraction studies on mLMM

The lamellar and lateral organizations of the mLMM were assessed by X-ray diffraction measurements performed at the station BM26B of the European Synchrotron Radiation facility (ESRF, Grenoble, France). For measurements, mLMM were hydrated for 24 hours (27% NaBr in demiwater) prior mounting in parallel to the primary beam in a sample holder with temperature controlled (25°C). Data were collected with a Pilatus 1M detector (1043 × 981 pixels at 172 x 172 µm spatial resolution) for small angle x-ray diffraction (SAXD) and with a Pilatus 300K (1475 × 195 pixels at 172 x 172 µm spatial resolution) for wide angle X-ray diffraction (WAXD). SAXD detector was calibrated using silver behenate (d = 5.838 nm) and the WAXD detector was calibrated using the two strongest reflections of high density polyethylene (HDPE, d = 0.416 and 0.378 nm). Cholesterol was also used as an internal standard as it is often a component of our synthetic lipid membranes. The X-ray wavelength was 0.1034 nm and the sample-to-detector distances were 1980 mm for Pilatus 1M detector and 3110 mm to the Pilatus 300K detector. Static measurements patterns were collected for 60 seconds and the scattering intensity I (in arbitrary units) was measured and calculated as a function of the scattering vector q (in reciprocal nm). Vector q was defined as $q = (4\pi \sin \theta)/\lambda)$ with θ representing the scattering angle and λ the wavelength. Using the positions of a sequence of equidistant peaks (q_n), the periodicity (d-spacing) of a lamellar phase was calculated ($q_n = 2n\pi/d$, n representing the order number of the diffraction peak). Peaks were integrated in a 40° angle perpendicular to the sample in the X-ray beam.

2.11 Permeability of mLMM to E-PABA

The barrier function of the murine epidermis lipids was investigated by the permeability of the mLMM to the model drug ethyl para-aminobenzoic acid (E-PABA; MW: 165.189 g/mol). For the permeation studies flow through Permegear inline diffusion cells (Bethlehem PA, USA) were used. mLMM were mounted into the diffusion cells (0.282 cm^2 diffusion area) and hydrated for at least 1 hour in the PBS acceptor phase (pH 7.4, filtered and degassed). The donor phase was a saturated and filtered E-PABA solution (concentration 0.65 mg/mL) in sodium acetate buffer (pH 5.0; 0.1 M acetic acid, 0.1 M sodium acetate, 1:2.5; v/v). To avoid evaporation from the donor phase adhesive tape was used to close the donor compartment. The acceptor phase was under constant stirring at 50 rpm perfused and perfused at a flow rate of 2-2.5 mL/min. The acceptor phase was sampled every hour for 10.5 hours (Isco Retriever IV; Teledyne Isco, Lincoln NE, USA). The amount of E-PABA in each sampled fraction was determined by UPLC-UV (Waters, Etten-Leur, The Netherlands) with a reversed phase C18 column (Alltima, C-18, 1.7 µm i.d., 2.1 x 50 mm, Waters, Ireland) at 40°C and an UV detector with excitation wavelength at 286 nm. The mobile phase consisted of acetonitrile with 0.1% trifluoroacetic acid :milliQ (40:60; v/v) at flow rate of 0.5mL/min. A calibration curve of E-PABA in ethanol was also measured. The software TargetLynx was used to process the data and calculate the flux of E-PABA.

2.12 Statistical analysis

Statistical analysis was performed using GraphPad Prism 7 (GraphPad Software Inc., CA, USA). Statistically significant differences between two groups were determined by two-tailed, unpaired Student's t-tests while differences among three groups were determined using One-way or Two-way ANOVAs with Holm-Šídák post-hoc test. Data is presented as mean ± SD and *p* values below 0.05 were considered significant.

3. RESULTS

3.1 Deficiency of *LDLR* or *APOE* results in (mild) hypercholesterolemia in chow-fed young adult mice but the skin morphology is preserved.

Non-fasted plasma lipid levels were determined by colorimetric enzymatic assays (Fig. 1a). On chow diet, *LDLR*$^{-/-}$ mice developed a mild hypercholesterolemia with increased plasma levels of free cholesterol (0.97±0.15 µg/µl plasma) and cholesteryl esters (CE) (2.05±0.54 µg/µl plasma) compared to WT controls (free cholesterol 0.36±0.05 µg/µl plasma and CE 0.97±0.15 µg/µl plasma). *APOE*$^{-/-}$mice on the same diet showed severe

hypercholesterolemia marked by 6-fold higher free cholesterol (2.3±0.49 µg/µl plasma) and 5-fold higher CE (4.59±1.03 µg/µl plasma). Plasma triglycerides were comparable among WT (1.02±0.15 µg/µl plasma), *LDLR*$^{-/-}$ (1.10±0.25 µg/µl plasma), and *APOE*$^{-/-}$ (1.13±0.16 µg/µl plasma) mice.

Subsequently, we assessed the impact of hypercholesterolemia on the skin morphology by hematoxylin and eosin and toluidine blue stainings (Fig. 1b). Hypercholesterolemic *LDLR*$^{-/-}$ and *APOE*$^{-/-}$ mice displayed similar skin morphology as the normolipidemic WT controls with a consistent number of epidermal layers (no hyperproliferation) and thin SC. In the dermis no striking morphological alterations or signs of inflammation were observed. Polarized light microscopy on skin sections did not show the presence of cholesterol crystals in the dermis.

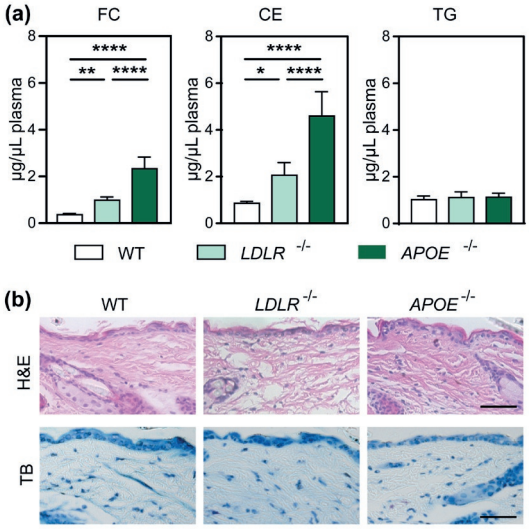

Figure 1. Chow-fed young-adult *APOE*$^{-/-}$ mice develop severe hypercholesterolemia but their skin shows no morphological changes or signs of inflammation compared to the chow-fed *LDLR*$^{-/-}$ mice and WT controls. (a) Plasma levels of free cholesterol (FC), cholesteryl esters (CE), and triglycerides (TG) were measured with enzymatic colorimetric assays. Animals were not fasted prior sacrifice (n= 4-6 animals/group). (b) Hematoxylin and eosin (H&E) and toluidine blue (TB) stainings of sections imaged with brightfield microscope (scale bar= 50 µm; representative images of n=3 animals/group; *p<0.05, **p <0.01, ****p<0.0001).

3.2 Increased amounts of shorter and unsaturated FFA species are present in the epidermis of *APOE*$^{-/-}$ but not in *LDLR*$^{-/-}$ mice

To examine whether the skin barrier was affected the three main SC lipid classes were analyzed by liquid-chromatography mass spectrometry (LC/MS). The amount of cholesterol did not differ among groups (Fig. 2a). Seven CER subclasses (detailed nomenclature as described by Motta *et al.* (1993) in Supplementary Fig. S1) were identified in the murine skin: CER NdS, CER NS, CER NP, CER AdS, CER AS, CER [EO], the latter representing CER EOdS and CER EOS (Fig. 2b). Abundance of CER NdS was significantly higher in *LDLR*$^{-/-}$ and *APOE*$^{-/-}$ epidermis (45% compared to 40% for WT controls) while the CER AS was lower in these mice (9% compared to 16% for WT controls). The average total CER chain length was 43-44 carbon atoms regardless the genetic background of the mice (Fig. 2c) and the ratio CER [EO]/CER [non-EO] both did not change (Supplementary Fig. S2a). CER NP and CER AdS could not be separated, thus these CERs are reported together representing about 5% of the total CERs.

Next, FFAs with chain length ranging from 20-30 carbon atoms were analyzed (Fig. 2d and Supplementary Fig. S2b). The epidermal FFA profile of the severely hypercholesterolemic *APOE*$^{-/-}$ mice strongly differed from that observed for the normolipidemic WT control and mild hypercholesterolemic *LDLR*$^{-/-}$ mice (Fig 2d-g). The *APOE*$^{-/-}$ epidermis contained 3 times the amount of FFA (Fig. 2e) with a 5-fold increase in the relative abundance of unsaturated FFA compared to WT and *LDLR*$^{-/-}$ epidermis, particularly the levels of FFA C20:1 were increased (Fig. 2d/f). In addition, *APOE*$^{-/-}$ epidermis showed a shift towards shorter FFA chains with on average 23 carbon atoms whilst in WT and *LDLR*$^{-/-}$ epidermis this average was around 25 carbon atoms (Fig. 2g). Over 50% of the FFA species in the *APOE*$^{-/-}$ epidermis contained less than 24 carbon atoms whilst for WT and *LDLR*$^{-/-}$ epidermis this value was around 20% (Supplementary Fig. S2c). In summary, in the *APOE*$^{-/-}$ epidermis FFA C20:1 was the most abundant FFA (25%) followed by FFA C24:0 (21%) and FFA C26:0 (16%) while for WT and *LDLR*$^{-/-}$ the most abundant species were FFA C24:0 and C26:0 representing nearly 28% and 40%, respectively. Additionally, the composition of unsaturated FFAs (C16-C18) was also altered in the *APOE*$^{-/-}$ epidermis with marked increase in the amounts of C16:1 (16-fold), C18:1 (18-fold) and C18:2 (8-fold) compared to the WT control (Supplementary Fig. S2d).

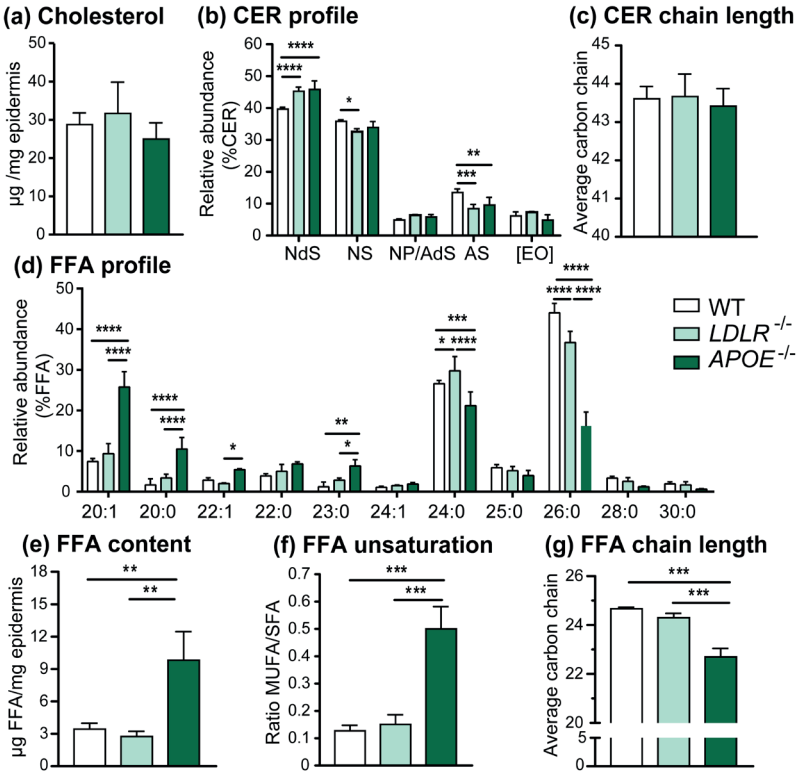

Figure 2. *APOE*$^{-/-}$ mice shows remarkably altered epidermal FFA profile compared to WT and *LDLR*$^{-/-}$ mice, while cholesterol and ceramides are not/minimally affected. LC/MS analysis of the three main classes of SC lipids: (a) cholesterol, (b-c) CERs, (d-g) FFAs. CER data plotted as a percentage of the total peak area after correction by internal standard. Nomenclature of ceramides subclasses based on different acyl chains (non-hydroxy fatty acid [N]; α-hydroxy fatty acid [A]; esterified ω-hydroxy fatty acid [EO]) and on the sphingoid base (dihydrosphingosine, [dS]; sphingosine [S]; phytosphingosine [P]). CER[EO] represents CER EOS and CER EOdS (n=3/group; *p<0.05; **p<0.01; ***p<0.001; ****p<0.0001).

3.3 *APOE*$^{-/-}$ mice downregulate cholesterol and FFA synthesis genes in the skin

The epidermal FFA composition of the *APOE*$^{-/-}$ mice greatly differed from that of the WT controls. Therefore, the expression of genes involved in lipid synthesis and uptake from circulation was assessed by quantitative real-time polymerase chain reaction (q-PCR) and compared to the WT controls to gain insight in the mechanisms underlying the changes in epidermal barrier lipids of *APOE*$^{-/-}$mice (Fig. 3). Expression of cholesterol synthesis and uptake genes was reduced in the skin of *APOE*$^{-/-}$ mice as

evidenced by the strong downregulation of *HMGCR* and *LDLR* (Fig. 3a). Expression of ATP-binding cassette genes (*ABCA1*, *ABCA12*, *ABCG1*) showed no differences between groups (Supplementary Fig. S3a). The expression of *CERS3* was not changed while *GBA* expression involved in the metabolism of glycolipids in the skin was downregulated in *APOE*$^{-/-}$ mice (Fig. 3b). No changes in expression were observed for CER degradation genes (Supplementary Fig. S3b). Genes involved in FFA synthesis (*ACACA*) and FFA elongation (*ELOVL1*) were remarkably reduced in the *APOE*$^{-/-}$ mice but no changes were observed between groups regarding FFA chain desaturation (*SCD1*) (Fig. 3c). Expression of other elongases (*ELOVL4, ELOVL6, ELOVL7*) and fatty acid transporters (*FABP5, CD36*) was not changed (Supplementary Fig. S3c-d). Furthermore, we evaluated whether the adapted lipid metabolism in the *APOE*$^{-/-}$ skin could affect keratinocyte proliferation and differentiation markers. However, mRNA levels of the proliferation marker *Ki-67*, early differentiation marker *K10*, late differentiation markers *IVL* and *FLG* did not differ in *APOE*$^{-/-}$ skin compared to WT skin (Supplementary Fig. S3e). Additionally, the q-PCR data did not reveal upregulation of pro-inflammatory genes in the skin of the *APOE*$^{-/-}$ mice regarding mast cells activation markers (*TPS1, TSP2*), pro-inflammatory cytokines (*IFNG, TNFA*), and macrophage marker (*CD68*) (data not shown).

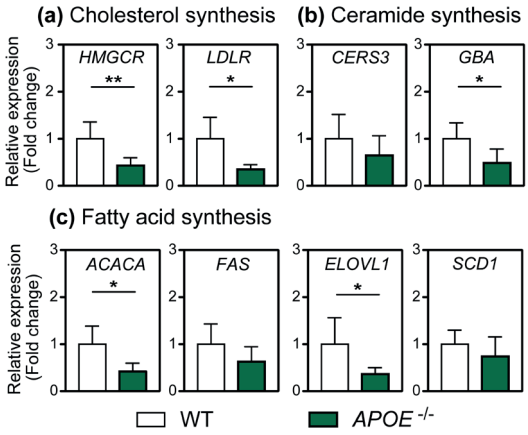

Figure 3. Downregulated mRNA expression of cholesterol, CER and FFA synthesis genes in the skin of hypercholesterolemic *APOE*$^{-/-}$ mice. The expression of genes encoding for key proteins and enzymes involved in (a) cholesterol, (b) ceramide and (c) fatty acid synthesis were measured: HMG-CoA reductase (*HMGCR*), LDL receptor (*LDLR*), ceramide synthase 3 (*CERS3*), glucocerebrosidase (*GBA*), acetyl-Coenzyme A carboxylase alpha (*ACACA*), fatty acid synthase (*FAS*), elongation of very long chain 1 (*ELOVL1*), stearoyl-Coenzyme A desaturase 1 (*SCD1*) (*p<0.05, ** p <0.01).

3.4 Lipids in the epidermis of *APOE*$^{-/-}$ mice adopt orthorhombic lateral packing

Changes in the epidermal lipid composition can alter the lateral organization of these lipids and, consequently, the integrity of the skin barrier. Therefore, the lateral organization of barrier lipids was determined by Fourier transform infrared spectrometry (FTIR). In all samples, at low temperatures the lipids had a low conformational disorder represented by frequencies below 2850 cm^{-1} for the CH_2 symmetric stretching vibrations and slightly increased with higher temperatures (Fig. 4a). From 38°C onwards this gradual shift was more pronounced indicating the transition of the lipids towards the fluid phase (frequencies above 2852 cm^{-1}). Throughout this transition the lipids in the *APOE*$^{-/-}$ epidermis showed slightly higher vibration frequencies than that of the lipids in epidermis of WT mice. The CH_2 rocking vibrations at 32°C (skin temperature) showed an orthorhombic lateral packing in a fraction of the lipids represented by the presence of a doublet: a strong peak at 719 cm^{-1} and a weaker peak at 730 cm^{-1} (Fig. 4b). The fraction of lipids in an orthorhombic packing is comparable between groups as the area ratio of the two peaks was similar for all samples (Fig. 4c). Transition temperature from orthorhombic to hexagonal phases was determined by the disappearance of the peak at 730 cm^{-1} and it was not different between groups, varying from 40-44°C (Supplementary Fig. S4).

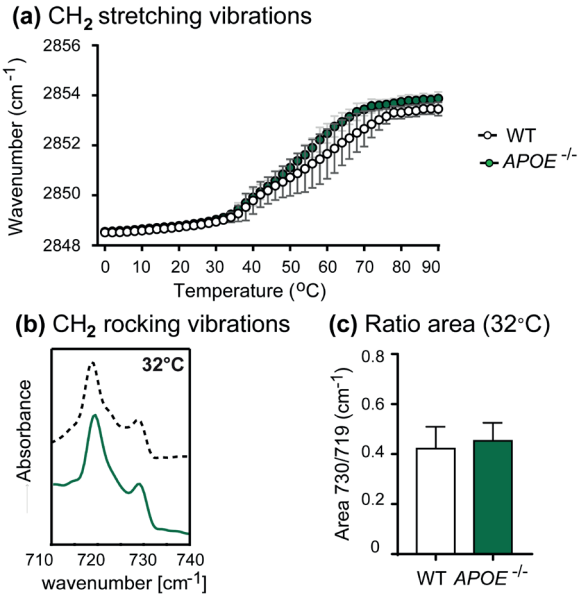

Figure 4. Altered epidermis FFA composition does not modify the orthorhombic lateral lipid organization in the skin *APOE*$^{-/-}$ mice. FTIR was used to determine the lateral packing of lipids in the epidermis of WT and *APOE*$^{-/-}$ mice. (a) CH_2 symmetric stretching vibrations (2848-2856 cm^{-1}) were plotted

against temperature (0-90°C) to follow the phase transition of the lipids; (b) CH_2 rocking vibrations (710-740 cm^{-1}) plotted at skin temperature (32°C); (c) ratio between peak area at 730 cm^{-1} and peak area at 719 cm^{-1} (32°C).

3.5 Altered FFA profile in the *APOE*$^{-/-}$ epidermis increases TEWL *in vivo* and the permeability in murine lipid model membranes (mLMM)

To examine whether the changes in FFA composition observed in the *APOE*$^{-/-}$ epidermis impairs skin barrier function, the TEWL (water loss from the skin) of WT and *APOE*$^{-/-}$ mice was measured. The TEWL of *APOE*$^{-/-}$ mice was significantly higher (12.9±0.5 g/m^2h) than that observed for the WT control (10.9±0.6 g/m^2h) (p<0.01). To further study whether the lipid barrier and in particular the change in FFA composition contributed to the impaired skin barrier function, permeation studies were performed using mLMMs. The mLMMs had a fixed CER composition, but a FFA composition mimicking that in the WT epidermis (WT_{LMM}) or in the *APOE*$^{-/-}$epidermis (*APOE*$^{-/-}{}_{LMM}$). The lamellar and lateral lipid organizations of the mLMMs were characterized by small- and wide-angle X-ray diffraction studies. The lipids in both WT_{LMM} and *APOE*$^{-/-}{}_{LMM}$ assembled in a long and short periodicity phases with no differences in the repeated distances (Fig. 5b). In the *APOE*$^{-/-}{}_{LMM}$ fewer lipids adopted an orthorhombic lateral packing compared to the WT_{LMM} as seen by the lower peak with 0.378 nm spacing in the wide-angle X-ray diffraction (Fig. 5c).

To assess the functionality of the barrier ethyl para-aminobenzoic acid (E-PABA), a commonly used topical anesthetic, was chosen as model drug for the permeability studies. A steady state flux of E-PABA was achieved in approximately 3 hours for both types of mLMM (Fig. 5d) with significantly increased flux through the *APOE*$^{-/-}{}_{LMM}$ in comparison to the WT_{LMM} (40±3.3 v.s. 14±2.2 μg/cm^2/h) (Fig. 5e). After diffusion, analysis of the donor and the collected acceptor solution showed nearly 100% drug recovery in both groups (data not shown).

4. DISCUSSION

In this study we showed for the first time that severe systemic hypercholesterolemia associated with apoE deficiency in young adult mice affects the lipid composition and barrier function of the epidermis, while in LDLR deficiency with mild hypercholesterolemia the epidermis was not affected. Here, we focused on chow diet fed and young adult mice to specifically investigate the effects of mild and severe hypercholesterolemia on barrier lipid composition and function.

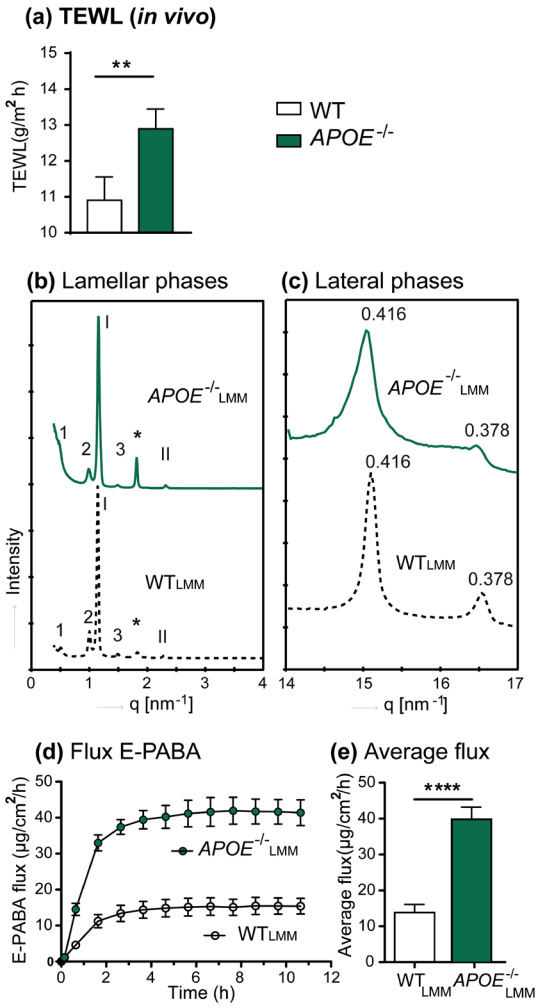

Figure 5. Skin of *APOE*$^{-/-}$ mice shows higher transepidermal water loss (TEWL) than WT control *in vivo* and epidermal lipid composition of *APOE*$^{-/-}_{LMM}$ mice shows remarkable increase in lipid barrier permeability to ethyl para-aminobenzoic acid (E-PABA). (a) Average TEWL at the skin surface of WT and *APOE*$^{-/-}$ mice. Data was collected for 90 s in vivo using a close-chamber evaporimeter. (b) Lamellar and (c) lateral organizations of murine lipid model membranes (mLMM) representing the epidermal lipids of the WT and *APOE*$^{-/-}$ mice determined by small angle- and wide angle X-ray diffraction, respectively. In Arabic numbers (1-3) the long periodicity phase orders, in Roman numbers (I-II) the short periodicity phase orders. Asterisk indicates the reflection of crystalline cholesterol. Flux of E-PABA through WT_{LMM} (open circles) and *APOE*$^{-/-}_{LMM}$ (closed circles) (d) over time (10.5 hours) and (e) at steady state (average). Data represents three different experiments (n=6-7/group) (**p<0.01; ****p<0.0001).

Analysis of the epidermal lipid composition showed similar levels of cholesterol in the *APOE*$^{-/-}$ epidermis compared to the WT controls despite the significant increase in circulating cholesterol[8,9]. However, based on the q-PCR data a higher cholesterol uptake from the circulation is expected and the skin cholesterol homeostasis is likely maintained by local reduction of cholesterol synthesis (*HMGCR*) and uptake from the circulation (*LDLR*). In line, higher intake of 25-hydroxy-cholesterol by keratinocytes *in vitro* reported downregulation of *HMGS1*[25] and suppressed the de novo cholesterol synthesis in these cells[26].

The FFA composition of the epidermis of *APOE*$^{-/-}$ mice greatly differed from the composition of the control mice with higher FFA content, characterized by a shift towards shorter and unsaturated chains. FFAs and CERs share a common biosynthetic pathway in the epidermis and alterations in the FFA chain length or unsaturation translate into similar trends in the CER profile[27,28]. Conversely, in our study the remarkable changes in FFA of the *APOE*$^{-/-}$ epidermis were not associated with alterations in the CER unsaturation and chain length profiles. This suggests that the observed changes in the FFAs may not be related to local biosynthesis, which is supported by the reduced expression of genes involved in FFA synthesis and elongation (*ACACA* and *ELOVL1*) in the *APOE*$^{-/-}$ epidermis. ELOVL1 is the main enzyme responsible for elongation of FA C20-C24 with especially high activity towards saturated and unsaturated FA C20-C22[29]. ELOVL1 activity can be inhibited *in vitro* by FA C18:1 in a dose-dependent manner[30]. Similar to the epidermis of *APOE*$^{-/-}$mice, in *ELOVL1*$^{-/-}$ mice the abundance of FFA and CER containing FA ≥C26 was strongly reduced with lower elongation activity towards FA C20-C22-CoA[27]. Interestingly, in this study no changes were observed in mRNA levels of *SCD1,* encoding for the rate-limiting enzyme in the desaturation of FFA[31]. However, SCD1 expression is strictly regulated in both gene and protein levels, usually showing a fast turn off; thus, further differences should be evaluated in protein and enzyme activity levels[32,33].

Altogether, our LC/MS and q-PCR data suggests an increased flux of cholesterol and FFA from the plasma into the skin. In the plasma, cholesterol is mainly transported as CE in the core of lipoproteins. After cellular uptake, the CE-rich core of the lipoprotein remnants is metabolized into free cholesterol and FA. In mice, plasma CE is mostly formed by esterification of cholesterol with unsaturated FA and LC/MS/MS analysis of hypercholesterolemic *APOE*$^{-/-}$ plasma shows more than 2-fold higher levels of FA C18:1-derived CE compared to the normolipidemic WT mice[7]. Similar to the plasma, we found increased amounts of FA C18:1 but also FA C18:2, an essential FA, in the epidermis of *APOE*$^{-/-}$ mice. Interestingly, the incubation of HaCaT keratinocytes with FA C18:1 increased the mRNA levels of *HMGCS1* and the activity of HMGCoA synthase promoter.

However, combined incubation of these cells with FA C18:1 and 25-hydroxy cholesterol resulted in downregulation of sterol synthesis[25]. Thus, it is possible that a higher uptake of CE-rich lipoproteins by keratinocytes of *APOE*$^{-/-}$ mice leads (1) to activation of compensatory feedback regulation in local lipid synthesis, at least on mRNA level, and (2) to the incorporation of FFAs derived from the CE-rich particles into the SC lipid matrix.

Modifications of skin lipid content and morphology have been previously described using other hyperlipidemic mouse models[8–10,34]. These modifications were mostly analyzed in double-knockout mice on *LDLR*$^{-/-}$ or *APOE*$^{-/-}$ backgrounds; in which two opposite effects occur: (1) hyperlipidemia by impaired (V)LDL pathway and (2) hypolipidemia by impaired high-density lipoprotein pathway. In these studies, double-knockout mice generated on *LDLR*$^{-/-}$ background (mild hyperlipidemic model) developed skin free cholesterol and CE accumulation, and inflammation in association with high cholesterol/high fat diets but not on chow diet. In contrast, the double-knockout with *APOE*$^{-/-}$ background (severe hyperlipidemic model) developed these alterations spontaneously in time. Thus, in line with our results this indicates that the severity of the hypercholesterolemia of the genetic background plays an important role in the development of the skin phenotypes.

Nonetheless, it is important to note that apoE and the LDLR are expressed in murine skin[18,35–37]. The role of apoE in the skin remains to be elucidated, but the role of LDLR as a mediator for the uptake of lipoproteins by the skin has been described[35]. Thus, the absence of these proteins/receptors in the skin of our mouse models may contribute to the changes reported in this study. Although CE levels are elevated in the plasma of *LDLR*$^{-/-}$ mice as compared to WT controls, the epidermal lipid profile is not affected in the skin of these mice. In this line, it could be hypothesized that LDLR deficiency in the skin of these mice prevented the accumulation of the CE-derived lipids. Additionally, considering the hypercholesterolemia as the driving factor altering the composition of the epidermal lipids, *LDLR*$^{-/-}$ mice on chow diet develop only a minor hypercholesterolemic phenotype[11], which in turn could have led to lower skin lipoprotein accumulation. In this view, skin-specific deletion of lipid transporters (*e.g.* LDLR, CD36) on a WT and on an *APOE*$^{-/-}$ background may help elucidate the mechanisms underlying this plasma-skin lipid crosstalk.

Studies using lipid model membranes or diseased skin reported that elevated FFA content increases the fraction of lipids assembled in an orthorhombic packing[28,38.] In contrast, shorter chain lengths and/or higher degree of unsaturation of FFA species also in the presence of the same CER composition favors a hexagonal packing and

higher permeability of the lipid barrier[24,39]. As all these changes are present in the *APOE*$^{-/-}$ epidermis, these opposite effects may counteract maintaining the dense lipid orthorhombic organization. However, when interpreting FTIR results one must remember that not only cholesterol, CERs and FFAs are present on the skin surface; and these vibrations are influenced by other lipid species; e.g. sebum lipids, which are abundantly present in mouse skin[40–42].

Direct *ex vivo* analysis of SC barrier function in non-nude mice is limited by the high density of hair follicles, which hinders the isolation of the few SC layers or the intact viable epidermis. Additionally, the high number of hair follicles offers an additional route of permeation for model drugs when studying skin barrier integrity[43,44]. TEWL is a well-established method to monitor the water loss from the skin and to assess the functionality of the SC barrier[45,46]. A decrease in TEWL values has been strongly correlated with a reduced chain length of the FFAs and CERs in the SC, emphasizing the importance of SC lipids for the skin barrier function[28]. Similarly, the skin of *APOE*$^{-/-}$ mice showed a reduced SC barrier function characterized by higher TEWL and a change in the fatty acid composition.

Additionally, mLMMs were used as *APOE*$^{-/-}$ SC substitutes to assess the contribution of the *APOE*$^{-/-}$ epidermal lipid composition to the impairment of the skin barrier function. Higher degree of unsaturation of the FFAs correlates with a lower the fraction of lipids forming an orthorhombic packing in the SC or lipid model membranes[24,28], while an increased abundance of short chain FFAs may, already at low levels, show higher mobility in lipid model membranes associated with a great increase in the permeability of the lipid model membrane to E-PABA[47]. In agreement, the altered FFA composition of *APOE*$^{-/-}$ epidermis resulted in higher permeability to E-PABA through $APOE^{-/-}_{LMM}$ compared to WT_{LMM}. Our mLMMs comprised 5% of FFA C16-C18 as we aimed to study the differences in permeability associated with epidermal barriers lipids. Higher levels of these short chain FFAs would only further increase the permeability of the $APOE^{-/-}_{LMM}$, especially considering that unsaturated FFA C16-C18 are higher in the *APOE*$^{-/-}$ epidermis.

In conclusion, we show that the hypercholesterolemia in young adult *APOE*$^{-/-}$ mice affects the skin lipid composition and is associated with a compromised lipid barrier function. Our data suggests that the severity of the hypercholesterolemia and plasma CE levels may play critical roles in the development of this skin phenotype. This highlights the relevance of investigating the composition and functionality of the skin barrier of hypercholesterolemic patients at young age and prior the development of inflammatory processes as to our knowledge this information is not yet available. In turn, it may be possible to protect the skin of these patients and prevent future development of skin

inflammatory phenotypes.

CONFLICT OF INTEREST

The authors have no conflict of interest.

ACKNOWLEDGEMENTS

We thank the company Evonik (Essen, Germany) for providing the synthetic ceramides; the DUBBLE beam line team for assissting with the X-ray diffraction studies at the European Synchrotron Radiation Facility (Grenoble, France). We thank Richard W. J. Helder, Dr. Ilze Bot and Prof. Johan Kuiper for supporting the TEWL studies. This research was supported by the Leiden Academic Centre for Drug Research (Leiden University, Leiden, The Netherlands).

REFERENCES

1. Harada-Shiba, M. et al. Guidelines for Diagnosis and Treatment of Familial Hypercholesterolemia 2017. J. Atheroscler. Thromb. 751–770 (2018). doi:10.5551/jat.CR003

2. Awan, Z. et al. APOE p.Leu167del mutation in familial hypercholesterolemia. Atherosclerosis 231, 218–222 (2013).

3. Holven, K. B. et al. Subjects with familial hypercholesterolemia are characterized by an inflammatory phenotype despite long-term intensive cholesterol lowering treatment. Atherosclerosis 233, 561–567 (2014).

4. Ohshiro, T., Shimabukuro, T., Sunagawa, M. & Ohta, T. An 11-year-old boy with familial hypercholesterolemia showing multiple xanthomas and advanced atherosclerosis, who responded to lipid-lowering therapy using statin. J. Atheroscler. Thromb. 16, 698–701 (2009).

5. Aljenedil, S., Ruel, I., Watters, K. & Genest, J. Severe xanthomatosis in heterozygous familial hypercholesterolemia. J. Clin. Lipidol. 12, 872–877 (2018).

6. Getz, G. S. & Reardon, C. A. Do the Apoe −/− and Ldlr −/− Mice Yield the Same Insight on Atherogenesis? Arterioscler. Thromb. Vasc. Biol. 36, 1734–1741 (2016).

7. Subbaiah, P. V. et al. Regulation of plasma cholesterol esterification by sphingomyelin: Effect of physiological variations of plasma sphingomyelin on lecithin-cholesterol acyltransferase activity. Biochim. Biophys. Acta - Mol. Cell Biol. Lipids 1821, 908–913 (2012).

8. Accad, M. et al. Massive xanthomatosis and altered composition of atherosclerotic lesions in hyperlipidemic mice lacking acyl CoA:cholesterol acyltransferase 1. J. Clin. Invest. 105, 711–719 (2000).

9. Arnaboldi, F. et al. High-density lipoprotein deficiency in genetically modified mice deeply affects skin morphology: A structural and ultrastructural study. Exp. Cell Res. 338, 105–112 (2015).

10. Zabalawi, M. et al. Inflammation and skin cholesterol in LDLr −/− , apoA-I −/− mice: link between cholesterol homeostasis and self-tolerance? J. Lipid Res. 48, 52–65 (2007).

11. Ishibashi, S., Goldstein, J. L., Brown, M. S., Herz, J. & Burns, D. K. Massive Xanthomatosis and Atherosclerosis in cholesterol-fed low density lipoprotein receptor-negative mice. J. Clin. Invest. 93, 1885–1893 (1994).

12. Feingold, K. R. et al. Apolipoprotein E Deficiency Leads to Cutaneous Foam Cell Formation in Mice. J. Invest. Dermatol. 104, 246–250 (1995).

13. Ang, L. S., Cruz, R. P., Hendel, A. & Granville, D. J. Apolipoprotein E, an important player in longevity and age-related diseases. Exp. Gerontol. 43, 615–622 (2008).

14. Hiebert, P. R. et al. Granzyme B contributes to extracellular matrix remodeling and skin aging in apolipoprotein E knockout mice. Exp. Gerontol. 46, 489–499 (2011).

15. Elias, P. M. Stratum corneum defensive functions: An integrated view. J. Invest. Dermatol. 125, 183–200 (2005).

16. Ponec, M., Weerheim, A., Lankhorst, P. & Wertz, P. New acylceramide in native and reconstructed epidermis. J. Invest. Dermatol. 120, 581–588 (2003).

17. Lin, M.-H. & Khnykin, D. Fatty acid transporters in skin development, function and disease. Biochim. Biophys. Acta 1841, 362–8 (2014).

18. Mommaas, M., Tada, J. & Ponec, M. Distribution of low-density lipoprotein receptors and apolipoprotein B on normal and on reconstructed human epidermis. J. Dermatol. Sci. 2, 97–105 (1991).

19. Tsuruoka, H. et al. Scavenger receptor class B type I is expressed in cultured keratinocytes and epidermis. Regulation in response to changes in cholesterol homeostasis and barrier requirements. J. Biol. Chem. 277, 2916–2922 (2002).

20. Out, R. et al. Macrophage ABCG1 Deletion Disrupts Lipid Homeostasis in Alveolar Macrophages and Moderately Influences Atherosclerotic Lesion Development in LDL Receptor-Deficient Mice. Arterioscler. Thromb. Vasc. Biol. 26, 2295–2300 (2006).

21. Boiten, W., Absalah, S., Vreeken, R., Bouwstra, J. & van Smeden, J. Quantitative analysis of ceramides using a novel lipidomics approach with three dimensional response modelling. Biochim. Biophys. Acta - Mol. Cell Biol. Lipids 1861, 1652–1661 (2016).

22. Motta, S. et al. Ceramide composition of the psoriatic scale. BBA - Mol. Basis Dis. 1182, 147–151 (1993).

23. Chomczynski, P. & Sacchi, N. The single-step method of RNA isolation by acid guanidinium thiocyanate–phenol–chloroform extraction: twenty-something years on. Nat. Protoc. 1, 581–585 (2006).

24. Mojumdar, E. H., Helder, R. W. J., Gooris, G. S. & Bouwstra, J. A. Monounsaturated fatty acids reduce the barrier of stratum corneum lipid membranes by enhancing the formation of a hexagonal lateral packing. Langmuir 30, 6534–6543 (2014).

25. Siefken, W., Höppner, H. & Harris, I. R. Regulation of cholesterol synthesis by oleic and palmitic acid in keratinocytes. Exp. Dermatol. 9, 138–145 (2000).

26. Ponec, M., Havekes, L., Kempenaar, J. & Jan Vermeer, B. Cultured Human Skin Fibroblasts and Keratinocytes: Differences in the Regulation of Cholesterol Synthesis. J. Invest. Dermatol. 81, 125–130 (1983).

27. Sassa, T. et al. Impaired Epidermal Permeability Barrier in Mice Lacking Elovl1, the Gene Responsible for Very-Long-Chain Fatty Acid Production. Mol. Cell. Biol. 33, 2787–2796 (2013).

28. van Smeden, J. et al. The importance of free fatty acid chain length for the skin barrier function in atopic eczema patients. Exp. Dermatol. 23, 45–52 (2014).

29. Ohno, Y. et al. ELOVL1 production of C24 acyl-CoAs is linked to C24 sphingolipid synthesis. Proc. Natl. Acad. Sci. 107, 18439–18444 (2010).

30. Sassa, T., Wakashima, T., Ohno, Y. & Kihara, A. Lorenzo's oil inhibits ELOVL1 and lowers the level of sphingomyelin with a saturated very long-chain fatty acid. J. Lipid Res. 55, 524–530 (2014).

31. Kim, H.-J., Miyazaki, M. & Ntambi, J. M. Dietary cholesterol opposes PUFA-mediated repression of the stearoyl-CoA desaturase-1 gene by SREBP-1 independent mechanism. J. Lipid Res. 43, 1750–1757 (2002).

32. Mauvoisin, D. & Mounier, C. Hormonal and nutritional regulation of SCD1 gene expression. Biochimie 93, 78–86 (2011).

33. Sampath, H. & Ntambi, J. M. Role of stearoyl-CoA desaturase-1 in skin integrity and whole body energy balance. J. Biol. Chem. 289, 2482–2488 (2014).

34. Aiello, R. J. et al. Increased atherosclerosis in hyperlipidemic mice with inactivation of ABCA1 in macrophages. Arterioscler. Thromb. Vasc. Biol. 22, 630–637 (2002).

35. Abd El-Latif, M. I. A., Murota, H., Terao, M. & Katayama, I. Effects of a 3-hydroxy-3-methylglutaryl coenzyme A reductase inhibitor and low-density lipoprotein on proliferation and migration of keratinocytes. Br. J. Dermatol. 128–137 (2010).

36. Gordon, D. A., Fenjves, E. S., Williams, D. L. & Taichman, L. B. Synthesis and secretion of apolipoprotein E by cultured human keratinocytes. J.Invest Dermatol. 92, 96–99 (1989)

37. Newman, T. C., Dawson, P. A., Rudel, L. L. & Williams, D. L. Quantitation of apolipoprotein E mRNA in the liver and peripheral tissues of nonhuman primates. J. Biol. Chem. 260, 2452–2457 (1985).

38. Groen, D., Poole, D. S., Gooris, G. S. & Bouwstra, J. A. Investigating the barrier function of skin lipid models with varying compositions. Eur. J. Pharm. Biopharm. 79, 334–342 (2011).

39. Groen, D., Poole, D. S., Gooris, G. S. & Bouwstra, J. A. Is an orthorhombic lateral packing and a proper lamellar organization important for the skin barrier function? Biochim. Biophys. Acta - Biomembr. 1808, 1529–1537 (2011).

40. Ludovici, M. et al. Influence of the sebaceous gland density on the stratum corneum lipidome. Sci. Rep. 8, 1–12 (2018).

41. Smith, K. R. & Thiboutot, D. M. Thematic review series: Skin Lipids. Sebaceous gland lipids: friend or foe? J. Lipid Res. 49, 271–281 (2008).

42. Westerberg, R. et al. Role for ELOVL3 and Fatty Acid Chain Length in Development of Hair and Skin Function. J. Biol. Chem. 279, 5621–5629 (2004).

43. Blume-Peytavi, U. et al. Follicular and percutaneous penetration pathways of topically applied minoxidil foam. Eur. J. Pharm. Biopharm. 76, 450–453 (2010).

44. Mohd, F., Todo, H., Yoshimoto, M., Yusuf, E. & Sugibayashi, K. Contribution of the hair follicular pathway to total skin permeation of topically applied and exposed chemicals. Pharmaceutics 8, (2016).

45. Nomoto, K. et al. Epidermal permeability barrier function and sphingolipid content in the skin of sphingomyelin synthase 2 deficient mice. Exp. Dermatol. 27, 827–832 (2018).

46. Fluhr, J. W., Feingold, K. R. & Elias, P. M. Transepidermal water loss reflects permeability barrier status : validation in human and rodent in vivo and ex vivo models. Exp. Dermatol. 15, 483–492 (2006).

47. Uchiyama, M., Oguri, M., Mojumdar, E. H., Gooris, G. S. & Bouwstra, J. A. Free fatty acids chain length distribution affects the permeability of skin lipid model membranes. Biochim. Biophys. Acta - Biomembr. 1858, 2050–2059 (2016).

SUPPLEMENTARY INFORMATION

1. MATERIALS AND METHODS

1.1 Chemicals

Ketamine and atropine were purchased from AUV Veterinary Services (Cuijk, The Netherlands); xylazine from ASTFarma (Oudewater, The Netherlands); Kaiser's glycerol gelatin and sodium chloride (NaCl) from Boom (Meppel, The Netherlands). Sodium phosphate dibasic (Na_2HPO_4), hematoxylin, eosin, toluidine blue, trypsin from bovine pancreas, trypsin inhibitor, cholesterol, free fatty acids (FFA) C16-C30, deuterated FFA C18 and deuterated FFA C24, chloroform, acetic acid, deuterated water (D_2O), sodium bromide (NaBr), ethyl-para-aminobenzoic acid (E-PABA), trifluoroacetic acid were purchased from Sigma-Aldrich (Zwijndrecht, The Netherlands). Potassium dihydrogen phosphate (KH_2PO_4), potassium chloride (KCl), and Entellan® were purchased from Merck (Darmstadt, Germany). CER[NS] (C24deuterated; C18protonated) and all synthetic CER were kindly provided by Evonik Industries (Essen, Germany). Heptane was purchased from ChemLab (Zedelgem, Belgium). Methanol, ethanol, isopropanol and acetonitrile were purchased from Biosolve (Valkenswaard, The Netherlands). All solvents used were analytical grade.

1.2 Liquid chromatography-mass spectrometry (LC/MS)

Table S1. Gradient of solvents used for cholesterol and CER analysis by UPLC-LC/MS.

Run time (min)	Solvent A[1] (%)	Solvent B[2] (%)
0	98	2
2.5	96	4
2.6	93	7
6	88	12
11	50	50
13	98	2

[1]**Solvent A - 100% Heptane**

[2]**Solvent B -Heptane:isopropanol:ethanol - 50:25:25; v/v/v**

Table S2. Gradient of the solvents used for FFA analysis by UPLC-LC/MS.

Run time (min)	Solvent A[1] (%)	Solvent B[2] (%)
0	100	0
2.5	0	100
5	0	100
8	100	0
11	100	0

[1]Solvent A - Acetonitrile/milliQ/chloroform/acetic acid -90:10:2:0.005; v/v/v/v

[2]Solvent B -Methanol/heptane/chloroform/acetic acid -90:10:2:0.005; v/v/v/v

1.3. Quantitative real-time PCR (q-PCR)

Table S3. Forward and reverse primer sequences used for q-PCR.

Protein (Gene)	Forward primer Reverse primer
Ribosomal protein, large, P0 (RPL0)	CTGAGTACACCTTCCCACTTACTGA CGACTCTTCCTTTGCTTCAGCTTT
Cytochrome c-1 (CYC1)	ACTGGGGTGTCATTGCGAGAAGGC GGTCATGCTCTGGTTCTGATGCCCA
Ribosomal protein S20 (RPS20)	GGACTTGATCAGAGGCGCCAAGGAAA CCCAGGTCTTGGAACCTTCACCACAA
Acetyl-Coenzyme A carboxylase alpha (ACACA)	GGAAGATGGCGTCCGCTCTGTG GTGAGATGTGCTGGGTCATGTGGAC
ATP-binding cassette, subfamily A, member 1 (ABCA1)	AGAGCAAAAAGCGACTCCACATAGAA CGGCCACATCCACAACTGTCT
ATP-binding cassette, subfamily A, member 12 (ABCA12)	TGACCTTCTGGAAACCAACAAGACTGC CACTTATGGTGGAACCTTGGCTACTGG
ATP-binding cassette, subfamily G, member 1 (ABCG1)	TTGACACCATCCCAGCCTAC CAGTGCAGGTCTTCTCGGT
Aldehyde dehydrogenase family 3, subfamily A2 (ALDH3A2)	CGGGTGATAGATGAGACCTCCAGTGG AGGGGCGCTGATGAGAAAAGGTATCA
N-acylsphingosine amidohydrolase 1 (ASAH1)	TTATTGATGACCGCAGAACACCGGC TACAAGGGTCTGGGCAATCTCGAAGG
Cluster of differentiation 36 (CD36)	ATGGTAGAGATGGCCTTACTTGGG AGATGTAGCCAGTGTATATGTAGGCTC
Cluster of differentiation 68 (CD68)	TGCCTGACAAGGGACACTTCGGG GCGGGTGATGCAGAAGGCGATG

Protein (Gene)	Forward primer Reverse primer
Ceramide kinase 1 (CERK1)	CTTGCTCAGCCTCCAGAAGCTCCT TCCTGGGCTTTGGGGTTCTTGCTTA
Ceramide synthase 3 (CERS3)	GGGCCTCCACGTTTACTGGGGT GCCCTTGGTGCTCTCTGCTTCCT
Elongation of very long chain fatty acids 1 (ELOVL1)	GGCAGAACTTGCCCCTGAGAAGAA TTCACAACAGCCTCCATCCTGGC
Elongation of very long chain fatty acids 4 (ELOVL4)	TGGAATCAAGTGGGTGGCTGGAGG AGCATGGTCAGGTATCGCTTCCACC
Elongation of very long chain fatty acids 6 (ELOVL6)	GGACCTGTCAGCAAATTCTGGGCTTA GGAGTACCAGGAGTACAGGAGCACA
Elongation of very long chain fatty acids 7 (ELOVL7)	ACAGCTGTGCACGTGGTCATGTATTC ACTGGGTACTGGTAATTGCAGTCCTCC
Fatty acid binding protein 5 (FABP5)	GGACGGGAAGGAGAGCACGATAACA GCACCTTCTCATAGACCCGAGTGCA
Fatty acid synthase (FAS)	GGCGGCACCTATGGCGAGG CTCCAGCAGTGTGCGGTGGTC
Fillagrin (FLG)	TTCTCAGAAGGCCAGGCAGTAGGAG CGCGTTGCTGTTCGTGCTGG
Glucocerebrosidase (GBA)	GCCCTTGCCAACAGTTCCCATGATG TGCCATGAACGTACTTAGCTGCCTCT
2-hydroxyacyl-CoA lyase 1 (HACL1)	GGTTTTGACGCTGACACCTGGGAAA CCTCAGCGAGTGTTGGAGCTCTTCT
3-hydroxy-3-methylglutaryl-CoA reductase (HMGCR)	CGAGCCACGACCTAATGAAGAATG TGCATCACTAAGGAACTTTGCACC
Interferon gamma (IFNG)	CCTTCTTCAGCAACAGCAAGGCGA GCGCTGGACCTGTGGGTTGT
Involucrin (IVL)	CCTCTGCCTTCTCCCTCCTGTGAGT ACACAGTCTTGAGAGGTCCCTGAACCA
Keratin 10 (K10)	GCGGCGACCAATCATCTAAAGGACC CCAGTGGCCCGTATGAAGAGACTCT
Antigen identified by monoclonal antibody Ki 67 (MKI67)	TCTGTGGAAGAGCAGGTTAGCACTGT TGGGCCTTGGCTGTTTTACATTGGTT
low density lipoprotein receptor (LDLR)	TGTGTGATGGAGACCGAGATTG CGTCAACACAGTCGACATCC
Stearoyl-Coenzyme A desaturase 1 (SCD1)	TACTACAAGCCCGGCCTCC CAGCAGTACCAGGGCACCA
Tumor necrosis factor alfa (TNFA)	GCCTCTTCTCATTCCTGCTTGTG ATGATCTGAGTGTGAGGGTCTGG
Tryptase alpha/beta 1 (TPS1)	ACCCTGTCCCCCTACCTCCT AATGGGAACTTGCACCTCCTTCAAA
Tryptase beta 2 (TPS2)	GCGGAGGTTCTCTCATCCATCCA CTGCTCACGAAGCTGCACCC

2. RESULTS

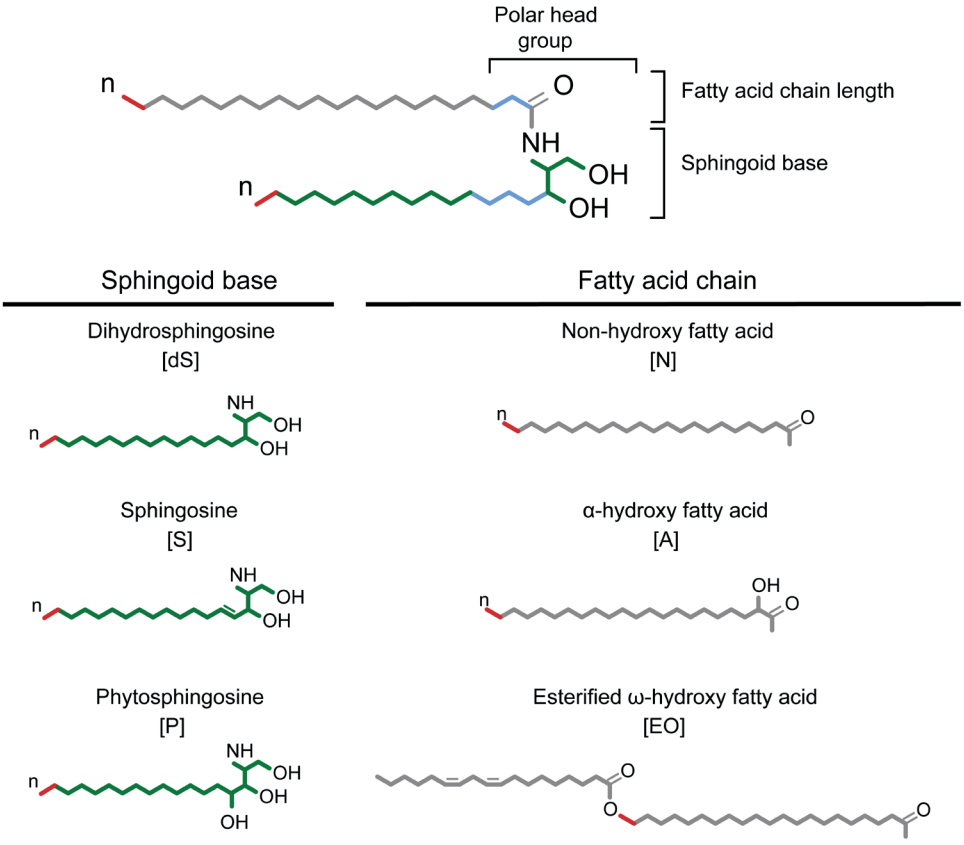

Figure S1. Schematic overview of a CER molecular structure and summary of the CER subclasses present in the epidermis of WT, *LDLR*$^{-/-}$ and *APOE*$^{-/-}$ mice. CERs consist of an acyl chain (in grey) and a sphingoid base (green), which can both vary in number of carbons (n; indicated in red). Nomenclature of ceramides subclasses (Motta *et al.* 1993)[1] based on different fatty acid acyl chains (non-hydroxy fatty acid [N]; α-hydroxy fatty acid [A]; esterified ω-hydroxy fatty acid [EO]) and on the sphingoid base (dihydrosphingosine, [dS]; sphingosine [S]; phytosphingosine [P]).

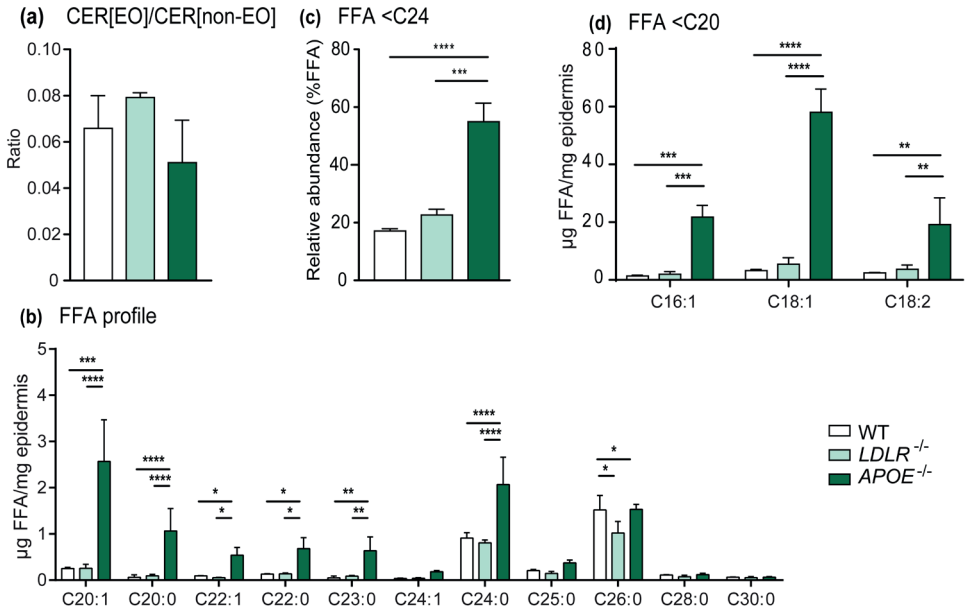

Figure S2. LC/MS analysis of WT, *LDLR*$^{-/-}$ and *APOE*$^{-/-}$ epidermal lipids. (a) Ratio CER[EO]/CER[non-EO], (b) absolute amounts FFA with chain length between C20-C30 per mg epidermis, (c) relative abundance of FFA with chain length below 24 carbon atoms, and (d)absolute amounts of FFA with chain length lower than 20 carbon atoms (n= 3 animals/group). FFA C16:0 and FFA C18:0 were not quantified due to manufacturer's contamination of the solvent with these FAs. Differences among groups were determined by One-way or Two-way ANOVAs using Holm-Šídák post-hoc test and represented as mean ± SD; *p<0.05, **p <0.01, ***p<0.001 and ***p<0.0001).

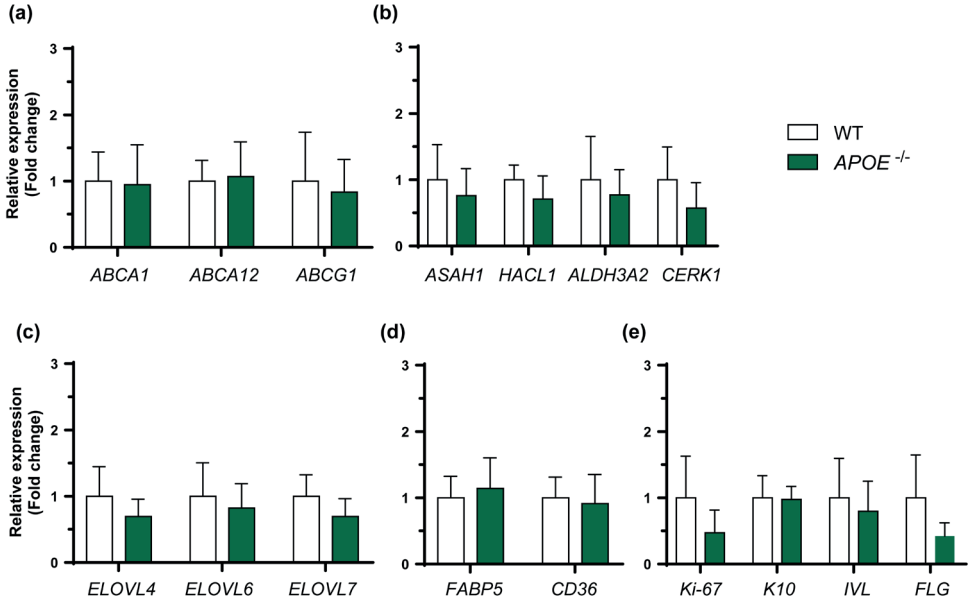

Figure S3. q-PCR of murine skin. mRNA expression of (a) ABC transporters, (b) ceramide degradation enzymes, (c) FFA elongases, (d) FFA transporters, and (e) keratinocyte proliferation and differentiation markers. Genes measured and encoded proteins: ABCA1 – ATP binding cassette class A member 1; ABCA12 – ATP binding cassette class A member 12; ABCG1 – ATP binding cassette class G member 1; ASAH1 – N-acylsphingosine amidohydrolase 1; HACL1 – 2-hydroxyacyl-CoA lyase 1; ALDH3A2 – Aldehyde dehydrogenase family 3, subfamily A2; CERK1 – Ceramide kinase 1; ELOVL4 – elongase of very long chain fatty acid 4; ELOVL6 – elongase of very long chain fatty acid 6; ELOVL7 – elongase of very long chain fatty acid 7; FABP5 – fatty acid binding protein 5; CD36 – cluster of differentiation 36; mitosis Ki-67 – Marker Of Proliferation Ki-67, K10 – early differentiation marker keratin 10, IVL – late differentiation marker involucrin; FLG – late differentiation marker filaggrin (n=6 animals/group). Statistical analysis by two-tailed unpaired students T-tests. Data presented as mean ± SD; no significant differences (p<0.05) were observed.

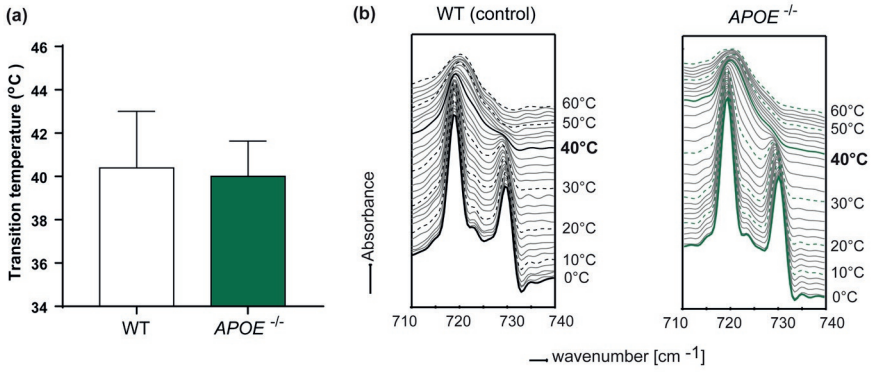

Figure S4. FTIR analysis of epidermal lipids in the skin of WT and *APOE*$^{-/-}$ mice. (a) Average transition temperature (TT) between orthorhombic and hexagonal phases determined by disappearance of the peak at 730 cm^{-1}, (b) CH_2 rocking vibrations plotted as a function of temperature (0-60°C) with TT marked in bold. (n= 4-5 animals/group). Differences between groups were determined by determined by two-tailed unpaired students T-tests. Data is presented as mean ± SD; no significant differences (p<0.05) were observed.

REFERENCES

1. Motta, S. *et al.* Ceramide composition of the psoriatic scale. BBA - Mol. Basis Dis. 1182, 147–151 (1993).

Chapter 3

Hyperalphalipoproteinemic scavenger receptor BI knockout mice exhibit a disrupted epidermal lipid barrier

Biochimica et Biophysica Acta Molecular and Cell Biology of Lipids 1865(3): 158592 (2020).

Renata Martins Cardoso[1], Eline Creemers[1], Samira Absalah[1], Gert S. Gooris[1], Menno Hoekstra[1], Joke A. Bouwstra[1*], Miranda Van Eck[1*]

[1]Division of BioTherapeutics, Leiden Academic Centre for Drug Research, Leiden University, Leiden, The Netherlands

*Both authors contributed equally

ABSTRACT

Scavenger receptor class B type I (SR-BI) mediates the selective uptake of cholesteryl esters (CE) from high-density lipoproteins (HDL). An impaired SR-BI function leads to hyperalphalipoproteinemia with elevated levels of cholesterol transported in the HDL fraction of the plasma. Accumulation of cholesterol in apolipoprotein B (apoB)-containing lipoproteins has been shown to alter skin lipid composition and barrier function in mice. To investigate whether these hypercholesterolemic effects on the skin also occur in hyperalphalipoproteinemia, we compared skins of wild-type and SR-BI knockout (*SR-BI*$^{-/-}$) mice. SR-BI deficiency did not affect the epidermal cholesterol content and induced only minor changes in the ceramide subclasses. The epidermal free fatty acid (FFA) pool was, however, enriched in short and unsaturated chains. Plasma CE levels strongly correlated with epidermal FFA C18:1 content. The increase in epidermal FFA coincided with downregulation of cholesterol and FFA synthesis genes, suggesting a compensatory response to increased flux of plasma cholesterol and FFAs into the skin. Importantly, the *SR-BI*$^{-/-}$ epidermal lipid barrier showed increased permeability to ethyl-paraminobenzoic acid, indicating an impairment of the barrier function. In conclusion, increased HDL-cholesterol levels in *SR-BI*$^{-/-}$ can alter the epidermal lipid composition and lipid barrier function similarly as observed in hypercholesterolemia due to elevated levels of apoB-containing lipoproteins.

Keywords: *High-density lipoprotein, hypercholesterolemia, hyperlipidemia, cholesteryl esters, epidermis, skin lipid metabolism, free fatty acids*

1. INTRODUCTION

Lipids are important components of the epidermal stratum corneum (SC), where they form a well-structured lipid matrix that functions as a protective barrier preventing dehydration and the penetration of pathogens and dangerous agents[1]. Cholesterol, ceramides (CERs), and free fatty acids (FFAs) are the main lipid classes present in the SC and are primarily synthesized by differentiating keratinocytes in the epidermis[2]. At the final stage of keratinocyte differentiation, these lipids are extruded into the intercellular space at the interface of the stratum granulosum and the SC and processed to form the SC lipid matrix[3].

Lipids of extracutaneous origin (*e.g.* plasma lipids) may also contribute to the formation of the matrix of SC lipids[4–7]. In plasma, lipids are primarily transported in the core of 4 classes of lipoproteins; chylomicrons, very-low-density lipoproteins (VLDL), and low-density lipoproteins (LDL), and high-density lipoproteins (HDL). Expression of the low-density lipoprotein receptor (LDLR), the apolipoprotein (apo) B/E receptor, in the liver is essential for maintaining normal plasma lipid levels transported by apoB-containing lipoproteins (chylomicrons, VLDL, LDL) and, hence, mutations in the LDLR leads to hyperlipidemia[8–10]. Recent work from our group showed that severe hypercholesterolemia associated with accumulation of apoB-containing lipoproteins can alter the composition of the epidermal lipids and the skin barrier function in mice[11]. Currently, it remains unknown whether the observed effects are specific for apo B-containing lipoproteins.

HDL represents a second important group of lipoprotein particles involved in the transport of cholesterol throughout the body, especially mediating reverse cholesterol transport. HDL particles interact with the ATP-binding cassette transporters ABCA1 and ABCG1[12] to promote cellular efflux of excess cholesterol, which is subsequently stored as cholesteryl esters (CE) in the core of these lipoproteins after esterification by the enzyme lecithin: cholesterol acyl transferase (LCAT)[13]. CE from mature HDL particles can be delivered via the scavenger receptor class B type I (SR-BI) to steroidogenic tissues for hormone production or to the liver to be redistributed to the body or excreted via the bile, the last step in the reverse cholesterol transport process[14,15].

SR-BI is a transmembrane glycoprotein that interacts with HDL and various native and modified lipoproteins (*e.g.* β-VLDL, oxidized LDL)[16,17]. In addition to its high expression in the liver and in steroidogenic tissues, SR-BI, like the LDLR, is also expressed in the epidermis; especially in keratinocytes in the basal epidermal layer close to the vascular bed in the dermis[4,7,18,19]. The expression of this receptor decreases towards the skin

surface but is increased in case of barrier disruption or inhibition of local synthesis by statins[4,7]. In contrast with apoB-containing lipoproteins, which deliver their lipid content via receptor mediated uptake, smaller HDL particles can more efficiently move through tissues (plasma to interstitial fluid) and get into the skin[20]. In fact, the skin is one of the largest body reservoirs of HDL[21].

In both mice and humans, impaired reverse cholesterol transport due to deficiency or polymorphisms in the gene encoding for SR-BI results in hyperalphalipoproteinemia marked by an accumulation of larger and abnormal HDL particles and increases HDL-cholesterol in the circulation[10,22,23]. Among others, HDL-driven hyperalphalipoproteinemia, a special form of hypercholesterolemia, has been related to altered platelet function[24,25] and reduced steroidogenesis[23,26,27].

In this study, we aimed to investigate whether hyperalphalipoproteinemia and the associated increase in HDL-cholesterol would affect the skin lipid barrier. For this purpose, we compared the skin of *SR-BI* knockout (*SR-BI*$^{-/-}$) mice, a model for hyperalphalipoproteinemia, to the skin of wild-type (WT) control mice of similar age and genetic background. Hereto, we assessed the skin morphology, the composition and organization of the epidermal lipids, and the lipid barrier function. The experimental mice were fed a low fat/low cholesterol diet as we aimed to specifically analyze the effects of HDL-driven hyperalphalipoproteinemia in absence of high fat/high cholesterol diet-induced increases in apoB-containing lipoproteins.

2. MATERIALS AND METHODS

2.1 Chemicals

Rodent chow diet low in fat and cholesterol (Rat and Mouse No.3 breeding diet) was purchased from Special Diets Services (United Kingdom). We obtained ketamine and atropine from AUV Veterinary Services (Cuijk, The Netherlands) and xylazine from ASTFarma (Oudewater, The Netherlands). Sodium phosphate dibasic (Na_2HPO_4), hematoxylin, eosin, toluidine blue, trypsin from bovine pancreas, trypsin inhibitor, cholesterol, FFA with carbon chains ranging from 16 to 30 carbon atoms (FFA C16-30), deuterated FFA C18, deuterated FFA C24, chloroform, acetic acid, deuterated water, natrium bromide (NaBr), ethyl-para-aminobenzoic acid (E-PABA), trifluoroacetic acid, synthetic CER N(24)dS(18), CER N(24)S(18), CER N(24)P(18), and CER A(24) S(18) were obtained from Sigma-Aldrich (Zwijndrecht, The Netherlands). Synthetic CER E(18:2)O(30)S(18) and CER[N(C24deuterated)S(C18protonated)] were kindly provided by Evonik Industries (Essen, Germany). Sodium chloride (NaCl) and Kaiser's

glycerol gelatin were purchased from Boom (Meppel, The Netherlands). Heptane was purchased from ChemLab (Zedelgem, Belgium). Potassium dihydrogen phosphate (KH_2PO_4), potassium chloride (KCl) and Entellan® were purchased from Merck (Darmstadt, Germany). Methanol, ethanol, isopropanol and acetonitrile were purchased from Biosolve (Valkenswaard, The Netherlands). All solvents used were analytical grade.

2.2 Animals

Female C57Bl/6 WT mice were obtained from The Jackson laboratory and bred at the Gorlaeus laboratories. Female homozygous *SR-BI*$^{-/-}$ mice were kindly provided by Monty Krieger and cross-bred at the Gorlaeus laboratories to a C57Bl/6 background. The experimental WT group consisted of the same mice as reported previously[11]. The mice were kept under standard laboratory conditions at 20°C and with light cycle of 12 hours light/12 hours dark. The mice received water and standard low-fat chow diet ad libitum (Rat and Mouse No. 3 breeding diet). At 16-18 weeks of age the mice were anesthetized with xylazine (70 mg/kg body weight), atropine (1.8 mg/kg body weight), and ketamine (350 mg/kg body weight) followed by retro-orbital bleeding and perfusion with phosphate buffered saline (PBS, 8.13 g/L NaCl, 2.87 g/L Na_2HPO_4, 0.2 g/L KH_2PO_4, 0.19 g/L KCl in milliQ water pH 7.4) at room temperature. Blood was collected in EDTA-containing tubes. The dorsal skin of the mice was shaved and the skin was processed further for morphological stainings, lipid and gene expression analysis. All experiments were in agreement with National guidelines and approved by the Animal Experiments Ethics Committee of Leiden University.

2.3 Plasma lipid analysis

Non-fasted plasma levels of free cholesterol (FC), cholesteryl esters (CE) and triglycerides were measured by enzymatic colorimetric assays performed as described previously (Roche Diagnostics, Almere, Netherlands)[28].

2.4 Skin morphology staining

4-5 µm paraffin sections of skin were stained with hematoxylin and eosin or with toluidine blue as described previously[11]. Stained sections were mounted in Entellan® and imaged with a Zeiss Axioplan 2 light microscope (Zeiss, Best, The Netherlands). The presence of cholesterol crystals was verified using a BH-2 polarized microscope (Olympus, Leiderdorp, The Netherlands).

2.5 Liquid chromatography-mass spectrometry (LC/MS)

Skin samples without the hypodermis were stretched on a paper filter soaked in 0.3 % w/v trypsin solution in PBS (pH 7.4) overnight at low temperature (4°C). The next day, the skin was incubated at 37°C (1 hour) for trypsin activation and subsequently the epidermis was isolated. Afterwards, the trypsin in the samples was neutralized by washing the samples in 0.1% w/v trypsin inhibitor in PBS (pH 7.4) and in demi-water. After air-drying, the epidermis was stored under argon atmosphere for further SC lipid extraction followed by LC/MS analysis, and Fourier transform infrared spectroscopy (FTIR). Epidermal lipids were extracted as described by Boiten *et. al.* (2016) and the extracts were stored in chloroform:methanol (2:1; v/v) at 4°C under argon atmosphere for LC/MS-based cholesterol, CER and FFA analysis[29].

Cholesterol and CER analysis

Epidermal cholesterol and CER analysis by LC/MS was performed as described previously[11]. In short, epidermal lipid extracts (dried at 40°C under a gentle flow of nitrogen) were reconstituted to a lipid concentration of 0.3 mg/ml in heptane:chloroform:methanol (95:2.5:2.5; v/v/v). Deuterated CER[N(C24deuterated) S(C18protonated)] was added to all samples as internal standard. Reconstituted epidermal lipid extracts (5 µl) were injected using an Acquity UPLC H-class system (Waters, Milford, MA, USA). Separation was achieved on a normal phase column (PVA-Sil column: 5 µm particle size, 100x2.1 mm i.d., YMC, Kyoto, Japan) with an eluent flow rate of 0.8 ml/min (Supplementary Table S1). The UPLC system was connected to a XEVO TQ-S mass spectrometer (Waters, Milford, MA, USA) with an atmospheric pressure chemical ionization (APCI) chamber. Samples were measured with positive ion detection mode for full scans (350-1200 amu) and the area under the curve (AUC) was determined using Waters MassLynx 4.1 software and corrected for the internal standard. Cholesterol data was plotted as absolute amount of cholesterol per epidermis weight (µg/mg) based on a calibration curve of cholesterol. CER composition data was plotted as relative percentage of each ceramide subclass based on AUC values corrected for internal standard. This method can underestimate the level of [EO] subclasses. CERs nomenclature as described by Motta *et al.* (1993) depicting the acyl chains (non-hydroxy fatty acid [N]; α-hydroxy fatty acid [A] or esterified ω-hydroxy fatty acid [EO]) and the sphingoid base (dihydrosphingosine, [dS]; sphingosine [S] or phytosphingosine [P])[30].

FFA analysis

Epidermal FFA analysis by LC/MS was performed using the same UPLC/MS system described above. Epidermal lipid extracts (dried at 40ºC under a gentle flow of nitrogen) were reconstituted in isopropanol to a lipid concentration of 0.75 mg/ml. Next, internal standards deuterated FFA C18 and deuterated FFA C24 were added to the samples. Reconstituted lipid extracts (2 µl) were injected in the UPLC system into a Purospher Star LiChroCART reverse phase column (3 µm particle size, 55x2 mm i.d., Merck, Darmstadt, Germany) with an eluent flow rate of 0.5 ml/min (Supplementary Table S2). The XEVO TQ-S mass spectrometer coupled to the APCI (probe temperature: 425°C, discharge current 3 µA.) was set to negative ion mode and the detector measured full scans (200-550 amu). Data was analyzed using Waters MassLynx 4.1 software to determine the AUC. The AUC was corrected for the internal standard FFA C24 and calculated to absolute amounts based on calibration curves of FFA C16-C30. FFA composition was plotted in absolute amounts and as relative percentage to the total amount FFA detected (%w/w). FFA C16:0 and C18:0 were not plotted as they were present in the solvent used for lipid extraction due to manufacturer's contamination with these FAs. Unsaturated FFA C16-C18, important components of sebum lipids, were plotted separately[31,32].

2.6 CER fragmentation by (LC/)MS/MS

Murine CERs present in the epidermal lipid extract (in chloroform-methanol 2:1) were separated using the UPLC-H class system described above for CER analysis while maintaining a continuous solvent flow of 98% heptane and 2% heptane:isopropanol:ethanol (50:25:25; v/v/v) at 0.8 ml/min. Fragmentation spectra (MS/MS) of murine epidermal CERs were obtained using the XEVO TQ-S mass spectrometer. The collision energy for MS/MS was set to 30 eV. All other parameters of the XEVO TQ-S mass spectrometer were identical to the setup described for CER analysis. Parent ions with masses of 647, 653 and 663 amu were fragmented and identification of the fragments was performed using Waters MassLynx 4.1.

2.7 q-PCR

Total RNA was isolated from skin samples after removal of the hypodermis using the guanidinium thiocyanate method[33]. 1 µg of RNA was used to synthesize cDNA using M-MuLV reverse transcriptase. SYBR Green Technology was used for the quantitative gene expression analysis with a 7500 Fast real-time PCR system (Applied Biosystems, Foster City, CA, USA). Gene expression was normalized by the expression of the

housekeeping genes ribosomal protein, large, P0 (*RPL0*), cytochrome c-1 (*CYC1*) and ribosomal protein S20 (*RPS20*). Relative gene expression was determined as the difference between the average threshold cycle (Ct) of the housekeeping genes and the Ct of the target gene followed by raising this difference to the power of 2. The expression of target genes in the *SR-BI*$^{-/-}$ skin were plotted as relative fold change compared to the WT controls. Forward and reverse primer sequences of the housekeeping genes and genes of interest are available in Supplementary Table S3.

2.8 Fourier transformed infrared spectroscopy

Epidermis was hydrated for 24 hours over 27% sodium bromide in deuterated water and placed between two silver bromide windows for Fourier transform infrared spectroscopy (FTIR) measurements (Varian 670-IR spectrometer, Agilent Technologies, Inc., Santa Clara, CA). The spectrometer was equipped with a broad-band mercury cadmium telluride detector. FTIR spectra (600-4000 cm^{-1}) were collected within a temperature range from 0-90°C rising at a rate of 0.5°C/min. Deconvolution of the spectra (half width of 4 cm^{-1}; enhancement factor of 1.7) was processed with Resolutions Pro 4.1 (Varian Inc.) software. Lateral organization of the SC lipids was monitored by CH_2 rocking vibrations (710-750 cm^{-1}). The ratio between the peak area at 730 cm^{-1} and the area peak at 719 cm^{-1} was used to assess changes in the fraction of lipids adopting the orthorhombic phase at 32°C (skin temperature). This area ratio was calculated by curve fitting these two main peaks in the region of CH_2 rocking vibrations of the FTIR spectra using a Lorentzian peak function. The transition temperature between the orthorhombic and hexagonal phases was determined by the disappearance of the vibration at the 730 cm^{-1}.

2.9 Transepidermial water loss (TEWL)

Transepidermal water loss (TEWL) was measured in the skin of WT and *SR-BI*$^{-/-}$ mice to assess the barrier the skin barrier function. For TEWL measurements the mice were anesthetized as described on section 2.2 and their dorsal skin was shaved. The closed-chamber of the evaporimeter (Aqua Flux AF200, Biox Systems Ltd, London, UK) was placed in upright position on their dorsal skin perpendicular to the skin surface. Transepidermal water loss was measured for 120 seconds. The temperature in the room (22°C) and the humidity (50.1%) were controlled during the measurements.

2.10 Murine lipid model membranes (mLMM)

Murine lipid model membranes (mLMM) mimicking either the lipid composition of

the epidermis of WT or *SR-BI*$^{-/-}$ mice were prepared based on the lipid composition determined by LC/MS in this study. All mLMM were prepared with a CER mixture containing CER N(24)dS(18), CER N(24)S(18), CER N(24)P(18), CER A(24)S(18), CER E(18:2)O(30)S(18) in a molar ratio of 40.5:36:5:14.5:4, respectively. The FFAs were composed of FFA C16:0, C18:0, C20:0, C20:1, C22:0, C22:1, C24:0, C26:0 in a molar ratio representative of either WT or *SR-BI*$^{-/-}$ mice SC FFA composition (Table 1). Briefly, for mLMM preparation all lipids were collected in a glass vial, dried under a gentle nitrogen flow and reconstituted in hexane:ethanol (2:1; v/v) to a lipid concentration of 5 mg/ml. The lipid mixtures were sprayed under a gentle nitrogen flow onto a polycarbonate membrane (0.05 µm pore size, 25 mm i.d., Whatmann, Kent, UK) using a 100 µl Hamilton syringe, Bonaduz, Switzerland). Spraying (5 µl/min) was performed by a Camag Linomat IV with an extended y-axis arm (Muttenz, Switzerland) to form a homogeneous square of 10 x 10 mm. Sprayed mLMMs were equilibrated at 85°C for 10 minutes, cooled down to room temperature for storage under argon atmosphere until their use in the permeability studies.

Table 1. FFA composition of mLMM prepared for permeability studies.

FFA Standard	FFA WT (%Molar ratio)	FFA *SR-BI*$^{-/-}$ (%Molar ratio)
C16:0	3.5	4.0
C18:0	1.5	1.0
C20:0	2.0	5.5
C20:1	10.0	20
C22:0	4.5	5.5
C22:1	3.5	4.0
C24:0	30.0	29.0
C26:0	45.0	31.0

2.11 Lamellar and lateral organization of mLMM

X-ray diffraction studies (station BM26B, European Synchrotron Radiation facility, Grenoble, France) were used to determine both lamellar and lateral organization of the mLMM. After hydration (24 hours, 27% sodium bromide in demiwater) the mLMM were mounted into a sample holder (parallel to X-ray beam; X-ray wavelength of 0.1034 nm, sample-to-detector distance of 1980 mm) with the temperature controlled at 25°C.

Small angle X-ray diffraction data were collected on a Pilatus 1M detector (1043 × 981 pixels at 172 x 172 µm spatial resolution) calibrated using silver behenate (d = 5.838 nm). Wide angle X-ray diffraction data were collected on a Pilatus 300K (1475 × 195 pixels at 172 x 172 µm spatial resolution, sample-to-detector distance of 3110 mm) calibrated using the high density polyethylene (HDPE, d = 0.416 nm and 0.378 nm). The scattering intensity I (in arbitrary units) of the static diffraction patterns (collected for 60 seconds at two positions) was calculated as a function of the scattering vector q (in reciprocal nm). Vector q was determined as shown in Equation 1 with θ representing the scattering angle and λ the wavelength. Diffraction rings were integrated over an angle of 40°. The periodicity (d-spacing) of the lamellar phase was calculated as shown in Equation 2 using the the positions of a sequence of equidistant peaks (q_n) with n representing the order number of the diffraction peak.

$$\textit{Equation 1: } q = (4\pi \sin\theta)/\lambda$$

$$\textit{Equation 2: } d = 2n\pi / q_n$$

2.12 Permeability studies with mLMM

Ethyl-para-aminobenzoic (E-PABA) was used as a model drug to assess the functionality of the mLMMs as a lipid barrier. mLMMs were mounted into Permegear inline diffusion cells (0.282 cm^2 diffusion area, Bethlehem PA, USA). The donor phase was composed of saturated E-PABA solution (0.65 mg/ml, pH 5.0), while the acceptor phase was comprised of PBS (pH 7.4, stirring at 50 rpm, flow rate 2-2.5 ml/min). For 10 hours the acceptor PBS phase was collected in 1 hour fractions (Isco Retriever IV; Teledyne Isco, Lincoln NE, USA) and the E-PABA content was determined by UPLC-UV (Waters, Etten-Leur, The Netherlands) with acetonitrile with 0.1% trifluoroacetic acid:milliQ (40:60; v/v) as mobile phase (flow rate of 0.5 ml/min). Separation occurred in a reversed phase C18 column (Alltima, C-18, 1.7 µm i.d., 2.1 x 50 mm, Waters, Ireland) followed by UV detection (excitation wavelength = 286 nm). A calibration curve of E-PABA in methanol was included in the UPLC-UV analysis for E-PABA quantification. Data was analyzed with the software TargetLynx. Average steady-state fluxes were calculated as the average flux measured from 3.5 to 10.5 hours.

2.13 Statistical analysis

Statistical analysis was performed using GraphPad Prism 7 (GraphPad Software Inc., CA, USA). Data are presented as means±SD. Significant differences between groups were determined by two-tailed unpaired students t-Test. Correlations between parameters were determined using a Pearson's correlation coefficient analysis and linear regression.

P values below 0.05 were considered significant.

3. RESULTS

3.1 Plasma lipid profile and skin morphology

The plasma lipid profile of non-fasted female WT and *SR-BI*$^{-/-}$ mice was determined by enzymatic colorimetric assays (Figure 1a). On a low-fat chow diet SR-BI deficiency in mice generally results in increased plasma cholesterol levels driven by an increase in HDL-cholesterol[10]. In agreement, *SR-BI*$^{-/-}$ mice in this study displayed a hypercholesterolemic plasma lipid profile marked by a significant increase in FC (1.20±0.25 µg/µl plasma; $p<0.0001$) and CE (1.37±0.3 µg/µl plasma; $p<0.0001$) levels compared to normolipidemic WT controls (FC 0.36±0.05 µg/µl plasma; CE 0.85±0.08 µg/µl plasma). The levels of plasma triglycerides in *SR-BI*$^{-/-}$ mice did not differ from those of WT mice.

Next, we evaluated the morphology of the skin of the mice by hematoxylin and eosin or toluidine blue stainings of paraffin sections (Figure 1b). Similar to WT controls, the skin of *SR-BI*$^{-/-}$ mice showed a thin SC, no epidermal hyperproliferation, and no evidence of inflammation as illustrated by the absence of immune cell infiltrates. The morphology of the dermis was also not altered. Polarized microscopy did not reveal the presence of cholesterol crystals in the sections (data now shown).

3.2 Epidermal lipid composition

The three main barrier lipid classes (cholesterol, CERs and FFAs) in the epidermis of *SR-BI*$^{-/-}$ mice were analyzed by LC/MS and compared to WT controls. The amount of cholesterol in the *SR-BI*$^{-/-}$ epidermis (27.4±5.3 µg/mg epidermis) was comparable to the WT control (28.7±3.1 µg/mg epidermis) (Figure. 2a). In both WT and *SR-BI*$^{-/-}$ epidermis seven subclasses of CER were detected: CER NdS, CER NS, CER NP, CER AdS, CER AS, CER EOdS, and CER EOS (Figure 2b-c). In the epidermis of *SR-BI*$^{-/-}$ mice, the abundance of CER AS (10.8±0.6%) was lower than in the WT control (13.5±1.1%; $p<0.01$). In contrast, the abundance of CER EOS was increased in the *SR-BI*$^{-/-}$ epidermis (6.9±1.0%) compared to the WT epidermis (4.6±0.7%; $p<0.01$). CER NP and CER AdS were not fully separated in the ion map; thus, these CER subclasses were grouped together, accounting for nearly 5% of the total CER content in the epidermis of both types of mice. Interestingly, a slight increase in the average CER chain length was observed in the *SR-BI*$^{-/-}$ epidermis for the non-ω-esterified (CER[nonEO]) (42.3±0.1 carbon atoms) and for the ω-esterified (CER[EO]) (68.2±0.1 carbon atoms) CER subclasses compared to

the WT epidermis (42.0±0.1 and 67.5±0.1 carbon atoms, respectively; $p<0.005$) (Figure 2d-e and Supplementary Figure S1).

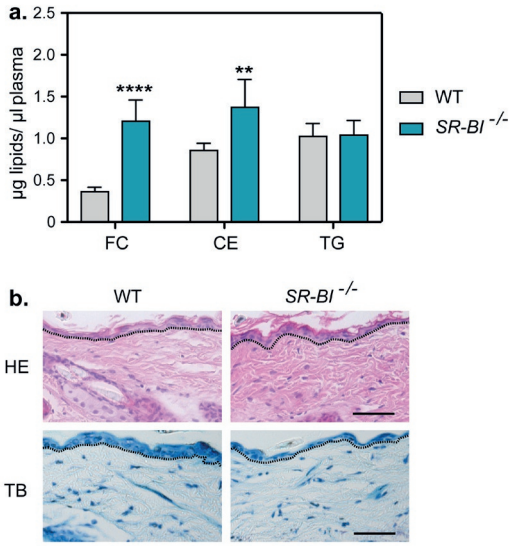

Figure 1. Non-fasted plasma lipids levels and skin morphology of WT and *SR-BI*$^{-/-}$ mice. a. Plasma levels of free cholesterol (FC), cholesteryl esters (CE), and triglycerides (TG) (n=5-6 animals/group). b. Representative paraffin sections of skin stained with hematoxylin and eosin (HE) or toluidine blue (TB). The interface between epidermis and dermis is marked by a black dashed line. Scale bar: 50 µm. Data shown as mean±SD. Significant differences between groups were determined by two-tailed unpaired student's t-Test. **$p<0.01$ and ****$p<0.0001$.

The CER chain length distribution revealed unusual abundance of CERs containing odd-numbered carbon chains (Figure 2d-e). In particular, CER[nonEO] containing 43 carbons atoms and CER[EO] containing 67 carbon atoms were abundantly present in both WT and *SR-BI*$^{-/-}$ epidermis. Further investigation with MS/MS fragmentation of CER NS C42 and CER NS C43, two CERs abundantly present in the epidermis, showed clear fragments for the fatty acid chain and the sphingosine base of these CERs as previously described[34]. For CER NS C42 with the parent ion $[M+H-H_2O]^+$ (m/z 632.3), fragments related to a fatty acid chain of 24 carbons atoms were detected at m/z 368.3 $[M+H-C_{16}H_{31}OH]^+$. Moreover, highly abundant fragments characteristic of a sphingosine base with 18 carbon atoms were found at m/z 252.3 $[M+H\text{-FA chain-}CH_3OH]^+$, 264.3 $[M+H\text{-FA chain-}H_2O]^+$ and 282.2 $[M+H\text{-FA chain}]^+$. Additionally, $[M+H\text{-FA chain-}H_2O]^+$ fragments, characteristic of sphingosine bases containing 16 and 17 carbon atoms, were detected at lower abundance at m/z

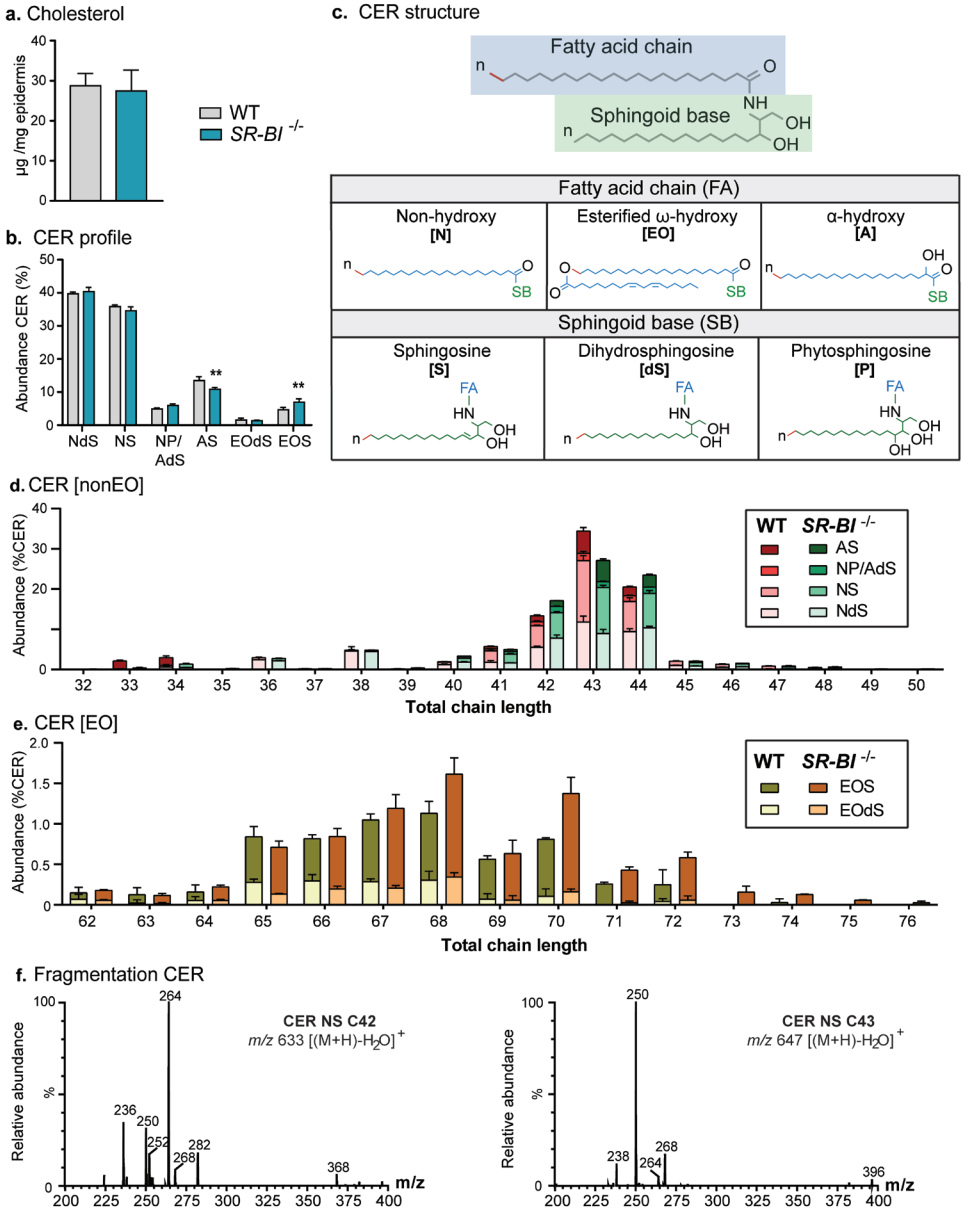

Figure 2. CER composition in the epidermis of WT and *SR-BI*$^{-/-}$ mice determined by LC/MS analysis. (a) Schematic representation of the molecular structure of CERs subclasses named as described by Motta *et. al.* (1993); (b) CER profile depicting the detected CER subclasses (NdS, NS, NP, AdS, AS, EOdS, EOS); (c) average total chain length of CERs with non-ω-esterified (CER[nonEO]) and ω-esterified (CER[EO]) fatty acid chains in their acyl chain; (d-e) CER chain length distribution of CER[nonEO] and CER[EO]; (f) MS/MS fragmentation of CER NS C42 and CER NS C43 showing an ion spectra in the range 200-700 m/z. Values are plotted as

mean±SD (n=3 animals/group). Statistical significance was determined by two-tailed unpaired student's t-Test. *p<0.05; **p<0.01.

236.1 and 250.1, respectively. In contrast, fragmentation of the CER NS C43 parent ion $[(M+H)-H_2O]^+$ at m/z 646.6 showed high abundance of fragments typical of a sphingoid base of 17 carbon atoms at m/z 238.1 $[M+H\text{-FA chain-}CH_3OH]^+$, 250.1 $[M+H\text{-FA chain-}H_2O]^+$, 268.1 $[M+H\text{-FA chain}]^+$. In addition, an abundant fragment of fatty acid with a chain of 26 carbons $[M+H-C_{18}H_{35}OH]^+$ was detected at m/z 396.2.

Epidermal FFA species with carbon chains ranging from 20-30 carbon atoms and abundant monounsaturated species were quantified by LC/MS (Figure 3a-b). Significant differences in the FFA profile between the *SR-BI*$^{-/-}$ mice and WT controls were detected. The epidermis of *SR-BI*$^{-/-}$ mice contained higher levels of FFAs with a chain length from 20 to 30 carbon atoms per mg of epidermis compared to WT controls (3.4±0.5 vs. 6.2±0.1 µg FFA/mg epidermis; p<0.01) (Figure 3c and Supplementary Figure S2). In the epidermis of both types of mice FFA C24:0 and FFA C26:0 were the most abundant FFA species. When focusing on the relative values (µg FFA/µg total FFA x 100%), FFA C26:0 represented 44% of the FFA species in the WT epidermis, while FFA C24:0 comprised 25% (Figure 3b). In contrast, in the epidermis of *SR-BI*$^{-/-}$ mice FFA C24 and FFA C26:0 were nearly equally abundant as a result of a strong reduction in the abundance of FFA C26:0 to only 28% (p<0.0001). Furthermore, the abundance of monounsaturated FFAs showed a 2-fold (p<0.05) increase in the *SR-BI*$^{-/-}$ epidermis (Figure 3d); in particular, FFA C20:1 (16%) was markedly increased compared to the WT controls (7.4%; p<0.0001). FFAs with a chain length containing less than 24 carbon atoms accounted for approximately 30% of the FFA species present in the epidermis of *SR-BI*$^{-/-}$ mice, while in WT mice these FFAs comprised 17% of FFAs (Figure 3e). As a result, the mean carbon chain length of the FFAs (including both saturated and unsaturated FFAs) in the *SR-BI*$^{-/-}$ mice was shorter than in the WT counterparts (Figure 3f; p<0.01).

3.3 Plasma cholesterol esters and skin FFA C18:1 and FFA C20:1 content

Our previous studies showed that the epidermis of hypercholesterolemic apolipoprotein E knockout mice (*APOE*$^{-/-}$) with severely elevated plasma CE levels is significantly enriched in FFA C18:1[11]. Likewise, in the current study *SR-BI*$^{-/-}$ mice with a mild increase in plasma CE exhibited higher levels of epidermal FFA C18:1 (Figure 4a). Therefore, the plasma CE concentration was plotted against the levels of FFA C18:1 in the epidermis of *SR-BI*$^{-/-}$mice (current study) and in the epidermis of *APOE*$^{-/-}$ mice (previously published study)[11]. The plasma CE levels WT and *SR-BI*$^{-/-}$ (moderately elevated CE) and

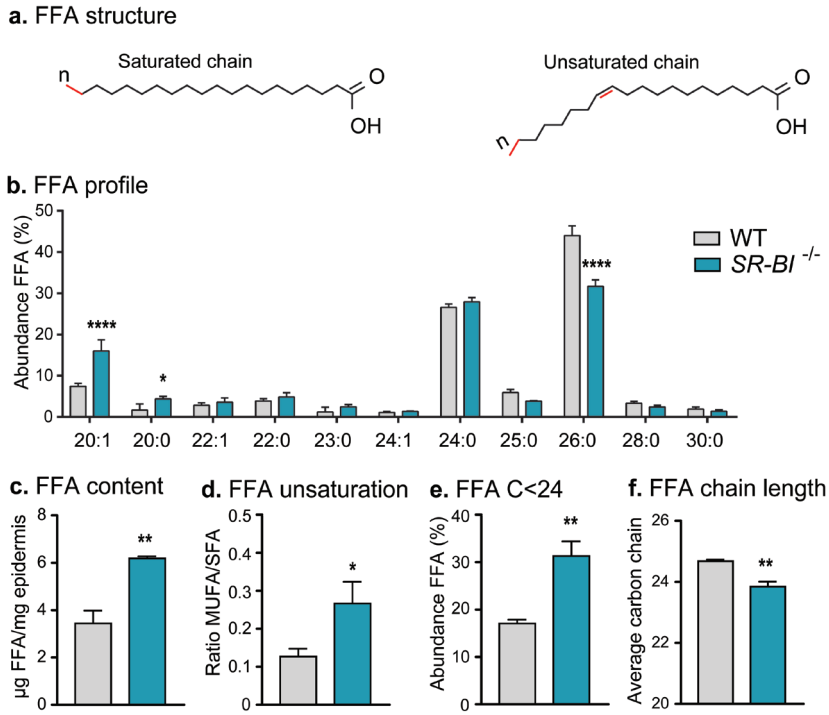

Figure 3. FFA composition in the epidermis of WT and *SR-BI*$^{-/-}$ mice determined by LC/MS analysis. (a) Schematic representation of the molecular structure of saturated and monounsaturated FFAs; (b) FFA profile; (c) Total FFA content (C20-C30) per mg of extracted epidermis; (d) FFA unsaturation ratio (MUFA-monounsaturated fatty acid, SFA- saturated fatty acid); (e) Abundance of FFA chains with less than 24 carbons atoms; (f) average FFA chain length. Values are plotted as mean±SD (n=3 animals/group). Statistical significance was determined by two-tailed unpaired student's t-Test. *p<0.05; **p<0.01; ****p<0.0001.

APOE$^{-/-}$ (severely elevated CE) showed a strong positive correlation with epidermal FFA C18:1 levels (Pearson's r = 0.9510, p<0.0001). In the epidermis FFA C18:1 can be elongated to FA C20:1[35]. Correspondingly, the epidermal levels of FFA C18:1 showed a significant linear correlation with the epidermal levels of FFA C20:1 (Pearson's r = 0.9448, p=0.0001; Figure 4c).

3.4 Skin gene expression

To gain insight in the effects and underlying causes of differences observed between the barrier lipid profile of WT control and *SR-BI*$^{-/-}$ mice, the expression of genes involved in skin lipid biosynthesis, uptake, efflux and degradation was analyzed by qPCR.

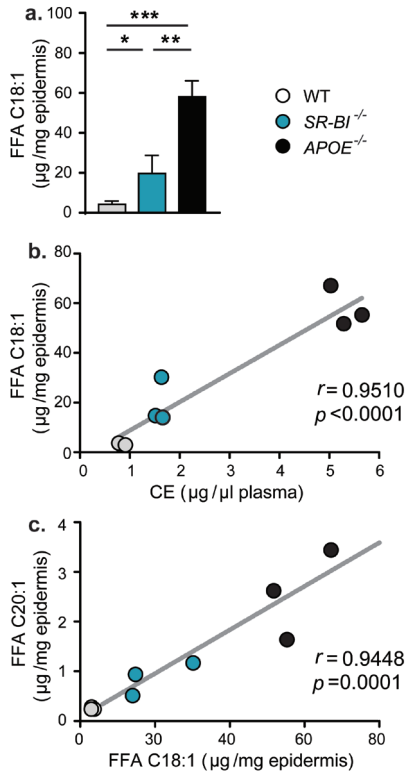

Figure 4. Correlation between plasma CE concentrations and unsaturated FFAs in the epidermis of WT, *SR-BI*$^{-/-}$ and *APOE*$^{-/-}$ mice. a. Epidermal levels of FFA C18:1; b. correlation between plasma CE concentration and epidermal FFA C18:1; c. correlation between epidermal FFA C18:1 and FFA C20:1. Plasma CE levels were determined by colorimetric enzymatic assays performed according to manufacturer's instructions. Epidermal FFA C18:1 and FFA C20:1 were determined by LC/MS analysis. Data regarding plasma CE, epidermal FFA C18:1 and FFA C20:1 levels of *APOE*$^{-/-}$ mice were obtained from a previous publication[11]. Data shown as mean±SD. Significant differences among groups were determined using One-way ANOVA with Holm-Šídák post-hoc test (*p<0.05; **p<0.01; ***p<0.001). Correlation between parameters was analyzed using Pearson's correlation analysis (r and p values) and linear regression (black line).

In the skin of *SR-BI*$^{-/-}$ mice the expressions of *HMGCS1* (cholesterol synthesis) and *LDLR* (lipoprotein uptake) were strongly downregulated (1.7-fold and 2.4-fold reduction, respectively) as compared to WT controls (p<0.05) (Figure 5a). For the CER metabolic pathways, comparable mRNA levels of *CERS3* (sphingolipid-based ceramice synthesis) were observed in the skin of WT and *SR-BI*$^{-/-}$ mice, while *GBA* (glucosylceramide metabolism) expression was reduced in the *SR-BI*$^{-/-}$ skin (1.6-

fold, p<0.05; Figure 5a). Regarding FFAs in the skin (Figure 5b), significantly lower mRNA levels of *ACACA* (2.1-fold; p<0.01) and *FAS* (1.7-fold; p<0.05), key enzymes in fatty acid synthesis, were detected in the *SR-BI*$^{-/-}$ skin, which was associated with a parallel reduction in the expression of *ELOVL1* (fatty acid chain elongation) (2.6-fold, p<0.05). *SCD1* expression (production of monounsaturated FFAs) in *SR-BI*$^{-/-}$ skin was equivalent to that observed in the WT controls. No significant differences were observed in the expression of genes encoding for ATP-binding cassette transporters, ceramide degradation enzymes and other elongases (Supplementary Figure S3). Despite the recently described *in vitro* effect of *SR-BI* knockdown on peroxisome proliferator-activated receptors[36], no differences on mRNA levels were noted for these genes in our experimental setting. In addition, in agreement with the morphological stainings, no significant differences were observed in the expression of genes related to keratinocyte proliferation and differentiation (*IVL, FLG, K10*) (data not shown).

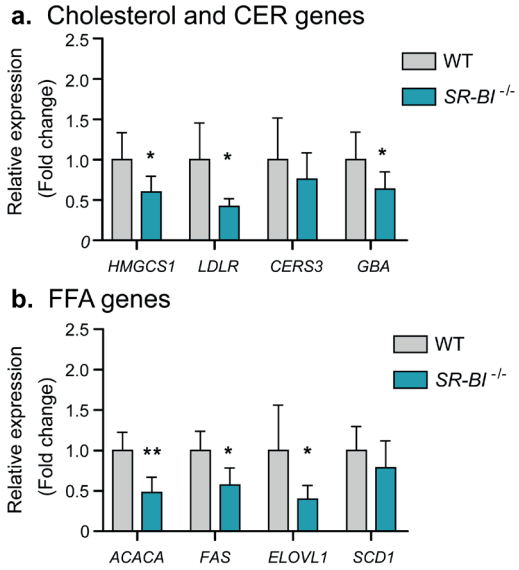

Figure 5. Effect of *SR-BI* deficiency on the expression of genes involved in lipid uptake and lipid synthesis in the skin. Relative mRNA expression levels of genes involved in (a) cholesterol and CER synthesis and (b) FFA synthesis. Genes and their respective encoded proteins/receptors: HMGCS1 - 3-hydroxy-3-methylglutaryl-Coenzyme A synthase 1; LDLR - low density lipoprotein receptor; CERS3 - ceramide synthase 3; GBA – glucocerebrosidase; ACACA - acetyl-Coenzyme A carboxylase alpha; FAS – fatty acid synthase; ELOVL1 - elongase of very long chain fatty acids 1; SCD1 - stearoyl-Coenzyme A desaturase 1. Values are plotted as mean±SD representing the fold change expression compared to the WT control (n=5-6 animals/group). Statistical significance was determined by two-tailed unpaired student's t-Test. *p<0.05; **p<0.01.

3.5 Lateral lipid organization

The epidermal lipid composition influences the lateral packing of these lipids, one of the determining parameters for the functionality of the skin barrier. The lateral lipid organization of the *SR-BI*$^{-/-}$ epidermis was analyzed by FTIR and compared to WT controls. In the spectrum region of the CH_2 rocking vibrations (710-740 cm^{-1}) a doublet at 710 cm^{-1} and at 730 cm^{-1}, indicative of a dense orthorhombic lateral lipid packing, was present in both WT and *SR-BI*$^{-/-}$ epidermis (Figure 6a). At 32°C (skin surface temperature) the fraction of lipids adopting an orthorhombic organization was comparable between the groups: a similar ratio between the peak area at 730 cm^{-1} and at 719 cm^{-1} was observed (Figure 6b). The orthorhombic to hexagonal transition temperature was determined by the disappearance of the peak at 730 cm^{-1} as a function of temperature. This transition temperature varied between 38°C and 44°C in both groups (Figure 6c).

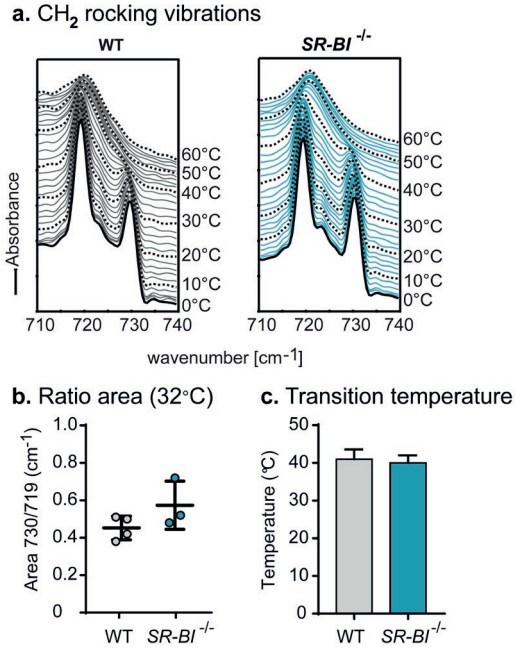

Figure 6. Lateral lipid organization in WT and *SR-BI*$^{-/-}$ epidermis. Lateral lipid organization was assessed by FTIR. (a) CH_2 rocking vibrations (710-740 cm^{-1}) were plotted as a function of temperature (0-60°C) to determine the lateral lipid packing; (b) area ratio between the peak at 730 cm^{-1} and the peak at 719 cm^{-1} at 32°C (skin surface temperature); (c) average transition temperature from orthorhombic and hexagonal phases. Values are plotted as mean±SD (n=3-4 animals/group). No statistical significant differences were observed by two-tailed unpaired student's t-Test.

3.6 Permeability studies using mLMMs

In non-nude mice, the isolation of SC or viable epidermis is hampered by the large number of hair follicles present in their skin. In addition, hair follicles may offer another route of permeation to compounds, which in turn compromises the analysis of the effects of the altered lipid barrier function[37,38]. Nonetheless, the inside-outside skin barrier function was analyzed *in vivo* by transepidermal water loss measurements; however, no differences were noted between *SR-BI*$^{-/-}$ (12.5±0.9 g/(m^{2}h)) and WT (12.5±0.7 g/(m^{2}h)) mice. Next, mLMMs were used as substitutes to investigate the specific impact of the altered epidermal FFA composition on the outside-inside lipid barrier function of *SR-BI*$^{-/-}$ mice. Small-angle X-ray diffraction showed that the lipids in the WT$_{LMM}$ and the *SR-BI*$^{-/-}_{LMM}$ were organized in both short and long periodicity phases (Figure 7a).

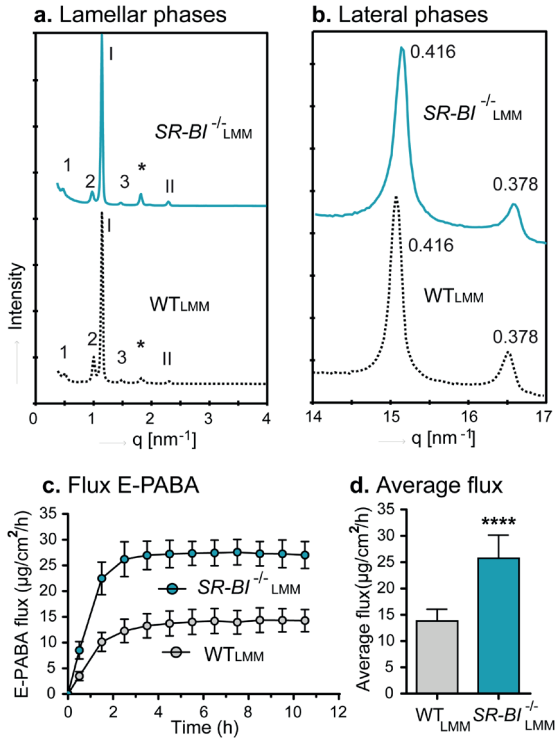

Figure 7. Lamellar and lateral lipid organizations in the WT$_{LMM}$ and *SR-BI*$^{-/-}_{LMM}$ and their permeability to E-PABA. a-b. Lamellar and lateral organizations of the mLMM were determined by small- and wide-angle X-ray diffraction studies, respectively. Long periodicity phase order indicated in Arabic numbers (1-3), short periodicity phase orders indicated in Roman numbers (I-II), and the reflection of crystalline cholesterol indicated with an asterisk (*). c. Permeability of WT$_{LMM}$ and *SR-BI*$^{-/-}_{LMM}$ to E-PABA over time. d. Average steady-state flux of E-PABA measured from 3.5-10.5 hours. Values are plotted as mean±SD; representative of three

different experiments (total n=6-7 mLMMs/group). Statistical significance was determined by two-tailed unpaired student's t-Test. ****p<0.0001.

The repeated distance of the long periodicity phase was increased in the *SR-BI*$^{-/-}_{LMM}$ compared to the WT_{LMM} (p<0.0001), but the short periodicity phase did not differ between both mLMM (Supplementary Figure. S4). Additionally, in both WT_{LMM} and the *SR-BI*$^{-/-}_{LMM}$ a high fraction of lipids in these synthetic models adopted an orthorhombic lateral packing characterized by the presence of two peaks at a position corresponding to a spacing of 0.416 nm and 0.378 nm in the wide-angle X-ray diffraction studies (Figure 7b). Next, the lipid barrier function of WT_{LMM} and the *SR-BI*$^{-/-}_{LMM}$ was assessed by measuring their permeability to E-PABA. The flux of E-PABA through both types of synthetic lipid membranes reached a steady-state after 3 hours (Figure 7c). In the steady-state, the *SR-BI*$^{-/-}_{LMM}$ showed nearly 2-fold higher permeability to E-PABA compared to the control WT_{LMM} (27.3±2.4 *vs*. 13.9±2.2 μg/cm^2/h, respectively; p<0.0001) (Figure 7d). At the end of the experiment, nearly 100% of E-PABA was recovered in all groups measuring the donor and acceptor phases (data not shown).

4. DISCUSSION

Despite the protective role of HDL in reverse cholesterol transport, we showed in this study that HDL-associated hyperalphalipoproteinemia can alter the epidermal lipid composition; thereby, negatively impacting the lipid barrier function of the skin. Additionally, these results support the hypothesis that the plasma levels of CE, independent of the type of lipoprotein carrier, play a crucial role in the maintenance of a proper skin barrier function.

Deficiency of SR-BI in mice impairs the clearance of HDL-CE from the circulation[39,40], which in turn leads to inhibition of LCAT activity and consequent FC accumulation[41]. Hence, *SR-BI*$^{-/-}$ mice, even on a low-fat/low cholesterol diet, develop a mild hyperalphalipoproteinemia characterized by increases in both FC and CE transported in the HDL fraction[10]. *In vitro*, *SR-BI* knockdown in human skin equivalents did not affect the cholesterol content of these skin models but led to downregulation of relevant lipid metabolism genes (*LDLR, PPAR-α, PPAR-γ*)[36]. Similarly, hyperalphalipoproteinemia in *SR-BI*$^{-/-}$ mice did not translate into changes in the epidermal cholesterol fraction in the skin of these mice. However, an increased flux of plasma cholesterol into their skin is expected as evidenced by downregulation of *LDLR* and *HMGCS1*; thereby, maintaining normal FC levels in the *SR-BI*$^{-/-}$ skin[11,42]. In addition, it is important to note that cholesterol

in the skin can be found as FC, CE, cholesterol sulfate and oxysterols[43,44]. In the SC, cholesterol sulfate comprises a minor fraction of the sterol content while FC is the major sterol component of the lipid matrix[45]. However, modified cholesterol species could not be measured with our LC/MS method and we cannot exclude that changes in the levels of these species contribute to the preserving the FC content in the SC.

As previously described in *APOE*$^{-/-}$ mice[11], unsaturated and short chain FFA species (below 24 carbons atoms) were strongly augmented in the epidermis of *SR-BI*$^{-/-}$ mice, which also showed downregulation of genes involved in FFA synthesis (*ACACA, FAS*) and elongation (*ELOVL1*) compared to WT controls. Although CERs and FFAs share biosynthetic pathways[46,47], the shift towards short chain and unsaturated FFA species in the *SR-BI*$^{-/-}$ epidermis did not result in a comparable profile in the CER composition, where only minor differences were observed in the percentage of a few subclasses compared to the WT controls. Thus, the altered FFA profile in the epidermal barrier of *SR-BI*$^{-/-}$ mice is likely not related to the biosynthetic pathway shared with CER but has rather an extracutaneous origin.

Analysis of the epidermal lipids also revealed increased amounts of FFA C18:1 in *SR-BI*$^{-/-}$ mice. As previously indicated, the LCAT activity is inhibited in the *SR-BI*$^{-/-}$ mice due to higher plasma levels of CE. Subbaiah *et. al.* (2013) demonstrated that low activity of LCAT in mice increases circulating levels of C16:0- and C18:1-containing CE, suggesting a direct link between C18:1-containing CE in plasma and elevated epidermal FFA C18:1[48]. The changes in the epidermal FFA species of the mild hypercholesterolemic *SR-BI*$^{-/-}$ mice showed a similar trend as that recently reported for the severely hypercholesterolemic *APOE*$^{-/-}$ mice[11]. In addition to their increased circulating CE concentrations, the epidermis of both *SR-BI*$^{-/-}$ and *APOE*$^{-/-}$ mice are enriched in FFA C18:1 and FFA C20:1, though to a lesser extend in the epidermis of *SR-BI*$^{-/-}$ mice. Simultaneous exposure of HaCaT keratinocytes to FFA C18:1 and 25-hydroxy cholesterol resulted in downregulation of HMGCoA synthase and a lower rate of acetate incorporation into FFA synthesis[42]. Hence, a higher flux of plasma CE into the epidermis of *SR-BI*$^{-/-}$ mice (similar to *APOE*$^{-/-}$mice) can be expected, which is also supported by the strong correlations between plasma CE and epidermal FFA C18:1 and the robust correlation between epidermal C18:1 and its elongated product FFA C20:1 in the epidermis.

Alterations in the epidermal lipid composition can affect the lipid organization and the functionality of the skin barrier[47]. In particular, short and unsaturated FFAs have been described to reduce the density of the lipid packing even in the presence of a similar CER composition[49,50]. Here, we analyzed the contribution of the altered lipid profile to the outside-inside lipid barrier function using LMMs. Our results show that a minor

increase in the short chain FFA fraction in LMMs can preserve the dense orthorhombic packing while increasing the mobility of the lipids within the lipid matrix, which in turn translates into a more permeable outside-inside lipid barrier[51]. In vivo transepidermal water loss measurements in *SR-BI*$^{-/-}$ mice revealed a functional inside-outside skin barrier despite the alteration in epidermal lipids (enriched in short chain FFAs). It is important to note that in the in vivo situation trans-corneocytes water transport, as well as hair follicles and other surface lipids will contribute to/influence the maintenance of transepidermal water loss levels. Hence, although the barrier lipids in the *SR-BI*$^{-/-}$ epidermis showed a dense orthorhombic organization, the lipid composition of the *SR-BI*$^{-/-}_{LMM}$ (enriched in short chain FFAs) resulted in a more permeable outside-inside lipid barrier.

Although SR-BI is expressed in both murine and human keratinocytes, its specific contribution to the skin lipid homeostasis is not yet clear due the lack of an *in vivo* keratinocyte-specific knockout mouse model. Recent data from a study using *SR-BI* knockout human skin equivalents suggests an involvement of SR-BI in lipid regulation in the upper epidermal layer; in particular in CER metabolism[36]. In our study, the CER composition was preserved in the total body *SR-BI*$^{-/-}$ mice while both cholesterol and FFA metabolism were shifted to a compensatory gene expression profile. This indicates that the hyperalphalipoproteinemia rather than the local absence of SR-BI in the skin may be the driving factor to the observed changes in epidermal lipids in these mice.

In conclusion, this study shows that hypercholesterolemia-related to elevated circulating levels of HDL particles alters the epidermal lipid composition, resulting in a compromised lipid barrier function in young adult *SR-BI*$^{-/-}$ mice on a low fat chow diet. In addition, a clear correlation between plasma CE levels and epidermal levels of FA C18:1 and FA C20:1 in hypercholesterolemic mice indicates that increased circulating CE may have a decisive role in the development of this skin phenotype. Although to date skin related problems have not been described in patients with SR-BI polymorphisms or hyperalphalipoproteinemia, this study demonstrates the relevance of analyzing the SC lipid composition in these patients to prevent the development of upcoming abnormalities in the functionality of the skin barrier.

CONFLICT OF INTEREST

The authors have no conflict of interest to declare regarding the content of this research article.

ACKNOWLEDGEMENTS

We thank the support of the DUBBLE beam line personnel in performing the X-ray diffraction studies at the European Synchrotron Radiation Facility (Grenoble, France), and the company Evonik (Essen, Germany) for providing us the synthetic ceramides used in our LC/MS analysis and in the preparation of our LMMs. We also thank Walter Boiten and Andreea Nădăban for their assistance with the interpretation of the MS/MS fragmentation data and Miréia N. A. Bernabé Kleijn for her assistance with transepidermal water loss measurements. This research was funded by the Leiden Academic Centre for Drug Research (Leiden, The Netherlands).

REFERENCES

1. Elias, P. M. Stratum corneum defensive functions: An integrated view. J. Invest. Dermatol. 125, 183–200 (2005).

2. Ponec, M., Weerheim, A., Lankhorst, P. & Wertz, P. New acylceramide in native and reconstructed epidermis. J. Invest. Dermatol. 120, 581–588 (2003).

3. Rassner, U., Feingold, K. R., Crumrine, D. A. & Elias, P. M. Coordinate assembly of lipids and enzyme proteins into epidermal lamellar bodies. Tissue Cell 31, 489–498 (1999).

4. Tsuruoka, H. et al. Scavenger receptor class B type I is expressed in cultured keratinocytes and epidermis. Regulation in response to changes in cholesterol homeostasis and barrier requirements. J. Biol. Chem. 277, 2916–2922 (2002).

5. Khnykin, D., Miner, J. H. & Jahnsen, F. Role of fatty acid transporters in epidermis. Dermatoendocrinol. 3, 53–61 (2011).

6. Haruta-Ono, Y. et al. Orally administered sphingomyelin in bovine milk is incorporated into skin sphingolipids and is involved in the water-holding capacity of hairless mice. J. Dermatol. Sci. 68, 56–62 (2012).

7. Abd El-Latif, M. I. A., Murota, H., Terao, M. & Katayama, I. Effects of a 3-hydroxy-3-methylglutaryl coenzyme A reductase inhibitor and low-density lipoprotein on proliferation and migration of keratinocytes. Br. J. Dermatol. 128–137 (2010). doi:10.1111/j.1365-2133.2010.09694.x

8. Accad, M. et al. Massive xanthomatosis and altered composition of atherosclerotic lesions in hyperlipidemic mice lacking acyl CoA:cholesterol acyltransferase 1. J. Clin. Invest. 105, 711–719 (2000).

9. Ishibashi, S., Goldstein, J. L., Brown, M. S., Herz, J. & Burns, D. K. Hypercholesterolemia in low density lipoprotein receptor knockout mice and its reversal by adenovirus-mediated gene delivery. J. Clin. Invest. 92, 883–93 (1993).

10. Van Eck, M. et al. Differential effects of scavenger receptor BI deficiency on lipid metabolism in cells of the arterial wall and in the liver. J. Biol. Chem. 278, 23699–23705 (2003).

11. Martins Cardoso, R. et al. Hypercholesterolemia in young adult APOE −/− mice alters epidermal lipid composition and impairs barrier function. Biochim. Biophys. Acta - Mol. Cell Biol. Lipids 1864, 976–984 (2019).

12. Vaughan, A. M. & Oram, J. F. ABCA1 and ABCG1 or ABCG4 act sequentially to remove cellular cholesterol and generate cholesterol-rich HDL. J. Lipid Res. 47, 2433–2443 (2006).

13. Nakamura, Y. et al. Molecular Mechanism of Reverse Cholesterol Transport: Reaction of Pre-β-Migrating High-Density Lipoprotein with Plasma Lecithin/Cholesterol Acyltransferase †. Biochemistry 43, 14811–14820 (2004).

14. Acton, S. et al. Identification of Scavenger Receptor SR-BI as a High Density Lipoprotein Receptor. Science (80-.). 271, 518–520 (1996).

15. Out, R. et al. Scavenger receptor class B type I is solely responsible for the selective uptake of cholesteryl esters from HDL by the liver and the adrenals in mice. J. Lipid Res. 45, 2088–2095 (2004).

16. Krieger, M. Scavenger receptor class b type I is a multiligand hdl receptor that influences diverse physiologic systems. J. Clin. Invest. 108, 793–797 (2001).

17. Shen, W.-J., Asthana, S., Kraemer, F. B. & Azhar, S. Scavenger receptor B type 1: expression, molecular regulation, and cholesterol transport function. J. Lipid Res. 59, 1114–1131 (2018).

18. Lin, M.-H. & Khnykin, D. Fatty acid transporters in skin development, function and disease. Biochim. Biophys. Acta 1841, 362–8 (2014).

19. Mommaas, M., Tada, J. & Ponec, M. Distribution of low-density lipoprotein receptors and apolipoprotein B on normal and on reconstructed human epidermis. J. Dermatol. Sci. 2, 97–105 (1991).

20. Randolph, G. J., Miller, N. E., Randolph, G. J. & Miller, N. E. Lymphatic transport of high-density lipoproteins and chylomicrons Find the latest version : Review series Lymphatic transport of high-density lipoproteins and chylomicrons. 124, 929–935 (2014).

21. Huang, L. et al. Interleukin-17 Drives Interstitial Entrapment of Tissue Lipoproteins in Experimental Psoriasis. Cell Metab. 29, 475-487.e7 (2019).

22. Brunham, L. R. et al. Novel mutations in scavenger receptor BI associated with high HDL cholesterol in humans. Clin. Genet. 79, 575–581 (2011).

23. Vergeer, M. et al. Genetic Variant of the Scavenger Receptor BI in Humans. N. Engl. J. Med. 364, 136–145 (2011).

24. Korporaal, S. J. A. et al. Deletion of the High-Density Lipoprotein Receptor Scavenger Receptor BI

in Mice Modulates Thrombosis Susceptibility and Indirectly Affects Platelet Function by Elevation of Plasma Free Cholesterol. Arterioscler. Thromb. Vasc. Biol. 31, 34–42 (2011).

25. Dole, V. S. et al. Thrombocytopenia and Platelet Abnormalities in High-Density Lipoprotein Receptor–Deficient Mice. Arterioscler. Thromb. Vasc. Biol. 28, 1111–1116 (2008).

26. Cai, L., Ji, A., de Beer, F. C., Tannock, L. R. & van der Westhuyzen, D. R. SR-BI protects against endotoxemia in mice through its roles in glucocorticoid production and hepatic clearance. J. Clin. Invest. 118, 364–375 (2008).

27. Hoekstra, M. et al. Absence of HDL cholesteryl ester uptake in mice via SR-BI impairs an adequate adrenal glucocorticoid-mediated stress response to fasting. J. Lipid Res. 49, 738–745 (2008).

28. Out, R. et al. Macrophage ABCG1 Deletion Disrupts Lipid Homeostasis in Alveolar Macrophages and Moderately Influences Atherosclerotic Lesion Development in LDL Receptor-Deficient Mice. Arterioscler. Thromb. Vasc. Biol. 26, 2295–2300 (2006).

29. Boiten, W., Absalah, S., Vreeken, R., Bouwstra, J. & van Smeden, J. Quantitative analysis of ceramides using a novel lipidomics approach with three dimensional response modelling. Biochim. Biophys. Acta - Mol. Cell Biol. Lipids 1861, 1652–1661 (2016).

30. Motta, S. et al. Ceramide composition of the psoriatic scale. BBA - Mol. Basis Dis. 1182, 147–151 (1993).

31. Smith, K. R. & Thiboutot, D. M. Thematic review series: Skin Lipids. Sebaceous gland lipids: friend or foe? J. Lipid Res. 49, 271–281 (2008).

32. Westerberg, R. et al. Role for ELOVL3 and Fatty Acid Chain Length in Development of Hair and Skin Function. J. Biol. Chem. 279, 5621–5629 (2004).

33. Chomczynski, P. & Sacchi, N. The single-step method of RNA isolation by acid guanidinium thiocyanate–phenol–chloroform extraction: twenty-something years on. Nat. Protoc. 1, 581–585 (2006).

34. van Smeden, J. et al. LC/MS analysis of stratum corneum lipids: ceramide profiling and discovery. J. Lipid Res. 52, 1211–1221 (2011).

35. Ohno, Y. et al. ELOVL1 production of C24 acyl-CoAs is linked to C24 sphingolipid synthesis. Proc. Natl. Acad. Sci. 107, 18439–18444 (2010).

36. Muresan, X. M. et al. Involvement of cutaneous SR-B1 in skin lipid homeostasis. Arch. Biochem. Biophys. 666, 1–7 (2019).

37. Mohd, F., Todo, H., Yoshimoto, M., Yusuf, E. & Sugibayashi, K. Contribution of the hair follicular pathway to total skin permeation of topically applied and exposed chemicals. Pharmaceutics 8, (2016).

38. Blume-Peytavi, U. et al. Follicular and percutaneous penetration pathways of topically applied minoxidil foam. Eur. J. Pharm. Biopharm. 76, 450–453 (2010).

39. Brodeur, M. R., Luangrath, V., Bourret, G., Falstrault, L. & Brissette, L. Physiological importance of SR-BI in the in vivo metabolism of human HDL and LDL in male and female mice. J. Lipid Res. 46, 687–696 (2005).

40. Rigotti, A. et al. A targeted mutation in the murine gene encoding the high density lipoprotein (HDL) receptor scavenger receptor class B type I reveals its key role in HDL metabolism. Proc. Natl. Acad. Sci. U. S. A. 94, 12610–12615 (1997).

41. Kosek, A. B., Durbin, D. & Jonas, A. Binding affinity and reactivity of lecithin cholesterol acyltransferase with native lipoproteins. Biochem. Biophys. Res. Commun. 258, 548–551 (1999).

42. Siefken, W., Höppner, H. & Harris, I. R. Regulation of cholesterol synthesis by oleic and palmitic acid in keratinocytes. Exp. Dermatol. 9, 138–145 (2000).

43. Sjövall, P. et al. Imaging the distribution of skin lipids and topically applied compounds in human skin using mass spectrometry. Sci. Rep. 8, 1–14 (2018).

44. Feingold, K. R. & Jiang, Y. J. The mechanisms by which lipids coordinately regulate the formation of the protein and lipid domains of the stratum corneum: Role of fatty acids, oxysterols, cholesterol sulfate and ceramides as signaling molecules. Dermatoendocrinol. 3, 113–118 (2011).

45. Elias, P. M., Williams, M. L., Choi, E. H. & Feingold, K. R. Role of cholesterol sulfate in epidermal structure and function: Lessons from X-linked ichthyosis. Biochim. Biophys. Acta - Mol. Cell Biol. Lipids 1841, 353–361 (2014).

46. Sassa, T. et al. Impaired Epidermal Permeability Barrier in Mice Lacking Elovl1, the Gene Responsible for Very-Long-Chain Fatty Acid Production. Mol. Cell. Biol. 33, 2787–2796 (2013).

47. van Smeden, J. et al. The importance of free fatty acid chain length for the skin barrier function in atopic eczema patients. Exp. Dermatol. 23, 45–52 (2014).

48. Subbaiah, P. V. et al. Regulation of plasma cholesterol esterification by sphingomyelin: Effect of physiological variations of plasma sphingomyelin on lecithin-cholesterol acyltransferase activity. Biochim. Biophys. Acta - Mol. Cell Biol. Lipids 1821, 908–913 (2012).

49. Mojumdar, E. H., Helder, R. W. J., Gooris, G. S. & Bouwstra, J. A. Monounsaturated fatty acids reduce the barrier of stratum corneum lipid membranes by enhancing the formation of a hexagonal lateral packing. Langmuir 30, 6534–6543 (2014).

50. Groen, D., Poole, D. S., Gooris, G. S. & Bouwstra, J. A. Is an orthorhombic lateral packing and a proper lamellar organization important for the skin barrier function? Biochim. Biophys. Acta - Biomembr. 1808, 1529–1537 (2011).

51. Uchiyama, M., Oguri, M., Mojumdar, E. H., Gooris, G. S. & Bouwstra, J. A. Free fatty acids chain length distribution affects the permeability of skin lipid model membranes. Biochim. Biophys. Acta - Biomembr. 1858, 2050–2059 (2016).

SUPPLEMENTARY INFORMATION

1. METHODS

1.1 Liquid chromatography-mass spectrometry (LC/MS)

Table S1. Gradient of solvents used for cholesterol and CER analysis by UPLC-LC/MS.

Run time (min)	Solvent A[1] (%)	Solvent B[2] (%)
0	98	2
2.5	96	4
2.6	93	7
6	88	12
11	50	50
13	98	2

[1]Solvent A - 100% Heptane

[2]Solvent B -Heptane:isopropanol:ethanol - 50:25:25; v/v/v

Table S2. Gradient of the solvents used for FFA analysis by UPLC-LC/MS.

Run time (min)	Solvent A[1] (%)	Solvent B[2] (%)
0	100	0
2.5	0	100
5	0	100
8	100	0
11	100	0

[1]Solvent A - Acetonitrile/milliQ/chloroform/acetic acid -90:10:2:0.005; v/v/v/v

[2]Solvent B -Methanol/heptane/chloroform/acetic acid -90:10:2:0.005; v/v/v/v

1.3. Quantitative real-time PCR (q-PCR)

Table S3. Forward and reverse primer sequences used for q-PCR.

Protein (Gene)	Forward primer Reverse primer
Ribosomal protein, large, P0 (RPL0)	CTGAGTACACCTTCCCACTTACTGA CGACTCTTCCTTTGCTTCAGCTTT
Cytochrome c-1 (CYC1)	ACTGGGGTGTCATTGCGAGAAGGC GGTCATGCTCTGGTTCTGATGCCCA
Ribosomal protein S20 (RPS20)	GGACTTGATCAGAGGCGCCAAGGAAA CCCAGGTCTTGGAACCTTCACCACAA
Acetyl-Coenzyme A carboxylase alpha (ACACA)	GGAAGATGGCGTCCGCTCTGTG GTGAGATGTGCTGGGTCATGTGGAC
ATP-binding cassette, subfamily A, member 1 (ABCA1)	AGAGCAAAAAGCGACTCCACATAGAA CGGCCACATCCACAACTGTCT
ATP-binding cassette, subfamily A, member 12 (ABCA12)	TGACCTTCTGGAAACCAACAAGACTGC CACTTATGGTGGAACCTTGGCTACTGG
ATP-binding cassette, subfamily G, member 1 (ABCG1)	TTGACACCATCCCAGCCTAC CAGTGCAGGTCTTCTCGGT
Aldehyde dehydrogenase family 3, subfamily A2 (ALDH3A2)	CGGGTGATAGATGAGACCTCCAGTGG AGGGGCGCTGATGAGAAAAGGTATCA
N-acylsphingosine amidohydrolase 1 (ASAH1)	TTATTGATGACCGCAGAACACCGGC TACAAGGGTCTGGGCAATCTCGAAGG
Ceramide kinase 1 (CERK1)	CTTGCTCAGCCTCCAGAAGCTCCT TCCTGGGCTTTGGGGTTCTTGCTTA
Ceramide synthase 3 (CERS3)	GGGCCTCCACGTTTACTGGGGT GCCCTTGGTGCTCTCTGCTTCCT
Elongation of very long chain fatty acids 1 (ELOVL1)	GGCAGAACTTGCCCCTGAGAAGAA TTCACAACAGCCTCCATCCTGGC
Elongation of very long chain fatty acids 4 (ELOVL4)	TGGAATCAAGTGGGTGGCTGGAGG AGCATGGTCAGGTATCGCTTCCACC
Elongation of very long chain fatty acids 6 (ELOVL6)	GGACCTGTCAGCAAATTCTGGGCTTA GGAGTACCAGGAGTACAGGAGCACA
Elongation of very long chain fatty acids 7 (ELOVL7)	ACAGCTGTGCACGTGGTCATGTATTC ACTGGGTACTGGTAATTGCAGTCCTCC
Fatty acid synthase (FAS)	GGCGGCACCTATGGCGAGG CTCCAGCAGTGTGCGGTGGTC
Glucocerebrosidase (GBA)	GCCCTTGCCAACAGTTCCCATGATG TGCCATGAACGTACTTAGCTGCCTCT
2-hydroxyacyl-CoA lyase 1 (HACL1)	GGTTTTGACGCTGACACCTGGGAAA CCTCAGCGAGTGTTGGAGCTCTTCT
3-hydroxy-3-methylglutaryl-CoA synthase 1 (HMGCS1)	AAAACACAGAAGGACTTACGCCCGG GTTGCAGGGAGTCTTGGCACTTTCT
Low density lipoprotein receptor (LDLR)	TGTGTGATGGAGACCGAGATTG CGTCAACACAGTCGACATCC

Protein (Gene)	Forward primer Reverse primer
Stearoyl-Coenzyme A desaturase 1 (SCD1)	TACTACAAGCCCGGCCTCC CAGCAGTACCAGGGCACCA

2. RESULTS

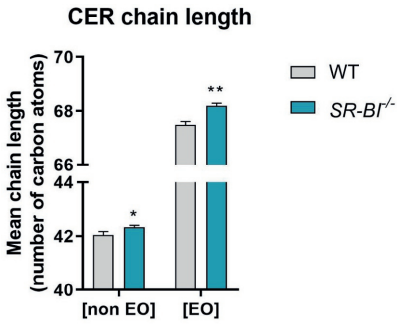

Figure S1. CER average chain length. Average total chain length of CERs with non-ω-esterified (CER[nonEO]) and ω-esterified (CER[EO]) fatty acid chains in their acyl chain. Values are plotted as mean ±SD (n=3 animals/group). Statistical significance was determined by unpaired students t-Test. *p<0.05, **p<0.01.

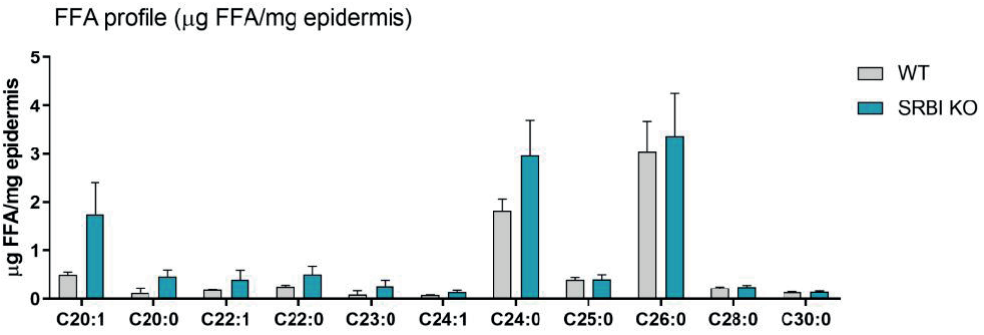

Figure S2. FFA composition in absolute values. FFA composition was determined by LC/MS. Values are plotted as mean ±SD (n=3 animals/group).

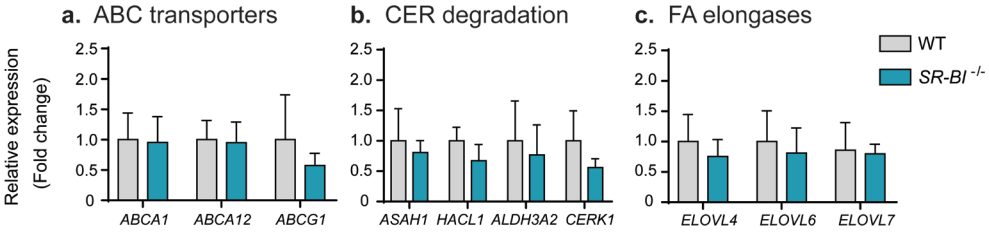

Figure S3. Expression of genes involved in lipid synthesis in the skin. Relative mRNA levels of (a) ABC transporters, (b) CER degradation enzymes, and (c) FA elongases. Genes and their respective encoded proteins/receptors: ABCA1 – ATP-binding cassette, subfamily A, member 1; ABCA12 – ATP-binding cassette, subfamily A, member 12; ABCG1 – ATP-binding cassette, subfamily G, member 1; ASAH1– N-acylsphingosine amidohydrolase 1; HACL1 – 2-hydroxyacyl-CoA lyase 1; ALDH3A2 – Aldehyde dehydrogenase family 3, subfamily A2; CERK1 – Ceramide kinase 1; ELOVL4 - elongase of very long chain fatty acids 4; ELOVL6 - elongase of very long chain fatty acids 6; ELOVL7 - elongase of very long chain fatty acids 7. Values are plotted as mean±SD and represent the fold change expression compared to the WT control (n=5-6 animals/group).

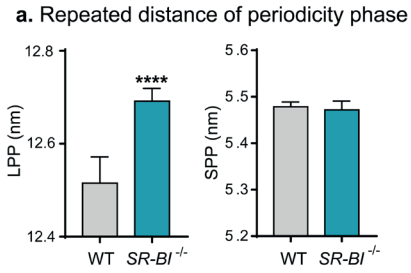

Figure S4. Repeated distances of the lamellar phases in WT and *SR-BI*$^{-/-}_{LMM}$. Repeated distances in the logng and short periodicity phases were determined by small-angle X-ray diffraction studies. espectively. Values are plotted as mean±SD (n=3 mLMM/group). Statistical significance was determined by unpaired students t-Test. ****p<0.000

Chapter 4

Compensatory lipid metabolism in the skin of apolipoprotein AI deficient mice in response to hypoalphalipoproteinemia

Manuscript in preparation

Renata Martins Cardoso[1], Samira Absalah[1], Menno Hoekstra[1], Joke A. Bouwstra[1*], Miranda Van Eck[1*]

[1]Division of BioTherapeutics, Leiden Academic Centre for Drug Research, Leiden University, Leiden, The Netherlands

*Both authors contributed equally

ABSTRACT

High-density lipoproteins (HDL) have a vital function in cholesterol metabolism. It involves a heterogeneous group of relatively small cholesterol-transporting particles that can efficiently traffic from plasma to interstitial fluid of various tissues, including the skin, and vice versa. . The importance of HDL for the transport of lipids into skin or efflux of excess lipids, produced by keratinocytes, out of the skin is currently unknown. In this study, we aimed to assess the impact of strongly reduced HDL levels (hypoalphalipoproteinemia) on skin lipid homeostasis. For that purpose, the skin of apolipoprotein AI knockout (*APOAI*$^{-/-}$) mice was compared to control wild type mice of the same age with particular focus on epidermal barrier lipids and the mRNA expression of enzymes involved in their synthesis. Despite the substantial decrease in plasma levels of cholesterol and triglycerides, *APOAI* deficiency did not affect the general morphology of the skin. Detailed analysis of the epidermal barrier lipids showed comparable cholesterol levels and ceramide and free fatty acid compositions between control and *APOAI*$^{-/-}$ mice. However, the unaltered barrier lipid composition did coincide with an increased expression of genes involved in cholesterol synthesis (*HMGCR, HMGCS1*), cholesterol uptake from lipoproteins (*LDLR, SR-BI*) and free fatty acid synthesis (*FAS, ACC*) in the skin of *APOAI*$^{-/-}$ mice. In summary, this study shows that neither the morphology or the epidermal lipid composition and organization of the skin of *APOAI*$^{-/-}$ mice is affected by hypoalphalipoproteinemia. A local compensatory mechanism marked by upregulation of lipid synthesis genes preserving the epidermal lipid profile in absence of HDL, suggests that HDL likely plays an important role in the delivery of essential lipids to the skin.

Keywords: *skin barrier lipids; apolipoprotein AI knockout; high-density lipoprotein; skin lipid metabolism*

1. INTRODUCTION

Apolipoprotein AI (APOAI) is the main protein component of high-density lipoprotein (HDL), a heterogeneous group of particles involved in the transport of cholesterol throughout the body[1,2]. APOAI is produced by enterocytes and hepatocytes and secreted into the plasma in a lipid-poor form[1,2]. Following interaction with ATP-binding cassette (ABC) transporter A1, plasma lipid-poor APOAI quickly acquires phospholipids and free cholesterol to form nascent HDL particles[2]. Maturation of nascent HDL continues with uptake of more lipids from peripheral tissues via ABCA1, ABCG1, and scavenger receptor class B member I (SR-BI) as well as by exchange from other lipoproteins[3]. The enzyme lecithin: cholesterol acyl transferase (LCAT) is a key player in the maturation of HDL particles as it generates cholesteryl esters (CE) for storage in the lipoprotein core[3,4].

HDL particles are relatively small and can efficiently traffic from plasma to interstitial fluid of various tissues, including the skin, and vice versa. In fact, both human and murine keratinocytes express ABCA1, ABCG1, cluster of differentiation 36 (CD36), and SR-BI facilitating the transit of lipids to and from HDL particles[5–7]. Lipids are key components of the stratum corneum (SC), the outermost dead layer of the skin, an organ that functions as a protective barrier in the interface between the body and the environment. The SC is mainly composed of cholesterol, free fatty acids (FFAs) and ceramides (CERs). Although most of the SC lipids are synthesized by keratinocytes[8], lipids of extracutaneous origin can be found in the skin[7,9–11], which are likely acquired via lipoprotein receptors expressed in keratinocytes (*e.g.* low-density lipoprotein receptor, SR-BI, and CD36)[7,10,12].

Recently, we have demonstrated that the skin of young adult *SR-BI* knockout (*SR-BI* $^{-/-}$) mice displayed an altered epidermal lipid composition and reduced lipid barrier functionality[13]. In these mice, SR-BI is not only absent in keratinocytes, but also in liver, the primary site for removal of HDL-CE from the circulation. As a result, the metabolism of HDL is severely impaired in SR-BI deficient mice, leading to augmented HDL cholesterol levels in the circulation (hyperalphalipoproteinemia).

In contrast, deficiency of APOAI leads to a virtual absence of HDL in the circulation, thereby impairing the transport of lipids (cholesterol, triglycerides) from peripheral tissues to the plasma via HDL particles[2]. Over 40 *APOAI* gene defects have been described in humans, which among others impact interactions with ABCA1 and/or activation of LCAT and severely affect HDL metabolism, leading to an increased risk for cardiovascular diseases[14–19]. Remarkably, enzymatic colorimetric analysis of whole

skin of *APOAI*$^{-/-}$ mice did not reveal changes in the overall cholesterol, phospholipids, and triglycerides contents[20]. However, the impact of the severely reduced HDL levels on specifically epidermal barrier lipids (CERs, FFAs) has not yet been assessed. Additionally, considering the large amount of HDL transiting through the skin via the vascular bed[21] and the epidermal barrier lipid alterations reported in *SR-BI*$^{-/-}$ mice[13], it is important to obtain more detailed insight in whether lipid metabolism is changed in the skin of *APOAI*$^{-/-}$ mice, in which HDL particles are virtually absent.

In the present study, the skin of *APOAI*$^{-/-}$ mice was compared to that of wild type (WT) mice to gain insight into skin lipid metabolism under conditions of an HDL-deficient hypolipidemic profile (hypoalphalipoproteinemia). Hereto, the epidermal lipid composition and organization were determined and the expression of genes involved in the local lipid synthesis and uptake was measured. The skin of *APOAI*$^{-/-}$ mice showed comparable epidermal barrier lipid composition and organization to the WT mice. However, gene expression analysis revealed that in *APOAI*$^{-/-}$ mice various genes related to lipid synthesis in the skin were upregulated, indicating a compensatory increase in local lipid synthesis.

2. MATERIALS AND METHODS

2.1 Chemicals

Rodent chow diet, low in fat and cholesterol (Rat and Mouse No.3 breeding diet), was purchased from Special Diets Services (United Kingdom). Ketamine and atropine from AUV Veterinary Services (Cuijk, The Netherlands). Xylazine from ASTFarma (Oudewater, The Netherlands). Sodium chloride (NaCl) from Boom (Meppel, The Netherlands). Sodium phosphate dibasic (Na_2HPO_4), hematoxylin, eosin, trypsin from bovine pancreas, trypsin inhibitor, cholesterol, FFA C16-C30, deuterated FFA C18 and deuterated FFA C24, chloroform, deuterated water (D_2O), natrium bromibe (NaBr), were purchased from Sigma-Aldrich (Zwijndrecht, The Netherlands). Potassium dihydrogen phosphate (KH_2PO_4), potassium chloride (KCl) and Entellan® were purchased from Merck (Darmstadt, Germany). CER[NS] (C24deuterated; C18protonated) and all synthetic CERs were kindly provided by Evonik Industries (Essen, Germany). Heptane was purchased from ChemLab (Zedelgem, Belgium). Methanol, ethanol and isopropanol were purchased from Biosolve (Valkenswaard, The Netherlands). All solvents used were analytical grade.

2.2 Animals

16-18 weeks old female C57BL/6 WT mice were obtained from The Jackson laboratory and bred at the Gorlaeus laboratories (Leiden, The Netherlands). Homozygous apolipoprotein AI knockout (*APOAI*$^{-/-}$) mice were rederived from *APOAI*/*LDLR* double knockout mice (C57Bl/6J background; kindly provided by Dr. Jan Albert Kuivenhoven, Department of Experimental Vascular Medicine, Academic Medical Centre, Amsterdam) by crossbreeding with C57BL/6 mice and subsequent intercrossing of the offspring[22]. All mice were kept under standard laboratory conditions at 20°C and with light cycle of 12h light/12h dark. The mice had access to water and standard low fat chow diet ad libitum. The non-fasted mice were anesthetized with a mixture of xylazine (70 mg/kg body weight); atropine (1.8 mg/kg body weight) and ketamine (350 mg/kg body weight) for retro-orbital bleeding. Next, the mice were perfused with phosphate buffered saline (PBS at pH 7.4; 8.13 g/L NaCl, 2.87 g/L Na_2HPO_4, 0.2 g/L KH_2PO_4, 0.19 g/L KCl in milliQ water) and the skin of their back was collected. All experiments were performed in agreement with National guidelines and approved by the Ethics Committee for Animals Experiments of Leiden University.

2.3 Plasma lipid analysis

Enzymatic colorimetric assays (Roche Diagnostics, Almere, Netherlands) were used to measure non-fasted plasma levels of free cholesterol (FC), cholesteryl esters (CE) and triglycerides as described previously[23].

2.4 Skin morphology staining

Paraffin embedded skin sections (4-5 μm) were deparaffinized, rehydrated and stained with hematoxylin and eosin according to manufacturer's instructions. Stained slides were mounted in Entellan® and imaged with a Zeiss Axioplan 2 light microscope (Zeiss, Best, The Netherlands).

2.5 Epidermis isolation

Skin samples without hypodermis were placed on a paper filter soaked with 0.3% w/v trypsin solution in PBS with the dermis side in contact with the paper. The skin was kept overnight at 4°C and, on the next day; the samples were incubated at 37°C for trypsin activity. After 1 hour the epidermis was separated and subsequently rinsed with trypsin inhibitor (0.1% w/v inhibitor in PBS) and in demi-water. The samples were dried overnight at room temperature and stored under argon atmosphere in a

container containing silica and protected from light until epidermal lipid extraction and FTIR measurements.

2.6 Lipid extraction and liquid chromatography-mass spectrometry (LC/MS)

Epidermal lipids were extracted as described by Boiten *et. al.* (2016)[24] and stored in chloroform:methanol (2:1; v/v) at 4°C under argon atmosphere for analysis of cholesterol, CERs, and FFAs using an Acquity UPLC H-class system (Waters, Milford, MA, USA) connected to an XEVO TQ-S mass spectrometer (MS; Waters, Milford, MA, USA) with an atmospheric pressure chemical ionization (APCI) chamber, as previously described[13,25]. In short, for cholesterol and CERs analysis, deuterated CER NS (C24 acyl chain deuterated; C18 sphingoid base protonated) was added as internal standard to all samples prior to injection into the UPLC/MS system. Upon completion of the measurements, the area under the curve (AUC) was determined using Software Waters MassLynx 4.1 for both cholesterol and CER analyses. Cholesterol AUC was divided by internal standard and further corrected for the response based on a calibration curve of cholesterol and the data was plotted as absolute amount of cholesterol (µg) per epidermis weight (mg). CER AUC data was divided by internal standard and plotted as relative percentage of ceramide subclasses calculated. In this work, CERs are named as according to Motta *et. al.* (1993) describing the acyl chain (non-hydroxy fatty acid [N]; α-hydroxy fatty acid [A]; esterified ω-hydroxy fatty acid [EO]) and the sphingoid base (dihydrosphingosine, [dS]; sphingosine [S]; phytosphingosine [P])[26]. For FFAs analysis, deuterated FFA C18 and FFA C24 were used as internal standard to all samples. The AUC was corrected by the internal standard FFA C24 and for the response based on calibration curves of FFA C16-C30. The data was plotted as absolute amounts and relative mass percentage to the total FFA content detected. Due to manufacturer's contamination of the chloroform extracting solvent with FFA C16:0 and C18:0, these FFAs were not determined. Their respective unsaturated species were not plotted as they are important components of sebum lipids.

2.7 Fourier transformed infrared spectroscopy (FTIR)

Fourier transformed infrared spectroscopy (FTIR) measurements were performed using a Varian 670-IR spectrometer (Agilent Technologies, Inc., Santa Clara, CA) equipped with a broad-band mercury cadmium telluride detector. Prior the measurement, the epidermis was hydrated for 24 hours in a deuterated water solution containing 27% w/v sodium bromide. Next, the epidermis was mounted between 2 silver bromide windows and FTIR spectra (600-4000 cm^{-1}) were collected with resolution of 1 cm^{-1} in a temperature range from 0-90°C (0.5°C/min). The spectra were deconvoluted (half

width of 4 cm^{-1}; enhancement factor of 1.7) and further processed with Resolutions Pro 4.1 (Varian Inc.) software. Lateral organization of the epidermal lipids was examined by analysis of the CH_2 rocking vibrations (710-740 cm^{-1}). The end of the orthorhombic to hexagonal phase transition was determined by the disappearance of the peak at 730 cm^{-1}.

2.8 qPCR

Total RNA was isolated from skin samples without hypodermis[27]. RNA (1 µg) was transcribed to cDNA using with M-MuLV reverse transcriptase. Quantitative gene analysis was done with QuantStudio 6 Flex Real-time PCR systems (Applied Biosystems, Foster City, CA, USA) using SYBR Green Technology for detection. Ribosomal protein, large, P0 (*RPL0*) and ribosomal protein L37 (*RPL37*) were used as reference genes. Relative gene expression was determined by subtracting the average threshold cycle (Ct) of the reference genes from the Ct of the target gene and raising the difference to 2 to the power. Gene expression was plotted as relative fold change compared to the WT control group. Primer sequences used in the gene expression analysis are available in Supplementary Table S1.

2.9 Statistical analysis

Data are presented as mean±standard deviation (SD). Statistical analysis was performed using GraphPad Prism 8 (GraphPad Software Inc., CA, USA). *P* values below 0.05 were considered significant.

3. RESULTS

3.1 *APOAI* deficiency in mice lowers plasma cholesterol without altering skin morphology

The non-fasted plasma lipid profile of WT and *APOAI*$^{-/-}$ mice was determined by enzymatic colorimetric assays to measure triglycerides, free cholesterol (FC), and cholesteryl esters (CE) (Fig 1a). *APOAI*$^{-/-}$ mice on low-fat chow diet showed reduced triglycerides levels (0.8±0.2 µg/ml plasma) compared to the WT control (1.1±0.1 µg/ml plasma) ($p<0.05$). The absence of *APOAI* leads to a strong reduction in circulating HDL-cholesterol[20]. As a result, *APOAI*$^{-/-}$ mice showed a large reduction in the FC fraction (0.23±0.05 µg/ml plasma) and CE fraction (0.31±0.05 µg/ml plasma) compared to the WT counterparts (0.36±0.05 µg/ml ($p<0.01$) and 0.86±0.08 µg/ml plasma ($p<0.0001$), respectively). Next, the morphology of the skin of WT and *APOAI*$^{-/-}$ mice was assessed by

hematoxylin and eosin staining (Fig 1b). Overall, the morphology of the *APOAI*$^{-/-}$ skin was comparable to the WT control with similar SC and epidermal and dermal morphology. At general inspection no signs of inflammation were observed (*e.g.* epidermal thickening).

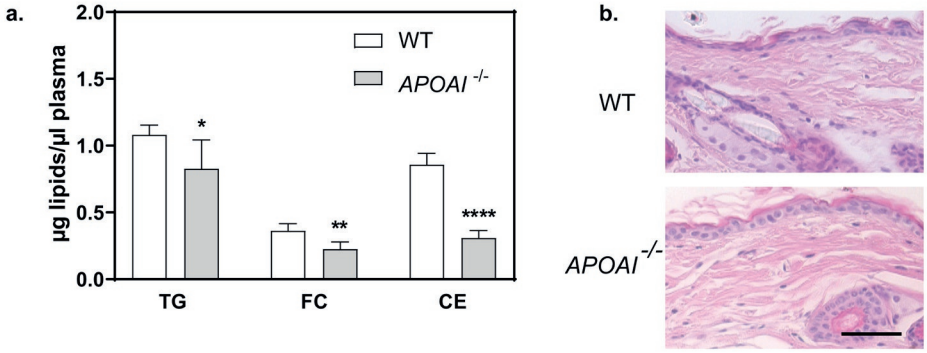

Figure 1. Deficiency of *APOAI* in young adult mice reduces plasma lipid levels but does not affect skin morphology. Non-fasted (a) plasma levels of triglycerides (TG); free cholesterol (FC) and cholesteryl esters (CE) were measured by enzymatic colorimetric reactions (n=5-6 animals/group) and (b) hematoxylin and eosin staining of paraffin skin sections of wild type (WT) and *APOAI* knockout (*APOAI*$^{-/-}$) mice. Representative micrographs (Scale bar = 50 µm). Data shown as mean ± SD. Significant differences between groups were determined by two-tailed unpaired Student's T-test; *p<0.05, **p<0.01 and ****p<0.0001.

3.2 Absence of *APOAI* minimally affects the epidermal lipid composition

The three main types of epidermal barrier lipids (cholesterol, CERs, and FFAs) were analyzed by LC/MS. The cholesterol content in the epidermis of *APOAI*$^{-/-}$ mice (30.7±1.3 µg/mg epidermis) was comparable to the WT control (28.7±3.1 µg/mg epidermis) (Fig 2a). Seven CER subclasses were detected in the epidermis of both types of mice (Fig 2b): CER NdS, CER NS, CER NP/AdS, CER AS, CER EOS, CER EOdS, nomenclature according to Motta *et. al.* (1993)[26]. The subclasses CER NP and CER AdS could not be completely separated in our method; thus, these CER subclasses are depicted in one group. In *APOAI*$^{-/-}$ mice, the percentage CER NdS was increased (42.3±1.5% versus 39.7±0.5% in WT, p<0.01), while the percentage of CER AS (11.1±0.9%) was lower in the *APOAI*$^{-/-}$ mice as compared to WT controls (13.5±1.1%; p<0.05). The abundance of CER NS, CER NP/AdS, CER EOdS and CER EOS was similar between groups. The total absolute FFA content did not differ between groups (Supplementary Fig S1a); hence the relative FFA composition in the epidermis of *APOAI*$^{-/-}$ mice was equivalent to that of WT controls (Fig 2c). In both groups of mice, FFA C24:0 and FFA C26:0 were the most abundant species, comprising nearly 70% of the total FFA content. Although no significant differences

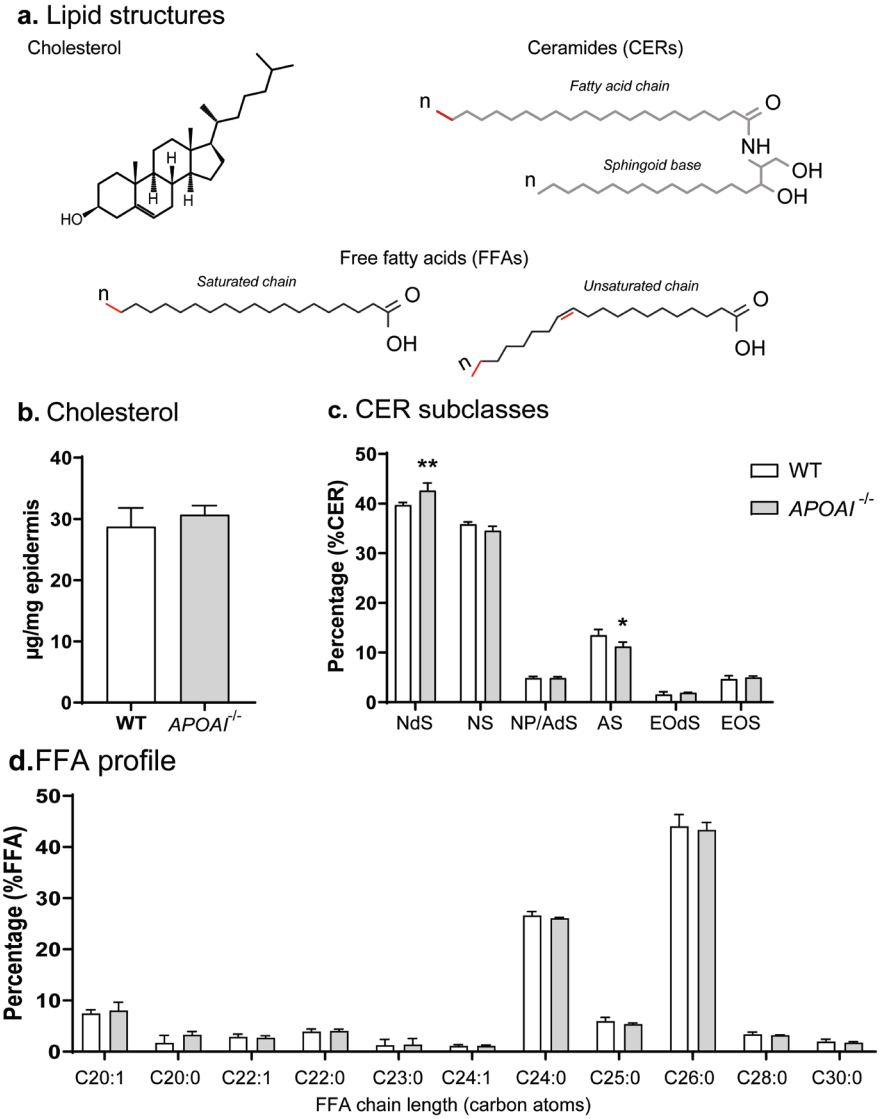

Figure 2. The epidermal lipid composition is minimally altered in young adult mice lacking *APOAI*. Epidermal lipids in wild type (WT) and *APOAI* knockout (*APOAI*$^{-/-}$) mice were analyzed by LC/MS: (a) the structure of the three main barrier lipids present in the skin, (b) cholesterol content, (c) CERs (CER subclasses: NdS, NS, NP/AdS, AS, EOdS, EOS) and (d) FFAs with chain length from 20-30 carbon atoms. CER subclasses named according to Motta *et. al.* (1993) describing the acyl chain (non-hydroxy fatty acid [N]; α-hydroxy fatty acid [A]; esterified ω-hydroxy fatty acid [EO]) and the sphingoid base (dihydrosphingosine, [dS]; sphingosine [S]; phytosphingosine [P]) 26. CER NP and CER AdS are represented together as these subclasses could not be fully separated. Data shown as mean±SD; n=3/group. Statistical significance was calculated by two-tailed unpaired Student's T-test and Two-way ANOVA followed by Holm-Šídák post-hoc test; *p<0.05; **p<0.01.

were noted between the FFA profiles, the epidermis of *APOAI*$^{-/-}$ mice showed a slight shift towards shorter FFA chains (below 24 carbon atoms), which comprised 19.3±1.3% of the total FFA species versus 17.1±0.8% in WT (p=0.058) (Supplementary Fig S1b). The ratio between unsaturated and saturated FFAs was comparable in both groups (0.13±0.02 in WT and 0.13±0.03 in *APOAI*$^{-/-}$ mice, (Supplementary Fig S1c).

3.3 Epidermal lipids in the skin of *APOAI*$^{-/-}$ mice adopt an orthorhombic organization

For the functionality of the skin barrier not only the lipid composition is of importance, but also the lateral organization of these lipids. Therefore next the lateral lipid organization in the skin of WT and *APOAI*$^{-/-}$ mice was analyzed by FTIR at temperatures ranging from 0°C to 50°C. At low temperatures, the CH_2 rocking vibrations (710-740 cm^{-1}) showed a doublet at 710 cm^{-1} and at 730 cm^{-1} for WT and *APOAI*$^{-/-}$ epidermis (Fig 3). The presence of the doublet in this region of the spectrum represents orthorhombic lateral packing, which was also present at normal skin surface temperature (~32°C) (Fig 3; red line)[28–30]. The temperature at which the lateral lipid organization shifts from orthorhombic to hexagonal was determined by the disappearance of the peak at 730 cm^{-1} as a function of temperature. The lipids in the epidermis of WT and *APOAI*$^{-/-}$ mice showed a shift towards the hexagonal phase at temperatures varying from 38°C to 42°C.

3.4 Skin of *APOAI*$^{-/-}$ mice shows adaptive expression of lipid synthesis genes in response to hypoalphalipoproteinemia

Altered plasma lipid profiles have been reported to affect the epidermal lipid composition[31–33]. To understand how the epidermal lipid composition was largely maintained in *APOAI*$^{-/-}$ mice despite the severe hypoalphalipoproteinemia, next the expression of genes involved in lipid synthesis and lipid uptake were determined. Regarding the synthesis of cholesterol, the expression of *HMGCR* (encoding for the enzyme 3-hydroxy-3-methyl-glutaryl-coenzyme A reductase) and *HMGCS1* (encoding for the enzyme 3-Hydroxy-3-Methylglutaryl-CoA Synthase 1) were strongly upregulated in *APOAI*$^{-/-}$ mice (1.9-fold and 1.7-fold increase, respectively) as compared to WT mice (p<0.01) (Fig 4a). Also, mRNA levels of plasma lipoprotein receptors *LDLR* (1.4-fold) and *SR-BI* (2.5-fold) were significantly higher in *APOAI*$^{-/-}$ mice (Fig 4a).

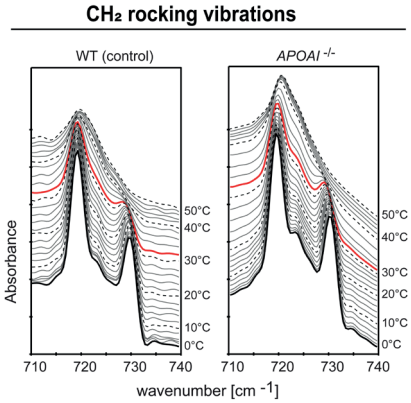

Figure 3. Epidermal lipids in *APOAI*$^{-/-}$ mice show orthorhombic lateral organization. Lateral packing of the epidermal lipids of wild type (WT) and *APOAI* knockout (*APOAI*$^{-/-}$) mice was assessed by FTIR using the spectrum in the CH2 rocking vibrations (710-740 cm^{-1}) plotted as a function of temperature (0-50°C). Lateral organization at skin temperature (~32°C) is indicated by the red line. Spectra are representative of 3-4 animals/group.

Analysis of FFA chain elongases in *APOAI*$^{-/-}$ skin revealed lower levels of *ELOVL1* (55% reduction, $p<0.01$), while the expressions of *ELOVL4* and *ELOVL6* remained unaltered (Fig 4c and Supplementary Fig S2). *SCD1* expression (encoding for stearoyl-CoA desaturase 1 involved in FFA desaturation) was similar in both groups of mice (Fig 4c). Interestingly, skin levels of *DGAT2*, a gene encoding for the enzyme diacylglycerol O-acyltransferase 2 involved in the synthesis of triglycerides, showed nearly 45% reduction ($p<0.01$) in the hypolipidemic *APOAI*$^{-/-}$ mice. In agreement with the upregulation of lipid synthesis genes, the levels of *IVL* (encoding for involucrin, a marker for keratinocyte differentiation) were increased by 40% ($p<0.05$) in the *APOAI*$^{-/-}$ mice; yet, *K10* expression (encoding for keratin 10, an early marker for keratinocyte differentiation) was comparable to the WT controls (Supplementary Fig S2).

4. DISCUSSION

In the present work, we analyzed the detailed composition and organization of the barrier lipids in hypolipidemic *APOAI*$^{-/-}$ mice and associated our findings with the expression of genes involved in lipid synthesis in the skin. Our data showed that the lipid composition and packing in the SC lipid matrix were preserved in *APOAI* deficient mice. More importantly, we demonstrated at gene expression level that compensatory mechanisms regulating local lipid synthesis and uptake likely contribute to the maintenance of skin lipid homeostasis.

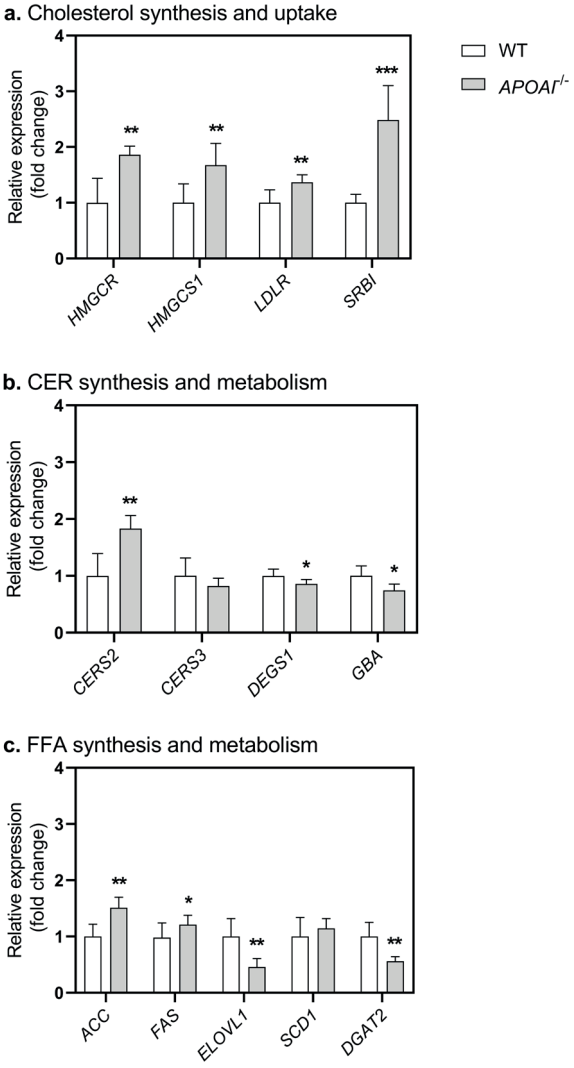

Figure 4. *APOAI* deficiency alters expression profile of various genes involved in lipid synthesis and uptake in the skin. Relative mRNA expression of genes related to (a) cholesterol; (b) CER and (c) FFA synthesis were determined in the epidermis of wild type (WT) and *APOAI* knockout (*APOAI*$^{-/-}$) mice. Data shown as mean±SD and plotted as fold change expression compared to the WT control (n=5-6 animals/group). Statistical significance was determined by two-tailed unpaired Student's t-Test. *p<0.05; **p<0.01; ***p<0.001.

HDL accounts for the largest fraction of lipoproteins in the plasma of WT mice, with APOAI being the major apolipoprotein in these particles[2,34]. In mice lacking APOAI, HDL

is strongly reduced and both free and esterified cholesterol levels in the plasma are largely decreased[20,35]. The severe hypocholesterolemia in *APOAI*$^{-/-}$ mice is associated with normal free cholesterol levels in the peripheral tissues but reduced levels of CE, particularly in steroidogenic tissues (*e.g.* adrenals)[35]. The skin is one of the main reservoirs of HDL in the body[21]. Yet, the reduced levels of circulating HDL particles and associated hypolipidemia did not affect the epidermal cholesterol content or general morphology of the skin of mice lacking APOAI[20]. The expression of key genes involved in skin cholesterol synthesis (*HMGCR, HMGCS1*) and lipoprotein uptake (*LDLR, SR-BI*) was strongly upregulated. This data suggests that local cholesterol content is maintained with a combination of increased: (1) local synthesis and (2) uptake of lipids from apolipoprotein B-containing lipoproteins. Importantly, it also indicates that that HDL is not essential for skin reverse transport of lipids but likely plays a role in the delivery of essential lipids to the skin.

Previous studies assessed the lipid composition of whole skin in *APOAI*$^{-/-}$ mice using enzymatic colorimetric assays but, in line with our findings, no differences were observed between the WT control and the *APOAI*$^{-/-}$ counterparts[20]. To our knowledge, we describe for the first time the detailed analysis of the compositions of CERs and FFAs in the epidermis of *APOAI*$^{-/-}$ mice using a LC/MS method, providing detailed information on subclass and chain length of these lipids. Alterations in the CER subclasses and chain length can lead to a less favorable organization of the SC lipids impacting the barrier function of the skin[31,36]. Similar effects have been described for changes in FFA chain length, in particular towards shorter FFA chains (below 24 carbons atoms)[33]. In line, with our method we demonstrate similar profiles of CER subclasses and FFA chain length distribution in the epidermis of WT and *APOAI*$^{-/-}$ mice. Tissues acquire substantial amounts of FFAs from plasma triglycerides and CEs. *APOAI*$^{-/-}$ mice show not only a reduction in plasma CEs, but also lower plasma triglycerides levels. Accordingly, it is unlikely that in the hypocholesterolemic *APOAI*$^{-/-}$ mice CERs and FFAs are maintained by increased uptake of triglycerides from the circulation. The expression of *FAS* and *ACC* (encoding for key enzymes in the fatty acid synthesis) were increased indicating compensatory epidermal fatty acid synthesis[37]. Moreover, the skin of *APOAI*$^{-/-}$ mice displayed reduced mRNA levels of *DGAT2*, encoding for the enzyme involved in the synthesis of triglycerides, thereby lowering the storage of FFA in the form of triglycerides[38]. Interestingly, Arnaboldi *et. al.* (2015) showed with colorimetric assays that also triglyceride and phospholipid content was preserved in the skin of *APOAI*$^{-/-}$ mice[20]. However, the mechanism underlying the preservation of the triglyceride levels in the skin of these mice remains unclear. Hence, our data indicate adaptations in lipid synthesis and uptake in the skin of *APOAI*$^{-/-}$ mice contributing to maintenance of local barrier lipid homeostasis. The organization of the epidermal lipids can be directly

influenced by changes in the barrier lipid composition. Consequently, the lateral lipid organization in the skin of *APOAI*$^{-/-}$ mice (orthorhombic packing) resembles that of the WT control as anticipated.

Other dyslipidemic double-knockout mouse models have been developed combining the hypolipidemic *APOAI*$^{-/-}$ background with an impaired metabolism of apolipoprotein B-containing lipoproteins (*LDLR*$^{-/-}$ and *APOE*$^{-/-}$ mice)[20,39,40]. Upon ageing or when challenged with a high fat/cholesterol diet, skin of the double-knockout *APOAI*$^{-/-}$/*LDLR*$^{-/-}$ model displays accumulation of both free and esterified cholesterol and marked inflammation[39,40]. In contrast, the double-knockout *APOAI*$^{-/-}$/*APOE*$^{-/-}$ mice develop similar dermatological alterations spontaneously in time when on a low-fat diet[20]. Deficiency of ATP-binding cassette A1 (ABCA1) results in hypolipidemia similar to that described for *APOAI*$^{-/-}$ mice, also without the development of any evident skin phenotypes[41]. However, the double-knockouts *ABCA1*$^{-/-}$/*LDLR*$^{-/-}$ on a lipid rich diet and *ABCAI*$^{-/-}$/*APOE*$^{-/-}$ show alterations in their skin comparable to those reported for the double knockouts in *APOAI*$^{-/-}$ background under similar circumstances[41].

The dermatological phenotypes in the *APOAI*$^{-/-}$/*LDLR*$^{-/-}$ on lipid rich diet and *APOAI*$^{-/-}$/*APOE*$^{-/-}$ mice are likely largely driven by the impaired metabolism of apoB-containing lipoproteins leading to a hypercholesterolemic phenotype. The skin lipid composition of mild hypercholesterolemic *LDLR*$^{-/-}$ mice on low fat/cholesterol diet did not differ from WT controls on that diet[25]. However, the skin of *APOE*$^{-/-}$ mice, with a more severe hypercholesterolemic phenotype under the same dietary conditions, showed an FFA profile enriched in short and unsaturated FFA species; thus, evidencing impact of apoB-containing lipoproteins levels on the skin[25]. It is important, however, to note that the dermatological alterations in skin of double knockout *APOAI*$^{-/-}$/*LDLR*$^{-/-}$ and *APOAI*$^{-/-}$/*APOE*$^{-/-}$ mice were more severe as compared to the single knockout *LDLR*$^{-/-}$ on a high fat/cholesterol diet or *APOE*$^{-/-}$ mice, indicating that absence of HDL might enhance the skin phenotype under hypercholesterolemic conditions. In contrast to mice that transport the majority of cholesterol in HDL, humans display high levels of LDL cholesterol[34]. Therefore, it might deem relevant to study the barrier lipid composition of individuals with APOAI polymorphism to better understand how HDL lipids and its metabolism can affect the skin in humans.

To conclude, we showed that hypoalphalipoproteinemia in *APOAI*$^{-/-}$ mice does not affect the skin morphology and that the epidermal lipid profile under hypolipidemic conditions is likely maintained by local compensatory mechanisms in the skin. Our data also suggest that HDL particles are a source of extracutaneous lipids and that the skin lipid profile warrants further investigation in patients with HDL-related dyslipidemias.

ACKNOWLEDGEMENTS

We thank Dr. A. B. Ouweneel for providing us the skin of the *APOAI*$^{-/-}$ mice. This research was funded by Leiden Academic Center for Drug Research (LACDR), Leiden University.

REFERENCES

1. Kosmas, C. E. et al. High-density lipoprotein (HDL) functionality and its relevance to atherosclerotic cardiovascular disease. Drugs Context 7, 1–9 (2018).

2. Lewis, G. F. & Rader, D. J. New Insights Into the Regulation of HDL Metabolism and Reverse Cholesterol Transport. Circ. Res. 96, 1221–1232 (2005).

3. Zannis, V. I., Chroni, A. & Krieger, M. Role of apoA-I, ABCA1, LCAT, and SR-BI in the biogenesis of HDL. J. Mol. Med. 84, 276–294 (2006).

4. Jonas, A. Lecithin cholesterol acyltransferase. Biochim. Biophys. Acta - Mol. Cell Biol. Lipids 1529, 245–256 (2000).

5. Jiang, Y. J., Lu, B., Kim, P., Elias, P. M. & Feingold, K. R. Regulation of ABCA1 expression in human keratinocytes and murine epidermis. J. Lipid Res. 47, 2248–2258 (2006).

6. Jiang, Y. J. et al. Regulation of ABCG1 expression in human keratinocytes and murine epidermis. J. Lipid Res. 51, 3185–3195 (2010).

7. Tsuruoka, H. et al. Scavenger receptor class B type I is expressed in cultured keratinocytes and epidermis. Regulation in response to changes in cholesterol homeostasis and barrier requirements. J. Biol. Chem. 277, 2916–2922 (2002).

8. Ponec, M., Weerheim, A., Lankhorst, P. & Wertz, P. New acylceramide in native and reconstructed epidermis. J. Invest. Dermatol. 120, 581–588 (2003).

9. Haruta-Ono, Y. et al. Orally administered sphingomyelin in bovine milk is incorporated into skin sphingolipids and is involved in the water-holding capacity of hairless mice. J. Dermatol. Sci. 68, 56–62 (2012).

10. Abd El-Latif, M. I. A., Murota, H., Terao, M. & Katayama, I. Effects of a 3-hydroxy-3-methylglutaryl coenzyme A reductase inhibitor and low-density lipoprotein on proliferation and migration of keratinocytes. Br. J. Dermatol. 128–137 (2010). doi:10.1111/j.1365-2133.2010.09694.x

11. Khnykin, D., Miner, J. H. & Jahnsen, F. Role of fatty acid transporters in epidermis: Implications for health and disease. Dermatoendocrinol. 3, 53–61 (2011).

12. Lin, M.-H. & Khnykin, D. Fatty acid transporters in skin development, function and disease. Biochim. Biophys. Acta 1841, 362–8 (2014).

13. Martins Cardoso, R. et al. Hyperalphalipoproteinemic scavenger receptor BI knockout mice exhibit a disrupted epidermal lipid barrier. Biochim. Biophys. Acta - Mol. Cell Biol. Lipids 1865, 158592 (2020).

14. Chroni, A., Duka, A., Kan, H.-Y., Liu, T. & Zannis, V. I. Point Mutations in Apolipoprotein A-I Mimic the Phenotype Observed in Patients with Classical Lecithin:Cholesterol Acyltransferase Deficiency †. Biochemistry 44, 14353–14366 (2005).

15. Huang, W. et al. A Novel Homozygous Missense Mutation in the Apo A-I Gene With Apo A-I Deficiency. Arterioscler. Thromb. Vasc. Biol. 18, 389–396 (1998).

16. Miettinen, H. E. et al. Apolipoprotein A-I FIN (Leu159→Arg) Mutation Affects Lecithin. Arterioscler. Thromb. Vasc. Biol. 17, 3021–3032 (1997).

17. Hovingh, G. K. et al. A novel apoA-I mutation (L178P) leads to endothelial dysfunction, increased arterial wall thickness, and premature coronary artery disease. J. Am. Coll. Cardiol. 44, 1429–1435 (2004).

18. Miller, M., Aiello, D., Pritchard, H., Friel, G. & Zeller, K. Apolipoprotein A-I Zavalla (Leu 159 →Pro). Arterioscler. Thromb. Vasc. Biol. 18, 1242–1247 (1998).

19. Tiniakou, I. et al. Natural human apoA-I mutations L141R Pisa and L159R FIN alter HDL structure and functionality and promote atherosclerosis development in mice. Atherosclerosis 243, 77–85 (2015).

20. Arnaboldi, F. et al. High-density lipoprotein deficiency in genetically modified mice deeply affects skin morphology: A structural and ultrastructural study. Exp. Cell Res. 338, 105–112 (2015).

21. Huang, L. et al. Interleukin-17 Drives Interstitial Entrapment of Tissue Lipoproteins in Experimental Psoriasis. Cell Metab. 29, 475-487.e7 (2019).

22. Ouweneel, A. B., van der Sluis, R. J., Nahon, J. E., Van Eck, M. & Hoekstra, M. Simvastatin treatment aggravates the glucocorticoid insufficiency associated with hypocholesterolemia in mice. Atherosclerosis 261, 99–104 (2017).

23. Out, R. et al. Macrophage ABCG1 Deletion Disrupts Lipid Homeostasis in Alveolar Macrophages and Moderately Influences Atherosclerotic Lesion Development in LDL Receptor-Deficient Mice. Arterioscler. Thromb. Vasc. Biol. 26, 2295–2300 (2006).

24. Boiten, W., Absalah, S., Vreeken, R., Bouwstra, J. & van Smeden, J. Quantitative analysis of ceramides using a novel lipidomics approach with three dimensional response modelling. Biochim. Biophys. Acta - Mol. Cell Biol. Lipids 1861, 1652–1661 (2016).

25. Martins Cardoso, R. et al. Hypercholesterolemia in young adult APOE −/− mice alters epidermal lipid composition and impairs barrier function. Biochim. Biophys. Acta - Mol. Cell Biol. Lipids 1864, 976–984 (2019).

26. Motta, S. et al. Ceramide composition of the psoriatic scale. BBA - Mol. Basis Dis. 1182, 147–151 (1993).

27. Chomczynski, P. & Sacchi, N. The single-step method of RNA isolation by acid guanidinium thiocyanate–phenol–chloroform extraction: twenty-something years on. Nat. Protoc. 1, 581–585 (2006).

28. Gordon, C. J. The mouse: An "average" homeotherm. J. Therm. Biol. 37, 286–290 (2012).

29. Gordon, C. J. The mouse thermoregulatory system: Its impact on translating biomedical data to humans. Physiol. Behav. 179, 55–66 (2017).

30. Mei, J. et al. Body temperature measurement in mice during acute illness: implantable temperature transponder versus surface infrared thermometry. Sci. Rep. 8, 3526 (2018).

31. Janssens, M. et al. Increase in short-chain ceramides correlates with an altered lipid organization and decreased barrier function in atopic eczema patients. J. Lipid Res. 53, 2755–2766 (2012).

32. Danso, M. et al. Altered expression of epidermal lipid bio-synthesis enzymes in atopic dermatitis skin is accompanied by changes in stratum corneum lipid composition. J. Dermatol. Sci. 88, 57–66 (2017).

33. van Smeden, J. et al. The importance of free fatty acid chain length for the skin barrier function in atopic eczema patients. Exp. Dermatol. 23, 45–52 (2014).

34. Kaabia, Z. et al. Plasma lipidomic analysis reveals strong similarities between lipid fingerprints in human, hamster and mouse compared to other animal species. Sci. Rep. 8, 15893 (2018).

35. Plump, A. S. et al. ApoA-I knockout mice: Characterization of HDL metabolism in homozygotes and identification of a post-RNA mechanism of apoA-I up-regulation in heterozygotes. J. Lipid Res. 38, 1033–1047 (1997).

36. van Smeden, J. et al. Intercellular Skin Barrier Lipid Composition and Organization in Netherton Syndrome Patients. J. Invest. Dermatol. 134, 1238–1245 (2014).

37. Kim, C.-W. et al. Acetyl CoA Carboxylase Inhibition Reduces Hepatic Steatosis but Elevates Plasma Triglycerides in Mice and Humans: A Bedside to Bench Investigation. Cell Metab. 26, 394-406.e6 (2017).

38. Roe, N. D., Handzlik, M. K., Li, T. & Tian, R. The Role of Diacylglycerol Acyltransferase (DGAT) 1 and 2 in Cardiac Metabolism and Function. Sci. Rep. 8, 4983 (2018).

39. Wilhelm, A. J. et al. Apolipoprotein A-I Modulates Regulatory T Cells in Autoimmune LDLr −/− , ApoA-I −/− Mice. J. Biol. Chem. 285, 36158–36169 (2010).

40. Zabalawi, M. et al. Inflammation and skin cholesterol in LDLr −/− , apoA-I −/− mice: link between cholesterol homeostasis and self-tolerance? J. Lipid Res. 48, 52–65 (2007).

41. Aiello, R. J. et al. Increased atherosclerosis in hyperlipidemic mice with inactivation of ABCA1 in macrophages. Arterioscler. Thromb. Vasc. Biol. 22, 630–637 (2002).

SUPPLEMENTARY INFORMATION

1. MATERIALS

Table S1. Forward and reverse primer sequences used for q-PCR.

Protein (Gene)	Forward primer Reverse primer
Ribosomal protein, large, P0 (RPL0)	CTGAGTACACCTTCCCACTTACTGA CGACTCTTCCTTTGCTTCAGCTTT
Ribosomal protein L37 (RPS37)	AGAGACGAAACACTACCGGGACTGG CTTGGGTTTCGGCGTTGTTCCCTC
Acetyl-Coenzyme A carboxylase alpha (ACC or ACACA)	GGAAGATGGCGTCCGCTCTGTG GTGAGATGTGCTGGGTCATGTGGAC
Ceramide synthase 2 (CERS2)	ACGTGTCTATGCCAAAGCCTCAGATC CGCAGTCGGGTTTTCTCCTTAACATTC
Ceramide synthase 3 (CERS3)	GGGCCTCCACGTTTACTGGGGT GCCCTTGGTGCTCTCTGCTTCCT
Delta(4)-desaturase, sphingolipid 1 (DEGS1)	GAGCACCATGACTTCCCCAACGTTC CAGGAGTTGTAGTGCGGGAGGTCAT
Diacylglycerol O-acyltransferase 2 (DGAT2)	TATTGGTTTCGCCCCCTGCATCTTC ATGTCTTTCTGGGTCGGGTGCTC
Elongation of very long chain fatty acids 1 (ELOVL1)	GGCAGAACTTGCCCCTGAGAAGAA TTCACAACAGCCTCCATCCTGGC
Elongation of very long chain fatty acids 4 (ELOVL4)	TGGAATCAAGTGGGTGGCTGGAGG AGCATGGTCAGGTATCGCTTCCACC
Elongation of very long chain fatty acids 6 (ELOVL6)	GGACCTGTCAGCAAATTCTGGGCTTA GGAGTACCAGGAGTACAGGAGCACA
Fatty acid synthase (FAS)	GGCGGCACCTATGGCGAGG CTCCAGCAGTGTGCGGTGGTC
3-hydroxy-3-methylglutaryl-CoA reductase (HMGCR)	CGAGCCACGACCTAATGAAGAATG TGCATCACTAAGGAACTTTGCACC
3-hydroxy-3-methylglutaryl-CoA synthase 1 (HMGCS1)	AAAACACAGAAGGACTTACGCCCGG GTTGCAGGGAGTCTTGGCACTTTCT
Involucrin (IVL)	CCTCTGCCTTCTCCCTCCTGTGAGT ACACAGTCTTGAGAGGTCCCTGAACCA
Keratin 10 (K10)	GCGGCGACCAATCATCTAAAGGACC CCAGTGGCCCGTATGAAGAGACTCT
Low density lipoprotein receptor (LDLR)	TGTGTGATGGAGACCGAGATTG CGTCAACACAGTCGACATCC
Stearoyl-Coenzyme A desaturase 1 (SCD1)	TACTACAAGCCCGGCCTCC CAGCAGTACCAGGGCACCA
Scavenger receptor class B member I (SR-BI)	AAACAGGGAAGATCGAGCCAGTAG CGTAGTGAAGAACCTGGGGCAT

2. RESULTS

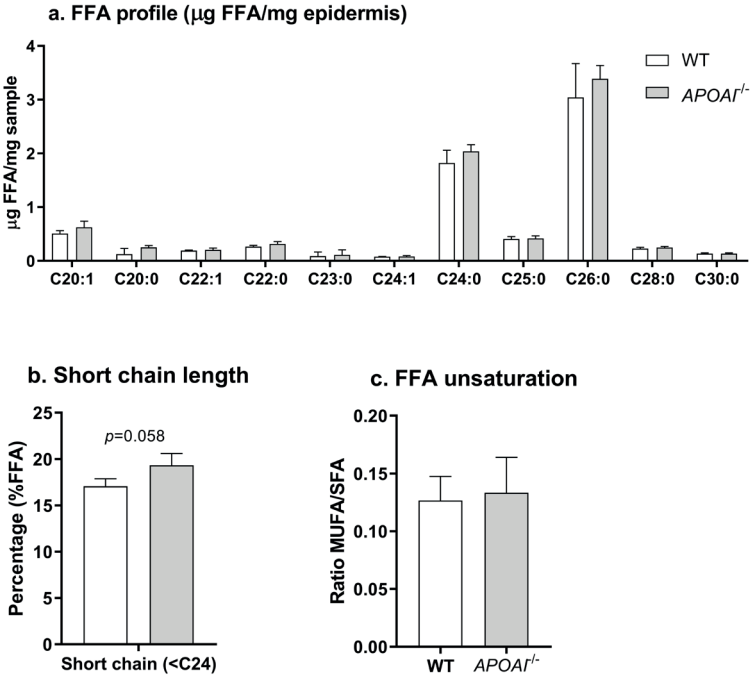

Figure S1. FFA composition in the skin of WT and *APOAI*$^{-/-}$ mice. A. Total absolute FFA content in the epidermis depicted according to the carbon chain length. B. The relative abundance of short chain FFAs defined as FFA species with less than 24 carbons. C. Ratio between unsaturated and saturated FFAs. Data shown as mean±SD and plotted (n=3 animals/group).

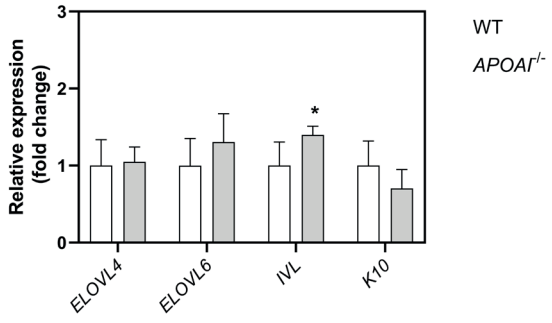

Figure S2. Gene expression profile in the skin of WT and *APOAI*$^{-/-}$ mice. Data shown as mean±SD and plotted as fold change expression compared to the WT control (n=5-6 animals/group). Statistical significance was determined by two-tailed unpaired student's t-Test. *p<0.05

Chapter 5

Barrier lipid composition and response to plasma lipids: a direct comparison of mouse dorsal back and ear skin

Experimental Dermatology 29(6): 548-555 (2020).

Renata Martins Cardoso[1], Samira Absalah[1], Miranda Van Eck[1*], Joke A. Bouwstra[*]

[1]Division of BioTherapeutics, Leiden Academic Centre for Drug Research, Leiden University, Leiden, The Netherlands

*Both authors contributed equally

ABSTRACT

The skin of the ear and the back are frequently selected sites in skin research using mouse models. However, distinct responses to treatment have been described between these two sites in several studies. Despite the crucial role of the stratum corneum (SC) in the skin barrier function of both dorsal back and ear skin, it remains unclear whether differences in lipid composition might underlie altered responses. Here, we compared the skin morphology and the barrier lipid composition of the ear with the back skin of wild-type mice. The ear contained more corneocyte layers in the SC and its barrier lipid composition was enriched with sphingosine ceramide subclasses, especially the short ones with a total chain length of 33-34 carbon atoms. The free fatty acid (FFA) profile in the ear skin shifted towards shorter chains, significantly reducing the mean chain length to 23.3 versus 24.7 carbon atoms in the back skin. In line, FFA species in the ear displayed a 2-fold increase in unsaturation index ($p<0.001$). Gene expression in the ear skin revealed low expression of genes involved in lipid synthesis and uptake, indicating a reduced metabolic activity. Finally, the effects of hypercholesterolemia on the SC FFA composition of the ear and the back skin was assessed in apolipoprotein E knockout (*APOE*$^{-/-}$) mice. Interestingly, the FFA profile in *APOE*$^{-/-}$ ear skin was minimally affected, while the FFA composition in the *APOE*$^{-/-}$ back skin was markedly changed in response to hypercholesterolemia. In conclusion, ear and back skin have distinct barrier lipids and respond differently to elevated plasma cholesterol.

Keywords: *Ceramides, fatty acids, wild-type mice, apolipoprotein E knockout mice*

1. INTRODUCTION

Our understanding of skin morphology and lipid composition has benefitted greatly from the use of *in vivo* animal models[1–3]. In particular, mouse models have been proven a valuable tool in skin research as it offers the possibility to genetically manipulate these animals to study the role of specific skin components (*e.g.* enzymes, proteins, receptors) and to generate *in vivo* diseased skin models[1,2]. In research, the back skin and the ear skin of mice are commonly used sites. However, previous studies reported differential effects/phenotypes on ear skin versus the back skin regarding, among others, drug treatment (*e.g.* imiquimod-induced psoriasis, allergic contact dermatitis), melanocyte function, and tissue regeneration[4–6]. The back skin comprises a relatively large area for performing experiments, but in hairy mice it contains a high density of hair follicles (fur) that can complicate the interpretation of the results[5]. In most studies, the fur is shaved to allow skin treatment and analysis. At the same time, the hair follicles may offer an alternative pathway for compound permeation[7,8]. In contrast, the ear represents an easily accessible, but small, skin area with a low density of hair follicles and centrally supported by a cartilaginous tissue framework[5].

Regardless of the skin site, the stratum corneum (SC) has a critical role in skin barrier function protecting against body desiccation and harmful chemicals and pathogens[9]. The SC is a well-organized structure of corneocytes (dead cornified keratinocytes) surrounded by an extracellular lipid matrix with free fatty acids (FFAs), ceramides (CERs), and cholesterol as major lipid classes[10]. Currently, however, there are no studies comparing SC lipids as the primary barrier components in the back versus ear skin. The lipids constituting the SC matrix are mostly synthesized by differentiating keratinocytes[10] or taken up from the plasma via lipoprotein receptors (*e.g.* low-density lipoprotein receptor, scavenger receptor class B member I (SR-BI), and cluster of differentiation 36 (CD36))[11–13]. For the skin barrier function the only continuous pathway connecting the environment with the viable epidermis is the SC extracellular lipid matrix[14]. Alterations in the composition of these lipids have been described in various skin pathologies, and it has been demonstrated that the SC lipids are crucial for the primary barrier components in the skin[15–20]. Exogenous molecules can penetrate the skin via this SC lipid matrix, particularly when the SC lipid profile is modified in response to (environmental) stressors and inflammatory processes.

Recently, we showed that increased plasma lipoprotein levels as described for apolipoprotein E knockout (*APOE*$^{-/-}$) and *SR-BI*$^{-/-}$ mice are associated with an altered lipid profile in the back skin at young age, affecting mainly the FFA composition[21,22]. In the severely hypercholesterolemic *APOE*$^{-/-}$ mice these epidermal lipids changes led

to functional differences in transepidermal water loss towards a less effective skin barrier. *APOE*$^{-/-}$ mice and other hypercholesterolemic mouse models have recently been used to study the relation between psoriasis and the comorbidities dyslipidemia and atherosclerosis[23–25]. Differential effects in *APOE*$^{-/-}$ mice have been described in response to the induction of psoriasis-like skin inflammation by topical application of compounds on ear *vs* back skin, with the back skin being more effective in generating the desired phenotype[6,26]. As lipids play a major role in the skin barrier, it is crucial to understand whether the epidermal lipid barrier in the ear is similarly impacted by hypercholesterolemia as previously demonstrated for the back skin of *APOE*$^{-/-}$ mice.

In this study, we used young adult wild-type (WT) mice to compare the morphology, lipid composition and gene expression between dorsal and ear skin. In addition, the epidermal lipid composition of the well-established hypercholesterolemic *APOE*$^{-/-}$ mice was also analyzed to assess whether the ear skin develops similar differences in lipid matrix composition in response to hypercholesterolemia as previously described for the back skin of these mice[22].

2. MATERIALS AND METHODS

2.1 Materials and chemicals

Rodent chow diet low in fat and cholesterol (Rat and Mouse No.3 breeding diet) purchased from Special Diets Services (United Kingdom). We obtained ketamine and atropine from AUV Veterinary Services (Cuijk, The Netherlands) and xylazine from ASTFarma (Oudewater, The Netherlands). Sodium phosphate dibasic (Na_2HPO_4), hematoxylin, eosin, trypsin from bovine pancreas, trypsin inhibitor, free fatty acids with 16 to 30 carbon atoms (FFA C16-30), deuterated FFA C18, deuterated FFA C24, chloroform, safranin-O, acetic acid, trifluoroacetic acid were obtained from Sigma-Aldrich (Zwijndrecht, The Netherlands). Heptane was purchased from ChemLab (Zedelgem, Belgium). Tissue-Tek O.C.T. was purchased from Sakura Finetek Europe B.V. (The Netherlands). Sodium chloride (NaCl) was purchased from Boom (Meppel, The Netherlands). Synthetic CER CER[N(C24deuterated)S(C18protonated)] were kindly provided by Evonik Industries (Essen, Germany). From Merck (Darmstadt, Germany) we bought potassium dihydrogen phosphate (KH_2PO_4), potassium chloride (KCl), potassium hydroxide and Entellan®. Methanol, ethanol, isopropanol and acetonitrile were from Biosolve (Valkenswaard, The Netherlands). All solvents had analytical grade.

2.2 Animals and samples

16-18 weeks old female C57BL/6 WT mice and female *APOE*$^{-/-}$ mice (obtained from The Jackson Laboratory and bred at the Gorlaeus laboratories) were kept under standard laboratory conditions (20°C and light cycle of 12 hours light/12 hours dark) with water and standard low-fat chow diet provided ad libitum (Rat and Mouse No.3 breeding diet). Prior sacrifice, the mice were anesthetized with a mixture of xylazine, atropine and ketamine (70 mg/kg; 1.8 mg/kg; 350 mg/kg body weight, respectively) and perfused with phosphate buffered saline (PBS; 8.13 g/L NaCl, 2.87 g/L Na_2HPO_4, 0.2 g/L KH_2PO_4, 0.19 g/L KCl in milliQ water; pH 7.4). The ears (WT and *APOE*$^{-/-}$ mice) and the shaved back skin (WT mice) were processed for morphological stainings (hematoxylin and eosin, and safranin-O), epidermal lipid composition analysis (liquid chromatography/mass spectrometry; LC/MS) and gene expression analysis (q-PCR). For sebum lipids analysis, hairs were collected from the back skin of both WT and *APOE*$^{-/-}$ mice. The sebum lipid composition was analyzed by LC/MS. Experiments were performed in agreement with National guidelines and approved Animal Experiments Ethics Committee of Leiden University.

2.3 Morphology stainings

Both ear and dorsal skin were embedded in tissue-tek and snap-frozen in liquid nitrogen. Frozen sample sections (8 µm) were rinsed in PBS and stained with hematoxylin and eosin according to manufacturer's protocol. The sections were mounted in DPX and imaged with a Zeiss Axioplan 2 light microscope (Zeiss, Best, The Netherlands). Frozen skin sections (8 µm) were fixed in cold acetone for 10 min and incubated with safranin-O solution (1% safranin-O in milliQ water) for 1 min. The sections were rinsed in milliQ to remove the excess of safranin-O and incubated with KOH solution (2% KOH in milliQ water) for 20 minutes[27]. The slides were covered with coverslip and imaged with a Zeiss Axioplan 2 light microscope (Zeiss, Best, The Netherlands).

2.4 Epidermal lipid extraction

The epidermis was isolated from the dorsal skin by trypsinization (0.3 % w/v trypsin in PBS; pH 7.4). Skin samples without the hypodermis were stretched on a paper filter soaked in 0.3 % w/v trypsin solution in PBS (pH 7.4) overnight at low temperature (4°C) for trypsin diffusion throughout the samples. Next day, the dorsal skin was incubated at 37°C (1 hour) for trypsin activation and subsequent isolation of the epidermis. Afterwards, the trypsin in the samples was neutralized by washing the samples in 0.1% w/v trypsin inhibitor in PBS and in demi-water. After air-drying, the samples were

placed under argon atmosphere for storage and further SC lipid extraction. The ears were used directly for lipid extraction as epidermal separation by trypsinization was not possible. Instead, a piece of the ear was completely submerged in the solvent mixes for lipid extraction. Considering that murine skin has few corneocytes layers and a thin epidermis compared to human skin, also for the ear likely the barrier lipids from the epidermis were extracted. Hairs were removed from the back skin using tweezers and used to extract sebum lipids. Epidermal lipids from the ear and the back and the sebum lipids surrounding the hairs were extracted with a modified Bligh and Dyer method described previously[28]. Lipid extracts in chloroform:methanol (2:1; v/v) and under argon atmosphere were kept at 4°C for liquid chromatography-mass spectrometry (LC/MS) CER and FFA analysis.

2.5 Liquid chromatography-mass spectrometry (LC/MS)

LC/MS analysis of epidermal and sebum CERs and FFAs was performed as described previously[22]. For CER analysis, 5 µL of lipid extracts reconstituted in heptane:chloroform:methanol (95:2.5:2.5; v/v/v) at a lipid concentration of 0.3 mg/mL were injected in an Acquity UPLC H-class system (Waters, Milford, MA, USA) connected to a triple-quadrupole XEVO TQ-S mass spectrometer (Waters, Milford, MA, USA). A normal phase column (PVA-Sil column: 5 µm particle size, 100x2.1 mm i.d., YMC, Kyoto, Japan) was used for CER separation with the solvent flow rate set to 0.8 ml/min (Supplementary Table S1). The MS was coupled to atmospheric pressure chemical ionization (APCI) chamber set to positive ion mode and the detector measured in full scans from 350-1200 amu. Software Waters MassLynx 4.1 was used to determine the area under the curve (AUC) followed by internal standard correction for CER analysis. Deuterated CER NS (C24 deuterated; C18 protonated) was used as internal standard. CERs were further analyzed according to a method described by Boiten *et. al.* (2016)[28]. CER data was plotted as relative molar percentage of ceramide subclasses based on the total amount of CERs. CER subclasses in this paper were identified using the nomenclature described by Motta *et. al.* (1993)[29]. For FFA analysis, 2 µl of lipid extracts reconstituted in isopropanol to a lipid concentration of 0.75 mg/mL were injected in the same UPLC-mass spectrometry system described for the CERs. As internal standards, deuterated FFA C18 and FFA C24 were added to all samples prior their injection into the UPLC-system. FFAs were separated in the UPLC system using a Purospher Star LiChroCART reverse phase column (3 µm particle size, 55x2 mm i.d., 55x2 mm, Merck, Darmstadt, Germany) with the solvent flow rate set to 0.5 mL/min (Supplementary Table S2). The XEVO TQ-S mass spectrometer connected to an APCI chamber (probe temperature: 425°C, discharge current 3 µA.) was set to negative mode and detector measured in full scan from 200-550 amu. FFA Data analysis was performed by Software

Waters MassLynx 4.1 to determine the AUC followed by internal standard correction. Response was calculated based on calibration curves of FFA C16-C30. Data was presented as relative molar percentage to the total amount of FFA detected. Saturated and unsaturated FFA C16-C18 are highly present in sebum lipids and were plotted separately (data not shown).

2.6 qPCR

Total RNA was isolated from ear and dorsal skin samples (without hypodermis) by the guanidinium thiocyanate method[30]. cDNA was synthetized from 1 µg total RNA (M-MuLV reverse transcriptase, ThermoFisher Technologies). Quantitative analysis of the genes (QuantStudio 6 Flex Real-time PCR systems, Applied Biosystems, Foster City, CA, USA) was done using SYBR Green detection technology. The expression of the target genes was normalized by the expression of the reference genes beta-actin (*β-actin*) and fatty acid binding protein 5 (*FABP5*). The expression of target genes in the ear and dorsal skin was plotted as relative fold change compared to the gene expression in the dorsal skin. Information regarding the forward and reverse primer sequences is available in Supplementary Table S3.

2.7 Statistical analysis

Data is presented as mean±SD and statistical significance was calculated using GraphPad Prism 8 (GraphPad Software Inc., CA, USA). *P* values below 0.05 were considered significant.

3. RESULTS

3.1 Thicker SC layer in the ear skin compared to the back skin

The general morphology of the ear skin and back skin of wild-type C57BL/6 mice was assessed by hematoxylin and eosin (HE), and safranin-O stainings (Fig. 1). HE staining of the ear showed a central cartilaginous structure. The hypodermis was more pronounced in the back skin than in ear skin. The dermis and epidermis presented comparable morphology between the two different skin sites. Safranin-O staining revealed a higher number of corneocyte layers in the ear SC compared to the back skin. In the latter, corneocytes showed more expansion in response to the alkali environment during the safranin-O staining

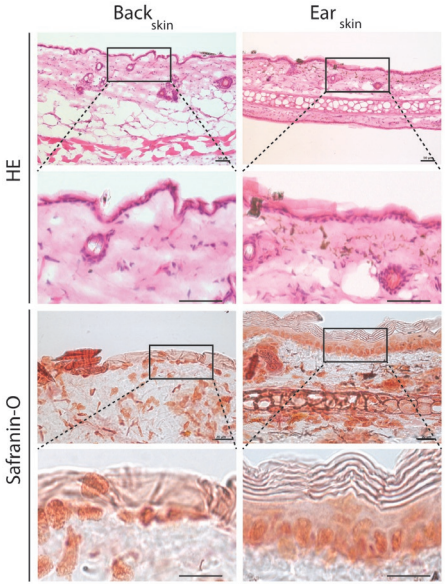

Figure 1. Epidermal and dermal morphology of back skin and ear skin. Back skin and ear cryostat sections (8 µm) stained with (a) hematoxylin and eosin (HE, scale bar: 50 µm) and (b) safranin-O (scale bar: 20 µm). Micrographs representative of 3 WT mice.

3.2 Epidermal CER composition strongly differs between dorsal and ear skin

For epidermal CER analysis, the epidermis was isolated from dermis in the back skin and used for lipid extraction (Fig. 2a). For the ear skin, lipids were extracted from the most distal section of the ear (Fig. 2b). Subsequently, the composition of CERs in the extracted lipids was analyzed by LC/MS. CER subclasses nomenclature is a combined representation of the acyl chains (non-hydroxy fatty acid [N]; α-hydroxy fatty acid [A] or esterified ω-hydroxy fatty acid [EO]) with the sphingoid base (dihydrosphingosine, [dS]; sphingosine [S] or phytosphingosine [P]) as reported by Motta *et. al.* (1993)[29]. The molar percentage distribution of the CER subclasses was strikingly different in the ear skin compared with the back skin (Fig 2c). The majority of the CERs are sphingosine base (CER[S]) at both skin sites (55% in the back skin vs 75% in the ear skin). Nonetheless, in the back skin CER NdS is most abundantly present (nearly 40%), while in ear skin NS and AS are present at higher concentrations (45% and 28%, respectively) than in back skin. The ω-esterified CERs (CER[EO]), composed of CER EOS and EOdS, represented 7% of the CERs in the back skin. In the ear skin CER EOS accounted for 14% of the CER content whereas CER EOdS was not detected. The CER[non-EO] chain length

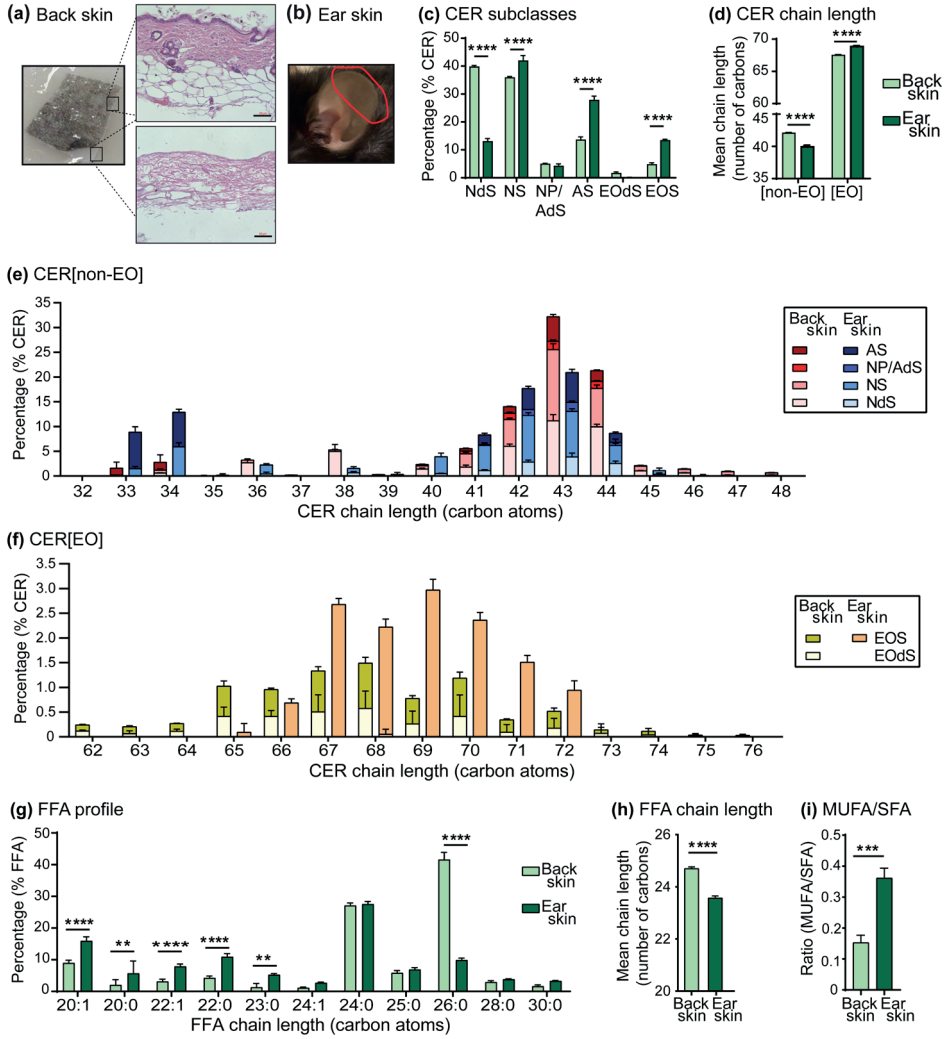

Figure 2. CER and FFA composition of the ear and back skin. CERs and FFAs were quantified by LC/MS. Representative images showing (a) epidermis isolation from back skin and (b) distal part of the ear (red circled area) used for lipid extraction. CERs are named according to nomenclature described by Motta *et. al.* (1993); (c) Distribution of CER subclasses (% molar); (d) CER mean chain length; total CER chain length distribution (e) CER[nonEO] and (f) CER[EO]; (g) FFA chain length distribution (molar %); (h) mean FFA chain length; (i) molar ratio between monounsaturated FAs (MUFA) and saturated FAs (SFA). Statistical significance was determined by Two-way ANOVA with Holm-Sĭdak post-hoc test and by two-tailed unpaired Student's T-test. Data presented as mean±SD (molar); n=3-4 samples/group; **p<0.01; ***p<0.001; ****p<0.0001.

distribution revealed higher abundance of long chain CERs (≥43 carbon atoms) in the back skin, while ear skin showed increased presence of short chain length CERs

(≤42 carbon atoms). Among the short chain CERs, the C33 and C34 CERs were strongly present in ear skin (22%) compared to back skin (5%) (Fig. 2d-e). The mean chain length of CER[non-EO] was shorter in the ear (39.5 carbon atoms vs. 41.8 carbon atoms in the back skin). When focusing on CER [EO], in the back skin, the mean chain length was 67.7 carbons while in the ear skin this average was 68.9 carbons (p<0.0001) with marked detection of CERs with 62-65 carbons, which were merely present in the ear skin (Fig. 2d-f).

3.3 Skin lipids in the ear are enriched in short and unsaturated FFA species

The composition of the FFAs with a chain length between 20-30 carbons atoms in the ear and the back skin was determined by LC/MS. The FFA composition of the ear skin showed a shift towards shorter and more unsaturated FFA species (Fig. 2g). In the back skin, FFA C24:0 and FFA C26:0 were most prevalent FFAs, accounting for nearly 70% of the total amount of FFAs (Fig. 2g). In the ear skin, FFA C20:1 and C24:0 were most abundant, comprising 43% of the FFAs with a striking four-fold reduction in the percentage of FFA C26:0 to only 10% (Fig. 2g). These differences strongly contributed to a shorter mean FFA chain length of 23.3 carbons in the ear compared to an average FFA chain length of 24.5 carbons atoms in the back skin (p<0.0001) (Fig. 2h). The mol ratio between mono-unsaturated FAs (MUFAs) and saturated FAs (SFAs) was 2-fold higher in the ear FFA species (0.36±0.03) than in the back FFAs (0.15±0.02) (p<0.001) (Fig. 2i).

3.4 Lower basal mRNA levels of genes involved lipid synthesis in the ear skin

The expression of genes involved in lipid synthesis and keratinocyte proliferation and differentiation was assessed to determine the underlying factors responsible for the differences in lipid composition in the ear and in the back skin. Basal mRNA levels of genes involved in cholesterol synthesis (*HMGCS1*; 2-fold), esterification (*ACAT1*; 3-4-fold) and uptake of lipoproteins (*LDLR*; 2-fold) were significantly lower in the ear compared to the back skin (Fig. 3a). In addition, the ear also showed a nearly 70% reduction in the expression *CERS3* and *GBA* (synthesis of esterified-ω-CERs and cleavage of glucosyl-CERs, respectively) with no changes in the expression of *DEGS1* (enzyme involved in synthesis step of CER[S] from CER[dS]) (Fig. 3b). Expression of fatty acid synthase (*FAS*) was reduced by 30% in the ear while expression of *SCD1*, an enzyme involved in fatty acid chain desaturation, was comparable between groups (Fig. 3c). The ear also showed reduced expression of genes involved in FFA chain elongation; *ELOVL1* (2-fold) and *ELOVL4* (3-fold) (Fig. 3c). In line with the lower expression of genes related to lipid synthesis, mRNA levels of *DGAT2* (triglyceride synthesis) and *ABCA12* (lipid transport to lamellar bodies) were also decreased in

the ear skin (Fig. 3d). The back skin showed higher expression of genes involved in keratinocyte differentiation (*IVL*) and proliferation (*K10*) markers (p<0.0001) (Fig. 3d).

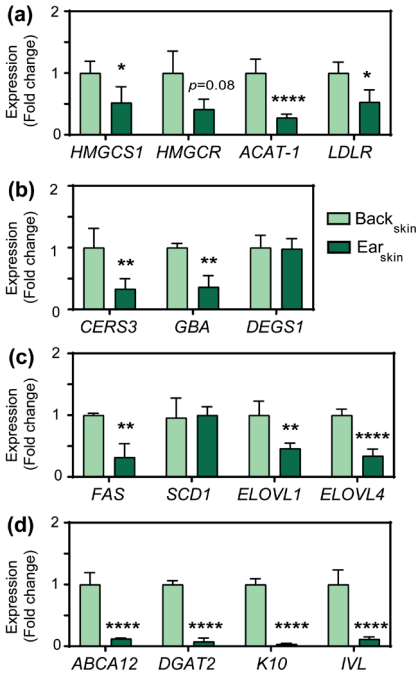

Figure 3. Ear skin shows lower expression levels of several genes involved in skin lipid metabolism and keratinocyte markers. mRNA levels of genes related to the synthesis or uptake of (a) cholesterol; synthesis of (b) CERs; and (c) FFAs. Expression of genes linked to (d) lipid transport in lamellar bodies; triglyceride (TG) synthesis; and keratinocyte proliferation and differentiation. Statistical significance was determined by two-tailed unpaired Student's T-test; *p<0.05; **p<0.01; ****p<0.0001. Data presented as mean±SD; n=5/group.

3.5 Changes in plasma lipid composition differentially affect dorsal and ear skin

The back skin of hypercholesterolemic *APOE*$^{-/-}$ mice shows an altered FFA profile in response to the massively increased levels of apolipoprotein B containing lipoprotein particles in the circulation at young age[22]. It remains unknown whether the skin in the ears is similarly affected by this hypercholesterolemic profile. Thus, next, we analyzed the FFA composition in the ear of *APOE*$^{-/-}$ mice and compared it to that described for WT ear skin in Figure 2g. The relative distribution of FFA (% total FFA) in the ear of *APOE*$^{-/-}$ mice was nearly comparable to the composition described for WT ear (Fig. 4a). The FFA composition in the ear of *APOE*$^{-/-}$ mice showed a significant increase in the percentage of FFA C20:0 (p<0.0001) accompanied by reduction in the percentage of FFA C24:0

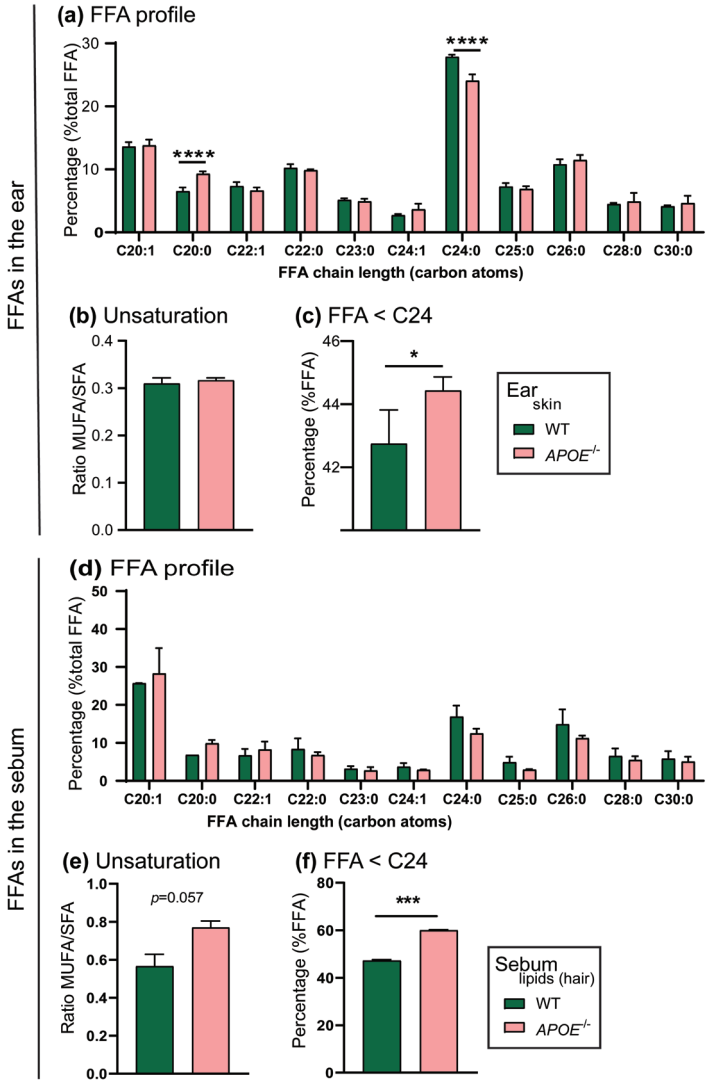

Figure 4. FFA composition of the ear and of sebum in normolipidemic WT and hypercholesterolemic *APOE*$^{-/-}$ mice. FFA profile: (a) FFA chain length distribution profile in the ear skin; (b) molar ratio between monounsaturated FFAs (MUFA) and saturated FFAs (SFA) in the ear skin; (c) percentage of short chain FFA (FFA chains containing less than 24 carbon atoms) in the ear skin; (d) FFA chain length distribution profile in the sebum lipids; (e) molar ratio between monounsaturated FFAs (MUFA) and saturated FFAs (SFA) in the sebum lipids; (f) percentage of short chain FFA (FFA chains containing less than 24 carbon atoms) in the sebum lipids. Statistical significance was determined by One-way ANOVA with Holm-Sĭdak post-hoc test and by two-tailed unpaired Student's T-test. Data presented as mean±SD; n=3-4 samples/group; *p<0.05; ****p<0.0001.

(p<0.0001). Consequently, a small shift towards a shorter chain length was observed in the ear of *APOE*$^{-/-}$ mice (Fig. 4b). The molar ratio between monounsaturated and saturated FFA species was not altered (Fig. 4c). Sebum lipids, produced by sebaceous glands, contribute to the skin surface lipid pool, particularly in back skin with a high density of hair follicles, and hence, sebaceous glands[31]. Triglycerides, a component of sebum lipids, may undergo hydrolysis by microbial lipases generating FFAs[32–34]. Thus, next we compared the composition of the FFAs in the sebum surrounding back skin hairs of both WT and *APOE*$^{-/-}$ mice to assess whether the sebum of *APOE*$^{-/-}$ mice was affected by the hypercholesterolemic profile of these mice. The sebum FFA composition of WT and *APOE*$^{-/-}$ mice was overall comparable (Fig. 4d), indicating that the observed differential response to hypercholesterolemia between back and ear skin cannot be explained by effects on the FFA content of sebum.

4. DISCUSSION

In mouse models both ear and back skin have been proven valuable assets in a large range of skin studies[1–3]. However, similarities and differences between ear and back skin are not extensively examined. In the present study, we provide evidence that the lipid composition of the skin barrier is fundamentally different between the two sites, as is the expression of genes related to lipid synthesis and keratinocytes differentiation and proliferation. In addition, the skin of the ear showed only a minimal response to hypercholesterolemic conditions as compared to the back skin.

The density of hair follicles and the number of corneocyte layers in the SC are important factors in skin research as they directly relate to skin permeability and, thus, barrier function. In hairy mice, the high density of hair follicles provides a smaller interfollicular area and comprises a permeation pathway into the skin. In the hairy C57Bl6 mouse strain, melanin production is restricted to the hair follicles and absent in the skin. Melanin is mostly produced during the anagen phase of the hair growth, giving the skin a dark pigmentation[35]. As hair growth in the murine skin occurs in waves, it leads to the formation of dark pigmented areas (dark patches) and non-pigmented areas ("white" patches). The dark skin patches with synchronized hair cycles appear after the age of 10 weeks[35]. In this study, "white" skin patches at similar position in the back skin were used for analysis as different hair cycles can influence the skin response to compounds and even the development of inflammation[25,36]. The SC in these "white" back skin patches of hairy mice has fewer number of corneocyte layers as compared to ear skin. The back skin of nude-mice with a larger interfollicular area displays a thicker SC with more corneocyte layers[37], suggesting that the reduced number of corneocyte layers in hairy mice is a direct effect of the presence of dense hair follicles and/or fur.

The reduced number of corneocyte layers in the back skin may require a faster turnover/replacement to preserve the barrier, whilst in the ear skin this turnover may take longer. Also, the ear skin has a lower density of blood vessels as well as lymphatic vessels than the back skin indicating a reduced metabolic activity and even drainage in the ear[6,38,39]. Accordingly, the basal expression of genes related to lipid synthesis/uptake and keratinocyte differentiation and proliferation was significantly higher in the back skin, likely reflecting the more active metabolic profile at this site.

The mRNA expression of the enzymes *CERS3, ELOVL1,* and *ELOVL4* was lower in ear skin as compared to back skin. *CERS3* encodes for the main ceramide synthase involved in the synthesis of CER[EO] and it regulates the elongation of FA chains by ELOVL1 and ELOVL4[40]. *In vitro* co-expression of *CERS3* with *ELOVL1* leads to an augmented production of CERs with a C26:0 acyl chain which is also accompanied by an increase in CERs with a C24:0 acyl chain[40]. Further elongation of C26:0 FAs is continued by ELOVL4 to generate both CER[non-EO] and CER[EO] with acyl chains containing more than 26 carbon atoms[40]. *In vivo*, *ELOVL1*$^{-/-}$ mice and *ELOVL4*$^{-/-}$ mice show a remarkable reduction in CER[EO] content and a shift towards CER containing acyl chains shorter than 24 carbons atoms[40,41]. Despite the low levels of *CERS3* in the ear skin, CER[EO] accounted for a relatively high percentage of the CERs in the ear skin, which may be a result of the overall percentage distribution of each subclass. Surprisingly, the mean chain length of CER[EO] was higher in the ear skin where reduced expressions of *ELOVL1* and *ELOVL4* were observed. Remarkably, the skin of *ELOVL4*$^{-/-}$ mice also showed major increases in the prevalence of CER NS and CER AS, especially containing acyl chain C26:0[42]. In the present study, the ear skin showed high prevalence of CER[S], while the expression of *DEGS1*, encoding for the desaturase enzyme that converts CER[dS] into CER[S][43], was comparable to the back skin, indicating that the reduced expression of *ELOVL4* can be related to the accumulation of CER NS and CER AS[42]. In line, the reduced expression of *CERS3, ELOVL1* and *ELOVL4* in the ear skin resulted in an increase in the fraction of sphingosine CERs with a total chain length of 33 and 34 carbon atoms, especially in CER NS and CER AS subclasses. Although CERs are essential components of the skin barrier, little information is available regarding the mechanism(s) involved in the regulation of ceramide synthesis[44]. Other factors, not included in the scope of this study (*e.g.* acyl-coenzyme A-binding protein), may also impact CER synthesis and contribute to the results described here[44].

The changes in the FFA composition in the ear corroborate with the reduced expression of *ELOVL1* and *ELOVL4* in the ear skin, leading to a FFA profile enriched with shorter chains. The ear skin also showed a higher presence of unsaturated FFA species compared to the back skin, although no changes were observed in the basal expression of *SCD1*,

an enzyme tightly regulated and subjected to fast turn on/off expression[45,46]. Altogether, our LC/MS and PCR data show that the skin lipid composition largely varies with the anatomical site even within young adult WT mice. Elucidation of the underlying causes for the reported differences between ear and back skin warrants further investigation.

As lipids are important components of the SC, variations in the skin lipid composition can affect the barrier function. In atopic dermatitis patients, the CER profile shows increased levels of CER NS and CER AS and a reduction of the average chain length linked to increased levels of C34 CERs in these subclasses[47]. These patients also have a higher percentage of short and unsaturated FFA species in their skin lipids[47]. Human skin equivalents, bioengineered *in vitro* models of human skin often containing activated keratinocytes, also show similar changes in lipid profile[48]. In both atopic dermatitis skin and in human skin equivalents samples, the altered lipid composition results in a reduced barrier function of the skin compared to native human skin[47,48]. In this view, it is likely that the changes in lipid composition described here for the ear skin is not favorable for an optimal lipid barrier, which may lead to higher number of corneocyte layers in order to compensate for this unfavorable lipid profile.

Lipids provided by plasma lipoproteins are also incorporated into the skin and hence an imbalance in lipoprotein profile may affect the composition of the barrier lipid pool[21,22,38,49]. Hypercholesterolemic *APOE*$^{-/-}$ mice develop skin inflammation and lipid deposits in the dermal compartment upon aging and when fed a high cholesterol/high fat diet[50,51]. Remarkably, already at young age, the back skin of these hypercholesterolemic mice shows altered epidermal lipid composition prior to the development of inflammatory skin profiles[22]. The FFA composition is especially affected in the back skin showing enrichment in short and unsaturated chains. In contrast, in the current study we found that the ear skin of young *APOE*$^{-/-}$ mice is minimally affected with only a minor shift towards shorter FFA chains. Considering the faster turnover of corneocyte layers in the back skin in combination with higher density of lymphatic and blood vessels, this skin site can more readily reflect the changes in the plasma lipids. Our findings provide insight why, as previously described, the ear and the back skin react differently to specific treatments leading to distinct outcomes; *e.g.* imiquimod-induced psoriasis[6].

In conclusion, the morphology and lipid composition of murine skin significantly varies depending on the body location, specifically in the ear and in the back skin. We suggest that the turnover rate of the corneocyte layer in combination with the level of metabolic activity of the skin site can be key players in the response to therapeutic intervention and to systemic lipid changes. Nonetheless, defining which skin site should be used in studies is not straightforward as the skin is a complex organ. It is important to further

characterize the morphological-, inflammatory-, and metabolic variations amongst skin sites in order to better match the skin site to the goal of the study.

CONFLICT OF INTEREST

The authors have declared no conflict of interest.

ACKNOWLEDGEMENTS

This research was funded by the Leiden Academic Centre for Drug Research (Leiden, The Netherlands).

REFERENCES

1. Avci, P. et al. Animal models of skin disease for drug discovery. Expert Opin. Drug Discov. 8, 331–355 (2013).

2. Abd, E. et al. Skin models for the testing of transdermal drugs. Clin. Pharmacol. Adv. Appl. Volume 8, 163–176 (2016).

3. Todo, H. Transdermal permeation of drugs in various animal species. Pharmaceutics 9, 1–11 (2017).

4. Nguyen, T. & Wei, M. L. Hermansky–Pudlak HPS1/pale ear Gene Regulates Epidermal and Dermal Melanocyte Development. J. Invest. Dermatol. 127, 421–428 (2007).

5. Metcalfe, A. D., Willis, H., Beare, A. & Ferguson, M. W. J. Characterizing regeneration in the vertebrate ear. J. Anat. 209, 439–446 (2006).

6. Madsen, M., Pedersen, T. X., Nielsen, L. B., Johansen, C. & Hansen, P. R. Differential Effects of Digoxin on Imiquimod-Induced Psoriasis-Like Skin Inflammation on the Ear and Back. Ann. Dermatol. 30, 485 (2018).

7. Mohd, F., Todo, H., Yoshimoto, M., Yusuf, E. & Sugibayashi, K. Contribution of the hair follicular pathway to total skin permeation of topically applied and exposed chemicals. Pharmaceutics 8, (2016).

8. Blume-Peytavi, U. et al. Follicular and percutaneous penetration pathways of topically applied minoxidil foam. Eur. J. Pharm. Biopharm. 76, 450–453 (2010).

9. Elias, P. M. Stratum corneum defensive functions: An integrated view. J. Invest. Dermatol. 125, 183–200 (2005).

10. Ponec, M., Weerheim, A., Lankhorst, P. & Wertz, P. New acylceramide in native and reconstructed epidermis. J. Invest. Dermatol. 120, 581–588 (2003).

11. Lin, M.-H. & Khnykin, D. Fatty acid transporters in skin development, function and disease. Biochim. Biophys. Acta 1841, 362–8 (2014).

12. Mommaas, M., Tada, J. & Ponec, M. Distribution of low-density lipoprotein receptors and apolipoprotein B on normal and on reconstructed human epidermis. J. Dermatol. Sci. 2, 97–105 (1991).

13. Tsuruoka, H. et al. Scavenger receptor class B type I is expressed in cultured keratinocytes and epidermis. Regulation in response to changes in cholesterol homeostasis and barrier requirements. J. Biol. Chem. 277, 2916–2922 (2002).

14. Sahle, F. F., Gebre-Mariam, T., Dobner, B., Wohlrab, J. & Neubert, R. H. H. Skin Diseases Associated with the Depletion of Stratum Corneum Lipids and Stratum Corneum Lipid Substitution Therapy. Skin Pharmacol. Physiol. 28, 42–55 (2015).

15. Zheng, Y. et al. PEG-Based Hydrogel Synthesis via the Photodimerization of Anthracene Groups. Macromolecules 35, 5228–5234 (2002).

16. Zhang, X. et al. Piezofluorochromic properties and mechanism of an aggregation-induced emission enhancement compound containing N-hexyl-phenothiazine and anthracene moieties. J. Phys. Chem. B 115, 7606–11 (2011).

17. Zhang, X.-X. et al. pH-Sensitive Fluorescent Dyes: Are They Really pH-Sensitive in Cells? Mol. Pharm. (2013). doi:10.1021/mp3006903

18. Janssens, M. et al. Increase in short-chain ceramides correlates with an altered lipid organization and decreased barrier function in atopic eczema patients. J. Lipid Res. 53, 2755–2766 (2012).

19. Hoekstra, M. et al. Absence of HDL cholesteryl ester uptake in mice via SR-BI impairs an adequate adrenal glucocorticoid-mediated stress response to fasting. J. Lipid Res. 49, 738–745 (2008).

20. van Smeden, J. et al. Intercellular Skin Barrier Lipid Composition and Organization in Netherton Syndrome Patients. J. Invest. Dermatol. 134, 1238–1245 (2014).

21. Martins Cardoso, R. et al. Hyperalphalipoproteinemic scavenger receptor BI knockout mice exhibit a disrupted epidermal lipid barrier. Biochim. Biophys. Acta - Mol. Cell Biol. Lipids 1865, 158592 (2020).

22. Martins Cardoso, R. et al. Hypercholesterolemia in young adult APOE −/− mice alters epidermal lipid composition and impairs barrier function. Biochim. Biophys. Acta - Mol. Cell Biol. Lipids 1864, 976–984 (2019).

23. Madsen, M. et al. Imiquimod-Induced Psoriasis-Like Skin Lesions Do Not Accelerate Atherosclerosis in Low-Density Lipoprotein Receptor–Deficient Mice. Am. J. Pathol. 188, 1486–1496 (2018).

24. Xie, X. et al. Imiquimod induced ApoE-deficient mice might be a composite animal model for the study of psoriasis and dyslipideamia comorbidity. J. Dermatol. Sci. 88, 20–28 (2017).

25. Madsen, M. et al. Effect of 12-O-tetradecanoylphorbol-13-acetate-induced psoriasis-like skin lesions on systemic inflammation and atherosclerosis in hypercholesterolaemic apolipoprotein E deficient mice. BMC Dermatol. 16, 9 (2016).

26. Schaper, K. et al. Sphingosine-1-phosphate exhibits anti-proliferative and anti-inflammatory effects in mouse models of psoriasis. J. Dermatol. Sci. 71, 29–36 (2013).

27. Oudshoorn, M. H. M. et al. Development of a murine model to evaluate the effect of vernix caseosa on skin barrier recovery. Exp. Dermatol. 18, 178–184 (2009).

28. Boiten, W., Absalah, S., Vreeken, R., Bouwstra, J. & van Smeden, J. Quantitative analysis of ceramides using a novel lipidomics approach with three dimensional response modelling. Biochim. Biophys. Acta - Mol. Cell Biol. Lipids 1861, 1652–1661 (2016).

29. Motta, S. et al. Ceramide composition of the psoriatic scale. BBA - Mol. Basis Dis. 1182, 147–151 (1993).

30. Chomczynski, P. & Sacchi, N. The single-step method of RNA isolation by acid guanidinium thiocyanate–phenol–chloroform extraction: twenty-something years on. Nat. Protoc. 1, 581–585 (2006).

31. Pappas, A., Johnsen, S., Liu, J.-C. & Eisinger, M. Sebum analysis of individuals with and without acne. Dermatoendocrinol. 1, 157–161 (2009).

32. Maier, H. et al. Normal Fur Development and Sebum Production Depends on Fatty Acid 2-Hydroxylase Expression in Sebaceous Glands. J. Biol. Chem. 286, 25922–25934 (2011).

33. Feldman, A. et al. Blimp1+ cells generate functional mouse sebaceous gland organoids in vitro. Nat. Commun. 10, 2348 (2019).

34. Dahlhoff, M. et al. Sebaceous lipids are essential for water repulsion, protection against UVB-induced apoptosis and ocular integrity in mice. Development 143, 1823–1831 (2016).

35. Plikus, M. V. & Chuong, C.-M. Complex Hair Cycle Domain Patterns and Regenerative Hair Waves in Living Rodents. J. Invest. Dermatol. 128, 1071–1080 (2008).

36. Hofmann, U., Tokura, Y., Nishijima, T., Takigawa, M. & Paus, R. Hair Cycle-Dependent Changes in Skin Immune Functions: Anagen-Associated Depression of Sensitization for Contact Hypersensitivity in Mice. J. Invest. Dermatol. 106, 598–604 (1996).

37. Rissmann, R., Oudshoorn, M. H. M., Hennink, W. E., Ponec, M. & Bouwstra, J. A. Skin barrier disruption by acetone: observations in a hairless mouse skin model. Arch. Dermatol. Res. 301, 609–613 (2009).

38. Liu, F., Smith, J., Zhang, Z., Cole, R. & Herron, B. J. Genetic heterogeneity of skin microvasculature.

Dev. Biol. 340, 480–489 (2010).

39. Huggenberger, R. et al. An important role of lymphatic vessel activation in limiting acute inflammation. Blood 117, 4667–4678 (2011).

40. Sassa, T. et al. Impaired Epidermal Permeability Barrier in Mice Lacking Elovl1, the Gene Responsible for Very-Long-Chain Fatty Acid Production. Mol. Cell. Biol. 33, 2787–2796 (2013).

41. Khnykin, D., Miner, J. H. & Jahnsen, F. Role of fatty acid transporters in epidermis: Implications for health and disease. Dermatoendocrinol. 3, 53–61 (2011).

42. Li, W. et al. Depletion of ceramides with very long chain fatty acids causes defective skin permeability barrier function, and neonatal lethality in ELOVL4 deficient mice. Int. J. Biol. Sci. 120–128 (2007). doi:10.7150/ijbs.3.120

43. Ternes, P., Franke, S., Zähringer, U., Sperling, P. & Heinz, E. Identification and Characterization of a Sphingolipid Δ4-Desaturase Family. J. Biol. Chem. 277, 25512–25518 (2002).

44. Ferreira, N. S. et al. Regulation of very-long acyl chain ceramide synthesis by acyl-CoA-binding protein. J. Biol. Chem. 292, 7588–7597 (2017).

45. Sampath, H. & Ntambi, J. M. Role of stearoyl-CoA desaturase-1 in skin integrity and whole body energy balance. J. Biol. Chem. 289, 2482–2488 (2014).

46. Mauvoisin, D. & Mounier, C. Hormonal and nutritional regulation of SCD1 gene expression. Biochimie 93, 78–86 (2011).

47. van Smeden, J. et al. The importance of free fatty acid chain length for the skin barrier function in atopic eczema patients. Exp. Dermatol. 23, 45–52 (2014).

48. Helder, R. W. J. et al. The effects of LXR agonist T0901317 and LXR antagonist GSK2033 on morphogenesis and lipid properties in full thickness skin models. Biochim. Biophys. Acta - Mol. Cell Biol. Lipids 1865, 158546 (2020).

49. Huang, L. et al. Interleukin-17 Drives Interstitial Entrapment of Tissue Lipoproteins in Experimental Psoriasis. Cell Metab. 29, 475-487.e7 (2019).

50. Feingold, K. R. et al. Apolipoprotein E Deficiency Leads to Cutaneous Foam Cell Formation in Mice. J. Invest. Dermatol. 104, 246–250 (1995).

51. Ang, L. S., Cruz, R. P., Hendel, A. & Granville, D. J. Apolipoprotein E, an important player in longevity and age-related diseases. Exp. Gerontol. 43, 615–622 (2008).

SUPPLEMENTARY INFORMATION

1. METHODS

1.1 Liquid chromatography-mass spectrometry (LC/MS)

Table S1. Gradient of solvents used for cholesterol and CER analysis by UPLC-LC/MS.

Run time (min)	Solvent A[1] (%)	Solvent B[2] (%)
0	98	2
2.5	96	4
2.6	93	7
6	88	12
11	50	50
13	98	2

[1]Solvent A - 100% Heptane

[2]Solvent B -Heptane:isopropanol:ethanol - 50:25:25; v/v/v

Table S2. Gradient of the solvents used for FFA analysis by UPLC-LC/MS.

Run time (min)	Solvent A[1] (%)	Solvent B[2] (%)
0	100	0
2.5	0	100
5	0	100
8	100	0
11	100	0

[1]Solvent A - Acetonitrile/milliQ/chloroform/acetic acid -90:10:2:0.005; v/v/v/v

[2]Solvent B -Methanol/heptane/chloroform/acetic acid -90:10:2:0.005; v/v/v/v

Table S3. Forward and reverse primer sequences used for q-PCR.

Protein (Gene)	Forward primer Reverse primer
Beta-actin (βACTIN)	CTTCTTTGCAGCTCCTTCGTTGCCG AATACAGCCCGGGGAGCATCGTC
Fatty acid binding protein 5 (FABP5)	GGACGGGAAGGAGAGCACGATAACA GCACCTTCTCATAGACCCGAGTGCA
ATP-binding cassette, subfamily A, member 12 (ABCA12)	GGAAGATGGCGTCCGCTCTGTG GTGAGATGTGCTGGGTCATGTGGAC
Acetyl-Coenzyme A acetyltransferase 1 (ACAT1)	AGCTGTTTCTCTGGGCCATCCAAT GAACTCTCCTGGCTTCAGGGCAT
Ceramide synthase 3 (CERS3)	GGGCCTCCACGTTTACTGGGGT GCCCTTGGTGCTCTCTGCTTCCT
Delta(4)-desaturase, sphingolipid 1 (DEGS1)	GAGCACCATGACTTCCCCAACGTTC CAGGAGTTGTAGTGCGGGAGGTCAT
Diacylglycerol O-acyltransferase 2 (DGAT2)	TATTGGTTTCGCCCCCTGCATCTTC ATGTCTTTCTGGGTCGGGTGCTC
Elongation of very long chain fatty acids 1 (ELOVL1)	GGCAGAACTTGCCCCTGAGAAGAA TTCACAACAGCCTCCATCCTGGC
Elongation of very long chain fatty acids 4 (ELOVL4)	TGGAATCAAGTGGGTGGCTGGAGG AGCATGGTCAGGTATCGCTTCCACC
Fatty acid synthase (FAS)	GGCGGCACCTATGGCGAGG CTCCAGCAGTGTGCGGTGGTC
Glucocerebrosidase (GBA)	GCCCTTGCCAACAGTTCCCATGATG TGCCATGAACGTACTTAGCTGCCTCT
3-hydroxy-3-methylglutaryl-CoA reductase (HMGCR)	CGAGCCACGACCTAATGAAGAATG TGCATCACTAAGGAACTTTGCACC
3-hydroxy-3-methylglutaryl-CoA synthase 1 (HMGCS1)	AAAACACAGAAGGACTTACGCCCGG GTTGCAGGGAGTCTTGGCACTTTCT
Involucrin (IVL)	CCTCTGCCTTCTCCCTCCTGTGAGT ACACAGTCTTGAGAGGTCCCTGAACCA
Keratin 10 (K10)	GCGGCGACCAATCATCTAAAGGACC CCAGTGGCCCGTATGAAGAGACTCT
Low density lipoprotein receptor (LDLR)	TGTGTGATGGAGACCGAGATTG CGTCAACACAGTCGACATCC
Stearoyl-Coenzyme A desaturase 1 (SCD1)	TACTACAAGCCCGGCCTCC CAGCAGTACCAGGGCACCA

Chapter 6

Complement receptor targeted liposomes encapsulating the liver X receptor agonist GW3965 accumulate in and stabilize atherosclerotic plaques

Advanced Healthcare Materials 9(10): 2000043 (2020).

Renata Martins Cardoso[1*], Naomi Benne[1*], Aimee L. Boyle[2], Alexander Kros[2], Wim Jiskoot[1], Johan Kuiper[1], Joke Bouwstra[1], Miranda Van Eck[1], Bram Slütter[1]

[1]Division of BioTherapeutics, Leiden Academic Centre for Drug Research, Leiden University, Leiden, The Netherlands
[2]Dept. Supramolecular & Biomaterials Chemistry, Leiden Institute of Chemistry, Leiden University, the Netherlands

*Both authors contributed equally

ABSTRACT

Atherosclerosis is the predominant underlying pathology of cardiovascular disease and is characterized by the retention of lipids, such as cholesterol, in macrophages (foam cells) in the intima of arteries. Liver X receptor agonists are promising compounds for treating atherosclerosis, since they induce reverse cholesterol transport in foam cells. However, LXR activation in the liver can lead to increased lipid levels. Therefore, in the present study we aimed to deliver LXR agonist GW3965 to atherosclerotic plaques by encapsulating it in liposomes. To increase the retention in atherosclerotic lesions, the liposomes were functionalized with the synthetic peptide Lyp-1 (CGNKRTRGC), which binds the p32 receptor on foam cells. Synthetic Lyp-1 was conjugated to DSPE-PEG2000-COOH and GW3965-containing (Lyp-1) liposomes (80 nm, PDI < 0.1, -20 mV) were prepared with nearly 100% encapsulation efficiency. Lyp-1 liposomes showed a 4-fold higher accumulation in foam cells compared to macrophages in vitro ($p < 0.05$). Moreover, in vivo targeting experiments showed significantly higher accumulation of Cy5-labeled Lyp-1 liposomes in atherosclerotic plaques compared to non-targeted liposomes, as shown by total (29-fold increase, $p < 0.01$) and relative radiant efficiency (25-fold increase, $p < 0.001$). Flow cytometric analysis demonstrated a 1.7-fold ($p < 0.05$) increase in the accumulation of Lyp-1 liposomes in atherosclerotic plaque macrophages as compared to controls. Finally, the effect of GW3965 loaded in Lyp-1 liposomes on atherosclerotic plaques was determined in low-density lipoprotein receptor knockout mice fed a western type diet for 13 weeks. Treatment with GW3965 loaded Lyp-1 liposomes twice a week for 5 weeks significantly reduced plaque macrophage content by nearly 50% ($p < 0.05$) and increased collagen content about 3-fold ($p < 0.01$) compared to PBS and free drug controls. Moreover, these changes in plaque stabilization were not accompanied by changes in plasma or hepatic lipid content. Thus, GW3965 loaded Lyp-1 liposomes successfully targeted the atherosclerotic plaque to allow plaque stabilization, in the absence of commonly observed side effects associated with the use of LXR agonists.

Keywords: *Lyp-1, foam cells, LXR, atherosclerosis, liposomes*

1. INTRODUCTION

Atherosclerosis is the predominant underlying pathology of cardiovascular disease and is one of the leading causes of death worldwide[1]. It is characterized by chronic inflammation in medium-and large-sized arteries caused by the subendothelial accumulation of oxidized low-density lipoprotein (oxLDL)[2]. This attracts immune cells, such as monocytes, which upon differentiation into macrophages clear oxLDL via scavenger receptors and can transform into large lipid-laden foam cells[3]. These foam cells are unable to migrate out of the vessel wall, leading to a build-up at the site of inflammation and the formation of atherosclerotic plaques[4].

There is increasing evidence that the migratory capacity of foam cells out of atherosclerotic plaques can be restored after cholesterol efflux[5]. Therefore, a promising treatment strategy to reverse the formation of foam cells is to stimulate this process[6]. Lipid-laden macrophages can actively transport excess cholesterol across their membrane via the ATP-binding cassette (ABC) transporters ABCA1 and ABCG1[7]. The liver X receptor (LXR) is a member of a family of nuclear transcription factors (LXRα; LXRβ) involved in the regulation of lipid homeostasis in response to altered sterol levels and controls the expression of both ABC transporters[7]. The deletion of these transcription factors in mice is associated with a remarkable increase in atherosclerotic lesions[8], implying therapeutic value of modulating LXR activity in atherosclerosis.

A class of small molecules, called LXR agonists (*e.g.* GW3965[9]), can activate this receptor to subsequently increase the efflux of excess cholesterol from foam cells via the induction of ABCA1 and ABCG1, reducing the local lipid content and enabling subsequent clearance of these cells from the plaque[10]. Several studies have demonstrated the beneficial effects of LXR agonists on reducing atherosclerotic plaque burden[11], however, LXR expression is not restricted to macrophages. LXRα is abundantly present in the liver, intestine, adipose tissue, spleen, and kidney[12] and LXRβ is ubiquitously expressed, although at a lower level. Therefore, when administered systemically, LXR agonists may affect several organs[12]. Activation of LXRα in the liver leads to high triglyceride levels in the plasma and liver[13-15]. This unwanted effect of LXR agonism could be prevented by altering the biodistribution of the active compound, directing it away from the liver and increasing the effective dose at the target site; the atherosclerotic lesion.

Encapsulation of active compounds in a drug delivery vehicle such as a nanoparticle is an effective strategy to alter their biodistribution[16]. In addition, conjugation of a targeting molecule to the drug delivery vehicle will direct the active compound to the required site of action[17]. Targeting to atherosclerotic plaques generally focuses on targeting to

endothelial cells1[8-22], clotted plasma proteins[23], or macrophages[24-26], by using HDL-like nanoparticles[27,28], or by passive targeting via sheer stress-mediated extravasation[29]. A common problem with many targeting strategies is lack of penetration into the plaque[22,23] or non-specificity[25,29].

The cyclic peptide Lyp-1 (CGNKRTRGC) has been identified as a valuable tool with a remarkable ability to penetrate into atherosclerotic plaques, making it superior for targeting macrophages in atherosclerotic plaques than other targeting peptides[30]. It binds to p32, also known as gC1q receptor, a receptor for the globular head domains of the complement component C1q. This receptor was originally found to be overexpressed on the cell surface of tumor cells[31] but is also expressed on foam cells in atherosclerotic plaques[32]. Nanoparticles coupled to Lyp-1 have been used for imaging of atherosclerotic plaques,[33,34] but so far, no studies have been performed using Lyp-1-targeted nanoparticles as treatment against atherosclerosis[35].

In this study, we aimed to design a particulate formulation combining the targeting properties of Lyp-1 with the therapeutic effect of an LXR agonist (GW3965) to promote cholesterol efflux from foam cells in atherosclerotic plaques to slow down atherosclerotic plaque development or reverse disease. We hypothesized that delivery of GW3965 with targeted liposomes will increase the retention of loaded particles in the atherosclerotic plaque, thereby reducing foam cell content in the plaque.

2. MATERIALS AND METHODS

2.1 Materials and chemicals

Rat and mouse no.3 breeding chow diet and Western-type diet (WTD) contained 0.25% cholesterol and 15% cocoa butter were purchased from Special Diet Services, Essex, UK. 1,2-dioleoyl-sn-glycero-3-phosphocholine (DOPC), DOPC-cyanine 5 (DOPC-Cy5), 1,2-dioleoyl-sn-glycero-3-phospho-L-serine (DOPS), 1,2-distearoyl-sn-glycero-3-phosphoethanolamine-polyethylene glycol (DSPE-PEG2000), and DSPE-N-[carboxy(polyethylene glycol)-2000] (DSPE-PEG2000-COOH) were purchased from Avanti Polar Lipids (Alabaster, AL, USA). O-(1H-6-chlorobenzotriazole-1-yl)-1,1,3,3-tetramethyluronium hexafluorophosphate (HCTU) and all amino acids used for synthesis were obtained from Novabiochem (Amsterdam, the Netherlands). N-N'-diisopropylethylamine (DIPEA) and Oxyma were purchased from Carl Roth (Karlsruhe, Germany). Dichloromethane (DCM) was obtained from Honeywell (Amsterdam, the Netherlands). Roswell Park Memorial Institute Medium (RPMI 1640), L-glutamine, and penicillin/streptomycin were purchased from Lonza (Basel, Switzerland). Fetal calf

serum (FCS) was bought from PAA Laboratories (Ontario, Canada) and polycarbonate track-etched pore size membranes (400 nm, 200 nm and 50 nm pore size) were obtained from Whatman® NucleoporeTM, GE Healthcare (Little Chalfont, UK). 70-µm cell strainer and 96-well plates were purchased from Greiner Bio-One B.V. (Alphen aan den Rijn, the Netherlands). Monosodium phosphate (NaH_2PO_4), disodium phosphate (Na_2HPO_4), diethyl ether, triisopropylsilane, iodine, diisopropylcarbodiimide, GW3965, Oil-red-O, Sirius Red, hematoxylin, NonidetTM P 40 Substitute, chloroform, collagenase I, collagenase XI, DNase, and hyaluronidase were purchased from Sigma-Aldrich (Zwijndrecht, The Netherlands). Dulbecco's Modified Eagle Medium (DMEM) low glucose, non-essential amino acids, pyruvate, oxidized LDL, Pierce™ BCA Protein Assay Kit, were purchased from ThermoFisher (MA, USA). Sodium chloride (NaCl) was obtained from Boom (Meppel, The Netherlands). Trifluoroacetic acid (TFA), piperidine, dimethylformamide (DMF), potassium dihydrogen phosphate (KH_2PO_4), potassium chloride (KCl), methanol and acetonitrile were purchased from Biosolve (Valkenswaard, the Netherlands). Optimal cutting temperature formulation Tissue-Tek®O.C.T. TM was purchased from Sakura Finetek (Alphen aan den Rijn, The Netherlands). Cholesterol and triglycerides colorimetric assays were obtained from Roche Diagnostics (Almere, The Netherlands). Rat anti-mouse macrophages/monocytes antibody (MOMA2) was purchased from Bio-Rad (Veenendaal, the Netherlands). Ketamine and atropine were purchased from AUV Veterinary Services (Cuijk, the Netherlands) and xylazine from ASTFarma (Oudewater, the Netherlands). CD45-AlexaFluor700 (30-F11) was obtained from Biolegend (San Diego, CA, USA). F4/80-FITC (BM8), fixable viability dye eFluor780, and MHC-II-eFluor450 (AF6-120.1) were purchased from eBioscience (San Diego, CA, USA). All solvents used were of analytical grade.

2.2 Animals

Wild-type (WT) and LDL receptor knockout ($LDLr^{-/-}$) mice on a C57BL/6 background were purchased from Jackson Laboratory (CA, USA), bred in-house under standard laboratory conditions, and provided with food and water ad libitum. Information about the diet used for individual experiments is described in each section. The regular laboratory diet (chow) was rat and mouse no.3 breeding diet. WTD contained 0.25 wt% cholesterol and 15 wt% cocoa butter. Animals had access to water and food ad libitum. All animal work was performed in compliance with the Dutch government guidelines and the Directive 2010/63/EU of the European Parliament. Experiments were approved by the Ethics Committee for Animal Experiments of Leiden University.

2.3 DSPE-PEG2000-Lyp-1 synthesis

The Lyp-1 peptide, GCGNKRTRGC with Cys residues protected by the non-acid-labile acetamidomethyl group, was synthesized using a Liberty Blue microwave-assisted peptide synthesizer. The synthesis was performed on a 0.1 mmol scale with a low-loading (0.18 mmol/g) tentagel R-RAM resin. Amino acid activation was achieved by using N,N'-diisopropylcarbodiimide as the activator and Oxyma as the base, while Fmoc-deprotection was achieved with 20% piperidine in DMF. Once the synthesis was complete, the resin was treated with 10 equivalents of iodine for one hour, to accommodate the concomitant deprotection and cyclization of the Cys residues. The resin was subsequently washed five times with DMF, five times with 2% acetic acid in DMF, five times with DMF and finally five times with DCM. The DSPE-PEG2000-COOH was manually coupled, on resin, to the N-terminus of an excess of the cyclized Lyp-1 by HCTU and DIPEA. The coupling reaction was left overnight, and the resin was subsequently washed with DMF and DCM. The DSPE-PEG2000-Lyp1 was cleaved from the resin by using a mixture of 97% TFA and 3% triisopropylsilane. The cleavage reaction was left to proceed for one hour, and the peptide was precipitated into ice-cold diethyl ether. The precipitate was collected by centrifugation. Levels of precipitate were low, likely due to the hydrophobic nature of the lipopeptide, therefore after centrifugation, the ether was separated from the precipitate and the ether was evaporated, leaving a white residue. This residue was combined with the original precipitate, dissolved in a mixture of acetonitrile and water, and dialyzed in a solution of 90% water and 10% acetonitrile to remove the excess uncoupled peptide and any scavengers or impurities that remained. The product was subsequently freeze-dried and analyzed using MALDI mass spectrometry to confirm the desired product had been formed.

2.4 Liposome preparation

Liposomes were prepared by using the thin film dehydration-rehydration method, as described previously[36]. Briefly, DOPC:DOPS:DSPE-PEG:DSPE-PEG-Lyp-1 in the molar ratio 76:19:4.3:0.7 were dissolved in chloroform and mixed in a round-bottom flask to obtain a final lipid concentration of 10 mg/mL. To this mixture, 2 mg of GW3965 was added. Chloroform was evaporated for 1 hour at 40°C in a rotary evaporator (Rotavapor R-210, Büchi, Switzerland). The lipid film was rehydrated with 1 mL Milli-Q water and homogenized by using glass beads and gentle swirling at room temperature (RT). The liposome dispersion was subsequently snap-frozen in liquid nitrogen, followed by freeze-drying overnight (Christ alpha 1–2 freeze-dryer, Osterode, Germany). The resulting dry lipid cake was gradually rehydrated at RT by using 10 mM phosphate buffer, pH 7.4 (PB); two volumes of 500 µL and one volume of 1000 µL PB were

successively added, with intervals of 30 min between each addition. The mixture was vortexed well between each hydration step, and the resulting dispersion was kept at RT for at least 1 hour. To obtain monodisperse liposomes, the multilamellar vesicles were sized by high-pressure extrusion at RT (LIPEX Extruder, Northern Lipids Inc., Canada). The liposome mixture was passed four times through stacked 400 nm and 200 nm polycarbonate track-etched pore size membranes and a further eight times through a 50 nm pore size membrane. To prepare fluorescently labeled liposomes, 0.1 mol% of DOPC was replaced with DOPC-Cy5. Liposomes were stored at 4°C and used for further experiments within 1 week.

2.5 Liposome characterization

The Z-average diameter and polydispersity index (PDI) of the liposomes were measured by dynamic light scattering (DLS) using a NanoZS Zetasizer (Malvern Ltd., Malvern, UK). Zeta-potential of the liposomes was determined by laser Doppler electrophoresis with the same instrument. Liposomes were diluted 100-fold in PB to a total volume of 1 mL prior to measuring. To determine the concentration of encapsulated GW3965 and Lyp-1, samples were analyzed by reversed-phase UPLC (Waters ACQUITY UPLC, Waters, MA, USA). 20 µL of the liposome dispersion was dissolved in 180 µL methanol. 10 µL of the sample was injected into a 1.7 µm BEH C18 column (2.1 x 50 mm, Waters ACQUITY UPLC, Waters, MA, USA). The column temperature and the temperature of the sample were set at 40°C and 4°C, respectively. The mobile phases were Milli-Q water with 0.1% TFA (solvent A) and acetonitrile with 0.1% TFA (solvent B). For detection, the mobile phases were applied in a linear gradient from 5% to 95% solvent B over 10.5 minutes at a flow rate of 0.370 mL/min. Lyp-1 was detected by absorbance at 220 nm using an ACQUITY UPLC TUV detector (Waters ACQUITY UPLC, Waters, MA, USA) and GW3965 was detected at 272 nm.

2.6 Bone marrow-derived macrophage (BMM) and foam cell culture

Bone marrow was isolated from the tibias and femurs of WT or $LDLr^{-/-}$ mice on a chow diet. The isolated bone marrow was passed through a 70-µm cell strainer. To differentiate the bone-marrow derived cells into macrophages, the cells were cultured in mixture of 60% complete RPMI medium (20% (v/v) FCS, 2 mM L-glutamine, 1 mM non-essential amino acids, 1 mM pyruvate, and 100 U/mL penicillin/streptavidin with 40% complete L929-conditioned DMEM low glucose medium (10% (v/v) FCS, 2 mM L-glutamine, and 100 U/mL penicillin/streptavidin) at 37˚C and 5% CO_2 for 7 days, as described previously[37]. The medium was refreshed every other day. To generate foam cells, macrophages were incubated with 75 µg/mL oxLDL for 30 hours.

2.7 Liposome association to BMMs and foam cells

BMMs and foam cells were cultured as described above. After 10 days of culture, 100,000 BMMs or foam cells were plated in 96-well plates and fluorescently labeled Lyp-1 liposomes or controls (PBS and fluorescently labeled non-targeted liposomes) were added at a concentration of 0.35 mg/mL Lyp-1 or an equivalent lipid dose. After 2 hours of incubation at 37˚C and 5% CO_2, excess liposomes were removed by washing the cells several times with medium. Cells were stained for F4/80 and viability dyes and were analyzed by flow cytometry (CytoFLEX S, Beckman Coulter, CA, USA). Data were analyzed by using FlowJo software (Treestar, OR, USA).

2.8 *In vivo* targeting to atherosclerotic plaques

Male $LDLr^{-/-}$ mice (6 to 10-week old) were fed WTD for 13 weeks to stimulate atherosclerotic lesion development. Subsequently, the mice were randomized into two groups (n = 10) injected intravenously with either Cy-5 fluorescently labeled non-targeting liposomes or Lyp-1 targeting liposomes (200 µL).The Lyp-1 concentration was 35 µg for Lyp-1 liposomes, and the equivalent lipid concentration was used for non-targeted liposomes. After 3 hours, the mice were anesthetized by using a mixture of ketamine (40 mg/mL), atropine (50 µg/mL), and sedazine (6.25 mg/mL) and perfused with PBS (8.13 g/L NaCl, 2.87 g/L Na_2HPO_4, 0.2 g/L KH_2PO_4, 0.19 g/L KCl, pH 7.4) via the left ventricle of the heart under physiological pressure after opening the thoracic cavity. After perfusion, the mice were imaged by using a fluorescence in vivo imaging system (IVIS, Perkin-Elmer IVIS Lumina Series III, Waltham, MA, USA) to provide information about the biodistribution of the liposomes. Afterward, spleen, lungs, liver, kidneys, hearts, and aortas were also imaged separately. Uptake by different organs was plotted as radiant efficiency and as relative radiant efficiency (%). To calculate relative radiant efficiency, the total sum of signals in organs was set to 100%, and the relative percentage per organ was calculated from this value. Aortas were further processed for flow cytometry analysis, as previously described[38]. Briefly, aortas were cut into small pieces, incubated with 450 U/mL collagenase I, 250 U/mL collagenase XI, 120 U/mL DNase, and 120 U/mL hyaluronidase (30 min at 37°C under constant agitation), and strained through a 70-µm cell strainer to obtain a single-cell suspension. Cells were stained for CD45, F4/80, MHC-II, and viability and analyzed by flow cytometry.

2.9 Analysis of atherosclerosis in mice

Male $LDLr^{-/-}$ mice (6 to 10-week old) were fed WTD for 8 weeks to develop atherosclerotic lesions. Next, these mice were randomized into 5 groups (n = 10 mice)

to receive intravenous injections twice a week (200 µL) of (1) PBS; (2) free GW3965; (3) empty Lyp-1 liposomes; (4) GW3965-loaded liposomes or (5) GW3965-loaded Lyp-1 liposomes. For GW3965-containing groups the dose was 6.5 mg/kg GW3965. The mice were treated for 5 weeks and continued to receive WTD during this time. After 5 weeks of treatment, the mice were anesthetized, exsanguinated and perfused, as described in the previous section. Hearts, livers, and blood were collected for further analysis. Hearts were embedded in OCT and stored at -80°C until further processing. Cryosections of the aortic root (10 µm, CM3050S cryostat, Leica, Rijswijk, The Netherlands) were collected. The sections were stained for Oil-Red-O to visualize lipid-rich plaques[39]. The largest Oil-red-O positive section of a sample and the two flanking sections were used to quantify the average plaque size. Macrophage positive area in the plaque was determined by using MOMA2 staining[40]. Macrophage positive area was calculated as the area positive for the MOMA2 staining divided by the total plaque area for the 3 largest consecutive sections. Collagen content in the plaques was measured by using Sirius Red staining[41]. Sections were visualized under polarized light[42] and the collagen content was determined by dividing the area positive for the Sirius Red staining by the total plaque area for the 3 largest consecutive sections. All stainings were imaged by using a Leica DM-RE microscope (Leica, Imaging Systems, UK) and analyzed using Leica QWin software.

2.10 Lipid quantification

Triglycerides were extracted from liver samples (± 50 mg tissue) homogenized with NonidetTM P 40 Substitute. To solubilize the triglycerides in the homogenate, the samples underwent two cycles of heat (90°C) and chill on ice. Subsequently, the homogenates were centrifuged (14000 rpm) to remove insoluble material and triglycerides were measured by a colorimetric enzymatic assay[43]. The Folch method[44] was used to extract cholesterol from liver samples (ca. 50 mg tissue). Cholesterol was then quantified by using a colorimetric enzymatic assay[43]. Both triglyceride and cholesterol levels were corrected for total protein concentration. Protein concentration was determined with a Pierce™ BCA Protein Assay Kit according to the manufacturer's instructions. Non-fasted plasma levels of cholesterol and triglycerides were measured by enzymatic colorimetric assays, as previously described by Out *et. al.*[43].

2.11 Statistical analysis

Statistical analysis was performed by using GraphPad Prism 8 (GraphPad Software Inc., CA, USA). Data are presented as mean ± standard deviation (SD) and *p* values below 0.05 were considered significant. For comparison of multiple treatment groups, unpaired

t-test, one-way ANOVA with Holm-Sidak post-test, or two-way ANOVA with Bonferroni's post-test were used, where appropriate.

3. RESULTS

3.1 Characterization of Lyp-1 starting materials and liposomes

The coupling reaction of cyclic Lyp-1 to DSPE-PEG2000-COOH generating DSPE-PEG2000-Lyp-1 is schematically represented in Figure 1 and was confirmed by MALDI-MS (Supplementary Figure S1). All GW3965-loaded liposomes showed an encapsulation efficiency of this drug of nearly 100% (Table I). The Z-average diameter of GW3965-loaded liposomes (ca. 75 nm) was slightly, but significantly ($p < 0.05$) smaller than that of empty liposomes (ca. 85 nm) (Table 1). The PDI was ca. 0.1 for all formulations, and the ζ-potential was about -20 mV (Table 1).

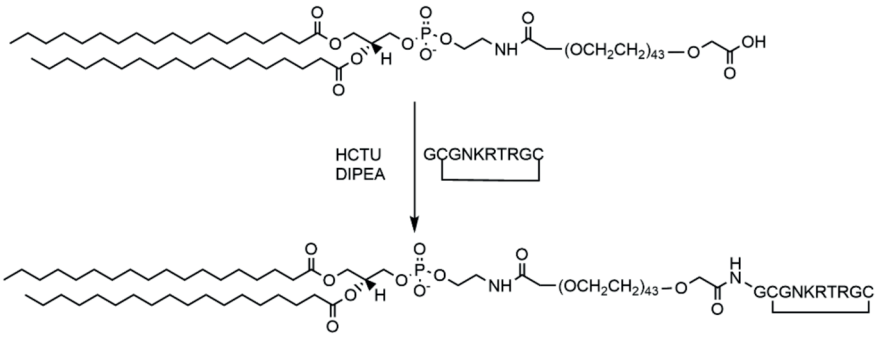

Figure 1. Synthesis of DSPE-PEG2000-Lyp-1. Schematic representation of the reaction coupling DSPE-PEG2000-COOH to cyclic peptide Lyp-1 to produce DSPE-PEG2000-Lyp-1.

Table 1: Physicochemical properties of liposomal formulations. Average particle diameter (Z-average diameter), PDI and ζ-potential were determined for all liposomal formulations. Encapsulation efficiency was calculated for liposomes loaded with GW3965 compound.

Formulation	Z-average diameter ± SD (nm)	PDI ± SD	ζ-potential ± SD (mV)	Encapsulation efficiency ± SD (%)
Empty Lyp-1 Liposomes	84.7 ± 3.9	0.09 ± 0.02	-19.3 ± 2.3	-
GW3965-loaded liposomes	73.8 ± 4.9*	0.10 ± 0.02	-19.7 ± 2.3	93.5 ± 19.9
GW3965-loaded Lyp-1 liposomes	77.5 ± 4.0*	0.09 ± 0.02	-19.5 ± 2.1	92.9 ± 22.5

*$p < 0.05$ compared to empty Lyp-1 liposomes

3.2 Lyp-1 liposomes preferentially associate with foam cells *in vitro*

To test the specific association of the liposomes to foam cells *in vitro*, fluorescently labeled liposomes were incubated with LDLr$^{-/-}$ mouse-derived non-differentiated BMMs (M0) and oxLDL-laden foam cells for 2 hours. Flow cytometric analysis showed that both non-targeted and targeted liposomes did not associate with M0 macrophages (Figure 2). Consistent with previous reports[22], foam cells showed enhanced association with both targeted and non-targeted liposomes. However, the interaction of Lyp-1 targeted liposomes was significantly increased as compared to not-targeted liposomes, marked by a higher fluorescent signal (Figure 2A and Figure 2B) and a nearly 4-fold increase in the percentage of liposome positive foam cells ($p < 0.05$) (Figure 2C). Similar results (4-fold increase, $p < 0.01$) were observed for M0 macrophages and foam cells both derived from WT mice containing a functional LDLr (data not shown).

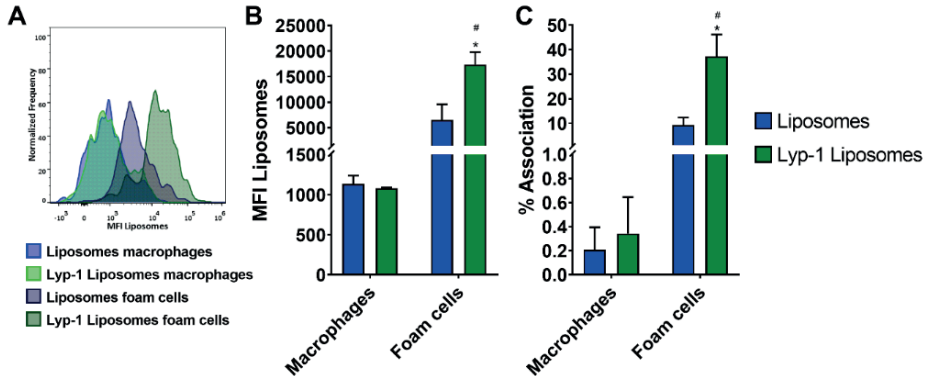

Figure 2. Preferential association of targeted Lyp-1 liposomes to foam cells in vitro. LDLr$^{-/-}$ M0 macrophages and oxLDL-laden foam cells were exposed to non-targeted liposomes or Lyp-1 liposomes labeled with DOPC-Cy5. After 2 hours of incubation, the liposomal association was determined by using flow cytometry. A) Representative MFI plots. Cell association was expressed as B) mean fluorescence intensity of the cells and C) percentage of cells positive for the fluorescent label. Graphs show means + SD of 3 independent experiments, *$p < 0.05$ comparing foam cells to M0 macrophages, #$p < 0.05$ comparing non-targeted to targeted liposomes, determined by two-way ANOVA and Bonferroni's post-test.

3.3 Lyp-1 liposomes are retained in plaque-residing foam cells of LDLr$^{-/-}$ mice

Next, we addressed the ability of the Lyp-1 liposomes to accumulate in foam cells residing in atherosclerotic plaques in vivo. LDLr$^{-/-}$ mice fed a WTD for 13 weeks were injected intravenously with fluorescently labeled Lyp-1 liposomes or non-targeted

liposomes. After 3 hours, mice were anesthetized and perfused, and the biodistribution of liposomes was assessed using fluorescence imaging (see Figure 3A and 3B for representative aortas) and flow cytometry (see Figure 3C and 3D for representative plots). Lyp-1 liposomes showed a significantly higher accumulation in atherosclerotic plaques compared to non-targeted liposomes, as shown by the total radiant efficiency (29-fold increase, $p < 0.01$, Figure 3E) and the relative fluorescence signal (25-fold increase, $p < 0.001$, Figure 3F). Flow cytometric analysis confirmed a 1.7-fold ($p < 0.05$) increase in the accumulation of Lyp-1 targeted liposomes in atherosclerotic plaque foam cells as compared to non-targeted control liposomes (Figure 3G). In addition, to determine the organ distribution of the liposomes, the liver, kidneys, heart, spleen, and lungs were collected and separately imaged with IVIS. Most liposomes (both targeted and non-targeted) accumulated in the spleen, liver and kidneys, and a small amount was recovered from the lungs and hearts (Figure S2). LDLr$^{-/-}$ mice that received chow diet instead of WTD, and therefore did not develop atherosclerotic plaques, did not show any liposomal signal in aortas (data not shown).

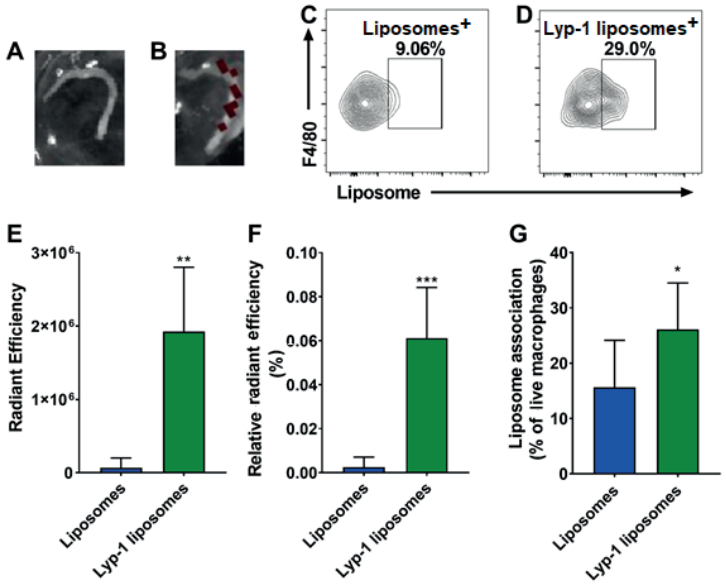

Figure 3. Association of fluorescently labeled non-targeted liposomes and Lyp-1 liposomes by plaque-residing foam cells in LDLr$^{-/-}$ mice fed WTD for 13 weeks. 3 hours after intravenous injection of liposomes, mice were perfused with PBS (pH 7.4 at RT). Representative IVIS images of descending aortas of mice that had received A) non-targeted and B) Lyp-1 liposomes. The dark brown signal indicates the presence of the Cy5 label. Representative FACS plots of pre-gated CD45^{+}MHC-II^{+}F4/80^{+} cells isolated from the aortic arch associated with C) non-targeted and D) Lyp-1 liposomes. E) Radiant efficiency of the fluorescent label in the descending aortas of mice measured by fluorescence imaging, n = 5. F) Aortic radiant efficiency as a

percentage of all organs, n = 5. G) Liposomes detected in $CD45^+MHC\text{-}II^+F4/80^+$ cells isolated from the aortic arch by flow cytometry, n = 8. Graphs show mean + SD, *p < 0.05, **p < 0.01, ***p < 0.001 determined by unpaired Student's T-test.

3.4 Treatment with GW3965-loaded Lyp-1 liposomes significantly reduces the macrophage content and increases the collagen content of atherosclerotic plaques

After confirming efficient targeting of the Lyp-1 liposomes to atherosclerotic foam cells, the effect of Lyp-1 liposomal targeting of the LXR agonist GW3965 on pre-established atherosclerotic lesions was assessed. Male $LDLr^{-/-}$ mice were fed WTD for eight weeks. At this point, the average plaque size in the aortic root area was ca. 0.12 ± 0.07 mm^2, with lesion area comprising of 57.1 ± 15.2% macrophages, and 1.3 ± 1.1% collagen. Subsequently, the mice were injected intravenously twice a week with PBS, free GW3965, empty Lyp-1 liposomes, GW3965-loaded liposomes or GW3965-loaded Lyp-1 liposomes for 5 weeks, during which the WTD was maintained. Upon sacrifice, no differences were observed in atherosclerotic plaque size between any of the groups as determined in Oil-red-O stained sections of the aortic roots (Figure 4A and 4D). However, the macrophage content, as measured with MOMA2 staining, was 2-fold ($p < 0.05$) lower in mice treated with Lyp-1 targeted GW3965-loaded liposomes compared to all other groups (Figure 4B and 4E). Previous studies have shown a positive correlation between the reduction in macrophage content and increase in collagen content in the plaque[45]. Indeed, we found that the percentage of collagen in the plaques was significantly increased (3-fold, $p < 0.01$) in mice treated with GW3965-loaded Lyp-1 liposomes as compared to all other groups (Figure 4C and 4F). Thus, foam cell delivery of GW3965 using Lyp-1 liposomes induced stabilization of established atherosclerotic plaques.

3.5 Free or encapsulated GW3965 does not affect plasma and liver lipid content

Despite the positive effects of LXR activation on atherosclerosis, the use of LXR agonists, such as GW3965, has been described to alter hepatic lipid metabolism often leading to an increase in circulating triglycerides and liver steatosis[10]. Triglyceride and cholesterol content (in both plasma and liver) showed no differences between any of the groups (Figure 5), suggesting that the GW3965 treatment with Lyp-1 targeted liposomes can stabilize atherosclerotic plaques without the confounding effects on serum and liver lipid levels.

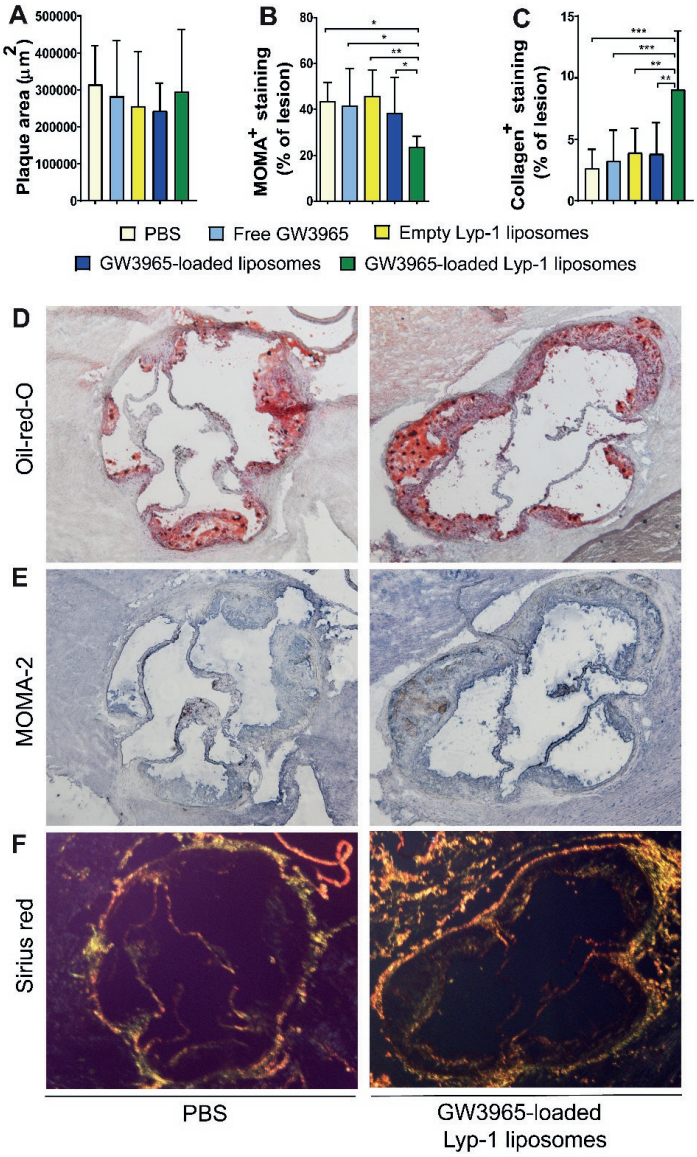

Figure 4. Effect of GW3965-loaded Lyp-1 targeted liposomes on plaque development in LDLr$^{-/-}$ mice. Mice were fed WTD for eight weeks before receiving intravenous injections of GW2965-loaded Lyp-1 liposomes or controls twice a week for five weeks while maintaining WTD. Upon sacrifice, hearts were collected and sectioned to reveal the aortic root area. Sections were stained for (A) Oil-Red-O to visualize lipids (B) MOMA2 to measure macrophage content, and (C) Sirius Red for collagen content, n = 10. Representative images of section stained for (D) Oil-red-O, (E) MOMA2 and (F) Sirius Red. Graphs show means + SD, *$p < 0.05$, **$p < 0.01$, ***$p < 0.001$ determined by one-way ANOVA with Holm-Sidak post-test.

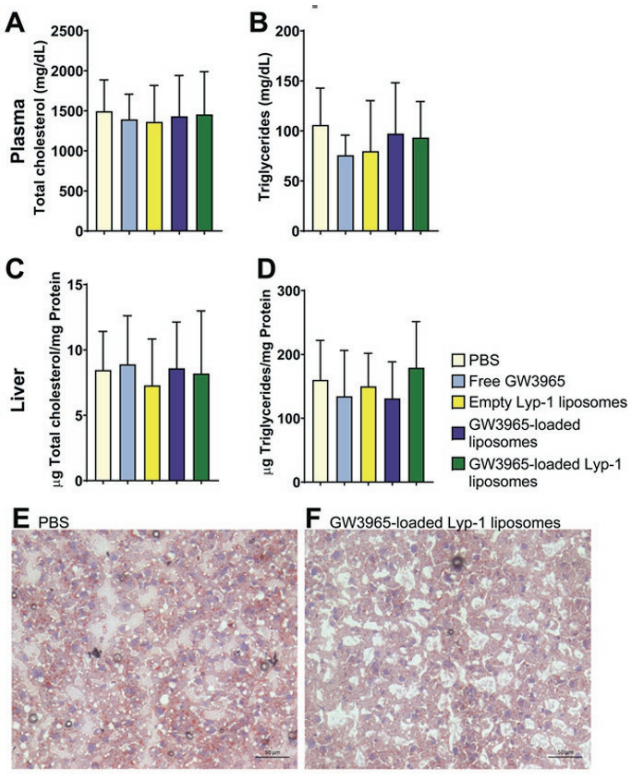

Figure 5. Effect of drug-loaded targeted liposomes and controls on plasma- and liver lipid levels in LDLr$^{-/-}$ mice on WTD. Mice received WTD for eight weeks before receiving intravenous injections of liposomes or controls twice a week for five weeks while maintaining WTD. Mice received the last injection 3 hours prior to sacrifice. Upon sacrifice, plasma and livers were collected for lipid analysis. (A) Total cholesterol and (B) triglyceride levels were measured in plasma. Livers were processed and total protein content in mg was determined. (C) Total cholesterol and (D) triglyceride levels were measured and normalized to protein content. (E) Representative image of Oil-Red-O stained liver of a mouse that received PBS, or (F) drug-loaded targeted liposomes, n = 10. Graphs show mean + SD, no significant differences found between groups.

4. DISCUSSION

LXR agonists are promising compounds for the treatment of atherosclerosis, but at therapeutic doses, they increase plasma triglyceride and cholesterol levels[13-15]. In this study, we showed that loading of an LXR agonist, GW3965, in Lyp-1-bearing liposomes induces a highly relevant stabilization of pre-established atherosclerotic lesions, in contrast to free GW3965 or GW3965 encapsulated in non-targeted liposomes. This is hypothesized to be due to the migration of macrophages out of lesions after LXR-agonist-

induced cholesterol efflux[5]. Liposomes consisting of DOPC:DOPS:DSPE-PEG:DSPE-PEG-Lyp-1 in a molar ratio of 76:19:4.3:0.7 were prepared to produce particles with fluid state membranes to improve the encapsulation of GW3965 and to prevent mononuclear phagocyte uptake upon injection into the circulation. Phosphatidylserine was added because of its anti-inflammatory properties[46-50] and reported ability to target foam cells[25]. Liposomes were PEGylated (5 mol%) to enhance their circulation time[51].

To minimize the undesired hepatic and metabolic effects, LXR agonists can be encapsulated into functionalized nanoparticles to target atherosclerotic plaques. Zhang *et. al.* formulated GW3965 in PEGylated PLGA nanoparticles containing phosphatidylserine on the surface to target atherosclerotic foam cells. The targeted PLGA particles (10 mg/kg GW3965; administered i.v. 3 times per week for 2 weeks) reduced the macrophage content in the lesion compared to untreated control. However, this effect was not enhanced when compared to free drug or drug encapsulated in non-targeted liposomes and was accompanied by increased hepatic and plasma triglyceride and cholesterol levels[25]. In a different approach, Yu *et. al.* encapsulated GW3965 in methoxy-PLA nanoparticles coated with 1,2-dilauroyl-sn-glycero-3-phosphocholine (DLPC):DSPE-PEG1000 functionalized with collagen-IV-targeting heptapeptide conjugated to DSPE-PEG2000 in the lipid layer. The GW3965-loaded collagen-targeting particles (8 mg/kg, administered intravenously 2 times per week for 5 weeks) significantly decreased the $CD68^+$ (macrophage) area in the lesion compared to free drug and non-targeted liposomes[18]. Neither of these previously described targeting approaches using collagen-IV and phosphatidylserine resulted in a reduction in total plaque size. Furthermore, the collagen content in the plaques, an important indicator of plaque stability, was not measured in these studies. It should be noted that, while in humans foam cells are mainly derived from macrophages[52], it has recently been discovered that foam cells can be derived from smooth muscle cells in the $ApoE^{-/-}$ mouse model[53]. Since the aforementioned studies and the study presented here are performed in $LDLr^{-/-}$ mice, it is unknown whether the therapeutic effect would be the same in $ApoE^{-/-}$ mice.

In this study, we made use of the interaction between the p32 receptor and Lyp-1 to target liposomes to foam cells in the plaque and deliver GW3965. Since the p32 receptor is not expressed on the surface of lipid-poor macrophages[31], the presence of Lyp-1 on the liposomal surface did not affect the in vitro association of the liposomes to undifferentiated macrophages but greatly and significantly enhanced their association to foam cells, confirming the selectivity of the targeting peptide. It should be noted that p32 has been found to be expressed in endothelial cells, foam cells, smooth muscle cells, and inflammatory cells present in the intima and media of human atherosclerotic

lesions[32]. However, similarly to the Lyp-1 liposomes described here, heat shock protein cages functionalized with Lyp-1 designed by Uchida *et. al.* showed accumulation in Mac-3^{+} foam cells in murine ligation-induced atherosclerotic plaques[33]. Seo *et. al.* also observed high aortic lesion retention of Lyp-1 dendrimers 3 hours after intravenous injection in ApoE$^{-/-}$ mice[34]. Remarkably, in our study, the presence of Lyp-1 on the liposomal surface leads to enough particle retention in the aorta to allow a clear therapeutic effect of a relatively low dose of GW3965 (ca. 6.5 mg/kg/injection). For reference, oral administration of high dose of free GW3965 (10 mg/kg) for 12 weeks significantly reduced lesion size. However, this effect was accompanied by higher serum triglycerides levels[14].

Administration of free or nanoparticle-encapsulated LXR agonist may not fully prevent unwanted effects in the plasma and in the liver[10]. In the present study, the high hepatic uptake of our GW3965-loaded Lyp-1 liposomes did not lead to the side effects typically associated with LXR agonists. Joseph *et. al.* showed that treatment with free GW3965 at a low dose (1 mg/kg for 12 weeks) did not result in plaque size reduction, hypertriglyceridemia or liver steatosis. The administration of a moderate dose of GW3965 (6.5 mg/kg in this study, *vs* 10 mg/kg by Zhang *et. al.*[25] and 8 mg/kg by Yu e*t. al.*[18]) may have contributed to maintenance of hepatic and serum lipid homeostasis, as free GW3965 also did not induce these unwanted effects. The aforementioned studies along with our own study demonstrate that uptake of nanoparticles by cells in the liver is difficult to avoid, especially by Kupffer cells[54], but nanoparticles can still protect against the unwanted effects of the LXR agonist while increasing the efficiency of the drug at the site of action. Nevertheless, high hepatic particle uptake in the long-term, especially with higher doses should be avoided. Thus, other liposomal formulations or even other types of particles could be explored to reduce the undesired particle removal by the liver.

In conclusion, our work shows that functionalizing liposomes with Lyp-1 is an excellent strategy for targeting to atherosclerotic plaques. We are, to our knowledge, the first to combine this targeting approach with an LXR agonist, and we show that GW3965 loaded in targeted liposomes can reduce plaque macrophage content and increase plaque stability. These findings suggest that it is possible to increase the efficacy of this LXR agonist and may contribute to the development of better atherosclerosis therapies.

ACKNOWLEDGMENTS

The authors thank P. J. van Santbrink, J. van Duijn, A. C. Foks, F. Lozano Vigario, R. J. T. Leboux, J. de Mol and I. Bot for their technical assistance during the animal studies.

REFERENCES

1. Frostegård, J. Immunity, atherosclerosis and cardiovascular disease. BMC Med 11, 117-117, doi:10.1186/1741-7015-11-117 (2013).

2 Pirillo, A., Norata, G. D. & Catapano, A. L. LOX-1, OxLDL, and atherosclerosis. Mediators Inflamm 2013, 152786, doi:10.1155/2013/152786 (2013).

3 Chistiakov, D. A., Melnichenko, A. A., Myasoedova, V. A., Grechko, A. V. & Orekhov, A. N. Mechanisms of foam cell formation in atherosclerosis. J Mol Med (Berl) 95, 1153-1165, doi:10.1007/s00109-017-1575-8 (2017).

4 Tabas, I. Macrophage death and defective inflammation resolution in atherosclerosis. Nat Rev Immunol 10, 36-46, doi:10.1038/nri2675 (2010).

5 Luo, Y. et al. Macrophagic CD146 promotes foam cell formation and retention during atherosclerosis. Cell Research 27, 352-372, doi:10.1038/cr.2017.8 (2017).

6 Tall, A. R. Cholesterol efflux pathways and other potential mechanisms involved in the athero-protective effect of high density lipoproteins. Journal of Internal Medicine 263, 256-273, doi:10.1111/j.1365-2796.2007.01898.x (2008).

7 Venkateswaran, A. et al. Control of cellular cholesterol efflux by the nuclear oxysterol receptor LXR alpha. Proc Natl Acad Sci U S A 97, 12097-12102, doi:10.1073/pnas.200367697 (2000).

8 Bischoff, E. D. et al. Non-redundant roles for LXRα and LXRβ in atherosclerosis susceptibility in low density lipoprotein receptor knockout mice. Journal of Lipid Research 51, 900-906, doi:10.1194/jlr.M900096-JLR200 (2010).

9 Collins, J. L. et al. Identification of a Nonsteroidal Liver X Receptor Agonist through Parallel Array Synthesis of Tertiary Amines. Journal of Medicinal Chemistry 45, 1963-1966, doi:10.1021/jm0255116 (2002).

10 Kirchgessner, T. G. et al. Beneficial and Adverse Effects of an LXR Agonist on Human Lipid and Lipoprotein Metabolism and Circulating Neutrophils. Cell Metab 24, 223-233, doi:10.1016/j.cmet.2016.07.016 (2016).

11 Levin, N. et al. Macrophage liver X receptor is required for antiatherogenic activity of LXR agonists. Arteriosclerosis, thrombosis, and vascular biology 25, 135-142, doi:10.1161/01.Atv.0000150044.84012.68

(2005).

12 Wojcicka, G., Jamroz-Wisniewska, A., Horoszewicz, K. & Beltowski, J. Liver X receptors (LXRs). Part I: structure, function, regulation of activity, and role in lipid metabolism. Postepy higieny i medycyny doswiadczalnej (Online) 61, 736-759 (2007).

13. Joseph, S. B. et al. Direct and indirect mechanisms for regulation of fatty acid synthase gene expression by liver X receptors. The Journal of biological chemistry 277, 11019-11025, doi:10.1074/jbc.M111041200 (2002).

14 Joseph, S. B. et al. Synthetic LXR ligand inhibits the development of atherosclerosis in mice. Proc Natl Acad Sci U S A 99, 7604-7609, doi:10.1073/pnas.112059299 (2002).

15 Schultz, J. R. et al. Role of LXRs in control of lipogenesis. Genes & Development 14, 2831-2838, doi:10.1101/gad.850400 (2000).

16 Tibbitt, M. W., Dahlman, J. E. & Langer, R. Emerging Frontiers in Drug Delivery. J Am Chem Soc 138, 704-717, doi:10.1021/jacs.5b09974 (2016).

17 Accardo, A. & Morelli, G. Review peptide-targeted liposomes for selective drug delivery: Advantages and problematic issues. Biopolymers 104, 462-479, doi:10.1002/bip.22678 (2015).

18 Yu, M. et al. Targeted Nanotherapeutics Encapsulating Liver X Receptor Agonist GW3965 Enhance Antiatherogenic Effects without Adverse Effects on Hepatic Lipid Metabolism in Ldlr-/- Mice. Adv Healthc Mater, doi:10.1002/adhm.201700313 (2017).

19 Kelly, K. A., Nahrendorf, M., Yu, A. M., Reynolds, F. & Weissleder, R. In Vivo Phage Display Selection Yields Atherosclerotic Plaque Targeted Peptides for Imaging. Molecular Imaging and Biology 8, 201, doi:10.1007/s11307-006-0043-6 (2006).

20 Park, K. et al. A new atherosclerotic lesion probe based on hydrophobically modified chitosan nanoparticles functionalized by the atherosclerotic plaque targeted peptides. Journal of Controlled Release 128, 217-223, doi:https://doi.org/10.1016/j.jconrel.2008.03.019 (2008).

21 Deosarkar, S. P. et al. Polymeric particles conjugated with a ligand to VCAM-1 exhibit selective, avid, and focal adhesion to sites of atherosclerosis. Biotechnol Bioeng 101, 400-407, doi:10.1002/bit.21885 (2008).

22 Namdee, K. et al. In vivo evaluation of vascular-targeted spheroidal microparticles for imaging and drug delivery application in atherosclerosis. Atherosclerosis 237, 279-286, doi:10.1016/j.atherosclerosis.2014.09.025 (2014).

23 Peters, D. et al. Targeting atherosclerosis by using modular, multifunctional micelles. Proc Natl Acad Sci U S A 106, 9815-9819, doi:10.1073/pnas.0903369106 (2009).

24 Cormode, D. P. et al. Nanocrystal Core High-Density Lipoproteins: A Multimodality Contrast Agent Platform. Nano Letters 8, 3715-3723, doi:10.1021/nl801958b (2008).

25 Zhang, X. Q. et al. Nanoparticles containing a liver X receptor agonist inhibit inflammation and atherosclerosis. Adv Healthc Mater 4, 228-236, doi:10.1002/adhm.201400337 (2015).

26 Zhaorigetu, S., Rodriguez-Aguayo, C., Sood, A. K., Lopez-Berestein, G. & Walton, B. L. Delivery of negatively charged liposomes into the atherosclerotic plaque of apolipoprotein E-deficient mouse aortic tissue. J Liposome Res 24, 182-190, doi:10.3109/08982104.2013.863208 (2014).

27 Binderup, T. et al. Imaging-assisted nanoimmunotherapy for atherosclerosis in multiple species. Science Translational Medicine 11, eaaw7736, doi:10.1126/scitranslmed.aaw7736 (2019).

28 Alaarg, A. et al. A systematic comparison of clinically viable nanomedicines targeting HMG-CoA reductase in inflammatory atherosclerosis. Journal of Controlled Release 262, 47-57, doi:https://doi.org/10.1016/j.jconrel.2017.07.013 (2017).

29 Lobatto, M. E. et al. Atherosclerotic plaque targeting mechanism of long-circulating nanoparticles established by multimodal imaging. ACS Nano 9, 1837-1847, doi:10.1021/nn506750r (2015).

30 Hamzah, J. et al. Specific penetration and accumulation of a homing peptide within atherosclerotic plaques of apolipoprotein E-deficient mice. Proc Natl Acad Sci U S A 108, 7154-7159, doi:10.1073/pnas.1104540108 (2011).

31 Laakkonen, P., Porkka, K., Hoffman, J. A. & Ruoslahti, E. A tumor-homing peptide with a targeting specificity related to lymphatic vessels. Nat Med 8, 751-755, doi:10.1038/nm720 (2002).

32 Peerschke, E. I. et al. Expression of gC1q-R/p33 and its major ligands in human atherosclerotic lesions. Mol Immunol 41, 759-766, doi:10.1016/j.molimm.2004.04.020 (2004).

33 Uchida, M. et al. Protein cage nanoparticles bearing the LyP-1 peptide for enhanced imaging of macrophage-rich vascular lesions. ACS Nano 5, 2493-2502, doi:10.1021/nn102863y (2011).

34 Seo, J. W. et al. (64)Cu-labeled LyP-1-dendrimer for PET-CT imaging of atherosclerotic plaque. Bioconjug Chem 25, 231-239, doi:10.1021/bc400347s (2014).

35 Song, N., Zhao, L., Zhu, M. & Zhao, J. Recent progress in LyP-1-based strategies for targeted imaging and therapy. Drug Deliv 26, 363-375, doi:10.1080/10717544.2019.1587047 (2019).

36 Benne, N. et al. Atomic force microscopy measurements of anionic liposomes reveal the effect of liposomal rigidity on antigen-specific regulatory T cell responses. J Control Release 318, 246-255, doi:10.1016/j.jconrel.2019.12.003 (2020).

37 Marim, F. M., Silveira, T. N., Lima, D. S., Jr. & Zamboni, D. S. A Method for Generation of Bone Marrow-Derived Macrophages from Cryopreserved Mouse Bone Marrow Cells. PLOS ONE 5, e15263, doi:10.1371/journal.pone.0015263 (2010).

38 van Duijn, J. et al. CD8+ T-cells contribute to lesion stabilization in advanced atherosclerosis by limiting macrophage content and CD4+ T-cell responses. Cardiovascular Research 115, 729-738, doi:10.1093/cvr/cvy261 (2018).

39 Mehlem, A., Hagberg, C. E., Muhl, L., Eriksson, U. & Falkevall, A. Imaging of neutral lipids by oil red O for analyzing the metabolic status in health and disease. Nat Protoc 8, 1149-1154, doi:10.1038/nprot.2013.055 (2013).

40 Kritikou, E. et al. Inhibition of lysophosphatidic acid receptors 1 and 3 attenuates atherosclerosis development in LDL-receptor deficient mice. Sci Rep 6, 37585, doi:10.1038/srep37585 (2016).

41 Wezel, A. et al. Complement factor C5a induces atherosclerotic plaque disruptions. J Cell Mol Med 18, 2020-2030, doi:10.1111/jcmm.12357 (2014).

42 Nadkarni, S. K. et al. Measurement of collagen and smooth muscle cell content in atherosclerotic plaques using polarization-sensitive optical coherence tomography. J Am Coll Cardiol 49, 1474-1481, doi:10.1016/j.jacc.2006.11.040 (2007).

43 Out, R. et al. Macrophage ABCG1 Deletion Disrupts Lipid Homeostasis in Alveolar Macrophages and Moderately Influences Atherosclerotic Lesion Development in LDL Receptor-Deficient Mice. Arteriosclerosis, thrombosis, and vascular biology 26, 2295-2300, doi:10.1161/01.ATV.0000237629.29842.4c (2006).

44 Folch, J., Lees, M. & Sloane Stanley, G. H. A simple method for the isolation and purification of total lipides from animal tissues. The Journal of biological chemistry 226, 497-509 (1957).

45 Dickhout, J. G., Basseri, S. & Austin, R. C. Macrophage Function and Its Impact on Atherosclerotic Lesion Composition, Progression, and Stability. Arteriosclerosis, thrombosis, and vascular biology 28, 1413-1415, doi:doi:10.1161/ATVBAHA.108.169144 (2008).

46 Rodriguez-Fernandez, S. et al. Phosphatidylserine-Liposomes Promote Tolerogenic Features on Dendritic Cells in Human Type 1 Diabetes by Apoptotic Mimicry. Front Immunol 9, 253, doi:10.3389/fimmu.2018.00253 (2018).

47 Krishna, S. M. et al. Anionic nanoliposomes reduced atherosclerosis progression in Low Density Lipoprotein Receptor (LDLR) deficient mice fed a high fat diet. J Cell Physiol, doi:10.1002/jcp.26610 (2018).

48 Hosseini, H. et al. Phosphatidylserine liposomes mimic apoptotic cells to attenuate atherosclerosis by expanding polyreactive IgM producing B1a lymphocytes. Cardiovasc Res 106, 443-452, doi:10.1093/cvr/cvv037 (2015).

49 Benne, N. et al. Anionic 1,2-distearoyl-sn-glycero-3-phosphoglycerol (DSPG) liposomes induce antigen-specific regulatory T cells and prevent atherosclerosis in mice. J Control Release 291, 135-146, doi:10.1016/j.jconrel.2018.10.028 (2018).

50 Pujol-Autonell, I. et al. Use of autoantigen-loaded phosphatidylserine-liposomes to arrest autoimmunity in type 1 diabetes. PLoS One 10, e0127057, doi:10.1371/journal.pone.0127057 (2015).

51 Abuchowski, A., McCoy, J. R., Palczuk, N. C., van Es, T. & Davis, F. F. Effect of covalent attachment of polyethylene glycol on immunogenicity and circulating life of bovine liver catalase. The Journal of biological chemistry 252, 3582-3586 (1977).

52 Fernandez, D. M. et al. Single-cell immune landscape of human atherosclerotic plaques. Nature Medicine 25, 1576-1588, doi:10.1038/s41591-019-0590-4 (2019).

53 Wang, Y. et al. Smooth Muscle Cells Contribute the Majority of Foam Cells in ApoE (Apolipoprotein E)-Deficient Mouse Atherosclerosis. Arteriosclerosis, thrombosis, and vascular biology 39, 876-887, doi:10.1161/atvbaha.119.312434 (2019).

54 Bieghs, V. et al. Internalization of modified lipids by CD36 and SR-A leads to hepatic inflammation and lysosomal cholesterol storage in Kupffer cells. PLoS One 7, e34378, doi:10.1371/journal.pone.0034378 (2012)

SUPPLEMENTARY INFORMATION

1. RESULTS

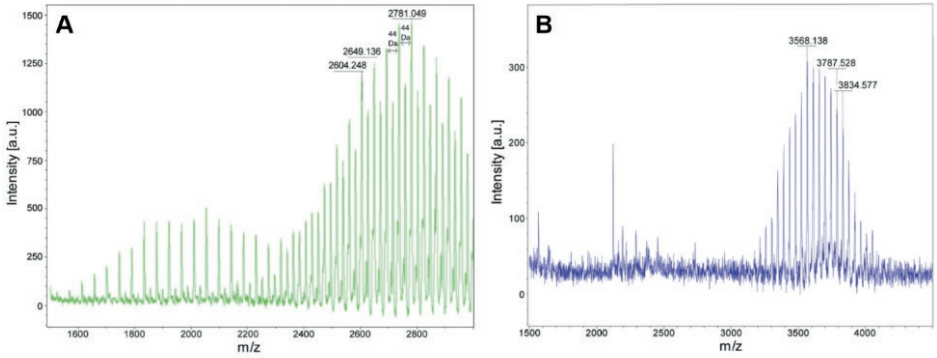

Figure S1. MALDI-MS spectra showing the coupling of DSPE-PEG2000-COOH to cyclic peptide Lyp-1. DSPE-PEG2000-COOH (A) was coupled to cyclic peptide Lyp-1 to produce DSPE-PEG2000-Lyp-1 (B). The mass change between the two spectra corresponds to the successful coupling of the peptide to the lipid.

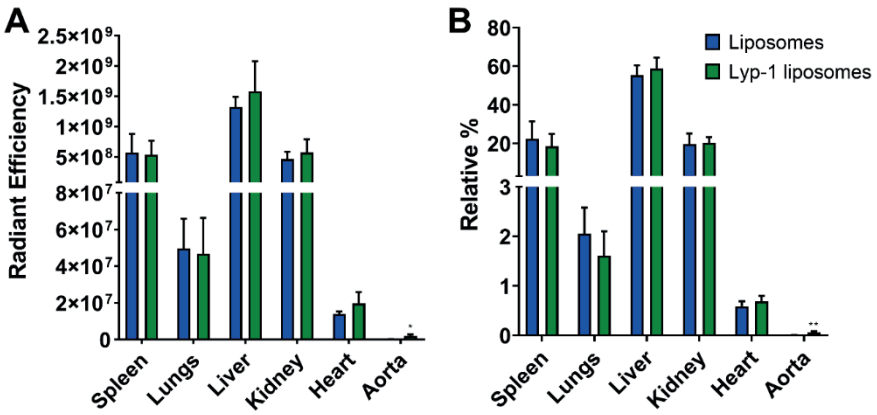

Figure S2. Absolute and relative radiant efficiency of liposomal signal in selected organs in LDLr$^{-/-}$ mice on WTD for 13 weeks, 3 hours after iv injection of non-targeted or Lyp-1 targeted liposomes. Radiant efficiency was measured in spleens, lungs, liver, kidneys, heart, and aorta. (A) Absolute radiant efficient values per organ. (B) The total sum of signals in organs was set to 100%, and the relative radiant efficiency was calculated from this value, n = 5. Graph shows mean + SD, *$p < 0.05$, ***$p < 0.001$ comparing Lyp-1 liposomes to non-targeted liposomes, determined by unpaired t-test.

Chapter 7

Summary, Discussion and Perspectives

INTRODUCTION

The skin represents the interface between the body and the environment. In this strategic position, this organ acts as a physical and immunological barrier protecting the organism against the excessive loss of water and nutrients and against the entry of chemicals and pathogens[1]. A key player in this protective role is the outermost layer of the skin - the stratum corneum (SC). The SC is composed of corneocytes (dead skin cells) embedded in a well-structured lipid matrix primarily composed of cholesterol, ceramides (CERs), and free fatty acids (FFAs) present in an equimolar ratio[2]. The functionality of the skin barrier relies on the organization of the lipid matrix as well as on the composition of the SC lipids, mostly synthesized by keratinocytes during their differentiation process to become corneocytes[3–8]. Extracutaneous lipids (*e.g.* lipoproteins) can also be found in the skin and may contribute to the formation of the SC lipid pool[9–13]. However, this crossroad between the local skin lipid synthesis and the uptake of extracutaneous lipids remains poorly understood.

In the plasma, lipids are mostly transported to and from peripheral tissues inside the core of four main groups of lipoproteins: chylomicrons, very-low-density lipoproteins (VLDL), low-density lipoproteins (LDL), and high-density lipoproteins (HDL). Impaired metabolism of these lipoproteins leads to dyslipidemia, namely abnormal levels of lipids in the plasma. The most common form of dyslipidemia is hyperlipidemia, a condition characterized by the increased levels of circulating lipoproteins and lipids in the plasma that arises from genetic mutations (*e.g.* familial hypercholesterolemia; FH) or an alternate underlying etiology (*e.g.* diabetes, poor life style, and unhealthy diet)[14]. Hyperlipidemia is an important risk factor for the development of atherosclerosis, a major cause of cardiovascular disease[14]. Atherosclerosis is a pathology marked by the formation of lipid plaque(s) inside the arterial wall caused by a chronic immune reaction in response to disturbed cholesterol metabolism. In time, these lipid plaques can harden and narrow the arteries, disturbing the blood flow and oxygen supply and posing a risk to the formation of thrombus and the occurrence of strokes, myocardial infarction, among others.

Liver X receptor (LXR) is a nuclear receptor that plays relevant roles in lipid metabolism and inflammation[15–17]. In the context of atherosclerosis, modulation of LXR by synthetic agonists (*e.g.* GW3965) can impact the plaque development by (1) promoting reverse cholesterol transport from lipid-laden macrophages (foam cells) and (2) by general inhibition of pro-inflammatory genes[16]. However, systemic administration of LXR agonists as free drug directly impacts hepatic lipid synthesis and may induce hypertriglyceridemia[18,19]. Hence, research has focused on encapsulation of these

molecules in delivery systems, which improves biodistribution and introduces the possibility of targeted delivery.

In addition to the increased risk of developing atherosclerosis, individuals with hyperlipidemia (familial or acquired) may develop in time yellow, cholesterol-rich deposits (xanthomas) in the skin around their eyes or joints[20–22]. Xanthomas are known dermatological signs for underlying lipid disorders[21]. Despite the crucial role of lipids in the skin, the link between dyslipidemia and skin lipid homeostasis remains unclear. In this thesis, we explored this knowledge gap to assess whether and how the skin can reflect changes in plasma cholesterol levels at early age prior to the development of xanthomas (or other dermatological disorders) and atherosclerosis. Lastly, we explored the interaction of synthetic peptide Lyp-1 with p32 receptor expressed on lipid-laden macrophages in atherosclerotic plaques[23,24]. We focused on the therapeutic value of Lyp-1 as a targeting peptide on liposomes to deliver the LXR agonist GW3965 to the atherosclerotic plaques in hypercholesterolemic mice.

SUMMARY

The impact of dyslipidemia on the skin

Familial hypercholesterolemia (FH) is a particular type of genetic lipoprotein disorder with an overall reported prevalence of 1:311, among the most common genetic disorders in the general population with similar distribution around the world[25]. This condition arises from mutations in low-density lipoprotein receptor (LDLR) gene and less common in other genes such as apolipoprotein B (APOB), proprotein convertase subtilisin/kexin type 9, apolipoprotein E (APOE) genes[26–28]. Although high cholesterol levels normally do not cause specific complaints early in life, FH patients often develop xanthomas around the eyelids, joints, tendons, and even in the margin of the iris in the long-term[29–31]. These dermatological signs are often the first indication of hypercholesterolemia, an important risk factor for atherosclerosis as described previously.

In **Chapter 2**, we examined the skin of young adult (16-18 weeks old) LDLR knockout (*LDLR*$^{-/-}$) and *APOE*$^{-/-}$ mice in search for early cutaneous disturbances related to hypercholesterolemia. Both *LDLR*$^{-/-}$ and *APOE*$^{-/-}$ mice are well-established hypercholesterolemic mouse models, and their skin is described to develop xanthomas upon prolonged high fat/high-cholesterol diet feeding or upon ageing. We showed that at young age the morphology of skin was preserved without signs of xanthomas, inflammation or hyperproliferation in both mouse models. Further analysis of the epidermis revealed that the barrier lipid composition was different between these two

models. The lipid composition in epidermis of the mild hypercholesterolemic *LDLR*$^{-/-}$ mice strongly resembled the lipid profile reported for normolipidemic wild-type control mice. In contrast, the epidermis of *APOE*$^{-/-}$ mice was enriched with unsaturated FFA species and short chain FFAs with less than 24 carbons atoms in their structure. Remarkably, the CER profile and cholesterol content were hardly impacted in the epidermis of *APOE*$^{-/-}$ mice. CERs and FFAs are known to share a common synthetic pathway in the skin with changes in the chain length and degree of unsaturation of FFA translating into similar trends in the CER profile[5,32]. As the changes observed for the epidermal FFA species were not accompanied by a similar profile in the CER group, we hypothesized that the short and unsaturated FFA species were likely of extracutaneous origin. In the plasma of *APOE*$^{-/-}$ mice cholesteryl esters (CE) are enriched with fatty acid C18:1-moiety[33]. Similarly, we reported increased levels of FFA 18:1 in the epidermis of the *APOE*$^{-/-}$ mice, which was accompanied by strong downregulation of mRNA of genes involved in both cholesterol (HMG-CoA reductase - *HMGCR*) and FFA (acetyl-Coenzyme A carboxylase alpha- *ACACA* or *ACC*) synthesis in the skin of these mice. This genetic profile indicates a compensatory downregulation of genes involved in the synthesis of cholesterol and fatty acids in response to the increased local levels of cholesterol and FFAs. Additionally, a reduction in mRNA levels of *LDLR* showed that the pathway to mediate uptake of lipids from lipoproteins was downregulated. Finally, the altered FFA pool in the epidermis of *APOE*$^{-/-}$ mice resulted in a reduced skin barrier function as shown by increased transepidermal water loss. In short, this study suggests that the severity of the hypercholesterolemia in mice, in particular the levels of CE in plasma, may contribute to the flux of extracutaneous lipids into the skin; thus, impacting the epidermal lipid composition and the functionality of the skin barrier already at young age. From the perspective of FH patients, our findings showed that the skin of hypercholesterolemic individuals may already be impacted on lipid composition and barrier function prior to the development of xanthomas or cardiovascular complications.

Hypercholesterolemic profiles may also emerge from accumulation of apolipoprotein A (APOA) carrying lipoproteins leading to hyperalphalipoproteinemia. Genetic factors such as deficiency of cholesteryl ester transfer protein (CETP) or rare mutations in scavenger receptor class B member I (SR-BI) are described as causes of hyperalphalipoproteinemia with striking increase in HDL-cholesterol levels in humans[34–36]. In contrast with FH patients, hyperalphalipoproteinemic patients are not reported to develop xanthomas[37]. However, the skin is one of the largest reservoirs of HDL in the body; thus, hyperalphalipoproteinemia may have an impact on the skin lipid homeostasis[38].

Next, in **Chapter 3** we assessed whether the hypercholesterolemia derived from

hyperalphalipoproteinemia could also impact the epidermal lipid pool. For this purpose we used young adult (16-18 weeks old) *SR-BI*$^{-/-}$ mice, a hypercholesterolemic mouse model of hyperalphalipoproteinemia, in which the clearance of HDL particles by the liver is impaired as well as their uptake by steroidogenic tissues[39–41]. Notably, the levels of total CE transported in lipoproteins in *SR-BI*$^{-/-}$ mice are significantly higher than the levels reported for *LDLR*$^{-/-}$ mice, but not as severe as seen for the *APOE*$^{-/-}$ mice (**Chapter 2**). Despite the protective role of HDL in reverse cholesterol transport, hyperalphalipoproteinemia had a negative impact on the epidermal FFA composition of the *SR-BI*$^{-/-}$ mice. Although to a lower extent as reported for the skin of *APOE*$^{-/-}$mice, the relative percentage of unsaturated and short carbon chain FFA species, including FFA C18:1, was augmented in the epidermis of *SR-BI*$^{-/-}$ mice in comparison with the normolipidemic wild-type controls. Similar to the epidermis of *APOE*$^{-/-}$ mice, the cholesterol content and CER profile were preserved in the epidermis of these mice. Thus, the altered FFA profile in the epidermal barrier of *SR-BI*$^{-/-}$ mice is likely not linked to the biosynthetic pathway shared with CERs but rather linked to lipids of extracutaneous origin[5,32]. This hypothesis is supported by the reduced mRNA levels of genes related to cholesterol (HMG-CoA synthase 1; *HMGCS1*) and FFA synthesis (*ACACA* and fatty acid synthase; *FAS*) as well as lower levels of *LDLR*. The accumulation of CE in the plasma of *SR-BI*$^{-/-}$ mice inhibits the activity of the enzyme lecithin-cholesterol acyl transferase (LCAT)[42]. Mice with reduced LCAT activity reportedly show increased circulating levels of CE containing fatty acid C16:0- and C18:1 moieties, supporting once more a direct link between fatty acid C18:1-containing CE in plasma and elevated epidermal FFA C18:1[33]. Synthetic stratum corneum lipid model membranes mimicking the epidermal composition of the *SR-BI*$^{-/-}$ mice showed a more permeable outside-inside lipid barrier. However, *in vivo* transepidermal water loss revealed a functional inside-outside skin barrier. Importantly, we showed that effects on epidermal lipids are closely correlated with plasma lipid levels and less dependent on the lipoprotein group involved in the lipid transport. Although dermatological signs (*e.g.* xanthomas) have not been described in patients with hyperalphalipoproteinemia, our data demonstrates that the skin is negatively affected by the changes in the plasma lipid profile. Hence, it is relevant to pay additional attention to the skin of these patients to prevent the development of dermatological abnormalities.

It is important to note that dyslipidemia may also refer to reduced levels of plasma lipids, namely hypolipidemia, caused by genetic abnormalities or other disorders. Mutations in APOAI can severely affect the metabolism of HDL leading to a virtual absence of these particles, which results in reduced cholesterol in the plasma (especially lower CE levels) and an increased risk of cardiovascular disease[43–48]. In **Chapter 4** we assessed the impact of HDL-driven hypolipidemia (hypoalphalipoproteinemia) on the skin

barrier lipid composition of *APOAI*$^{-/-}$ mice. Hypoalphalipoproteinemia in the *APOAI*$^{-/-}$ mice did not impact the general morphology of the skin or the epidermal lipid profile. However, the mRNA expression of various genes involved in lipid synthesis and uptake of lipoproteins was upregulated in the skin of these mice (*e.g. HMGCR, LDLR, FAS, SR-BI*). In line, the downregulation of *DGAT2* (diacylglycerol O-acyltransferase 2) mRNA levels in the skin of these mice suggests a reduction in the storage of fatty acids in the form of triglycerides. Altogether, our data indicates that (1) HDL particles are not crucial for the skin reversed cholesterol transport but (2) contribute to the delivery of essential lipids to the skin. Importantly, the epidermal lipid barrier can be maintained by a compensatory rise in local lipid synthesis and in the uptake of lipid from apolipoprotein B-containing lipoproteins in the virtual absence of HDL.

The relevance of the skin site to research – a barrier lipid assessment

The studies described in the previous sections (**Chapters 2-4**) were performed using the back skin of the mice as it comprised a large area for sampling and analysis. However, skin of both ear and back are commonly used for research in mouse models and these sites strongly differ in the density of hair follicles and the number of cell layers in the SC. Furthermore, these skin sites may yield different effects/phenotypes regarding for instance drug treatment and tissues regeneration studies[49–51]. Despite these differences little information is available regarding the composition of their lipid barrier, especially regarding the ear epidermis.

In **Chapter 5**, we provide evidence that the epidermal lipid composition and the mRNA gene expression profile are fundamentally different between the ear and the back skin in a normolipidemic background. Compared to the back skin, the epidermis of the ears revealed stronger prevalence of sphingosine base (CER[S]) in the overall CER pool, including short chain CERs (33-34 carbons). Additionally, the ear epidermis was enriched with shorter and unsaturated FFA species, leading to a reduction in the mean chain length of the FFA pool. Both unsaturated- and short chains lipids in the SC are associated with reduced barrier function of the skin. For instance, the skin of atopic dermatitis patients shows a higher percentage of CER [S], 34 carbon chain CERs, short FFAs, and unsaturated FFAs[5]. This profile in atopic dermatitis accounts for a reduced barrier function of the skin marked by an increased transepidermal water loss in these patients[5]. However, in the case of the murine model, the ear skin may compensate for this unfavorable lipid profile with an increased number of corneocyte layers in the epidermis. In addition to the reported differences in the epidermal lipid profile, the ear skin showed a reduction in the mRNA expression of genes involved in the lipid synthesis (*e.g. FAS, elongases, HMGCS1*) and late differentiation markers for keratinocytes (keratin

10 and involucrin), indicating a lower metabolic activity in this skin site. In agreement, the network of blood- and lymphatic vessels is less prominent in the ear[52,53].

Further in **Chapter 5**, we described that the skin of the ear marginally responded to hypercholesterolemia as compared to the back skin in *APOE*$^{-/-}$ mice[54]. The FFA epidermal profile of the ears of normolipidemic and hypercholesterolemic mice was fairly comparable, with only a minimal increase in the overall percentage of the short chain FFA species. Further, we showed that changes in the FFA component of sebaceous lipids do not account for the striking changes reported in the back skin of *APOE*$^{-/-}$ mice. These findings indicate that the back skin is likely a more active metabolic site compared to the ear skin and these sites respond differently to specific treatments leading to distinct outcomes as previously reported[49–51]. Thus, the selection of the skin site can have an impact on the outcome of a study and should be carefully considered to match the goal of the study. For instance, studies to assess the penetration of topically applied compounds could be performed on the ears due to their larger interfollicular area and higher number of corneocyte layers; which more closely resembles human skin.

Lyp-1: small peptide to target liposomes to atherosclerotic lesion macrophages

In addition to its effects on the skin, hypercholesterolemia is an important risk factor for atherosclerosis, a disease characterized by the pathologic narrowing of large and medium arteries[55]. The onset and development of this pathology is primarily driven by lipid (LDL and other lipoprotein remnants) buildup in macrophages in the intima of these vessels, leading to the formation of atherosclerotic plaques[55–57]. In **Chapter 6**, we described our efforts to design a liposome formulation to deliver LXR agonist GW3965 to plaque macrophages stimulating reverse cholesterol transport and ultimately promoting plaque stabilization[58–60]. Atherosclerotic plaques show high expression of C1q-binding protein, also known as p32, in particular in lipid-rich macrophages (foam cells)[23,24]. Lyp-1 is a small cyclic peptide (CGNKRTRGC) known to bind to p32[23]. To date, the potential of Lyp-1 as targeting molecule has been mostly explored for plaque imaging purposes, which also benefits from macrophages propensity to take up nanoparticles[61,62].

In our study, liposome functionalization with Lyp-1 was the key strategy in our formulation design to increase target and retention time of the liposomes in the plaque. Despite their inherited properties towards particle uptake, lipid-rich murine macrophages displayed uptake preference towards Lyp-1-containing liposomes compared to the Lyp-1-free particles in the in vitro setting. In agreement, *LDLR*$^{-/-}$ mice on Western type diet treated with GW3965-loaded liposomes showed increased retention

for the particles functionalized with Lyp-1 in the aorta. In line with the *in vitro* data, the percentage of aortic macrophages "positive" for Lyp-1-targeting liposomes was superior to the Lyp-1-free liposomes. Although no impact in plaque size was observed in this study, the group treated with GW3965-loaded Lyp-1 liposomes had reduced plaque macrophage content and enhanced plaque stability as evidenced by increased collagen content. Additionally, treatment with the functionalized GW3965-loaded liposomes did not impact liver and serum lipid content. Hence, liposomes functionalized with Lyp-1 are a valuable tool to target lipid-rich macrophages in the atherosclerotic lesions and may increase efficacy of a moderate dose of GW3965, paving the way to the development of better therapies for atherosclerosis.

DISCUSSION AND PERSPECTIVES

The research described in this thesis broadens our perspective of how dyslipidemia impacts the quality of life of the individuals beyond cardiovascular- and metabolic diseases. It highlights the relevance of unraveling the governance of the skin lipid homeostasis in response to dyslipidemic profiles to properly advice and to treat these patients on dermatological disorders they may develop. In turn, this knowledge may facilitate the future development of therapies that could tackle both sides of this spectrum.

Some dermatological disorders (*e.g.* psoriasis) with chronic and systemic inflammatory components have been associated with plasma lipid abnormalities[22]. Also, individuals suffering from dyslipidemia are generally unaware of their condition unless in case of a severe profile. As a consequence, skin signs like xanthomas may be the first indication of an imbalanced metabolic lipid profile[21,22]. For instance, patients with FH present increased plasma cholesterol levels from birth; however, the development of skin xanthomas can occur at different stages of life and likely dependent on the severity of the dyslipidemic profile[28]. Here, we report that skin lipid composition can be negatively impacted prior to the development of macroscopic dermatological abnormalities in dyslipidemic mice fed a regular chow diet (low-fat diet).

It is important to note that the dyslipidemic murine models used in this thesis are a result of total body gene deletion; hence, the deletion affects all organs in the body in which the gene of interest is normally expressed. The deletion of *SR-BI* and *LDLR* in the liver impacts the metabolism of lipoproteins strongly contributing to the dyslipidemic profiles seen in the mice. However, *SR-BI*, *LDLR*, and *APOE* are also expressed in the skin, especially in keratinocytes in the basal layer[63–65]. In our studies, the consequences of the local gene deletion could not be evaluated with our full body knockout models;

thus, a potential local effect cannot be discarded. The roles of SR-BI and APOE in the skin remain unclear. To differentiate local (skin) effect from systemic effects (plasma-derived), the generation of skin-specific knockout models by Cre-LoxP system can be a valuable tool to assess the role of these genes and their respective protein/receptor exclusively in the skin[66,67]. In line with previous studies, we showed that different results may be obtained depending on the skin site used in the research[49–51,68]. Also for this topic, skin specific knockout of genes may help shed some light on the diversity of responses of the skin sites, in particular between areas where differences in metabolic activity are anticipated.

In addition to genetic predisposition, dietary habits affect the composition and the metabolism of plasma lipids. In both mice and humans, hypercholesterolemia may also derive from dietary habits such as the regular intake of lipid-rich diet as commonly observed in Western countries. In our studies, the use of young adult mice fed a regular low-fat diet allowed us to assess the impact of "naturally occurring" (genetically) imbalanced lipid metabolism on the skin without the contribution of ageing and unhealthy diets. Several studies in murine models have reported the negative impact of lipid-rich diets on the skin[69–73]. For instance, *LDLR*$^{-/-}$ mice fed a diet containing 1.25% cholesterol, 7.5% cocoa butter, 7.5% casein and 0.5% cholate for 5 to 7 months developed strong skin xanthoma, a phenotype not observed upon challenge with Western-type diet, containing 0.15% cholesterol and 21% fat for 3 to 5 months[74,75]. These studies demonstrate that the composition of the diet and its duration determine development of dermatological abnormalities in mice. However, it is important to note that these extreme hyperlipidemic models do not develop human-like lipoproteins profiles. APOE*3-Leiden.huCETP mice have reduced clearance of apolipoprotein B containing lipoproteins and express human CETP, a protein that facilitates the exchange of triglycerides between HDL and apolipoprotein B containing lipoproteins[76,77]. As a result, these mice develop a human-like lipoprotein profile when challenged with a cholesterol-rich Western type diet[78,79]. Hence, analysis of the skin of APOE*3-Leiden.huCETP with and without the challenge of lipid rich diets is important to facilitate the translation of these dermatological findings to the human situation.

Hypercholesterolemia is also a well-defined risk factor for the development of atherosclerosis, a pathology marked by impaired cholesterol metabolism. To expand our knowledge on the plasma lipid changes underlying the development of atherosclerosis metabolomics (in particular lipidomics) could be employed. In *SR-BI*$^{-/-}$ mice, plasma metabolomics identified potential biomarkers for cardiovascular disease[80]. Similarly, a wide-ranging plasma metabolomics analyses of *APOE*$^{-/-}$ mice revealed distinct glycerophospholipid and sphingolipid metabolites profiles associated with different

stages of atherosclerosis development in these mice detectable from 5-15 weeks of age[81]. Importantly, glycerophospholipids and sphingolipids have also been reported to be altered in the plasma of psoriatic patients[82,83]. In addition, literature reports that FH patients with xanthomas have a higher risk of developing cardiovascular disease compared to those without these dermatological signs[84]. Although much remains to be understood regarding the plasma-skin interaction as described in the previous paragraphs, these findings bring forward the opportunity to explore the connection between atherosclerosis development and early dermatological disorders. This knowledge (metabolomics) may in the future ratify epidermal lipid screening as a marker for dyslipidemia and other metabolic disorders to bring the opportunity of early detection and treatment to improve the quality of life of the patients.

As atherosclerosis remains a leading cause of death worldwide, identifying novel therapeutic targets and strategies to treat this pathology is crucial, in particular at an early stage of disease development[85]. In this battle against atherosclerosis, synthetic LXR agonists have extensively been investigated to stimulate reversed cholesterol transport from atherosclerotic plaques[60]. It is clear that systemic administration of LXR agonists as free drugs can lead to an unwanted rise in hepatic- and serum lipids, thereby limiting their anti-atherogenic effects[86–88]. For instance, oral administration of free GW3965 at 10 mg/kg for 12 weeks strongly reduced atherosclerotic lesion size[87]. However, this effect was accompanied by hypertriglyceridemia in mice. Thus, encapsulation of these small molecules in drug carriers is an useful tool to modify the biodistribution of these compounds[89]. The use of drug delivery systems also brings the opportunity to employ targeting molecules to increase delivery to the atherosclerotic plaque. The synthetic cyclic peptide Lyp-1 interacts with p32, a receptor highly expressed in macrophage foam cells in atherosclerotic lesions[24]. Hence, functionalization of GW3965-loaded liposomes with this small peptide can enhance targeting of plaque macrophages. The targeting properties of Lyp-1 increased the efficacy of a moderate dose of GW3965 (6.5 mg/kg) yielding a plaque with reduced macrophage content and higher collagen content. The atherosclerotic lesion size was not impacted by treatment with free-GW3965 or GW3065-loaded-lyp-1 liposomes, which can be driven by the moderate dose used in our studies. To achieve plaque size reduction by treatment with Lyp-1 liposomes loaded with a higher dose of GW3965 (*e.g.* 10 mg/kg), it is crucial to concurrently explore strategies to minimize hepatic uptake of these particles. In our study we used poly-ethylene glycol (PEG) to create a stealthy particle surface and reduce removal of the liposomes by the reticuloendothelial system (RES). Yet, we observed a significant hepatic accumulation of PEG-coated-Lyp-1 liposomes. Other strategies to increse circulation time and/or evade the immune system can be evaluated to improve the performance of the Lyp-1 liposomes such as polyvinyl pyrrolidone, polyoxazolines, CD47-mimicking peptide, PEG-

based copolymers[90,91]. Another interesting strategy to evade the RES system comprises "RES blockage" in which pre-administration of empty liposomes to occupy the RES system enables a longer circulation time of subsequently administered nanoparticles[92]. However, the effectiveness of this approach is controversial and the biodistribution of the subsequent dose could be affected in other ways that aimed for. The delivery of other drug classes (*e.g.* microRNAs, atorvastatin) could also be considered as macrophages are also involved in the local inflammatory response in the atherosclerotic plaque[93–96]. Different delivery systems yield different particle biodistribution. In line, other drug delivery systems could be functionalized with Lyp-1 as this small peptide has been reported to deliver supramagnetic iron oxide nanoworm-based magnetic resonance imaging probes and dendrimers to the atherosclerotic plaque[23,62]. For instance, (co) Polymeric systems such as poly(lactic-co-glycolic acid) (PLGA) may also be investigated as they are easy to functionalize and PLGA particles have already been successfully employed to deliver GW3965 to atherosclerotic plaques[97]. In summary, we showed that Lyp-1 is a valuable tool to target atherosclerotic lesions and it enhanced the therapeutic window of a moderate dose of LXR agonist. Future studies could explore functionalization of Lyp-1 (1) on other types of delivery systems, (2) in combination with different surface stealth materials, and (3) even evaluate the impact of targeted delivery of other drugs (*e.g.* anti-inflammatory drugs).

In view of the potential value of LXR agonists in atherosclerosis, it is important to note that LXR is also expressed in the skin of both humans (LXRα and LXRβ) and mice (LXRβ). In human skin, LXRα is the predominant isoform and its expression can be impacted in diseased skin as previously reported for psoriasis[98]. Lesional psoriatic skin shows reduced expression of LXRα compared to non-lesional and control skin[98]. In contrast, in murine skin LXRβ is the predominant isoform and the deletion of LXRα in normolipidemic mice did not affect keratinocyte differentiation or skin morphology[99]. The deletion of LXRβ in normolipidemic mice resulted in thinner epidermis and mild reduction in the expression of differentiation markers[99]. In the skin, naturally occurring LXR agonists (*e.g.* 22(R)-hydroxy-cholesterol) drive keratinocyte differentiation and improve barrier function[99–101]. Synthetic LXR agonists (*e.g.* T0901317 and GW3965) have been shown to reduce skin inflammation, inhibit fibrosis, prevent photo- and chronological aging, and induce cholesterol efflux in both human and murine skin by upregulation of ABCA1 in normolipidemic backgrounds[102–104]. However, to date the effect of LXR activation on the skin in hypercholesterolemic backgrounds remains to be investigated. One of the main downstream targets of LXR is stearoyl-CoA desaturase-1, a desaturase with crucial role in the formation of unsaturated fatty acids[105]. As previously mentioned, rises in the fraction of unsaturated lipids have a negative impact in the barrier organization and function. Human skin equivalents are *in vitro* 3D models of skin cultured with

human skin cells (keratinocytes and fibroblasts)[106]. The SC lipid composition of these models is enriched with short and unsaturated CERs and FFAs species, sharing to some extend similarities with the *APOE*$^{-/-}$ epidermal lipid profile[106]. In these *in vitro* models, exposure to T0901317 was further detrimental to the SC lipid composition with further increase in the pool of unsaturated and short FFAs and CERs[106]. Another key point to be considered is that LXR agonists can also induce the expression of other members of the nuclear receptor family. LXR agonist T0901317 also induces the expression of farsenoid-X-receptor (FXR) and peroxisome-X-receptor (PXR), both expressed in the skin[107–109] . Activation of FXR (EC_{50}=5 μM) by small heterodimer partner (SHP) downregulates LXR and its target genes (*e.g. SREBP-1C* and *FAS*)[109]. In particular, activation of PXR has been associated with hepatic steatosis and impaired skin barrier function[110]. In contrast, the LXR agonist GW3965 is a strong activator of LXR but without inducing FXR or PXR expression to the same extent as described for T0901317[110]. This more selective profile of GW3965 favors this compound as a frontrunner in future investigations when aiming for concomitant tackling of dermatological and atherogenic disturbances. In addition to its effects in modulating cholesterol metabolism, LXR also plays a role in regulation of inflammation[111,112]. The skin of young adult *APOE*$^{-/-}$ mice does not present signs of inflammation but with aging accumulation of lipid-laden macrophages (foam cells) in the skin of these mice has been reported[113]. Activation of LXR leads to downregulation of diverse inflammatory mediators such as interleukin-1 and tumor necrosis factor-alpha in keratinocytes[111]. These anti-inflammatory properties derived from LXR activation have been reported to ameliorate irritant and allergic contact dermatitis and to reduce aging related photo damage in murine models. In short, it remains unclear whether LXR activation in the skin would be beneficial for the barrier lipid profile in hypercholesterolemia. Nonetheless, there is evidence on both sides that shows that it may be worthy to investigate it.

The findings described in this thesis focused on dyslipidemic mouse models and should not be directly applied to the human situation without further considerations and studies. Mice and humans will present similarities and differences in all research topics explored in this thesis (skin, lipid metabolism, atherosclerosis development)[114–117]. For instance, both plasma and skin lipidomics have identified differential lipid fingerprints between the two species but also strong similarities, in particular when compared to other animal research models (*e.g.*; non-human primates and rats)[114]. Additionally, it is important to mention that, although not explored in depth in this thesis, the skin is an active immunological site[118]. Also here, the two species present convergent and divergent immunologic profiles that should be carefully considered when translating findings in mouse models to the human situation[118]. Importantly, these differences should not discourage the use of mouse models as they have greatly contributed to

landmark discoveries in the research fields explored in this thesis. Instead, awareness of these differences is important to help scientists better design their experiments and later appropriately translate their findings to the human situation. Lastly, the next step in this research should certainly focus on the evaluation of the skin lipid composition and barrier functionality in individuals suffering from FH. The data generated from such study would be the first step to understand the value of using dyslipidemic murine models to comprehend the crossroads between the skin, the plasma and dyslipidemic related pathologies for the human situation.

In summary, the research described in this thesis shows that hypercholesterolemia, a well-established risk factor for atherosclerosis, can impact skin lipid pool and barrier function already at young age. Elucidation of the mechanisms underlying this intercommunication between plasma and skin may also bring valuable opportunities to prevent and treat dermatological pathologies in dyslipidemic patients; perhaps in combination with anti-atherogenic therapies. Thus, by deepening our knowledge we may improve our advice to the patients and ultimately improve their quality of life.

REFERENCES

1. Elias, P. M. Stratum corneum defensive functions: An integrated view. J. Invest. Dermatol. 125, 183–200 (2005).

2. Ponec, M., Weerheim, A., Lankhorst, P. & Wertz, P. New acylceramide in native and reconstructed epidermis. J. Invest. Dermatol. 120, 581–588 (2003).

3. Janssens, M. et al. Increase in short-chain ceramides correlates with an altered lipid organization and decreased barrier function in atopic eczema patients. J. Lipid Res. 53, 2755–2766 (2012).

4. Thakoersing, V. S. et al. Modulation of stratum corneum lipid composition and organization of human skin equivalents by specific medium supplements. Exp. Dermatol. 24, 669–674 (2015).

5. van Smeden, J. et al. The importance of free fatty acid chain length for the skin barrier function in atopic eczema patients. Exp. Dermatol. 23, 45–52 (2014).

6. White, S. H., Mirejovsky, D. & King, G. I. Structure of lamellar lipid domains and corneocyte envelopes of murine stratum corneum. An x-ray diffraction study. Biochemistry 27, 3725–3732 (1988).

7. Boncheva, M., Damien, F. & Normand, V. Molecular organization of the lipid matrix in intact Stratum corneum using ATR-FTIR spectroscopy. Biochim. Biophys. Acta - Biomembr. 1778, 1344–1355 (2008).

8. Bouwstra, J., Gooris, G. & Ponec, M. The lipid organisation of the skin barrier: liquid and crystalline domains coexist in lamellar phases. J. Biol. Phys. 28, 211–23 (2002).

9. Haruta-Ono, Y. et al. Orally administered sphingomyelin in bovine milk is incorporated into skin sphingolipids and is involved in the water-holding capacity of hairless mice. J. Dermatol. Sci. 68, 56–62 (2012).

10. Bhattacharyya, A. K., Connor, W. E. & Spector, A. A. Excretion of sterols from the skin of normal and hypercholesterolemic humans. Implications for sterol balance studies. J. Clin. Invest. 51, 2060–70 (1972).

11. Khnykin, D., Miner, J. H. & Jahnsen, F. Role of fatty acid transporters in epidermis: Implications for health and disease. Dermatoendocrinol. 3, 53–61 (2011).

12. Hansen, H. S. & Jensen, B. Essential function of linoleic acid esterified in acylglucosylceramide and acylceramide in maintaining the epidermal water permeability barrier. Evidence from feeding studies with oleate, linoleate, arachidonate, columbinate and α-linolenate. Biochim. Biophys. Acta - Lipids Lipid Metab. 834, 357–363 (1985).

13. Bibel, D. J. et al. Antimicrobial Activity of Stratum Corneum Lipids from Normal and Essential Fatty Acid-Deficient Mice. J. Invest. Dermatol. 92, 632–638 (1989).

14. Nelson, R. H. Hyperlipidemia as a Risk Factor for Cardiovascular Disease. Prim. Care Clin. Off. Pract. 40, 195–211 (2013).

15. Wang, B. & Tontonoz, P. Liver X receptors in lipid signalling and membrane homeostasis. Nat. Rev. Endocrinol. 14, 452–463 (2018).

16. Im, S.-S. & Osborne, T. F. Liver X Receptors in Atherosclerosis and Inflammation. Circ. Res. 108, 996–1001 (2011).

17. Schulman, I. G. Liver X receptors link lipid metabolism and inflammation. FEBS Lett. 591, 2978–2991 (2017).

18. Zhang, Y. et al. Liver LXRα expression is crucial for whole body cholesterol homeostasis and reverse cholesterol transport in mice. J. Clin. Invest. 122, 1688–1699 (2012).

19. Heckmann, B. L. et al. Liver X receptor α mediates hepatic triglyceride accumulation through upregulation of G0/G1 Switch Gene 2 expression. JCI Insight 2, (2017).

20. Sugiyama, N. et al. Immunohistochemical distribution of lipoprotein epitopes in xanthomata from patients with familial hypercholesterolemia. Am. J. Pathol. 141, 99–106 (1992).

21. Dwivedi, S. Cutaneous markers of coronary artery disease. World J. Cardiol. 2, 262 (2010).

22. Shenoy, C., Shenoy, M. & Rao, G. Dyslipidemia in dermatological disorders. N. Am. J. Med. Sci. 7, 421 (2015).

23. Hamzah, J. et al. Specific penetration and accumulation of a homing peptide within atherosclerotic plaques of apolipoprotein E-deficient mice. Proc. Natl. Acad. Sci. 108, 7154–7159 (2011).

24. Peerschke, E. et al. Expression of gC1q-R/p33 and its major ligands in human atherosclerotic lesions. Mol. Immunol. 41, 759–766 (2004).

25. Hu, P. et al. Prevalence of Familial Hypercholesterolemia Among the General Population and Patients With Atherosclerotic Cardiovascular Disease. Circulation 141, 1742–1759 (2020).

26. Fairoozy, R. H. et al. The Genetic Spectrum of Familial Hypercholesterolemia (FH) in the Iranian

Population. Sci. Rep. 7, 17087 (2017).

27. Rashidi, O. M., H.Nazar, F. A., Alama, M. N. & Awan, Z. A. Interpreting the Mechanism of APOE (p.Leu167del) Mutation in the Incidence of Familial Hypercholesterolemia; An In-silico Approach. Open Cardiovasc. Med. J. 11, 84–93 (2017).

28. Defesche, J. C. et al. Familial hypercholesterolaemia. Nat. Rev. Dis. Prim. 3, 17093 (2017).

29. Ohshiro, T., Shimabukuro, T., Sunagawa, M. & Ohta, T. An 11-year-old boy with familial hypercholesterolemia showing multiple xanthomas and advanced atherosclerosis, who responded to lipid-lowering therapy using statin. J. Atheroscler. Thromb. 16, 698–701 (2009).

30. Aljenedil, S., Ruel, I., Watters, K. & Genest, J. Severe xanthomatosis in heterozygous familial hypercholesterolemia. J. Clin. Lipidol. 12, 872–877 (2018).

31. Palacio, C. H., Harring, T. R., Nguyen, N. T. T., Goss, J. A. & O'Mahony, C. A. Homozygous familial hypercholesterolemia: case series and review of the literature. Case Rep. Transplant. 2011, 154908 (2011).

32. Sassa, T. et al. Impaired Epidermal Permeability Barrier in Mice Lacking Elovl1, the Gene Responsible for Very-Long-Chain Fatty Acid Production. Mol. Cell. Biol. 33, 2787–2796 (2013).

33. Subbaiah, P. V. et al. Regulation of plasma cholesterol esterification by sphingomyelin: Effect of physiological variations of plasma sphingomyelin on lecithin-cholesterol acyltransferase activity. Biochim. Biophys. Acta - Mol. Cell Biol. Lipids 1821, 908–913 (2012).

34. Hirano, K. et al. Disease-associated marked hyperalphalipoproteinemia. Mol. Genet. Metab. Reports 1, 264–268 (2014).

35. Oates, C. P. et al. Novel polymorphisms associated with hyperalphalipoproteinemia and apparent cardioprotection. J. Clin. Lipidol. 12, 110–115 (2018).

36. Helgadottir, A. et al. Rare SCARB1 mutations associate with high-density lipoprotein cholesterol but not with coronary artery disease. Eur. Heart J. 39, 2172–2178 (2018).

37. Miettinen, H. E. et al. Molecular Genetic Study of Finns With Hypoalphalipoproteinemia and Hyperalphalipoproteinemia. Arterioscler. Thromb. Vasc. Biol. 18, 591–598 (1998).

38. Randolph, G. J. & Miller, N. E. Lymphatic transport of high-density lipoproteins and chylomicrons. J. Clin. Invest. 124, 929–935 (2014).

39. Acton, S. et al. Identification of Scavenger Receptor SR-BI as a High Density Lipoprotein Receptor. Science (80-.). 271, 518–520 (1996).

40. Rigotti, A. et al. A targeted mutation in the murine gene encoding the high density lipoprotein (HDL) receptor scavenger receptor class B type I reveals its key role in HDL metabolism. Proc. Natl. Acad. Sci. U. S. A. 94, 12610–12615 (1997).

41. Brodeur, M. R., Luangrath, V., Bourret, G., Falstrault, L. & Brissette, L. Physiological importance of SR-BI in the in vivo metabolism of human HDL and LDL in male and female mice. J. Lipid Res. 46, 687–696 (2005).

42. Kosek, A. B., Durbin, D. & Jonas, A. Binding affinity and reactivity of lecithin cholesterol acyltransferase with native lipoproteins. Biochem. Biophys. Res. Commun. 258, 548–551 (1999).

43. Sorci-Thomas, M. G. & Thomas, M. J. The Effects of Altered Apolipoprotein A-I Structure on Plasma HDL Concentration. Trends Cardiovasc. Med. 12, 121–128 (2002).

44. Chroni, A., Duka, A., Kan, H.-Y., Liu, T. & Zannis, V. I. Point Mutations in Apolipoprotein A-I Mimic the Phenotype Observed in Patients with Classical Lecithin:Cholesterol Acyltransferase Deficiency †. Biochemistry 44, 14353–14366 (2005).

45. Huang, W. et al. A Novel Homozygous Missense Mutation in the Apo A-I Gene With Apo A-I Deficiency. Arterioscler. Thromb. Vasc. Biol. 18, 389–396 (1998).

46. Miettinen, H. E. et al. Apolipoprotein A-I FIN (Leu159→Arg) Mutation Affects Lecithin. Arterioscler. Thromb. Vasc. Biol. 17, 3021–3032 (1997).

47. Hovingh, G. K. et al. A novel apoA-I mutation (L178P) leads to endothelial dysfunction, increased arterial wall thickness, and premature coronary artery disease. J. Am. Coll. Cardiol. 44, 1429–1435 (2004).

48. Plump, A. S. et al. ApoA-I knockout mice: Characterization of HDL metabolism in homozygotes and identification of a post-RNA mechanism of apoA-I up-regulation in heterozygotes. J. Lipid Res. 38, 1033–1047 (1997).

49. Madsen, M., Pedersen, T. X., Nielsen, L. B., Johansen, C. & Hansen, P. R. Differential Effects of Digoxin on Imiquimod-Induced Psoriasis-Like Skin Inflammation on the Ear and Back. Ann. Dermatol. 30, 485 (2018).

50. Nguyen, T. & Wei, M. L. Hermansky–Pudlak HPS1/pale ear Gene Regulates Epidermal and Dermal Melanocyte Development. J. Invest. Dermatol. 127, 421–428 (2007).

51. Metcalfe, A. D., Willis, H., Beare, A. & Ferguson, M. W. J. Characterizing regeneration in the vertebrate ear. J. Anat. 209, 439–446 (2006).

52. Liu, F., Smith, J., Zhang, Z., Cole, R. & Herron, B. J. Genetic heterogeneity of skin microvasculature. Dev. Biol. 340, 480–489 (2010).

53. Huggenberger, R. et al. An important role of lymphatic vessel activation in limiting acute inflammation. Blood 117, 4667–4678 (2011).

54. Martins Cardoso, R. et al. Hypercholesterolemia in young adult APOE −/− mice alters epidermal lipid composition and impairs barrier function. Biochim. Biophys. Acta - Mol. Cell Biol. Lipids 1864, (2019).

55. Pirillo, A., Norata, G. D. & Catapano, A. L. LOX-1, OxLDL, and Atherosclerosis. Mediators Inflamm. 2013, 1–12 (2013).

56. Tabas, I. Macrophage death and defective inflammation resolution in atherosclerosis. Nat. Rev. Immunol. 10, 36–46 (2010).

57. Chistiakov, D. A., Melnichenko, A. A., Myasoedova, V. A., Grechko, A. V. & Orekhov, A. N. Mechanisms of foam cell formation in atherosclerosis. J. Mol. Med. 95, 1153–1165 (2017).

58. Collins, J. L. et al. Identification of a Nonsteroidal Liver X Receptor Agonist through Parallel Array Synthesis of Tertiary Amines. J. Med. Chem. 45, 1963–1966 (2002).

59. Levin, N. et al. Macrophage Liver X Receptor Is Required for Antiatherogenic Activity of LXR Agonists. Arterioscler. Thromb. Vasc. Biol. 25, 135–142 (2005).

60. Kirchgessner, T. G. et al. Beneficial and Adverse Effects of an LXR Agonist on Human Lipid and Lipoprotein Metabolism and Circulating Neutrophils. Cell Metab. 24, 223–233 (2016).

61. Uchida, M. et al. Protein Cage Nanoparticles Bearing the LyP-1 Peptide for Enhanced Imaging of Macrophage-Rich Vascular Lesions. ACS Nano 5, 2493–2502 (2011).

62. Seo, J. W. et al. 64 Cu-Labeled LyP-1-Dendrimer for PET-CT Imaging of Atherosclerotic Plaque. Bioconjug. Chem. 25, 231–239 (2014).

63. Abd El-Latif, M. I. A., Murota, H., Terao, M. & Katayama, I. Effects of a 3-hydroxy-3-methylglutaryl coenzyme A reductase inhibitor and low-density lipoprotein on proliferation and migration of keratinocytes. Br. J. Dermatol. 128–137 (2010). doi:10.1111/j.1365-2133.2010.09694.x

64. Tsuruoka, H. et al. Scavenger receptor class B type I is expressed in cultured keratinocytes and epidermis. Regulation in response to changes in cholesterol homeostasis and barrier requirements. J. Biol. Chem. 277, 2916–2922 (2002).

65. Grehan, S., Allan, C., Tse, E., Walker, D. & Taylor, J. M. Expression of the apolipoprotein E gene in the skin is controlled by a unique downstream enhancer. J. Invest. Dermatol. 116, 77–84 (2001).

66. Taylor, C. A., Shawlot, W., Ren, J. X. & Mukhopadhyay, S. Generation and Validation of Tissue-Specific Knockout Strains for Toxicology Research. Curr. Protoc. Toxicol. 81, (2019).

67. Son, J. W., Shin, J. J., Kim, M.-G., Kim, J. & Son, S. W. Keratinocyte-specific knockout mice models via Cre–loxP recombination system. Mol. Cell. Toxicol. 17, 15–27 (2021).

68. Martins Cardoso, R., Absalah, S., Van Eck, M. & Bouwstra, J. A. Barrier lipid composition and response to plasma lipids: A direct comparison of mouse dorsal back and ear skin. Exp. Dermatol. 29, 548–555 (2020).

69. Getz, G. S. & Reardon, C. A. Diet and Murine Atherosclerosis. Arterioscler. Thromb. Vasc. Biol. 26, 242–249 (2006).

70. Accad, M. et al. Massive xanthomatosis and altered composition of atherosclerotic lesions in hyperlipidemic mice lacking acyl CoA:cholesterol acyltransferase 1. J. Clin. Invest. 105, 711–719 (2000).

71. Nakamizo, S. et al. High fat diet exacerbates murine psoriatic dermatitis by increasing the number of IL-17-producing γδ T cells. Sci. Rep. 7, 14076 (2017).

72. Herbert, D. et al. High-Fat Diet Exacerbates Early Psoriatic Skin Inflammation Independent of Obesity: Saturated Fatty Acids as Key Players. J. Invest. Dermatol. 138, 1999–2009 (2018).

73. Hartvigsen, K. et al. A Diet-Induced Hypercholesterolemic Murine Model to Study Atherogenesis Without Obesity and Metabolic Syndrome. Arterioscler. Thromb. Vasc. Biol. 27, 878–885 (2007).

74. Ishibashi, S., Goldstein, J. L., Brown, M. S., Herz, J. & Burns, D. K. Massive Xanthomatosis and Atherosclerosis in cholesterol-fed low density lipoprotein receptor-negative mice. J. Clin. Invest. 93, 1885–1893 (1994).

75. Reardon, C. A., Blachowicz, L., Lukens, J., Nissenbaum, M. & Getz, G. S. Genetic Background Selectively Influences Innominate Artery Atherosclerosis. Arterioscler. Thromb. Vasc. Biol. 23, 1449–1454 (2003).

76. Lutgens, E. et al. Atherosclerosis in APOE*3-Leiden Transgenic Mice. Circulation 99, 276–283

(1999).

77. Paalvast, Y. et al. Male apoE*3-Leiden.CETP mice on high-fat high-cholesterol diet exhibit a biphasic dyslipidemic response, mimicking the changes in plasma lipids observed through life in men. Physiol. Rep. 5, (2017).

78. Havekes, L. et al. Apolipoprotein E3-Leiden. A new variant of human apolipoprotein E associated with familial type III hyperlipoproteinemia. Hum. Genet. 73, 157–163 (1986).

79. Westerterp, M. et al. Cholesteryl Ester Transfer Protein Decreases High-Density Lipoprotein and Severely Aggravates Atherosclerosis in APOE*3-Leiden Mice. Arterioscler. Thromb. Vasc. Biol. 26, 2552–2559 (2006).

80. Liu, J., Zhao, M., Zhu, Y., Zheng, L. & Yin, Y. Plasma Metabolomic and Lipidomic Profiling of a Genetically Modified Mouse Model of Scavenger Receptor Class B Type I. Proteomics 20, 2000050 (2020).

81. Dang, V. T., Huang, A., Zhong, L. H., Shi, Y. & Werstuck, G. H. Comprehensive Plasma Metabolomic Analyses of Atherosclerotic Progression Reveal Alterations in Glycerophospholipid and Sphingolipid Metabolism in Apolipoprotein E-deficient Mice. Sci. Rep. 6, 35037 (2016).

82. Zeng, C. et al. Lipidomics profiling reveals the role of glycerophospholipid metabolism in psoriasis. Gigascience 6, (2017).

83. Checa, A. et al. Circulating levels of sphingosine-1-phosphate are elevated in severe, but not mild psoriasis and are unresponsive to anti-TNF-α treatment. Sci. Rep. 5, 12017 (2015).

84. Oosterveer, D. M., Versmissen, J., Yazdanpanah, M., Hamza, T. H. & Sijbrands, E. J. G. Differences in characteristics and risk of cardiovascular disease in familial hypercholesterolemia patients with and without tendon xanthomas: A systematic review and meta-analysis. Atherosclerosis 207, 311–317 (2009).

85. Frostegård, J. Immunity, atherosclerosis and cardiovascular disease. BMC Med. 11, 117 (2013).

86. Joseph, S. B. et al. Direct and Indirect Mechanisms for Regulation of Fatty Acid Synthase Gene Expression by Liver X Receptors. J. Biol. Chem. 277, 11019–11025 (2002).

87. Joseph, S. B. et al. Synthetic LXR ligand inhibits the development of atherosclerosis in mice. Proc. Natl. Acad. Sci. 99, 7604–7609 (2002).

88. Schultz, J. R. Role of LXRs in control of lipogenesis. Genes Dev. 14, 2831–2838 (2000).

89. Tibbitt, M. W., Dahlman, J. E. & Langer, R. Emerging Frontiers in Drug Delivery. J. Am. Chem. Soc. 138, 704–717 (2016).

90. Nag, O. & Awasthi, V. Surface Engineering of Liposomes for Stealth Behavior. Pharmaceutics 5, 542–569 (2013).

91. Hayat, S. M. G., Jaafari, M. R., Hatamipour, M., Penson, P. E. & Sahebkar, A. Liposome Circulation Time is Prolonged by CD47 Coating. Protein Pept. Lett. 27, 1029–1037 (2020).

92. Liu, T., Choi, H., Zhou, R. & Chen, I.-W. RES blockade: A strategy for boosting efficiency of nanoparticle drug. Nano Today 10, 11–21 (2015).

93. Charo, I. F. & Taub, R. Anti-inflammatory therapeutics for the treatment of atherosclerosis. Nat. Rev. Drug Discov. 10, 365–376 (2011).

94. Peng, R. et al. Macrophage-Based Therapies for Atherosclerosis Management. J. Immunol. Res. 2020, 1–11 (2020).

95. Martinet, W., Coornaert, I., Puylaert, P. & De Meyer, G. R. Y. Macrophage Death as a Pharmacological Target in Atherosclerosis. Front. Pharmacol. 10, (2019).

96. Meyer, I. De, Martinet, W. & Meyer, G. R. Y. De. Therapeutic strategies to deplete macrophages in atherosclerotic plaques. (2012). doi:10.1111/j.1365-2125.2012.04211.x

97. Zhang, X.-Q. et al. Nanoparticles Containing a Liver X Receptor Agonist Inhibit Inflammation and Atherosclerosis. Adv. Healthc. Mater. 4, 228–236 (2015).

98. Gupta, D. S., Kaul, D., Kanwar, A. J. & Parsad, D. Psoriasis: crucial role of LXR-α RNomics. Genes Immun. 11, 37–44 (2010).

99. Kömüves, L. G. et al. Oxysterol Stimulation of Epidermal Differentiation is Mediated by Liver X Receptor-β in Murine Epidermis. J. Invest. Dermatol. 118, 25–34 (2002).

100. Fowler, A. J. et al. Liver X Receptor Activators Display Anti-Inflammatory Activity in Irritant and Allergic Contact Dermatitis Models: Liver-X-Receptor-Specific Inhibition of Inflammation and Primary Cytokine Production. J. Invest. Dermatol. 120, 246–255 (2003).

101. Man, M.-Q. et al. Basis for Improved Permeability Barrier Homeostasis Induced by PPAR and LXR Activators: Liposensors Stimulate Lipid Synthesis, Lamellar Body Secretion, and Post-Secretory Lipid

Processing. J. Invest. Dermatol. 126, 386–392 (2006).

102. Chang, K. C. N. et al. Liver X Receptor Is a Therapeutic Target for Photoaging and Chronological Skin Aging. Mol. Endocrinol. 22, 2407–2419 (2008).

103. Hyter, S. & Indra, A. K. Nuclear hormone receptor functions in keratinocyte and melanocyte homeostasis, epidermal carcinogenesis and melanomagenesis. FEBS Lett. 587, 529–541 (2013).

104. Ouedraogo, Z. G., Fouache, A., Trousson, A., Baron, S. & Lobaccaro, J.-M. A. Role of the liver X receptors in skin physiology: Putative pharmacological targets in human diseases. Chem. Phys. Lipids 207, 59–68 (2017).

105. Chu, K., Miyazaki, M., Man, W. C. & Ntambi, J. M. Stearoyl-Coenzyme A Desaturase 1 Deficiency Protects against Hypertriglyceridemia and Increases Plasma High-Density Lipoprotein Cholesterol Induced by Liver X Receptor Activation. Mol. Cell. Biol. 26, 6786–6798 (2006).

106. Helder, R. W. J. et al. The effects of LXR agonist T0901317 and LXR antagonist GSK2033 on morphogenesis and lipid properties in full thickness skin models. Biochim. Biophys. Acta - Mol. Cell Biol. Lipids 1865, 158546 (2020).

107. Oetjen, L. K., Trier, A. M. & Kim, B. S. PXR: A New Player in Atopic Dermatitis. J. Invest. Dermatol. 138, 8–10 (2018).

108. Elentner, A. et al. Epidermal Overexpression of Xenobiotic Receptor PXR Impairs the Epidermal Barrier and Triggers Th2 Immune Response. J. Invest. Dermatol. 138, 109–120 (2018).

109. Houck, K. A. et al. T0901317 is a dual LXR/FXR agonist. Mol. Genet. Metab. 83, 184–187 (2004).

110. Mitro, N., Vargas, L., Romeo, R., Koder, A. & Saez, E. T0901317 is a potent PXR ligand: Implications for the biology ascribed to LXR. FEBS Lett. 581, 1721–1726 (2007).

111. Schmuth, M., Moosbrugger-Martinz, V., Blunder, S. & Dubrac, S. Role of PPAR, LXR, and PXR in epidermal homeostasis and inflammation. Biochim. Biophys. Acta - Mol. Cell Biol. Lipids 1841, 463–473 (2014).

112. Bedewi, A. El, Awad, M. & Nada, E. Role of Tissue Liver X-Receptors Level in Skin Diseases. Int. J. Pept. Res. Ther. 19, 275–279 (2013).

113. Ang, L. S., Cruz, R. P., Hendel, A. & Granville, D. J. Apolipoprotein E, an important player in longevity

and age-related diseases. Exp. Gerontol. 43, 615–622 (2008).

114. Kaabia, Z. et al. Plasma lipidomic analysis reveals strong similarities between lipid fingerprints in human, hamster and mouse compared to other animal species. Sci. Rep. 8, 15893 (2018).

115. Zomer, H. D. & Trentin, A. G. Skin wound healing in humans and mice: Challenges in translational research. J. Dermatol. Sci. 90, 3–12 (2018).

116. von Scheidt, M. et al. Applications and Limitations of Mouse Models for Understanding Human Atherosclerosis. Cell Metab. 25, 248–261 (2017).

117. Schneider, M. R. Genetic mouse models for skin research: Strategies and resources. genesis 50, 652–664 (2012).

118. Mestas, J. & Hughes, C. C. W. Of Mice and Not Men: Differences between Mouse and Human Immunology. J. Immunol. 172, 2731–2738 (2004).

Appendix

Nederlandse Samenvatting
(Dutch Summary)

INTRODUCTIE

De huid vormt een essentiële fysieke barrière tussen het lichaam en de omgeving die het organisme beschermt tegen overmatig verlies van water en voedingsstoffen en het organisme beschermt tegen het binnendringen van chemicaliën en pathogenen[1]. Een belangrijke speler in deze beschermende rol is de buitenste laag van de huid - het stratum corneum (SC). Het SC is samengesteld uit corneocyten (dode huidcellen) ingebed in een lipidenmatrix die voornamelijk bestaat uit cholesterol, ceramiden en vrije vetzuren1. De huidbarrièrefunctie is afhankelijk van de samenstelling en rangschikking (genoemd organisatie) van de lipiden in de matrix in het SC[2–7]. De SC barrièrelipiden worden voornamelijk gesynthetiseerd door keratinocyten tijdens hun differentiatieproces met als eindproduct de corneocyten. Extracutane lipiden (bijv. lipoproteïnen) worden ook in de huid opgenomen en kunnen bijdragen aan de vorming van de SC lipidenpoel[8–12]. Het samenspel tussen de lokale lipidensynthese in de huid en de opname van extracutane lipiden is nog niet uitgebreid onderzocht.

In het plasma worden lipiden voornamelijk getransporteerd van en naar perifere weefsels door lipoproteinen. De vier hoofdgroepen zijn chylomicronen, lipoproteïnen met zeer lage dichtheid (VLDL), lipoproteïnen met lage dichtheid (LDL) en lipoproteïnen met hoge dichtheid (HDL). Een verstoord metabolisme van deze lipoproteïnen leidt tot abnormale concentraties lipiden in het plasma, ook wel genoemd dyslipidemie. De meest voorkomende vorm van dyslipidemie is hyperlipidemie, een aandoening die wordt gekenmerkt door een toename van circulerende lipoproteïnen en lipiden in het plasma als gevolg van genetische mutaties (bijv., Familiaire hypercholesterolemie; FH) of een andere onderliggende etiologie (bijv., Diabetes, slechte levensstijl en ongezond dieet)[13]. Hyperlipidemie is een belangrijke risicofactor voor het ontstaan van atherosclerose, een belangrijke oorzaak van hart- en vaatziekten[13]. Atherosclerose is een pathologie die wordt gekenmerkt door de vorming van lipiden plaque(s) in de arteriële wand veroorzaakt door een chronische immuunreactie waar een verstoord cholesterolmetabolisme aan ten grondslag ligt. Na verloop van tijd kunnen deze lipidenplaques de slagaders verharden en vernauwen, de bloedstroom en zuurstoftoevoer verstoren en een risico vormen voor de vorming van thrombus en het optreden van beroertes, en/of een myocardinfarct.

Liver-X-receptor (LXR) is een nucleaire receptor die een relevante rol speelt bij het vetmetabolisme en ontsteking[14–17]. In de context van atherosclerose kan “activatie” van LXR door synthetische agonisten (bijv. GW3965) de plaqueontwikkeling beïnvloeden door (1) het bevorderen van cholesteroltransport van vetrijke macrofagen (schuimcellen) terug naar de lever en (2) door algemene remming van pro-inflammatoire genen[15].

Directe systemische toediening van LXR-agonisten heeft echter een negatieve invloed op synthese van lipiden door de lever en kan hypertriglyceridemie induceren[17,18]. Daarom is een deel van het onderzoek beschreven in dit proefschrift gericht op het verpakken van een LXR-agonist in specifieke afgiftesystemen, met als doel een verhoogde aflevering van het medicament in macrofagen in de plaques.

Naast het verhoogde risico op het ontwikkelen van atherosclerose, kunnen personen met hyperlipidemie (familiair of verworven) na verloop van tijd gele, cholesterolrijke afzettingen (xanthomen) ontwikkelen in de huid rond hun ogen of gewrichten[19–21]. Xanthomen zijn bekende dermatologische symptomen van onderliggende lipidenstoornissen[20]. Ondanks de cruciale rol van lipiden in de huid, is het verband tussen dyslipidemie en lipidenhomeostase van de huid onduidelijk. In dit proefschrift hebben we deze relatie onderzocht om er achter te komen of en hoe veranderingen in het cholesterolgehalte in het plasma op jonge leeftijd de lipidensynthese en/of de samenstelling van barrièrelipiden verandert voorafgaand aan de ontwikkeling van xanthomen (of andere dermatologische aandoeningen) en atherosclerose. Ten slotte hebben we de interactie onderzocht van de synthetische peptide Lyp-1 met de p32-receptor die tot expressie wordt gebracht op met lipiden beladen macrofagen in atherosclerotische plaques[22,23]. We concentreerden ons op Lyp-1 als een peptide geassocieerd met liposomen om de daarin verpakte LXR-agonist GW3965 specifiek af te leveren aan de atherosclerotische plaques in hypercholesterolemische muizen.

SAMENVATTING

De impact van dyslipidemia op de huid

Hypercholesterolemie

Hypercholesterolemie (hoge cholesterol niveaus in plasma) werd in het onderzoek beschreven in dit proefschrift onderzocht omdat het wereldwijd de meest voorkomende vorm van dyslipidemie is. Familiaire hypercholesterolemie (FH) is een bepaald type genetische lipoproteïnestoornis die leidt tot hoge concentraties van apolipoproteine B-bevattende lage dichtheidslipoproteïnen in plasma. Met een algemene gerapporteerde prevalentie van 1:311 is FH één van de meest voorkomende genetische aandoeningen bij de bevolking, met een vergelijkbare verspreiding over de hele wereld[24]. Hoewel een hoog cholesterolgehalte op jonge leeftijd meestal geen specifieke klachten veroorzaakt, ontwikkelen FH-patiënten op de lange termijn vaak xanthomen rond de oogleden, gewrichten, pezen en zelfs in de rand van de iris[25–27]. Deze dermatologische symptomen zijn vaak de eerste indicatie van hypercholesterolemie, een belangrijke risicofactor

voor de ontwikkeling van atherosclerose op jonge leeftijd, zoals eerder beschreven.

In **Hoofdstuk 2** hebben we de huid van jonge volwassen lage dichtheidslipoproteïn receptor knockout (*LDLR*$^{-/-}$) en apolipoproteïne E knockout (*APOE*$^{-/-}$) muizen onderzocht. Zowel *LDLR*$^{-/-}$ als *APOE*$^{-/-}$ muizen zijn bekende hypercholesterolemische muismodellen en er is beschreven dat hun huid, analoog aan mensen met deze aandoening, xanthomen ontwikkelt bij langdurige voeding met een hoog vet/hoog cholesterolgehalte of bij veroudering. Bij een vetarm/cholesterolarm dieet leidt LDLR deficiëntie tot een milde hypercholesterolemie met voornamelijk ophoping van LDL in het plasma. Daarentegen ontwikkelen *APOE*$^{-/-}$ muizen een ernstiger hypercholesterolemisch profiel met een duidelijke toename van de VLDL fracties. Uit analyse van de epidermale lipidensamenstelling bleek dat ernstige systemische hypercholesterolemie bij jongvolwassen *APOE*$^{-/-}$ muizen het vrije vetzuren-profiel beïnvloedt waardoor de epidermale barrièrefunctie vermindert. De epidermis van de *APOE*$^{-/-}$ muizen was verrijkt met korte keten vrije vetzuren (minder dan 24 koolstofatomen) en onverzadigde vrije vetzuren, terwijl de lipidensamenstelling in de epidermis van de milde hypercholesterolemische *LDLR*$^{-/-}$ muizen niet veranderde. Het genregulatie profiel waargenomen in de huid van *APOE*$^{-/-}$ muizen wijst op een compenserende neerwaartse regulatie van de expressie van genen die betrokken zijn bij de synthese van cholesterol en vetzuren als reactie op de verhoogde lokale niveaus van cholesterol en vrije vetzuren. Ten slotte resulteerde de veranderde vrije vetzuren-poel in de epidermis van *APOE*$^{-/-}$ muizen in een verminderde huidbarrièrefunctie, zoals blijkt uit een verhoogd transepidermaal waterverlies. Kortom, uit deze studie blijkt dat de ernst van de hypercholesterolemie bij muizen kan bijdragen aan de flux van extracutane lipiden in de huid, waardoor het de epidermale lipidensamenstelling en de functionaliteit van de huidbarrière al op jonge leeftijd beïnvloedt. Onze bevindingen suggereren dat de huid van hypercholesterolemische personen met FH mogelijk al aan een veranderde lipidensamenstelling onderhevig is voordat de xanthomen of cardiovasculaire complicaties zich ontwikkelen, waardoor mogelijk de barrièrefunctie vermindert.

Hypercholesterolemische plasmaprofielen kunnen ook het gevolg zijn van accumulatie van lipoproteïnen met apolipoproteïne A (APOA) als structurele eiwitcomponent, wat leidt tot hyper-alfalipoproteïnemie. Genetische factoren zoals deficiëntie van cholesterylester transfer proteïne (CETP) of zeldzame mutaties in scavenger receptor klasse BI (SR-BI) worden beschreven als oorzaken van hyper-alfalipoproteïnemie met opvallende toename van HDL-cholesterol concentraties bij mensen[28–30]. In tegenstelling tot FH-patiënten worden bij hyper-alfalipoproteïnemische patiënten geen xanthomen gemeld[31]. De huid is echter één van de grootste reservoirs van HDL in het lichaam;

hyper-alfalipoproteïnemie kan dus de lipidenhomeostase van de huid beïnvloeden[32].

In het onderzoek beschreven in **Hoofdstuk 3** hebben we daarom onderzocht of de hypercholesterolemie veroorzaakt door hyperalphalipoproteïnemie ook de epidermale lipidenpoel zou kunnen beïnvloeden. Voor dit doel gebruikten we jongvolwassen (16-18 weken oud) *SR-BI*$^{-/-}$ muizen, een hypercholesterolemisch muismodel van hyper-alfalipoproteïnemie, waarbij de klaring van HDL-deeltjes door de lever is belemmerd, evenals hun opname door steroïdogene weefsels[33–35]. Met name het niveau van CE getransporteerd in lipoproteïnen in *SR-BI*$^{-/-}$ muizen is significant hoger dan het niveau gerapporteerd voor *LDLR*$^{-/-}$ muizen, maar niet zo ernstig als waargenomen in de *APOE*$^{-/-}$ muizen (**Hoofdstuk 2**). Ondanks de beschermende rol van HDL bij het transport van cholesterol van perifere weefsels naar de lever had hyper-alfalipoproteïnemie een negatieve invloed op de epidermale vrije vetzuren-samenstelling van de *SR-BI*$^{-/-}$ muizen. Hoewel in mindere mate dan gerapporteerd voor de huid van *APOE*$^{-/-}$ muizen, werd ook het relatieve percentage onverzadigde en vrije vetzuren-soorten met een korte koolstofketen, inclusief vrij vetzuur C18:1 was verhoogd in de epidermis van *SR-BI*$^{-/-}$ muizen in vergelijking met de normolipidemische wild-type controles. Net als bij *APOE*$^{-/-}$ muizen, vertoonde het genregulatie profiel van de huid van *SR-BI*$^{-/-}$ muizen lagere niveaus van mRNA van die genen welke coderen voor enzymen die betrokken zijn bij de synthese van vrije vetzuren en cholesterol en voor receptoren die betrokken zijn bij de opname van lipoproteïnen. Belangrijk is dat we hebben aangetoond dat de waargenomen samenstelling veranderingen van epidermale lipiden nauw gecorreleerd zijn met de lipiden concentraties in plasma. Ze zijn minder afhankelijk zijn van de specifieke lipoproteïnegroep die betrokken is bij het transport van de lipiden. Hoewel dermatologische symptomen (bijv. xanthomen) niet zijn beschreven bij patiënten met hyper-alfalipoproteïnemie, laten onze studies zien dat de huid negatief wordt beïnvloed door de veranderingen in het plasmalipidenprofiel. Daarom is het belangrijk om extra aandacht te besteden aan de huid van deze patiënten om de ontwikkeling van dermatologische afwijkingen te voorkomen.

Hypolipidemie

Uiteraard kan dyslipidemie ook verwijzen naar verlaagde concentraties plasmalipiden, namelijk hypolipidemie, wat ook veroorzaakt kan worden door bepaalde genetische afwijkingen. Mutaties in APOAI kunnen de vorming van HDL ernstig beïnvloeden, wat leidt tot een vrijwel volledige afwezigheid van deze deeltjes, een verlaagd cholesterol in het plasma (vooral lagere CE-waarden) en een verhoogd risico op hart- en vaatziekten[36–41]. In het onderzoek beschreven in **Hoofdstuk 4** hebben we de gevolgen van een HDL-gedreven hypolipidemie (hypo-alfalipoproteïnemie) op

de lipidensamenstelling van de huidbarrière van *APOAI*$^{-/-}$ muizen onderzocht. Hypoalfalipoproteïnemie bij de *APOAI*$^{-/-}$ muizen had geen invloed op de morfologie van de huid of het epidermale lipidenprofiel. De mRNA-expressie van verschillende genen die betrokken zijn bij de synthese van lipiden en opname van lipoproteïnen was echter verhoogd in de huid van deze muizen (bijv. *HMGCR, LDLR, FAS, SR-BI*). Dit suggereert dat de neerwaartse regulering van *DGAT2* (diacylglycerol O-acyltransferase 2) mRNA-niveaus in de huid van deze muizen een vermindering in de opslag van vetzuren in de vorm van triglyceriden veroorzaakt. Samenvattend, laat ons onderzoek zien dat (1) HDL-deeltjes niet cruciaal zijn voor het transport van cholesterol vanuit de huid naar de lever, maar in plaats daarvan (2) juist bijdragen aan de afgifte van essentiële lipiden aan de huid. Belangrijk is dat de epidermale lipidenbarrière kan worden gehandhaafd door een compenserende toename van de lokale lipidensynthese en opname van lipiden uit apolipoproteïne B-bevattende lipoproteïnen in de afwezigheid van HDL.

De relevantie van de huid voor onderzoek – een vergelijking van de barrièrelipiden profielen

De onderzoeken die in de vorige paragrafen (**Hoofdstukken 2-4**) zijn beschreven, werden uitgevoerd met behulp van de rughuid van de muizen, aangezien dit gebied een voldoende groot oppervlakte heeft voor het doen van de betreffende analyses. Naast de huid van de rug wordt echter ook vaak huid van het oor gebruikt voor onderzoek in muismodellen. Echter verschillen deze locaties sterk in de dichtheid van haarzakjes en het aantal cellagen in het SC. Bovendien kunnen deze huidlocaties verschillende effecten/fenotypes opleveren met betrekking tot bijvoorbeeld medicamenteuze behandeling en weefselregeneratiestudies[42–44]. Ondanks deze verschillen is er weinig informatie beschikbaar over de samenstelling van hun lipidenbarrière en eventuele verschillen daarin. Vooral over de epidermis van het oor is nog weinig informatie beschikbaar.

In **Hoofdstuk 5** laten we zien dat de epidermale lipidensamenstelling en het mRNA-genexpressieprofiel fundamenteel verschillen tussen oor- en rughuid van de muis in een normolipidemische achtergrond. In vergelijking met de epidermis van de rug is er een hogere fractie onverzadigde vetzuren en ceramiden (vooral ceramiden met een sfingo base) in de epidermis van de oren. De oorhuid is ook verrijkt met korte keten vrije vetzuren en korte keten (33-34 koolstofatomen) ceramiden. Verder blijkt uit onderzoek beschreven in **Hoofdstuk 5** dat de huid van het oor bij *APOE*$^{-/-}$ muizen marginaal reageerde op hypercholesterolemie in vergelijking met de rughuid bij *APOE*$^{-/-}$ muizen[45]. Het epidermale vrije vetzurenprofiel van de oren van normolipidemische en hypercholesterolemische muizen was redelijk vergelijkbaar, met slechts een minimale

toename van het totale percentage van de vrije vetzuren-soorten met een korte keten. Uit deze bevindingen blijkt dat de huid van de rug van muizen waarschijnlijk een actievere metabole plaats is in vergelijking met de huid van het oor en dat deze plaatsen anders reageren op specifieke behandelingen die tot verschillende resultaten kunnen leiden, zoals eerder gerapporteerd[42–44]. De selectie van de plek van de huid voor onderzoek kan dus impact hebben op de uitkomst en moet zorgvuldig worden overwogen.

Lyp-1: klein peptide om liposomen te gericht te sturen naar macrofagen in atherosclerotische laesies

Naast de effecten op de huid is hypercholesterolemie een belangrijke risicofactor voor atherosclerose, een ziekte die wordt gekenmerkt door de pathologische vernauwing van grote en middelgrote slagaders[46]. Het begin en de ontwikkeling van deze pathologie wordt voornamelijk gedreven door de ophoping van lipiden (LDL en andere gemodificeerde lipoproteïnen) in macrofagen in de intima van deze bloedvaten, wat leidt tot de vorming van atherosclerotische plaques[46–48]. Het onderzoek beschreven in **Hoofdstuk 6** heeft als doel een liposoomformulering te ontwikkelen die LXR-agonist GW3965 gericht aflevert aan macrofagen in atherosclerotische plaques met als beoogd gevolg verhoging van het cholesterol transport uit de macrofagen en bevordering van plaquestabilisatie[49–51]. Atherosclerotische plaques vertonen een hoge expressie van C1q-bindend eiwit, ook bekend als p32, met name in vetrijke macrofagen (schuimcellen)[22,23]. Lyp-1 is een klein cyclisch peptide (CGNKRTRGC) waarvan bekend is dat het bindt aan p32[22]. Tot op heden is het potentieel van Lyp-1 als richtmolecuul vooral onderzocht voor plaque-beeldvormingsdoeleinden[52,53]. In onze studie was liposoomfunctionalisatie met Lyp-1 de belangrijkste strategie om het zo specifiek mogelijk GW3965 naar macrofagen in de atherosclerotische plaques te kunnen sturen en daarnaast om ook de retentietijd van de liposomen in de plaque te verlengen. Hoewel er in deze studie geen effect op de plaquegrootte werd waargenomen, had de muizengroep die met GW3965-geladen Lyp-1-liposomen was behandeld, een verlaagd gehalte aan plaque-macrofagen en een verbeterde plakstabiliteit, zoals bleek uit een verhoogd collageengehalte. Bovendien had de behandeling met de gefunctionaliseerde GW3965-geladen liposomen geen invloed op het gehalte aan lipiden in de lever en serum. Liposomen, gefunctionaliseerd met Lyp-1, zijn dus een waardevol hulpmiddel om de werkzaamheid en effecten van GW3965 te verhogen en zo macrofaag-schuimcellen in de atherosclerotische laesies aan te pakken, wat de weg vrijmaakt voor de ontwikkeling van betere therapieën voor atherosclerose.

DISCUSSIE EN PERSPECTIEVEN

Het onderzoek beschreven in dit proefschrift verbreedt onze kennis omtrent de kwaliteit

van leven van individuen met dyslipidemie. Het geeft inzicht in de lipidenhomeostase in de huid, kennis die mogelijk kan bijdragen aan de ontwikkeling van zo optimaal mogelijke behandeling van dyslipidemie patiënten met dermatologische aandoeningen.

De bevindingen die in dit proefschrift zijn beschreven zijn gericht op onderzoek in dyslipidemische muismodellen en kunnen niet rechtstreeks worden toegepast op de menselijke situatie, zonder verdere studies. Muizen en mensen vertonen overeenkomsten en verschillen in alle onderzoeksaspecten van dit proefschrift (huid, lipidenmetabolisme, en de ontwikkeling van atherosclerose)[54–57]. Uit zowel plasma- als huid lipidomics blijken verschillen en overeenkomsten tussen muizen en mensen. Evenzo hebben muismodellen, met de eventuele beperkingen, een belangrijke bijdrage geleverd om processen betrokken bij de ontwikkeling van atherosclerose in mensen beter te begrijpen. Dit is uiteraard met in acht neming van de convergerende en uiteenlopende kenmerken tussen mensen en de verschillende diermodellen[54]. Bovendien is het ook belangrijk ons te realiseren dat, hoewel dit aspect niet diepgaand wordt onderzocht in dit proefschrift, de huid een actief immunologisch orgaan is en dat muizen en mensen convergente en divergerende immunologische profielen vertonen waarmee bij de translatie van bevindingen in de muis naar de mens rekening gehouden moet worden[58]. Belangrijk is dat deze verschillen het gebruik van muismodellen niet mogen ontmoedigen, aangezien muismodellen enorm hebben bijgedragen aan de baanbrekende ontdekkingen in de onderzoeksgebieden die in dit proefschrift zijn beschreven. Het bewustzijn van deze verschillen is belangrijk om experimenten optimaal te ontwerpen en met de toekomstige bevindingen daarna de juiste vertaalslag naar de menselijke situatie te maken. Ten slotte, voor het toepassen van de bevindingen beschreven in dit proefschrift, zou het onderzoeken de barrièrefunctie en de lipidensamenstelling en organisatie in de huid bij personen die lijden aan FH een belangrijke stap zijn. De gegevens die in een dergelijke studie worden gegenereerd, zouden de eerste stap zijn om de translationele waarde van dyslipidemische muizenmodellen aangaande de relatie tussen de huid, het plasma en dyslipidemische pathologieën beter te leren begrijpen.

Samenvattend, het onderzoek beschreven in dit proefschrift laat zien dat hypercholesterolemie, een bekende risicofactor voor atherosclerose, al op jonge leeftijd invloed kan hebben op de lipidenpoel en de barrièrefunctie van de huid. Opheldering van de mechanismen die ten grondslag liggen aan deze relatietussen het plasma en de huid biedt ook waardevolle aanknopingspunten om dermatologische pathologieën bij dyslipidemische patiënten te voorkomen en/of te behandelen; misschien in combinatie met anti-atherogene therapieën. Met vergroting van de kennis en inzicht in de betrokken processen, kan op termijn het advies aan patiënten worden verbeterd met uiteindelijk een verbetering van de kwaliteit van leven tot gevolg.

REFERENCES

1. Elias, P. M. Stratum corneum defensive functions: An integrated view. J. Invest. Dermatol. 125, 183–200 (2005).

2. Janssens, M. et al. Increase in short-chain ceramides correlates with an altered lipid organization and decreased barrier function in atopic eczema patients. J. Lipid Res. 53, 2755–2766 (2012).

3. Thakoersing, V. S. et al. Modulation of stratum corneum lipid composition and organization of human skin equivalents by specific medium supplements. Exp. Dermatol. 24, 669–674 (2015).

4. van Smeden, J. et al. The importance of free fatty acid chain length for the skin barrier function in atopic eczema patients. Exp. Dermatol. 23, 45–52 (2014).

5. White, S. H., Mirejovsky, D. & King, G. I. Structure of lamellar lipid domains and corneocyte envelopes of murine stratum corneum. An x-ray diffraction study. Biochemistry 27, 3725–3732 (1988).

6. Boncheva, M., Damien, F. & Normand, V. Molecular organization of the lipid matrix in intact Stratum corneum using ATR-FTIR spectroscopy. Biochim. Biophys. Acta - Biomembr. 1778, 1344–1355 (2008).

7. Bouwstra, J., Gooris, G. & Ponec, M. The lipid organisation of the skin barrier: liquid and crystalline domains coexist in lamellar phases. J. Biol. Phys. 28, 211–23 (2002).

8. Haruta-Ono, Y. et al. Orally administered sphingomyelin in bovine milk is incorporated into skin sphingolipids and is involved in the water-holding capacity of hairless mice. J. Dermatol. Sci. 68, 56–62 (2012).

9. Bhattacharyya, A. K., Connor, W. E. & Spector, A. A. Excretion of sterols from the skin of normal and hypercholesterolemic humans. Implications for sterol balance studies. J. Clin. Invest. 51, 2060–70 (1972).

10. Khnykin, D., Miner, J. H. & Jahnsen, F. Role of fatty acid transporters in epidermis: Implications for health and disease. Dermatoendocrinol. 3, 53–61 (2011).

11. Hansen, H. S. & Jensen, B. Essential function of linoleic acid esterified in acylglucosylceramide and acylceramide in maintaining the epidermal water permeability barrier. Evidence from feeding studies with oleate, linoleate, arachidonate, columbinate and α-linolenate. Biochim. Biophys. Acta - Lipids Lipid Metab. 834, 357–363 (1985).

12. Bibel, D. J. et al. Antimicrobial Activity of Stratum Corneum Lipids from Normal and Essential Fatty Acid-Deficient Mice. J. Invest. Dermatol. 92, 632–638 (1989).

13. Nelson, R. H. Hyperlipidemia as a Risk Factor for Cardiovascular Disease. Prim. Care Clin. Off. Pract. 40, 195–211 (2013).

14. Wang, B. & Tontonoz, P. Liver X receptors in lipid signalling and membrane homeostasis. Nat. Rev. Endocrinol. 14, 452–463 (2018).

15. Im, S.-S. & Osborne, T. F. Liver X Receptors in Atherosclerosis and Inflammation. Circ. Res. 108, 996–1001 (2011).

16. Schulman, I. G. Liver X receptors link lipid metabolism and inflammation. FEBS Lett. 591, 2978–2991 (2017).

17. Zhang, Y. et al. Liver LXRα expression is crucial for whole body cholesterol homeostasis and reverse cholesterol transport in mice. J. Clin. Invest. 122, 1688–1699 (2012).

18. Heckmann, B. L. et al. Liver X receptor α mediates hepatic triglyceride accumulation through upregulation of G0/G1 Switch Gene 2 expression. JCI Insight 2, (2017).

19. Sugiyama, N. et al. Immunohistochemical distribution of lipoprotein epitopes in xanthomata from patients with familial hypercholesterolemia. Am. J. Pathol. 141, 99–106 (1992).

20. Dwivedi, S. Cutaneous markers of coronary artery disease. World J. Cardiol. 2, 262 (2010).

21. Shenoy, C., Shenoy, M. & Rao, G. Dyslipidemia in dermatological disorders. N. Am. J. Med. Sci. 7, 421 (2015).

22. Hamzah, J. et al. Specific penetration and accumulation of a homing peptide within atherosclerotic plaques of apolipoprotein E-deficient mice. Proc. Natl. Acad. Sci. 108, 7154–7159 (2011).

23. Peerschke, E. et al. Expression of gC1q-R/p33 and its major ligands in human atherosclerotic lesions. Mol. Immunol. 41, 759–766 (2004).

24. Hu, P. et al. Prevalence of Familial Hypercholesterolemia Among the General Population and Patients With Atherosclerotic Cardiovascular Disease. Circulation 141, 1742–1759 (2020).

25. Ohshiro, T., Shimabukuro, T., Sunagawa, M. & Ohta, T. An 11-year-old boy with familial hypercholesterolemia showing multiple xanthomas and advanced atherosclerosis, who responded to lipid-lowering therapy using statin. J. Atheroscler. Thromb. 16, 698–701 (2009).

26. Aljenedil, S., Ruel, I., Watters, K. & Genest, J. Severe xanthomatosis in heterozygous familial hypercholesterolemia. J. Clin. Lipidol. 12, 872–877 (2018).

27. Palacio, C. H., Harring, T. R., Nguyen, N. T. T., Goss, J. A. & O'Mahony, C. A. Homozygous familial hypercholesterolemia: case series and review of the literature. Case Rep. Transplant. 2011, 154908 (2011).

28. Hirano, K. et al. Disease-associated marked hyperalphalipoproteinemia. Mol. Genet. Metab. Reports 1, 264–268 (2014).

29. Oates, C. P. et al. Novel polymorphisms associated with hyperalphalipoproteinemia and apparent cardioprotection. J. Clin. Lipidol. 12, 110–115 (2018).

30. Helgadottir, A. et al. Rare SCARB1 mutations associate with high-density lipoprotein cholesterol but not with coronary artery disease. Eur. Heart J. 39, 2172–2178 (2018).

31. Miettinen, H. E. et al. Molecular Genetic Study of Finns With Hypoalphalipoproteinemia and Hyperalphalipoproteinemia. Arterioscler. Thromb. Vasc. Biol. 18, 591–598 (1998).

32. Randolph, G. J. & Miller, N. E. Lymphatic transport of high-density lipoproteins and chylomicrons. J. Clin. Invest. 124, 929–935 (2014).

33. Acton, S. et al. Identification of Scavenger Receptor SR-BI as a High Density Lipoprotein Receptor. Science (80-.). 271, 518–520 (1996).

34. Rigotti, A. et al. A targeted mutation in the murine gene encoding the high density lipoprotein (HDL) receptor scavenger receptor class B type I reveals its key role in HDL metabolism. Proc. Natl. Acad. Sci. U. S. A. 94, 12610–12615 (1997).

35. Brodeur, M. R., Luangrath, V., Bourret, G., Falstrault, L. & Brissette, L. Physiological importance of SR-BI in the in vivo metabolism of human HDL and LDL in male and female mice. J. Lipid Res. 46, 687–696 (2005).

36. Sorci-Thomas, M. G. & Thomas, M. J. The Effects of Altered Apolipoprotein A-I Structure on Plasma HDL Concentration. Trends Cardiovasc. Med. 12, 121–128 (2002).

37. Chroni, A., Duka, A., Kan, H.-Y., Liu, T. & Zannis, V. I. Point Mutations in Apolipoprotein A-I Mimic the Phenotype Observed in Patients with Classical Lecithin:Cholesterol Acyltransferase Deficiency †. Biochemistry 44, 14353–14366 (2005).

38. Huang, W. et al. A Novel Homozygous Missense Mutation in the Apo A-I Gene With Apo A-I Deficiency. Arterioscler. Thromb. Vasc. Biol. 18, 389–396 (1998).

39. Miettinen, H. E. et al. Apolipoprotein A-I FIN (Leu159→Arg) Mutation Affects Lecithin. Arterioscler. Thromb. Vasc. Biol. 17, 3021–3032 (1997).

40. Hovingh, G. K. et al. A novel apoA-I mutation (L178P) leads to endothelial dysfunction, increased arterial wall thickness, and premature coronary artery disease. J. Am. Coll. Cardiol. 44, 1429–1435 (2004).

41. Plump, A. S. et al. ApoA-I knockout mice: Characterization of HDL metabolism in homozygotes and identification of a post-RNA mechanism of apoA-I up-regulation in heterozygotes. J. Lipid Res. 38, 1033–1047 (1997).

42. Madsen, M., Pedersen, T. X., Nielsen, L. B., Johansen, C. & Hansen, P. R. Differential Effects of Digoxin on Imiquimod-Induced Psoriasis-Like Skin Inflammation on the Ear and Back. Ann. Dermatol. 30, 485 (2018).

43. Nguyen, T. & Wei, M. L. Hermansky–Pudlak HPS1/pale ear Gene Regulates Epidermal and Dermal Melanocyte Development. J. Invest. Dermatol. 127, 421–428 (2007).

44. Metcalfe, A. D., Willis, H., Beare, A. & Ferguson, M. W. J. Characterizing regeneration in the vertebrate ear. J. Anat. 209, 439–446 (2006).

45. Martins Cardoso, R. et al. Hypercholesterolemia in young adult APOE −/− mice alters epidermal lipid composition and impairs barrier function. Biochim. Biophys. Acta - Mol. Cell Biol. Lipids 1864, (2019).

46. Pirillo, A., Norata, G. D. & Catapano, A. L. LOX-1, OxLDL, and Atherosclerosis. Mediators Inflamm. 2013, 1–12 (2013).

47. Tabas, I. Macrophage death and defective inflammation resolution in atherosclerosis. Nat. Rev. Immunol. 10, 36–46 (2010).

48. Chistiakov, D. A., Melnichenko, A. A., Myasoedova, V. A., Grechko, A. V. & Orekhov, A. N. Mechanisms of foam cell formation in atherosclerosis. J. Mol. Med. 95, 1153–1165 (2017).

49. Collins, J. L. et al. Identification of a Nonsteroidal Liver X Receptor Agonist through Parallel Array Synthesis of Tertiary Amines. J. Med. Chem. 45, 1963–1966 (2002).

50. Levin, N. et al. Macrophage Liver X Receptor Is Required for Antiatherogenic Activity of LXR Agonists. Arterioscler. Thromb. Vasc. Biol. 25, 135–142 (2005).

51. Kirchgessner, T. G. et al. Beneficial and Adverse Effects of an LXR Agonist on Human Lipid and Lipoprotein Metabolism and Circulating Neutrophils. Cell Metab. 24, 223–233 (2016).

52. Uchida, M. et al. Protein Cage Nanoparticles Bearing the LyP-1 Peptide for Enhanced Imaging of Macrophage-Rich Vascular Lesions. ACS Nano 5, 2493–2502 (2011).

53. Seo, J. W. et al. 64 Cu-Labeled LyP-1-Dendrimer for PET-CT Imaging of Atherosclerotic Plaque. Bioconjug. Chem. 25, 231–239 (2014).

54. Kaabia, Z. et al. Plasma lipidomic analysis reveals strong similarities between lipid fingerprints in human, hamster and mouse compared to other animal species. Sci. Rep. 8, 15893 (2018).

55. Zomer, H. D. & Trentin, A. G. Skin wound healing in humans and mice: Challenges in translational research. J. Dermatol. Sci. 90, 3–12 (2018).

56. von Scheidt, M. et al. Applications and Limitations of Mouse Models for Understanding Human Atherosclerosis. Cell Metab. 25, 248–261 (2017).

57. Schneider, M. R. Genetic mouse models for skin research: Strategies and resources. genesis 50, 652–664 (2012).

58. Mestas, J. & Hughes, C. C. W. Of Mice and Not Men: Differences between Mouse and Human Immunology. J. Immunol. 172, 2731–2738 (2004).

Appendix

Curriculum Vitae

List of Publications

CURRICULUM VITAE

Renata Martins Cardoso was born in Vitória (Espírito Santo, Brazil) on the 8th of April 1986. She did her bachelor studies in Pharmacy with a minor in Biochemistry at the Federal University of Espírito Santo (Vitória, Brazil). During her bachelor studies, she did a research internship in the Department of Physiology led by Prof. Dr. Margareth Moysés studying the impact of adrenergic activity induced by ultrasound stimulation on plasma sodium levels in obese Wistar rats.

In early 2011, she moved to The Netherlands where a year later she started her Master's research program in Drug Innovation at Utrecht University. During her Master's program she dedicated herself to the research of drug delivery systems. Her first master's project took place in the department of Pharmaceutics under supervision of Dr. Rene van Nostrum and Prof. Dr. Wim Hennink. The research focused on the development of UV-crosslinkable thermosensitive micelles for drug delivery. Next, she joined the group of Prof. Dr. Raymond Schiffelers at the department of Clinical Chemistry and Hematology of the Utrecht University Medical Centre (UMC Utrecht) where she explored different labelling strategies for tracking of extracellular vesicles.

Starting in 2014 Renata performed her Ph.D. studies at Leiden University in the Division of BioTherapeutics of the Leiden Academic Centre for Drug Research under supervision of Prof. Dr. Joke Bouwstra and Prof. Dr. Miranda van Eck. Her research mostly focused on the impact of dyslipidemia on the skin lipid homeostasis and barrier function. In addition, she collaborated with a fellow Ph.D. student (Naomi Benne) to explore the homing properties of a small peptide to target liposomes to macrophages (foam cells) in the atherosclerotic plaques. Renata also collaborated with the group of Dr. Tanja X. Pedersen (University of Copenhagen, Denmark) to investigate the effects of imiquimod-induced psoriasis on the development of atherosclerosis. During her Ph.D. trajectory, she won several presentation prizes (including best poster prize for three consecutive years at the LACDR Spring Symposium) and was invited to give a short communication at the Gordon Research Conference on Barrier Function of Mammalian Skin conference (United States).

Since 2020, Renata works at Janssen Vaccines and Prevention (Leiden, The Netherlands) in the Drug Product Development department.

LIST OF PUBLICATIONS

Martins Cardoso R., Absalah S., Eck M. van[1], Bouwstra J.A.[1] (2020). Barrier lipid composition and response to plasma lipids: A direct comparison of mouse dorsal back and ear skin. Experimental Dermatology 29(6): 548-555.

Martins Cardoso R.[1], Benne N.[1], Boyle A.L., Kros A., Jiskoot W., Kuiper J., Bouwstra J., Eck M. van, Slütter B.A. (2020). Complement Receptor Targeted Liposomes Encapsulating the Liver X Receptor Agonist GW3965 Accumulate in and Stabilize Atherosclerotic Plaques. Advanced Healthcare Materials 9(10): 2000043.

Martins Cardoso R., Creemers E., Absalah S., Hoekstra M., Gooris G.S., Bouwstra J.A.[1], Eck M. van[1] (2020). Hyperalphalipoproteinemic scavenger receptor BI knockout mice exhibit a disrupted epidermal lipid barrier. Biochimica et Biophysica Acta Molecular and Cell Biology of Lipids 1865(3): 158592.

Martins Cardoso R., Creemers E., Absalah S., Gooris G.S., Hoekstra M., Eck M. van[1], Bouwstra J.A.[1] (2019). Hypercholesterolemia in young adult *APOE*$^{-/-}$ mice alters epidermal lipid composition and impairs barrier function. Biochimica et Biophysica Acta Molecular and Cell Biology of Lipids 1864(7): 976-984.

Madsen M., Hansen P.R., Nielsen L.B., **Martins Cardoso R**., Eck M. van., Pedersen T.X. (2018), Imiquimod-Induced Psoriasis-Like Skin Lesions Do Not Accelerate Atherosclerosis in Low-Density Lipoprotein Receptor-Deficient Mice. American Journal of Pathology 88(6): 1486-1496.

Shi Y.; **Martins Cardoso R**., Nostrum C.F. van, Hennink W. van (2015). Anthracene functionalized thermosensitive and UV-crosslinkable polymeric micelles. Polymer Chemistry 11(6):2048-2053.

[1]Both authors contributed equally